

SINGLE-CRYSTAL-TO-SINGLE-CRYSTAL  
[2+2] PHOTODIMERIZATIONS  
THROUGH ABSORPTION-TAIL IRRADIATION

BY

KATHLEEN NOVAK

A DISSERTATION PRESENTED TO THE GRADUATE SCHOOL OF  
THE UNIVERSITY OF FLORIDA IN PARTIAL FULFILLMENT  
OF THE REQUIREMENTS FOR THE DEGREE OF  
DOCTOR OF PHILOSOPHY

UNIVERSITY OF FLORIDA

1993

This dissertation is dedicated to my family.

To my sister and brother,

*Jeanne Annette Novak*

and

*Michael Anthony Novak*

And to our parents,

*Dolores Marlene Novak*

and

*James Joseph Novak*

It was a family effort, as always.

## ACKNOWLEDGEMENTS

I have looked forward to writing these pages of this dissertation--my thank you to the many people contributing to this work--more than any other. It is certainly the part I am most qualified to author.

If I was forced to choose only one person to thank here, it would be Professor Ken Wagener, of course. I could write a dissertation on his skill as an advisor, his commitment and generosity to his graduate students (as well as to any of the other graduate students in the Chemistry Department and to the undergraduates in his courses), and the joy and magic that he finds in the science of chemistry and reveals to those students. Professor Wagener has created an exchange program with Professor Gerhard Wegner from the Max-Planck-Institut für Polymerforschung (MPI-P) in Mainz, Germany. My participation in this program was generously funded by the 3M Company of St. Paul, Minnesota, and brought me to the MPI-P for two years during the course of my doctoral work.

At our first meeting Professor Wegner suggested I irradiate the styrylpyrylium salt crystals in their absorption tail to create single crystals of photoproduct. This method became the primary theme of the investigations, resulting in work that was eventually presented at the ICCOSS XI conference in Jerusalem, 1993. I am deeply grateful for the opportunity, made possible by Professor Wegner, to attend this conference. It was an invaluable professional experience that has had a significant bearing on the development of this dissertation. I also thank Professor Wegner for welcoming me to the MPI-P two years ago and for all his support, encouragement and patience since then.

I smile at the thought of "acknowledging" anyone mentioned here, but especially Dr. Volker Enkelmann. His ideas and labor are the heart of this dissertation. He was

working on the twenty-fifth full x-ray crystal structure associated with this research when I left the Max-Planck-Institut. I wish I could describe how edifying and enlightening all our discussions of this work were to me. But what measure exists for the gratitude an apprehensive student possesses for a good and patient teacher?

Dr. Werner Köhler is the force behind the work in Chapter 6. He adapted equipment he had been using in forced Raleigh scattering experiments and realized how kinetic data could be obtained from thermal decay of the grating. He turned otherwise tedious data collection monitoring into fascinating tutorials on holographic gratings.

Michael Steiert created many of the crystals used in Chapters 5 and 6, while Bernhard Zimmer prepared the laser setup used for the styrylpyrylium triflate irradiation. I owe their expertise and diligence an incalculable debt. Special thanks go to Herr Zimmer, who spent days modifying and fine-tuning the laser setup used for the irradiations reported in Chapter 3. Dr. Günter Lieser's expertise with the photomicroscope was also invaluable.

During my last days at MPI, Elke Muth slaved over the characterizations of many of the compounds. Her crucial support is deeply appreciated. Carsten Fülber generously donated his time during the course of his own doctoral work to create the PV-Wave plots found in Chapter 6. I thank Dr. Jeremy Titman for performing the C-13 solid state NMRs as well as Walter Scholdei and Dr. Wolfgang Meyer for helpful discussions and advice.

I would also like to thank Lorraine Williams for her tireless efforts in arranging all the paperwork associated with my travel and study overseas. If it were not for her and Dr. Fabio Zuluaga, Dr. Dennis Smith and Dr. Will Vaughan taking care of my University of Florida concerns, the trip to Germany would have been very difficult. Special thanks go to Will Vaughan for the  $^1\text{H}$ -NMR in Figure 2-4. Finally, I would like to thank Dr. James Konzelman, Dr. Jeffrey Linert and Professor James Deyrup for all their advice and encouragement over the last four years. I am particularly grateful to Jim Konzelman for his patient help with my first experiments and preparation for my seminars.

## TABLE OF CONTENTS

	<u>page</u>
ACKNOWLEDGEMENTS.....	iii
ABSTRACT.....	viii
CHAPTERS	
1 INTRODUCTION.....	1
Motivation .....	1
Preview .....	4
Background .....	5
[2+2] Photodimerizations of Styrylpyrylium Salts .....	5
Topochemistry .....	9
Beyond Cinnamic Acids .....	18
Appearance of the Product Phase: Homogeneous vs. Heterogeneous Mechanisms .....	28
Summary of Results Presented in this Dissertation.....	38
2 EXPERIMENTAL .....	41
Instrumentation and Analysis.....	41
General Information.....	41
X-ray Structure Analysis .....	41
Solid State C-13 Measurement .....	42
Crystal Preparation.....	42
Syntheses.....	45
Recrystallizations .....	50
Irradiation.....	53
Photodimer Single-Crystal Preparation .....	53
Micrographs .....	54
Kinetic Studies.....	55
Characterization .....	63
Elemental Analyses .....	64
Infrared Analyses.....	66
Mass Spectral Analyses .....	71
NMR Analyses.....	73

3	CRYSTALLINE-STATE PHOTODIMERIZATION OF A STYRYLPYRYLIUM TRIFLATE .....	84
	Introduction .....	84
	Topochemical Reactions: A Type of Phase Transition .....	85
	Homogeneous vs. Heterogeneous Product Formation .....	90
	Single-Crystal-to-Single-Crystal Topochemical Reactions: Phase "Transitions" Involving Dimensionally Similar Lattices .....	94
	Results .....	98
	Crystal Modifications of a Styrylpyrylium Triflate and its Photoproducts: The Overall Scheme .....	98
	[2+2] Photodimerization: The Forward Reaction .....	102
	Thermal Cycloreversion: The Backward Reaction .....	109
	Substitutional Mixed Crystals: What Happens "In-Between" .....	115
	Future Studies .....	125
4	CINNAMIC ACID: A REPRISE .....	127
	Introduction .....	127
	Results .....	128
	<i>t</i> -Butyl Amine Salt of <i>trans</i> -Cinnamic Acid .....	128
	$\alpha$ - <i>trans</i> -Cinnamic Acid .....	130
	Future Studies .....	140
5	STYRYLPYRYLIUM SALTS: VARIATIONS ON A THEME .....	141
	Introduction .....	141
	Crystal Packing .....	141
	Kinetic Investigations on [2+2] Photodimerizations .....	142
	Results .....	143
	Crystal Structures .....	143
	Kinetic Studies .....	157
	Thermal Cycloreversion of Photodimers .....	165
	A bis(Styrylpyrylium Triflate) .....	171
	Future Studies .....	172
6	THERMALLY REVERSIBLE HOLOGRAPHIC GRATINGS .....	174
	Introduction .....	174
	Background .....	174
	The Setup .....	178
	Theory .....	179
	Results .....	186
	Writing the Grating .....	186
	Energy of Activation for Cyclobutane Cleavage .....	187
	Energy of Activation for Photodimerization .....	193
	Future Studies .....	194

APPENDIX VISUALIZING PRODUCT PHASE EVOLUTION: THE DRAWINGS OF M. C. ESCHER.....	196
REFERENCES.....	198
BIOGRAPHICAL SKETCH .....	204

Abstract of Dissertation Presented to the Graduate School  
of the University of Florida in Partial Fulfillment of the  
Requirements for the Degree of Doctor of Philosophy

SINGLE-CRYSTAL-TO-SINGLE-CRYSTAL  
[2+2] PHOTODIMERIZATIONS  
THROUGH ABSORPTION-TAIL IRRADIATION

By

Kathleen Novak

December, 1993

Chairman: Kenneth B. Wagener  
Major Department: Chemistry

A method for controlling the mechanism of product phase evolution in topochemical reactions of photoactive molecular crystals is described that produces rare single-crystal-to-single-crystal transformations. In the case of the [2+2] photodimerizations of cinnamic acids and styrylpyrylium salts, a heterogeneous mechanism, typical of solid state photodimerizations, has been observed. In such cases, the photoproduct is obtained as a polycrystalline powder and a full x-ray structure analysis is not possible unless the product is recrystallized. However, a homogeneous mechanism is induced when these photodimerizable monomer crystals are irradiated with wavelengths in the long-wavelength tail of their electronic absorption spectra. This leads to the formation of single crystals of photoproduct. Thus full x-ray structure analyses may be done on the as-formed photoproduct and crystals of intermediate conversion.



Twenty-one crystal structures are reported in this dissertation: seven for the styrylpyrylium triflate, its photodimer, and solid solutions of both and five analogous structure analyses for the photodimerization of  $\alpha$ -trans-cinnamic monomer crystals. In both cases, the lattice evolves from the monomer to the product phase through a side-group swivel. The analyses on the solid solutions are the first such crystal structures reported on substitutional mixed crystals formed through a topochemical photodimerization.

The crystal modification obtained by homogeneously forming the photoproduct may or may not be different from that obtained through heterogeneous conversion, as determined by x-ray powder measurements. However, the recrystallized photoproduct for styrylpyrylium photodimerization is vastly different from its as-dimerized modification. The as-dimerized cyclobutane crystals thermally revert to single crystals of monomer in the first documented single-crystal-to-single-crystal topochemical back reaction.

Two kinetic studies were performed: one was on the heterogeneous photodimerization of an isomorphous series of styrylpyrylium salts, and the other involved writing a thick phase grating into a single crystal. The growth and thermal decay of the diffracted intensities provide data on the activation energies for the photodimerization and thermal cycloreversion. This is the first use of holography to study the kinetic behavior of a low molecular weight organic substance reacting in the crystalline state.

## CHAPTER 1 INTRODUCTION

### Motivation

The subject of this dissertation is single-crystal-to-single-crystal [2+2] photodimerization reactions in organic solid state chemistry. In a recent review on bimolecular photoreactions in crystals, Ramamurthy and Venkatesen write, "There is a clear lack of understanding of the mechanism of solid state reactions. Present knowledge exists only on the initial and final stages of the organic solid state reactions."<sup>1</sup> Until now, crystallographic investigations have been limited because photoreactive crystals typically disintegrate into polycrystalline powder during the reaction. This dissertation reports on investigations of a general method for obtaining single-crystal-to-single-crystal transformations of photoactive crystals and presents the first full x-ray structures of crystals at an intermediate stage of a solid state photodimerization.

The initial motivation for this study arose from the interest in developing systems applicable to thermally reversible crosslinking in polymers;<sup>2,3</sup> therefore, adduct forming reactions, were sought which produced the original edducts on heating. The thermally reversible solid state photodimerization<sup>4</sup> of (*E*)-2,6-Di-*tert*-butyl-4-[2-(4-methoxyphenyl)-ethenyl]pyrylium trifluoromethanesulfonate--hereafter referred to as the styrylpyrylium triflate, 1-1c--shown in Figure 1-1 and Figure 3-6, falls into this category and was chosen to be investigated. At that time, the photoreaction of this styrylpyrylium salt under typical irradiation conditions--that is, irradiation corresponding to wavelengths in the range of its absorption maximum--was known to proceed, as most [2+2] crystalline-state photoreactions, with disintegration of the crystal into a polycrystalline powder due to a heterogeneous mechanism of product phase evolution.

For example, it was known that the [2+2] photo-oligomerization of the diolefin distyrylpyrazine (DSP) occurs with disintegration of the reactant single crystals into a polycrystalline powder when those crystals were irradiated with wavelengths absorbed strongly by the DSP monomer.<sup>5-9</sup> However, it had also been proven by Braun<sup>6,7,10</sup> that intact single crystals of DSP oligomer could be obtained if the irradiation was effected with wavelengths corresponding to the long-wavelength tail of the monomer absorption.<sup>11,6,7,10</sup> While crystal disintegration was ascribed to heterogeneous evolution of the product phase within the crystal, homogeneous product formation was suggested as the origin of the single-crystal-to-crystal transformation. Thus the mechanism of phase transition could be controlled by proper choice of irradiation conditions.

The photodimerization of the styrylpyrylium triflate described in this dissertation was found to show the same behavior as DSP; that is, intact single crystals of photoproduct were obtained with tail-irradiation, even though crystal disintegration occurred otherwise. Only one other single-crystal-to-single-crystal [2+2] photodimerization had ever been demonstrated in the literature and no reversible single-crystal-to-single-crystal transformations had ever been found.<sup>12,13</sup> A recent reviewer of bimolecular photoreactions in crystals writes, "Reversible photodimerizations in crystals are expected to find wide application in molecular-scale devices. Successful application can be found only for systems that are truly single-crystal-single-crystal transformations."<sup>13</sup> Since single-crystal-to-single-crystal transformations in general are quite rare and of significant academic as well as technological interest, the work was redirected from the crosslinking to carry out the following investigations and to answer the following questions.

For the styrylpyrylium triflate, crystallographic analysis of the crystals of the monomer and as-dimerized dimer would verify that this reaction was topochemical and show how much the lattice changed during the reaction. Viewing the photodimerizing single crystals with an optical microscope would indicate whether phase boundaries did emerge or if the reaction was single-phase. If the reaction was single-phase, could single

crystals of partial conversion be obtained and what could be learned about the mechanism of the reaction from their analysis? For example, a recent challenge to Schmidt's Topochemical Principle,<sup>14,15</sup> the foundation of much of organic solid state chemistry, had appeared in the literature. What could be learned from this study to contribute to this debate? Though several single-crystal-to-single-crystal reactions in the literature existed,<sup>6,7,10,12,16-20</sup> no examples of a single-crystal-to-single-crystal back reaction had ever been demonstrated. The photodimerization of the styrylpyrylium triflate was known to be thermally reversible, and since single crystals of the photodimer were now obtainable, could single crystals of the thermally reversed monomer be achieved and how would they compare to the original monomer? Furthermore, how would the crystal structure of the recrystallized dimer compare to that of the as-dimerized dimer, and how would their thermal behavior compare? How would the photoproduct obtained heterogeneously compare to the product formed homogeneously?

To broaden the investigation to other styrylpyrylium salts, the synthesis of an isomorphous series of salts through counter-anion replacement was planned. If this piece of "crystal engineering" were possible,<sup>21-24</sup> how would the structures and reactivities of the members this series compare to one another? In addition to varying the counterion, would it be possible to link two styrylpyrylium salts with either a methylene bridge or through sharing an aromatic ring to create a photopolymerizable crystal that forms single crystals of polymer?<sup>9,25-37</sup>

Most importantly, how general is the method of tail-irradiation for inducing single-crystal-to-single-crystal reactions? Along these lines, it was planned to try to induce a single-crystal-to-single-crystal transformation for the quintessential organic solid state dimerization, that of a cinnamic acid derivative. Expecting that the single-crystal-to-single-crystal photodimerization of cinnamic acid itself would not be possible, the synthesis of a series of ammonium salts of several cinnamic acids was planned involving large

substituents on the nitrogen atom, with the idea of mimicking the styrylpyrylium salt photodimerization.

As originally suggested by Hesse and Hünig,<sup>4</sup> the thermally reversible photochromic behavior of the styrylpyrylium triflate, 1-1c, might be applicable to reversible information storage. A few examples of holographic recording systems based on creating a spatial variation of the refractive index (a phase grating) within single crystals of photochromic materials through photodimerization reactions exist in the literature.<sup>38-41</sup> These systems have been shown to be photochemically reversible but suffered eventually from the typical crystal deterioration, as described above for DSP. Would it be possible to write a holographic grating into a single crystal of a styrylpyrylium salt? If so, could this grating be thermally erased and rewritten? What kinetic information about the photodimerization and thermal cycloreversion could be extracted from holography?<sup>32,42,43</sup>

### Preview

Descriptions of the investigations and inquiries posed in the preceding four paragraphs are fully addressed in chapters 3, 4, 5 and 6, respectively, and summarized at the end of this chapter. Besides outlining the initial work done on the photodimerization of styrylpyrylium salts, the purpose of the balance of this chapter is to introduce certain aspects of organic solid state chemistry through a brief review of the literature most pertinent to issues discussed in this dissertation, primarily the evolution of the product phase in topochemical reactions.

The Background section is divided into two parts. First, a synopsis is given of the original work on the solid state photodimerization of styrylpyrylium salts that initiated the work reported in this dissertation. In the second part, topochemistry is distinguished from other types of organic solid state reactions. An outline of Schmidt's work on cinnamic acids is presented as it pertains to the foundation of topochemistry, Schmidt's topochemical principle, and some post-Schmidt conceptual refinements to the topochemical

principle are introduced. Specifically, the concepts “reaction cavity” and homogeneous vs. heterogeneous mechanisms of product phase formation are introduced to explain single-crystal-to-single-crystal transformations. Finally, a survey of selected examples of organic solid state reactions is presented to compare and contrast various mechanisms of product phase formation thus far reported in the literature. Separate introductions to chapters 3, 5 and 6 contain further background information from the literature specific to those chapters.

The field of organic solid state chemistry is widely acknowledged to be a largely underdeveloped but rapidly growing science. Sophisticated and elegant investigations of a number of fascinating issues, related to the topics of this dissertation but not having a direct bearing, have been reported in the literature. Some of the most often-cited of these reports and collections of papers have been summarized in the section The literature of topochemistry (see p. 20).

## Background

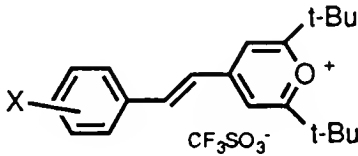
### [2+2] Photodimerizations of Styrylpyrylium Salts

The synthesis of a series of nineteen  $\alpha$ -styrylpyrylium salts has been reported, and their photochemistry in the solid state and in solution, as well as the thermal behavior of their photoproducts, has been explored by Hünig and Hesse.<sup>4</sup> This section of the introduction to this dissertation briefly reviews their results. A summary is shown in Table 1-1. The solid state photoactivity was tested by irradiating KBr pellets of each of the salts. The preparative irradiations were done in hexane suspensions with wavelengths strongly absorbed by the salts and thus no single-crystal-to-single-crystal transformations were observed. The styrylpyrylium salts that are photoactive in the solid state were shown to dimerize to form cyclobutane rings as illustrated in Figure 1-1.

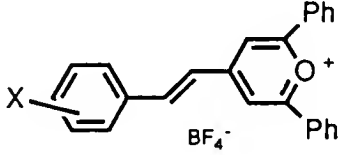
Table 1-1. Previous work on the solid state photoactivity of some styrylpyrylium salts and the solid state thermal behavior of their photodimers.<sup>4</sup>

salt	substituent, X	photoactivity	dimer	thermal behavior of dimer
1-1	a 4-NMe <sub>2</sub>	no	---	---
	b 3,4,5-(OMe) <sub>3</sub>	99%	1-4b	100% cycloreversion
	c 4-OMe	99%	1-4c	100% cycloreversion
	d 4-Me	100%	1-4d	100% cycloreversion
	e 4-Cl	100%	1-4e	modification/melting
	f 4-H	100%		melting
	g 4-CF <sub>3</sub>	no	---	---
	h 4-NO <sub>2</sub>	99%		melting
	i 4-CN	99%	1-4i	modification/melting

1-2	a 4-NMe <sub>2</sub>	no	
	c 4-OMe	no	
	d 4-Me	no	
	f 4-H	86%	
	h 4-NO <sub>2</sub>	no	
	i 4-CN	no	

1-3	c 4-OMe	no	
	d 4-Me	71%	
	f 4-H	53 %	
	i 4-CN	no	

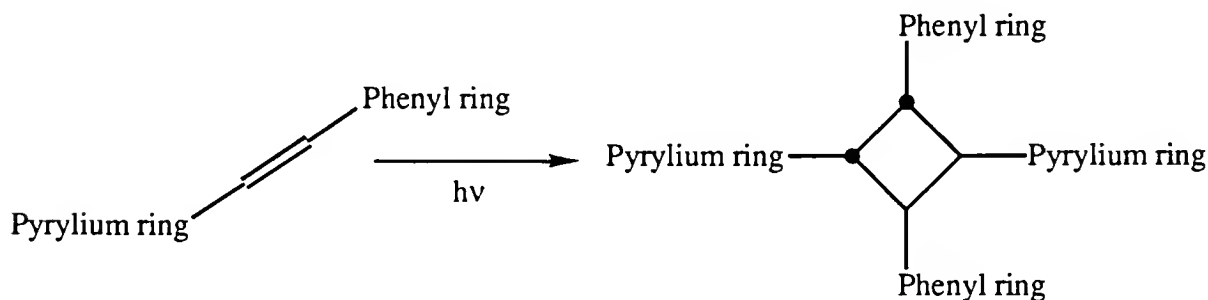


Figure 1-1. The [2+2] photodimerization of the styrylpyrylium salts in Table 1-1 occur to give head-to-tail (htt) dimers with an *r-ctt* (reference-cis,trans,trans) configuration. See reference 44 for more details on the IUPAC rules for specifying the stereochemistry of rings.

The preparative irradiations gave the yields indicated in Table 1-1. For 1-3d and 1-3f, edge filters ( $\lambda > 390$  nm) were used to inhibit excitation of the product cyclobutane back to monomer, but this did not improve the yield. This resulted in the conclusion that the change in lattice parameters, that is, the lattice contraction, during the dimerization is so severe that the unreacted molecules are shifted to unreactive orientations and distances. The photostability of 1-1a was suggested to be due to an unreactive crystal structure or the strong delocalization of  $\pi$ -electrons in the exocyclic double bond. Through IR and NMR analyses, the structure and E-configuration of the double bond in each of the salts was verified. The stereochemical configuration of all the photodimers reported in this paper were determined to be of the type [*r-ctt* htt],<sup>44</sup> see Figure 1-1, by <sup>1</sup>H-NMR analysis of the cyclobutane proton signals in o-chlorophenol.

The compounds in series 1-1 form strongly fluorescent solutions in acetic acid (series 1-2 and 1-3 are insoluble). Compounds 1-1c and 1-1d photodimerize in this solution to form only the cyclobutane isomer obtained from irradiation in their crystalline state, [*r-ctt* htt dimer].<sup>44</sup> The other possible dimers, [*r-tct* htt], [*r-ctt* hth], and [*r-tct* hth], that would be expected from the reaction of an excited trans monomer with a ground state trans monomer, were not isolated, which indicates a pre-orientation of reacting partners in solution. Concerning the solution photodimerization of 1-1c, it is stated, "Nach einiger Zeit fallen orangefarbene Kristalle aus . . . (64%) orangefarbene monokline Kristalle, Schmp. 185 - 190°C, laut <sup>1</sup>H-NMR [1-1c:dimer] (19:1)."<sup>44</sup> It is unclear whether these mixed crystals obtained from solution irradiation are of the same crystal modification as the dimer formed from solid state irradiation or a second form, characteristic of the recrystallized dimer. The latter is most likely the case, meaning the crystals were, based on the results reported in this dissertation, not monoclinic, rather orthorhombic. Only in the case of 1-1h was cis-trans isomerization observed when an acetic acid solution of the salt was irradiated. However, it should be noted that an excited cis monomer reacting with a



ground state cis monomer would also give the [*r-ctt* htt dimer] found in the cases of 1-1c and 1-1d above.

The thermal behavior of the monomers and photodimers were analyzed by differential scanning calorimetry (DSC). The only photodimers that undergo 100% cycloreversion are 1-4b-d, summarized in Part I of Table 1-2. Because these systems involve a shift to shorter wavelengths in the absorption spectrum of the photoproduct, they are called inverse photochromic systems. Since they are thermally reversible, they may be called thermochromic as well. Hünig and Hesse<sup>4</sup> suggested these systems might have uses involving thermal information storage and erasure through irradiation. The large differences in  $\lambda_{\text{max}}$  between the monomer and photodimer, 173 - 128 nm, was pointed out as a favorable asset. The monomers 1-1b and 1-1d also undergo thermal modifications that are reversible, as are the melting transitions. The photoactivity of the modified monomers 1-4b' and 1-4d' was not reported. However, the interconversion of 1-1c and 1-4c was cycled several times without noticeable side reaction. It is interesting to note that the monomers 1-3c (photostable) and 1-3d (photoactive) also undergo modifications on heating; however, they are irreversible transitions and such that 1-3d, at 176°C, is rendered photostable. It was not reported if the photostability of 1-3c changes on heating. Of the rest of the photodimers investigated, 1-4f and 1-4h simply melt on heating while 1-4e and 1-4i melt then recrystallize, as shown in Part II of Table 1-2. For 1-4e, it was determined by <sup>1</sup>H-NMR that at 170°C the cyclobutane had epimerized to a less strained isomer, for example, the lower energy *r-tct* isomer.

The thermal stability of the 1-4c was tested in solution with the following results: in o-chlorophenol and T=155°C, in 220 minutes, 78% of 1-4c had cycloreverted to 1-1c. It was concluded that the crystal packing was vital for a fast back reaction at a defined temperature and since both donar substituents and polar solvents favored the cycloreversion, a zwitterionic intermediate was indicated.

Table 1-2. Thermal behavior of styrylpyrylium salts and photodimers reported by Hünig and Hesse.<sup>4</sup>

---

Part I. Photodimers undergoing cycloreversion reactions back to monomer.

photodimer	monomer	modification of monomer	monomer melting
1-4b--->	1-1b(148°C)	---> modification 1-1b'(164°C)	---> 1-1b' melts (245°C)
1-4c--->	1-1c(101°C)		---> 1-1c melts (209°C)
1-4d--->	1-1d(180°C)	--->[modification 1-1d'(171°C)]	---> 1-1d' melts (211°C)

---

Part II. Photodimers that recrystallize in a different modification after melting.

photodimer	first melting	modification of photodimer	second melting
1-4e--->	melts(157°C)--->	crystallizes 1-4e'(165°C)--->	1-4e' melts (219°C)
1-4i--->	melts(167°C)--->	crystallizes 1-4i'(183°C)--->	1-4i' melts (240°C)

---

## Topochemistry

### Topochemical vs. nontopochemical processes

The photodimerizations described above fall into the broad class of organic solid state reactions known as topochemical reactions. G.M.J. Schmidt began his seminal work on the photodimerization of cinnamic acids,<sup>45</sup> which laid the foundation for the topochemical principle in organic solid state chemistry, in this way:

The analysis of the mechanism of solid state reactions has for some time now centered around the study of lattice imperfections . . . This focus on lattice irregularities has tended to ignore the major feature of the crystalline state, namely three-dimensional regularity and its effect on reaction mechanism, rate, and products. The work in progress here is intended to analyse the role of lattice geometry and thereby to extend our understanding of solid state chemistry.

This passage suggests two broad categories of reactions: those whose progress and outcome are controlled by the three-dimensional regularity of the lattice of the reacting phase, that is, topochemical reactions, and those that are not controlled by the lattice, but rather trace their origin and/or propagation to disorder in the lattice, that is,

nontopochemical reactions. Since topochemical reactions are solid state reactions controlled by the lattice geometry of the reacting species, if a reaction begins or continues in a region of the crystal where the parent lattice is nonexistent, the reaction is said to proceed nontopochemically. The parent lattice may become disordered by propagation of defects in the crystal, which can be due to several causes, including by a reaction in the ordered lattice or reaction at an incipient defect. Nucleation of the product phase within the crystal may occur preferentially at defects in the parent lattice or may itself initiate disordering. Whenever local melting occurs due to product “impurity” in the reactant lattice, the reaction is no longer topochemical.

One type of crystal defect is a line defect or dislocation and may be caused by an accumulation of vacancies within the lattice.<sup>46</sup> The enhanced reactivity of solids at dislocations has been attributed to a number of factors including the following. Dislocations can act as energy traps. Furthermore, the relative stereochemical orientation of neighboring molecules as well as the conformational freedom of molecules at a defect is different compared to the regular lattice. Also, heterogeneous nucleation is easier “because the stresses and strains set up during nucleation can be ameliorated more readily at a dislocation.”<sup>46</sup>

Schmidt described a process that may cause a defect within an ordered lattice, beginning with a polymerizable monomer stack of molecules A-D regularly spaced:<sup>47</sup>

Suppose that, on absorption of the activating radiation, the reactive monomer  $A^*$  . . . reacts with its neighbor B to form the reactive dimer  $AB^*$ . The covalent link formed between A and B pulls these two monomer units together and, in so doing, increases the separation between B and its other neighbor C. If this separation is still not too great to permit further reaction, formation of the the trimer  $ABC^*$  will open a still wider gap between C and D, so that eventually the orderly propagation of the polymer chain along the stack will be arrested.

This explains why some topochemical reactions never reach quantitative conversion, for example, 1-2f, 1-3d and 1-3f in Table 1-1. In other words, as yet unreacted partners are pulled out of their reactive conformation by distortion of the lattice

from previous reactions. Reaction may cease at this point or the nontopochemical process may proceed in the disrupted crystal structure. For example, disordered reactant around the defect may continue to react by random translational movement to the center of reactivity. As Wegner describes it, "In many cases reaction proceeds by diffusion of the reactants to centers of reactivity or by nucleation of the new phase at certain centers of disorder and, therefore, increased mobility under complete destruction of the parent crystal."<sup>11</sup>

One phenomenon in solid state reactions is nucleation of the product phase at an interface with the parent lattice where there is a coherent phase boundary. This may lead to oriented growth of the product such that the product lattice and reactant lattice are related by certain crystallographic equivalencies. One may contrast this with the idea that a daughter crystal growing from a parent crystal, forms as it would from the melt and that no special orientation exists. If the reaction proceeds through the bulk of the reactant, this type of reaction is said to be topotactic. For example, in crystals of the cyclic monomer trioxane, the molecules are aligned  $4.3\text{\AA}$  apart along a certain crystallographic axis. The ring-opening polymerization occurs to form crystalline polyoxymethylene with the chains aligned along the direction of that same monomer axis in the original crystal.<sup>47</sup> This reaction, once thought to be topochemical, has been shown to be nontopochemical.<sup>48</sup>

#### The photodimerization of 9-cyanoanthracene

The product for this photodimerization is not predicted by applying the topochemical principle to the geometry of the regular crystal lattice, but it may be explained by considering the geometry of well-defined defect sites within the crystal "where the structure of the reaction product is predefined by the arrangement of the molecules around the particular defect."<sup>11</sup> As Thomas puts it, "[Defects] could, on topochemical grounds, favour the 'wrong' product."<sup>46</sup> The "wrong" product here refers to a non-topochemical product. 9-Cyanoanthracene packs in a  $\beta$ -type structure with highly overlapping stacks and an interplanar distance of  $3.5\text{\AA}$ . The  $\beta$  packing--that is, a mirror symmetry relates the

closest monomers in a stack--should give head-to-*head* dimers, but head-to-*tail* dimers are formed instead. By examining pairs of cleaved crystal surfaces, one of which had been etched and one of which had been photodimerized, Thomas and coworkers were able to correlate stacking faults in the crystal with centers of dimerization.<sup>49</sup> The photodimerization of 9-cyanoanthracene was shown to occur preferentially at these defects in the anthracene crystal. The relative orientation of the monomers at these faults could then be related to the stereochemistry of the anthracene dimer as shown in Figure 1-2.

However, it has been noted that it may not be the specific geometry that causes the dimerization reaction to center at the dislocations. In correlating the etch pit surface with the irradiated surface, the latter surface was examined for certain textures associated with the 20% increase in crystal volume associated with the dimerization.<sup>46</sup> Thus it may be that these defects serve only to facilitate the crystallization of the photoproduct. Then how may the head-to-*tail* dimer form? Later studies revealed the existence of a stress-induced metastable phase within the regular parent lattice with a shorter head-to-*head* distance than in the parent lattice.<sup>50</sup> Other anthracenes also show such nontopochemical behavior.<sup>51,52</sup>

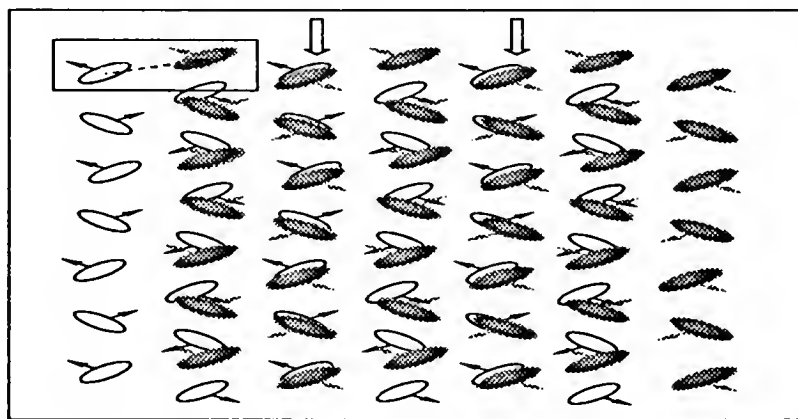


Figure 1-2.<sup>46,49</sup> This figure shows how head-to-*tail* anthracene photodimers might form near a lattice defect. The closed arrows indicate the orientation of the substituent in the 9-position on the anthracene. In the regular parent lattice the dimers would be oriented so that nearest neighbors would have the substituents pointing in the same direction. But here, one layer of anthracene molecules has slid relative to the parent lattice as indicated by the dashed arrow. The open arrows indicate the stacks that would produce the photodimers with substituents on opposite sides.

The concept of defect-controlled reactions is important when considering the final outcome of phase transformations in organic solid state reactions, since phase transformations, such as nucleation or recrystallization, are often initiated by crystal texture.

#### Schmidt's topochemical principle

Lattice control. As described above, organic solid state reactions can be broadly classified as topochemical or nontopochemical. The purpose of the preceding paragraphs was to provide contrasting examples for the type of chemistry described in the balance of this section, that is, topochemistry, in order to better illustrate this concept. In topochemical reactions the chemical transformation is directed by the parent lattice throughout the transformation. Thus there is a direct transition from the reactant to product "without destruction of the crystal lattice and without formation of non-crystalline intermediates."<sup>11</sup> Whereas in nontopochemical reactions there is random diffusion of molecules to a center of reactivity, in the ideal topochemical reactions, the center of mass of each molecule is stationary; therefore the molecules do not lose their location in the lattice. For example, in the cases of topochemical polymerizations, the molecules are often pictured as swiveling *on their lattice positions* to come within bonding distance of one another. This notion was first described by Hirshfeld and Schmidt<sup>47</sup> and first realized in the laboratories of Wegner and coworkers for the polymerization of diacetylenes.<sup>16</sup>

This lattice-point swivel motion is shown in Figure 1-3a, a schematic illustration of the polymerization of diacetylenes. However, this type of motion also applies to the polymerization of distyrylpyrazine as shown in Figure 1-3b. The two remaining olefins in the dimer pictured in the central stack of Figure 1-3b are now closer to their reacting partners than they were in the unreacted monomer stack. Also, in dimerization reactions, the molecule is seen to pucker. That is, the center moves in one direction while the edges move in the opposite direction, and thus the center of mass is kept constant. Figure 1-3b demonstrates how this is the case for [2+2] photopolymerizations as well.

Though the concept had been previously described, the first systematic investigations that offered evidence of topochemical reactions in molecular crystals were conducted by G.M.J. Schmidt and coworkers at the Weizmann Institute in Israel. These investigations were reported in the *Journal of the Chemical Society* in a seminal series<sup>53,45,54</sup> that has since been republished in part with a selection of subsequent reports and review articles by Schmidt and his collaborators.<sup>55</sup> Jack Dunitz writes in a retrospective on Schmidt's contributions to science,<sup>56</sup> that up until the early 1960s, x-ray crystallography had been used primarily to determine molecular geometry, for example, interatomic distances and angles, or characteristic separations between nonbonded atoms. But for most organic chemists, "a molecule in a crystal was a dead molecule" and organic solid state reactions were largely regarded as a nuisance. Schmidt's genius was the "synthesis of crystallography and chemistry."<sup>56</sup> He looked beyond the individual molecule to the way in which molecules approached one another in the crystal. He shifted the focus from molecular geometry to molecular *packing*. Once the correlation between crystal structure and solid state reactivity had been made, "Everything fell into place; order had been created out of chaos."<sup>56</sup>

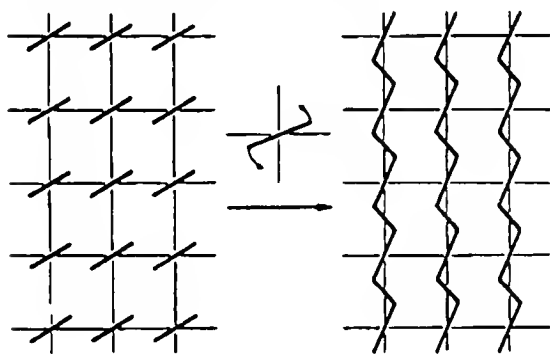


Figure 1-3a.

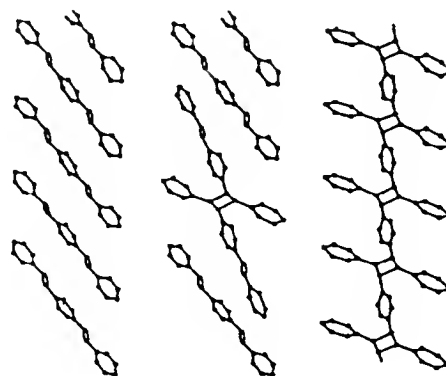


Figure 1-3b.

Figure 1-3. Topochemical polymerization: stacks of difunctional monomers may react in a regularly ordered crystal lattice, without the aid of defects, by rotating on their lattice rotates. The rotation of one molecule brings its reactive ends into contact with two others and so on in a zipper-like mechanism.

- a) schematic diagram of diacetylene chain polymerization<sup>57</sup>
- b) illustration of [2+2] step polymerization of DSP<sup>37</sup>

Cinnamic-acid investigations of G.M.J. Schmidt. The subject of Schmidt's most heralded studies is the [2+2] photodimerizations of cinnamic acids and was initiated by a dispute in the literature. In 1964, trans-cinnamic acid had been long known as dimorphic; that is, it could exist in two types of crystalline forms,  $\alpha$  and  $\beta$ , and that the  $\alpha$  form gave truxillic acid, the head-to-tail dimer. The argument centered over the stereochemistry of the cyclobutane dimer formed from the  $\beta$  modification of trans-cinnamic acid which seemed to give mixtures of both truxillic and truxinic acid, the head-to-head dimer.

In the first part of the series,<sup>45</sup> Schmidt and Cohen state the thesis and three related tenets supported by the studies reported in the following parts of the work and other examples from the literature. This thesis, known as Schmidt's topochemical principle, states that "*reaction in the solid state occurs with a minimum amount of atomic or molecular movement.*" The tenets are:<sup>45</sup>

(1) chemically closely-related compounds show significant differences in chemical behaviour in the solid state; (2) a given compound reacts differently in the solid and dispersed phases; (3) polymorphic modifications of a given compound show significant differences in chemical behaviour.

Tenets (1) and (3) have found expression in the research reported in this dissertation: (1) in chapter 4 in comparison of the photoactivities of various counteranion-substituted styrylpyrylium salts and (3) in chapter 3 in comparison of the thermal behavior of recrystallized vs. as-dimerized styrylpyrylium triflate photodimer, 1-4c.

In the second part of the series,<sup>54</sup> Schmidt and coworkers resolve the controversy surrounding the photochemistry of the  $\beta$  form of cinnamic acid by showing that there is a phase transition from the  $\beta$  to the  $\alpha$  around room temperature and that when the  $\beta$  modification is irradiated at temperatures that exclude this transition, truxinic acid is formed exclusively. Otherwise, irradiation of the  $\beta$  form gives a mixture of photodimers, the truxillic acid arising from the  $\alpha$  modification. These transformations are outlined in Figure 1-4. (Almost 30 years later, the kinetics<sup>58,59</sup> and mechanism of the  $\beta$  to  $\alpha$



transformation in trans-cinnamic acid continues to be investigated and has been shown to be topotactic.<sup>60</sup>) In the second part of Schmidt's classic work, the preparation of crystal modifications of thirty-six substituted cinnamic acids is also reported and their photoproducts, if any, identified.

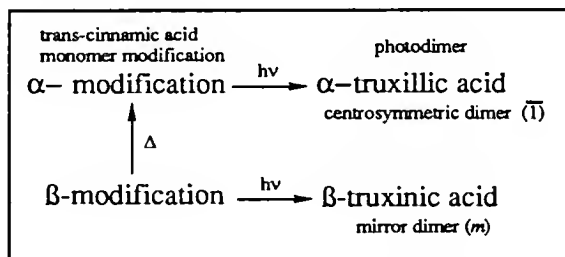


Figure 1-4. Crystalline modifications of trans-cinnamic acid and the photoproducts arising from each. Note that these two forms may be distinguished visually, the  $\alpha$  modification being in the form of squarish platelets and the  $\beta$  modification being in a longer, narrower lath shape.

The irradiation of each of the acids either produced only truxillic and/or truxinic-type photodimers, or the crystal was photostable. Detailed experimental data and references are given for the preparation and irradiation of the cinnamic acids with the “plea that workers in solid state chemistry specify in sufficient detail the reacting crystalline phase . . .”<sup>45</sup> Once the identity and exclusivity of the photoproducts of dimerization had been decisively established, Schmidt, in the third and culminating part of the series,<sup>53</sup> related the *molecular* symmetry of the photoproducts with the *crystallographic* symmetry of the reacting monomers. Crystallographic data on twenty-eight cinnamic acids are presented in this part of the series.<sup>54</sup> Analysis of their cell parameters compared with crystal structures of five selected compounds revealed that among all the acids investigated, three types of crystal modifications exist,  $\alpha$ ,  $\beta$  and  $\gamma$ , and that six of the acids are dimorphic and one occurs in all three modifications. The five crystal structures presented are one  $\beta$  type, p-chloro-trans-cinnamic acid; two  $\gamma$  types,  $\alpha$ -bromo-trans-cinnamic acid and m-chloro-trans-cinnamic acid; and two  $\alpha$  types,  $\alpha$ -trans-cinnamic acid and trans-

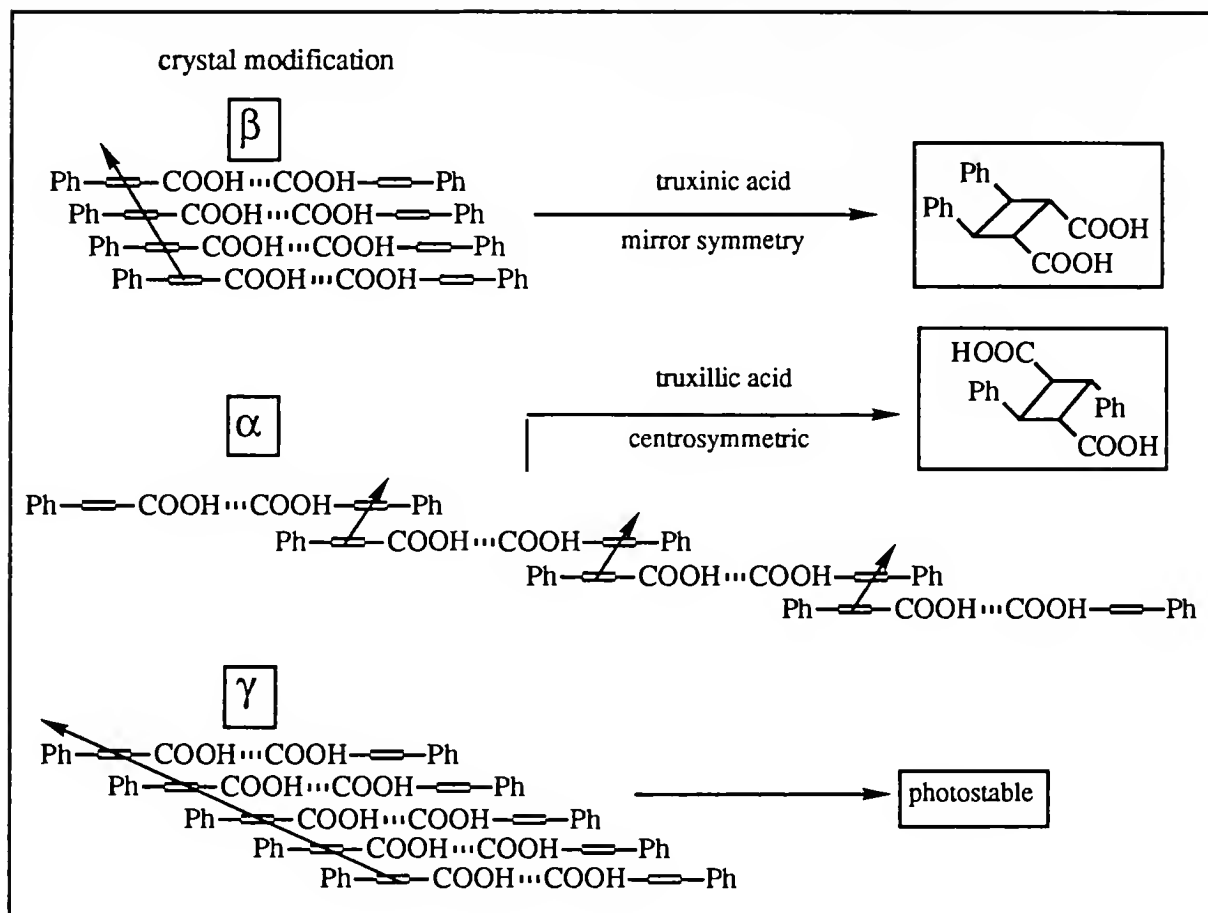


Figure 1-5. The crystal modifications of cinnamic acids have been identified with their lattice symmetries and in turn with the stereochemical identity of their photoproducts or with their photostability.<sup>61</sup>

cinnamide. Figure 1-5 shows that each type is built from a unit of two monomers, hydrogen-bonded to one another and approximately in the same plane. These units form parallel stacks that bring monomers within certain distances and relative orientations to one another. In the  $\beta$  form the monomers in a stack are highly overlapped compared to the other two modifications and the distance between reactive centers, which are related by mirror symmetry, is approximately 4Å. In the  $\gamma$  form, the decreased overlap within the stack results in a distance between nearest double bond contacts of 5Å. In the  $\alpha$  form, the overlap offset is so great, that the closest monomer pairs in a reactive orientation are not in the same stack, but in neighboring stacks. Thus, while neighbors within a stack are related

by mirror symmetry and are over 5.5Å apart, the reacting pairs are only 4Å apart and are related to one another by a center of symmetry.

Thus it is easily seen that in the  $\beta$  lattice, the most easily formed dimer--the dimer formed with the least atomic or molecular motion--is the head-to-*head* dimer. However, in the  $\alpha$  lattice the head-to-*tail* dimer is the dimer formed with the least lattice disturbance. In all twenty-eight cases investigated by Schmidt, the lattice symmetry matched the stereochemistry of the products or predicted the photostability of the lattice in the cases where the  $\gamma$  modification occurred.

Schmidt went on to investigate the photoreactions of heterocyclic analogs of cinnamic acid,<sup>62-65</sup> providing examples of the first tenet of the topochemical principle: that chemically closely related compounds could show significantly different behavior in the solid state. Thus, the lattice controls not only the reactivity of the compound stereochemistry of any products, but in some cases, even the reaction *type*. For the first time, it was demonstrated that the same crystalline phase could house two competing reactions, in this case, dimerization and polymerization:

thienyl acrylic acid	$\beta$ -----> dimer
	$\gamma$ -----> oligomer (ring participation)
furylacrylic acid	$\beta$ -----> dimer + oligomer (ring participation)

Spectroscopic evidence from the product oligomers indicate that the heteroaromatic rings participate.

### Beyond Cinnamic Acids

Schmidt's first work on the [2+2] photodimerization of cinnamic acids described above allowed topochemical reactions to be identified as a class of organic solid state reactions. Since then numerous other solid state reactions, both thermal and

photochemical, including unimolecular, bimolecular and polymeric, have also been shown to be topochemical.<sup>9,16,66</sup> The study of these has led to refinements of the original principle and a deeper understanding of the mechanisms involved in topochemical processes. Though there are many examples of thermally initiated solid state reactions in crystals, most notably the thermal polymerization of diacetylenes and the thermochromism of various classes of chromophores, it should be noted that photochemical transformations dominate investigations into topochemical processes. Scores of examples of [2+2] photodimerizations and polymerizations exist in the literature,<sup>66,13</sup> and the most deeply investigated solid state reaction is the  $\gamma$ -radiation induced polymerization of diacetylenes.

Other chromophores investigated by Schmidt include butadiene and hexatriene derivatives,<sup>67</sup> p-quinones, chalcones,<sup>68-70</sup> and the eight-center photodimerization of a 3-keto-1,4-pentadiene derivatives.<sup>71</sup> Schmidt and collaborators went on to investigate cis-trans isomerization<sup>64</sup> and photochromism in the solid state.<sup>72,64</sup>

Reviewing solid state organic photochemistry, Schmidt outlined its progress as having begun with the "phase of the topochemical principle," which was being followed by the "phase of the locus of the reaction".<sup>73</sup> On a microscopic scale, the locus refers to the conformation of the photoreactants as it relates to the structure of the rigid matrix surrounding them, that is, the "reaction cavity." On a macroscopic scale, the question of the reaction locus involves the issues of crystal texture, for example, dislocations and phase boundaries, on the outcome of the solid state reaction, as well as energy transfer within a crystal. Thus the question, is the reaction defect-controlled or does it proceed in the bulk of the crystal?

Schmidt called the third phase the "phase of crystal engineering."<sup>73</sup> Along these lines investigations into the photochemistry of solid solutions of photoactive species were initiated.<sup>74,75</sup> The first asymmetric syntheses through lattice-controlled reactions in chiral crystals were also demonstrated.<sup>76-78</sup> Also, "steering groups" have been investigated in efforts to develop ways to control crystal packing, an intensely sought and highly prized

goal of solid state chemists. A text on various aspects of crystal engineering has recently been published.<sup>79</sup> Under the category of crystal engineering, one might include host-guest topochemistry occurring in channel inclusion complexes such as the deoxycholid acid example in Table 3-1, or matrix polymerization also represented in Table 3-1 with the butadiene polymerization in the layered perovskite structure.

### The literature of topochemistry

Most of the references cited above have been gathered into a collection of selected papers by Schmidt and his collaborators, *Solid State Photochemistry*,<sup>55</sup> that explores the relationship between the geometrical properties of lattices of molecular crystals and the photochemistry of those molecules. Besides reports of original research, it contains four review articles, one on solid state polymerization,<sup>47</sup> one on asymmetric synthesis<sup>78</sup> and two general reviews on solid state photochemistry,<sup>64</sup> one focusing on dimerizations.<sup>73</sup>

Two other collections of papers centered involving the topic of solid state photochemistry have also recently been produced: *Photochemistry in Organized and Constrained Media*<sup>80</sup> and *Organic Solid State Chemistry*.<sup>81</sup> Pertinent to this work, the first reference contains a review article on bimolecular photoreactions in crystals,<sup>13</sup> a reprise of a larger review article encompassing both unimolecular and bimolecular photochemical reactions of organic crystals.<sup>66</sup> Besides covering some of the prominent fields of research in topochemistry (such as the photodimerization of benzylidenecyclopentanones, intramolecular hydrogen abstraction in the solid state, “four-center” photopolymerization of distyrylpyrazine, and host-guest topochemistry), the latter reference emphasizes the interdisciplinary nature of organic solid state chemistry by including articles in the areas of theoretical chemistry and solid state physics. Many short overviews of organic solid state chemistry exist in texts devoted to solid state chemistry or to photochemistry, but a short, comprehensive introduction to organic solid state chemistry is a review article by M. D. Cohen and Bernhard S. Green,<sup>61</sup> collaborators of Schmidt. The first single-crystal-to-single-crystal transformation of an organic substance reported in the literature is the

polymerization of a diacetylene,<sup>16,82</sup> which contributed much to the understanding of product phase evolution in the solid state. Thus introductions to various issues involving the mechanisms of solid state polymerizations by Gerhard Wegner are important to mention here.<sup>6,7,11,48,57,83</sup> Topochemical polymerizations are dominated by the two examples in Figure 1-3: diacetylene photopolymerization<sup>84</sup> and “four-center” photopolymerizations. Hasegawa, the principal investigator of the latter type, has written several reviews.<sup>9,34,36,37</sup> Phonon spectroscopy has been used as a tool to investigate the mechanism of product phase evolution in organic solid state reactions, most notably the controversial DSP “four-center” reaction. A review by Prasad of investigations using this technique may be found in *Organic Solid State Chemistry*, mentioned above.<sup>8</sup> Polymerizations of unsaturated compounds by photocycloaddition reactions, primarily [2+2] reactions, have been extensively reviewed by Dilling.<sup>35</sup>

In general, very few thorough kinetic studies exist for reactions in the solid state, with the exception of diacetylene polymerization, easily the most well-investigated of organic solid state reactions. Here Baughman has advanced a model that is based on the idea that the kinetics of homogeneously polymerizing crystals (single phase) is dependent on the strain induced within the crystal due to polymer-monomer lattice mismatch.<sup>85</sup> In the case of [2+2] photodimerizations, Hasegawa has proposed a reaction model for the photoreaction of olefin crystals based on the temperature-dependent deviation of the two olefin bonds from the optimal positions for the reaction.<sup>86</sup> The only other method applied to the kinetics of topochemical reactions in the literature is that refined by Hancock, Sharp and Brindley for heterogeneous processes in barium and magnesium salts.<sup>87,88</sup> Heyes has used this method to explain the time vs. conversion curves of the [2+2] photodimerizations of cinnamic acid, its o-methoxy derivative, the intramolecular [2+2] reactions of a benzoquinone and cyclopentadiene adduct, the solid state racemization of a coboxalime complex and the  $\beta$  to  $\alpha$  phase transition of cinnamic acid.<sup>59</sup> In this method, slopes from  $\ln(\ln(1-\text{conversion}))$  vs.  $\ln(\text{time})$  are used to identify reaction mechanisms such as

diffusion-control, nucleation and growth and phase-boundary control. Time vs. conversion curves have been reported for the [2+2] photodimerization of azastilbenes and coumarins.<sup>23,89</sup> Quantum yield studies<sup>90</sup> and a multiplicity study<sup>91</sup> have been reported for a few solid state intramolecular photoreactions.

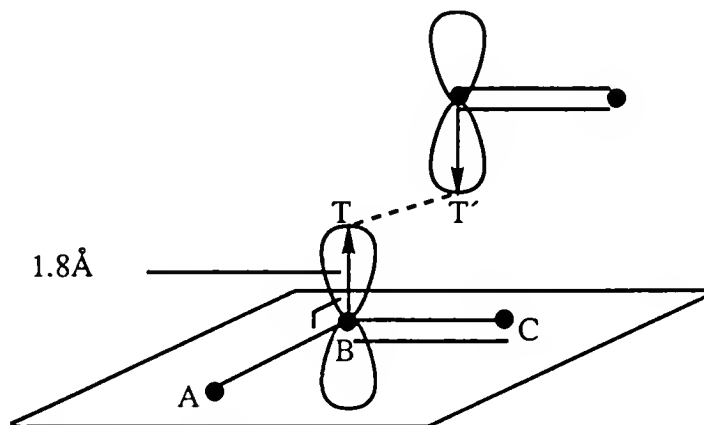


Figure 1-6. The orbital overlap is defined as the distance T-T', which is the distance between points 1.8 Å, the van der Waals radius of carbon, along an axis passing through the carbon atom, normal to the double bond plane.<sup>92</sup>

### Geometric models

Since Schmidt's original formulation of the topochemical principle, hundreds of examples of topochemical reactions have been investigated. Certain molecular crystals expected to be reactive on the basis of their lattice geometry are not reactive, while many expected to be stable are, in fact, reactive. These investigations have led to additional efforts to explain the photoreactivity and selectivity of organic solid state reactions. An informal rule for [2+2] photodimerizations is that the species must be within 4.2 Å for a reaction to be possible. Kearsley refines this parameter by suggesting a measure of the orbital overlap between reacting orbitals as the distances between the apices of the reacting atomic orbital lobes of carbon as shown in Figure 1-6.<sup>92</sup> The overlap, SUM, is defined as the sum of these two distances for a pair of double bonds and, along with the lateral displacement of the double bonds, is calculated for almost 70 various photoactive and photostable crystals. Kearsley also presents projections of carbon p-orbital contours

(based on electron density of H atomic orbitals) for nine compounds, an example of which is shown in Figure 1-7 for benzyl benzylidenecyclopentanone (BBCP) and a naphthalenone derivative (NAPTH). It is clear why the BBCP is photoreactive but it was left to the development of the concept of the "reaction cavity" by Cohen, described below, to explain the photostability of NAPTH (see Table 1-3).

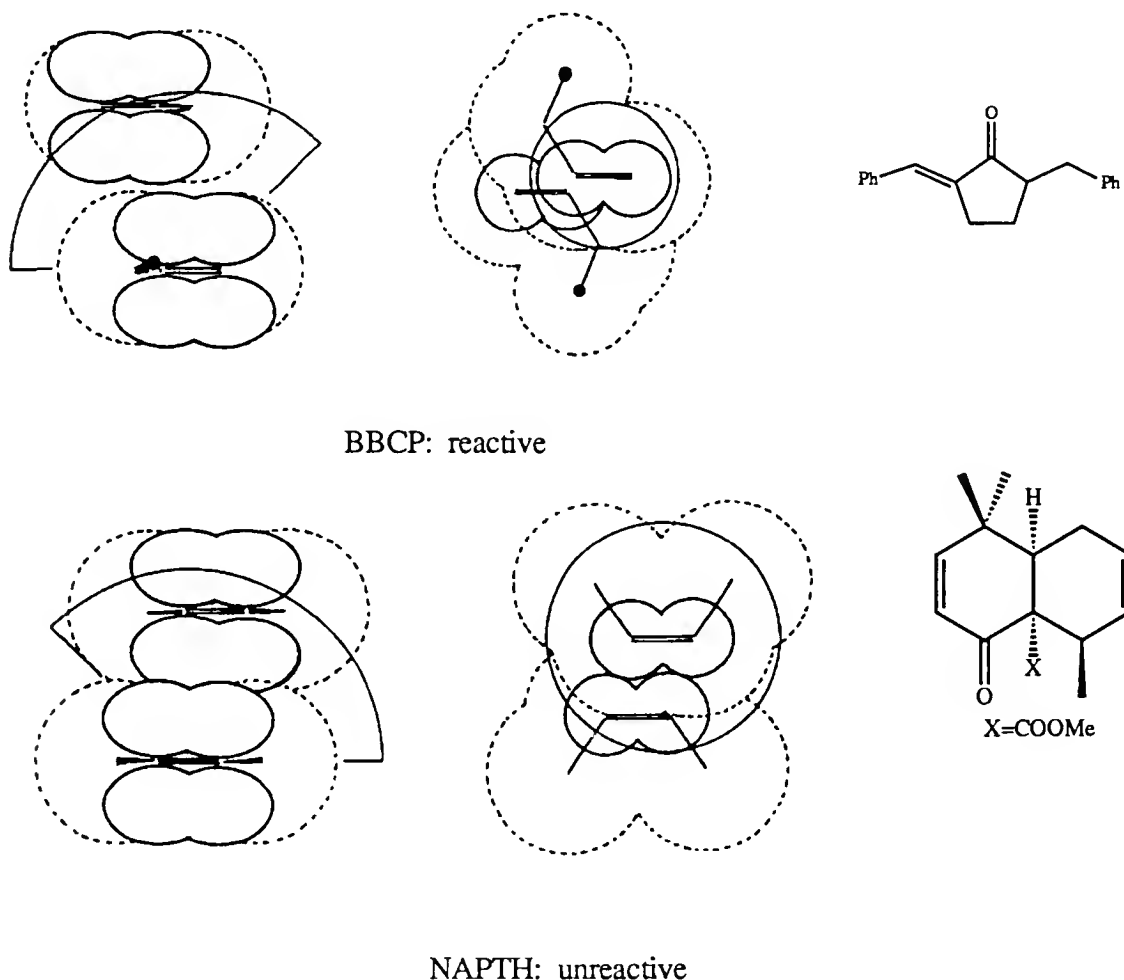


Figure 1-7. p-orbital contours for BBCP and NAPTH double bonds (enone). The arc in the left-hand projection is a cross-section of a 4.2 Å spherical shell originating from the midpoint of the lower double bond, whereas the solid circle on the right is the intersection of this shell with the plane of conjugation of the other double bond. The dashed lines are the full van der Waal radii of the indicated portion of the molecule whereas the partial circles represent a 1.75 Å cross-section of the p-orbitals on the conjugated carbon atoms.

Another method of elaborating on relative molecular orientations in a lattice measures the angles swept out by a parallelogram constructed from the planes of two



neighboring double bonds,  $\theta_2$  and  $\theta_3$ , shown in Figure 1-8.<sup>89</sup> If the bonds are skewed then  $\theta_1$  is considered. Though both of these methods, based on geometrical relationships between potentially reacting pairs of molecules in the lattice, explain certain anomalies not consistent with the simple 4.2 Å rule, they fail to take into consideration the steric effect of the neighboring molecules on the potential of the reaction to proceed as well as the overall flexibility of the lattice. This has been addressed by Cohen with the concept of the reaction cavity, as discussed below.

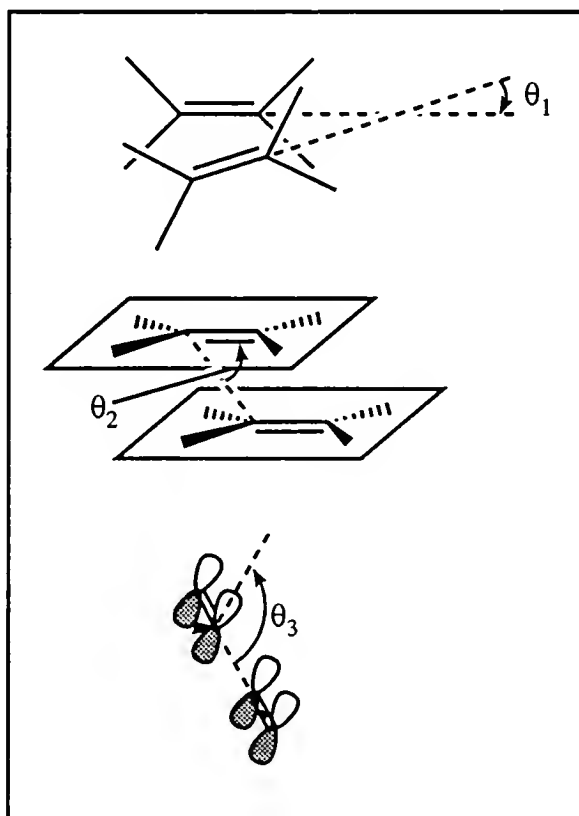


Figure 1-8. Angles considered to predict reactivity of double bonds in a crystal lattice. Ideal values are  $\theta_1=0^\circ$ ,  $\theta_2=90^\circ$ ,  $\theta_3=180^\circ$ .

A highly predictive geometrical analysis of a series of topochemical reactions was that performed for the polymerization of diacetylenes.<sup>82</sup> Figure 1-9 and Figure 1-10 show how the diacetylene monomers are stacked according to repeat distance,  $d$ , and tilted with respect to the axis of the monomer stack,  $\phi$ , so that the minimum van der Waals distance,

$R_V$ , is maintained. In order for the end carbons of the diacetylene unit to approach within bonding distance, the monomer must rotate with the reacting carbons starting from a separation distance of  $R$ , as determined by  $d$  and  $\phi$ . The closed circles in Figure 1-10 represent reactive diacetylenes and the open circles, the unreactive monomer. Clearly,  $d$  and  $\phi$  must be such that  $R$  falls within 4 Å or less for a structure to be reactive. The one closed circle beyond the 4 Å border is for the diacetylene DCH, ( $\text{Cz-CH}_2\text{-C}\equiv\text{C-C}\equiv\text{C-CH}_2\text{-Cz}$ , Cz=carbazolyl) discussed in chapter 3. Figure 1-10 emphasizes the first tenet of Schmidt's topochemical principle as described by Enkelmann: "The reactivity is controlled by the monomer packing and not by the chemical nature of the substituents."<sup>82</sup>

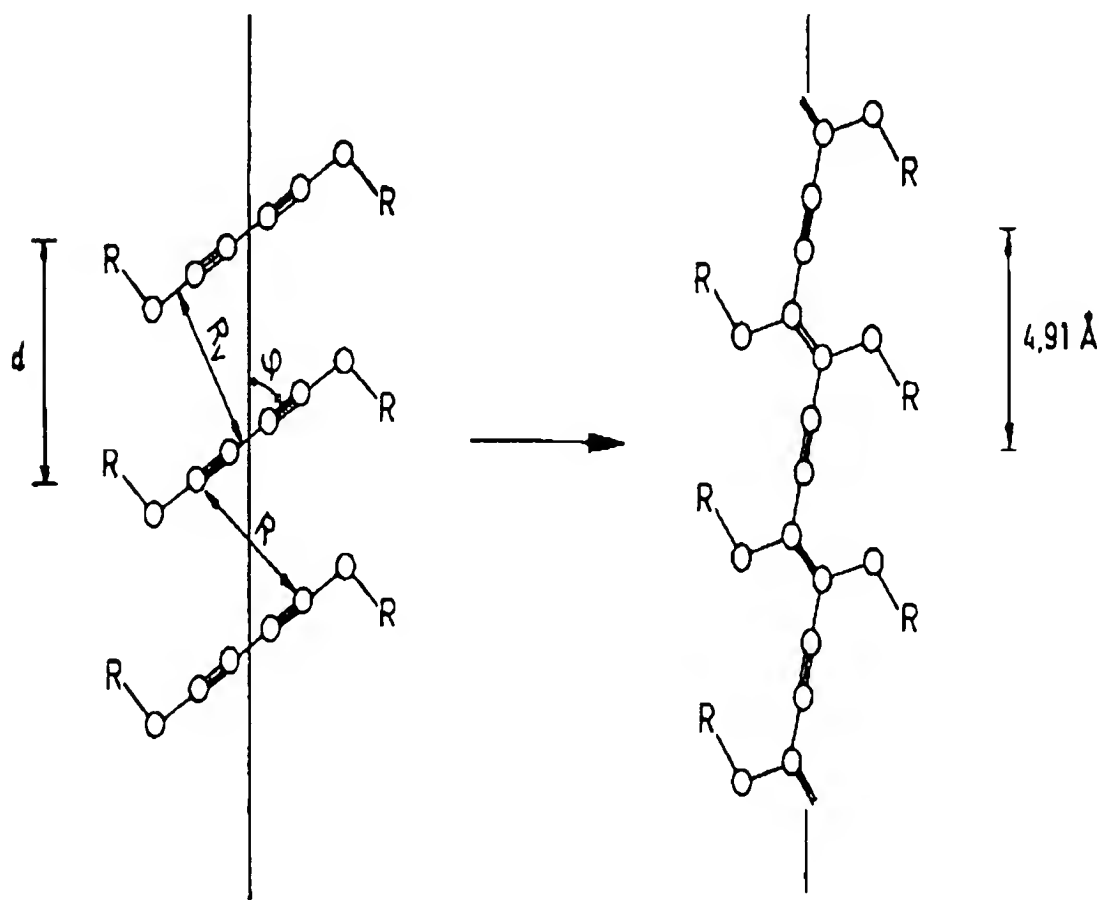


Figure 1-9. Geometrical parameters  $d$  and  $\phi$  in the topochemical polymerization of a diacetylene monomer stack.<sup>82</sup>

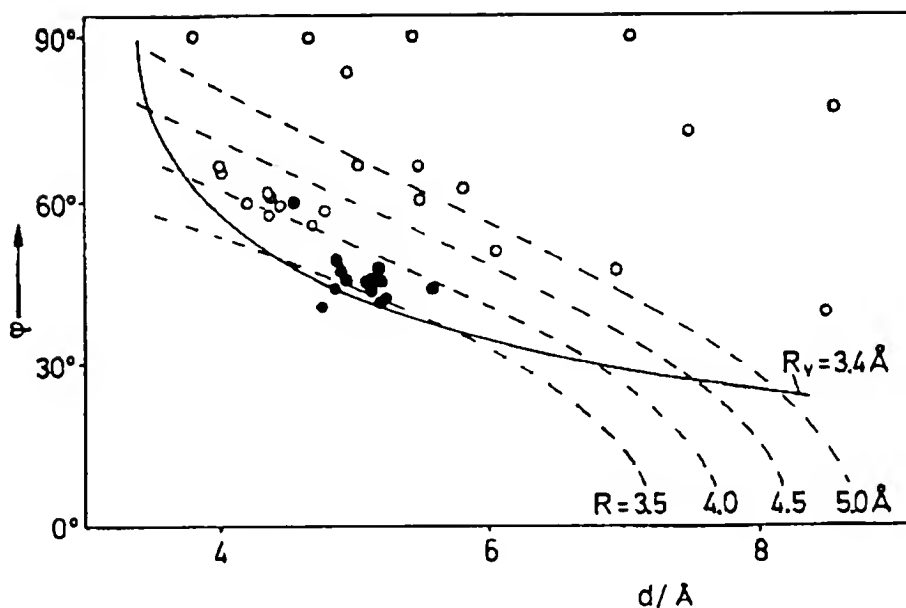


Figure 1-10.  $d$  vs  $\phi$  for various reactive (•) and unreactive (o) diacetylenes.  $R_v$  is the van der Waals distance.<sup>82</sup>

### Reaction cavity concept

Cohen reasoned that, if a reaction was controlled by the parent lattice, “at least up to the transition state, the reaction complex maintains close contact with its environment in the crystal.”<sup>93,94</sup> The contours of the inner boundaries of this environment form a space of fixed size and shape in which the reaction may occur. This is the reaction cavity or cage. Cohen restates the topochemical principle as this: distortion of the size and shape of the reaction cavity due to the rotations and translations involved in bond formation and breaking are minimized in a lattice-controlled reaction. Formation of voids within the cavity are disfavored since they would lead to a large decrease in attractive forces that had existed among the reacting molecules and their environment, while extrusions from the cavity are disfavored due to an increase in repulsive forces that must arise. Thus, the close-packed environment in a crystal resists large shape changes in the packed units. This is illustrated in Figure 1-11.

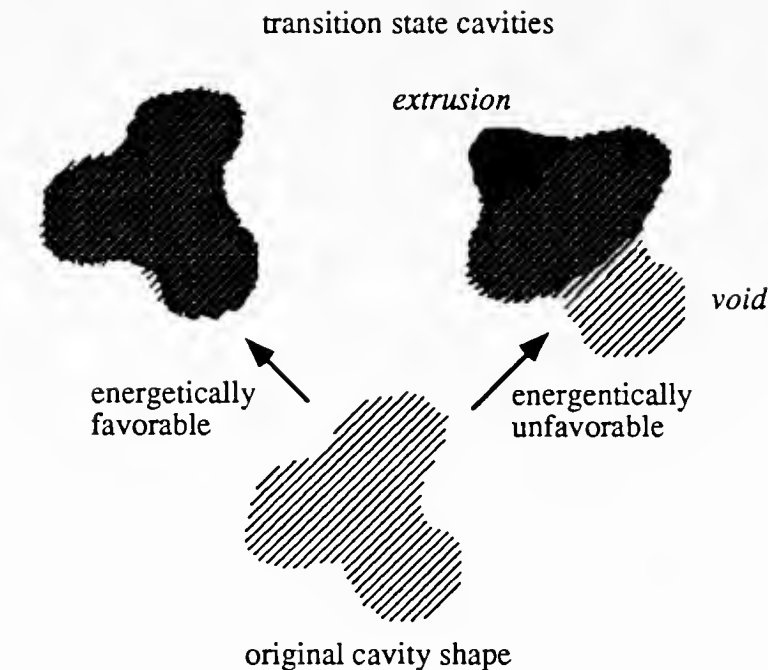


Figure 1-11. The original reaction cavity undergoes minimum distortion in a favorable reaction. However, creation of extrusions and voids is energetically unfavorable.

This concept has been applied to a number of examples of solid state reactions to rationalize their specificity when two products are feasible and to explain the photostability of favorably aligned molecules and the photoreactivity of unfavorably aligned molecules.<sup>93,94</sup>

Computational investigations on the crystal structure of potentially photoactive organic solids have been reported that take into consideration the influence of the environment on the reactivity of molecules in crystals. One investigation calculated the relative energies associated with the steric compression involved for hybridization of two potentially reactive centers in a unimolecular H-abstraction to explain the specificity of the product formation.<sup>95,96,66</sup> Calculations involving lattice energies have also predicted product specificity for dimerization reactions as well as photostability despite a favorable geometric arrangement.<sup>95-97,66,13</sup> Table 1-3 contrasts strictly geometrical parameters with calculations considering reaction cavity principles for predictive value. Another type of

calculation involves computing packing density maps of crystal structures that allow the identification of void space.<sup>98</sup> These maps may explain why some molecules with unfavorable geometric orientation, in contrast to above, nevertheless do react because of an enhanced lattice flexibility.

Table 1-3. Calculations to predict topochemistry based on reaction environment where simple geometrical considerations fail.

### Specificity

Unimolecular H-abstraction<sup>95,96,66</sup>

GEOMETRY	C...H	steric compression	REACTIVITY
	distance	ENERGY	
C <sub>1</sub> ...H	2.74 Å	0 kcal / mole	yes
C <sub>2</sub> ...H	2.70 Å	12 kcal / mole	no

Photodimerizable

Olefins	center to center double bond	rise in lattice	
	distance	ENERGY	
7-chlorocoumarin <sup>97,66</sup>	4.45 Å	160 kcal / mole	yes
translational pairs			
centrosymmetric pairs	4.12 Å	18,000 kcal / mole	no

### Photoactivity

naphthalenone derivative<sup>95,96,66,97</sup>

$\theta_1=0^\circ, \theta_2=82^\circ, \theta_3=154^\circ$	3.79 Å	1500 kcal / mole	no
7-methoxycoumarin <sup>97,66</sup>	3.83 Å	160 kcal / mole	yes
$\theta_1=68^\circ, \theta_2=110^\circ, \theta_3=160^\circ$			

Related to the idea of reaction cavity distortion is the concept of dynamical preformation advanced by Craig and coworkers.<sup>13,66</sup> It is well accepted that the molecular geometry of the excited state may be radically different from that in the ground state, and this must also be considered in the context of the reaction cavity principle.

### Appearance of the Product Phase: Homogeneous vs. Heterogeneous Mechanisms

The topochemical principle organizes the issues involving lattice packing, reactivity and product identity in solid state reactions. However, the mechanism by which the reactant phase transforms into the product phase lacked a cohesive explanation. The

concept of the shape of a reaction cavity in determining the topochemistry of a solid state reaction applies to transition state geometries but may also inform the discussion on how the product builds within the crystal. But up until the discovery of the first single-crystal-to-single-crystal transformation of a molecular crystal, only speculation existed on the course of the phase transformation from reactant to product. With the discovery of the solid state topochemical reaction of diacetylene monomer crystals to yield single crystals of polymer, new light was shed on the issue of phase transformations in the organic solid state.

### Conceptual developments

Structural mimicry. Schmidt's original proposal on the appearance of the product phase provides a rough outline that accommodates subsequent observations on the mechanisms of phase transformations of topochemical reactions:<sup>53</sup>

It is reasonable to assume that the dimer goes into solid solution in the lattice of the monomer and that as the dimer concentration rises the solubility limit is exceeded and the new phase precipitated. However, since the solubility of dimer in the monomer lattice and the stability of this solid solution must vary from compound to compound . . . no generalisations are as yet possible.

Schmidt observed "a wide variety of effects," including that in X-ray powder diffraction studies, powder lines of the product phase appear over a wide range of product concentrations for various substances. Schmidt also observed that some of the  $\beta$  acids "crystallise during the course of reaction in a metastable form not identical with the modification obtained by crystallisation from solvent." As for single-crystal-to-single-crystal transformations, Schmidt proposed that<sup>53</sup>

the absence of orientation [of the product phase] is due to too large a difference between the crystal structures of the monomers and dimers and that, where two structures are sufficiently closely related . . . direct single-crystal transitions are in fact possible.

Ten years later when introducing the concept of the reaction cavity in organic solid state reactions, Cohen refined the proposal that organic solid state reactions begin with the formation of a solid solution of reactant and product with the idea that due to the

geometrical constraints of the cavity, the product molecules are not only a substitutional solute in the parent crystal but that the conformation of the product molecules was that “which best fits them to solid-solubility in the reactant crystal.”<sup>53,94,93</sup> Therefore, solid solubility was dependent on conformational mimicry. Moreover, he stated that this will be most readily observed when the product molecule is “intrinsically readily deformable.” Along these lines, the remarkable case of the single-crystal-to-single-crystal conversion of diacetylene monomer crystals to polymer crystals was informative. For this case, Cohen notes that “complete conversion can be achieved without phase change since the polymer formed is crystallographically isomorphous with the starting monomer.”<sup>94,93</sup>

The role of van der Waals contacts among side groups. Van der Waals contacts among bulky side groups determine the packing of a monomer in the solid state. The diacetylene examples illustrate that these groups stabilize the packing of the reacting monomer throughout the transformation to photoproduct. Since the side groups do not react, their final conformation in the daughter lattice is similar to that in the parent lattice. In this way, the side groups control the production of a structure isomorphous with the incipient structure. Figure 1-12 demonstrates this concept by superimposing projections of monomer and polymer crystal structures of bis(p-toluene sulfonate of dodeca-5,7-diyne-1,12-diol) PTS-12. The side groups move very little in the transformation from reactant to product. It was noted that although these ideas were true for a type of polymerization reaction, for reactions producing low-molecular weight products such as photodimerizations, “lattice control of the conformation of the product is less clearly established.”<sup>94,93</sup> A single-crystal-to-single-crystal photodimerization has also now been achieved. The full crystal structure of the photoproduct superimposed on that of the reactant is also seen in Figure 1-12.<sup>12</sup>

Solid solutions. The terms “homogeneous” and “heterogeneous” were established to describe the two types of mechanisms by which topochemical polymerizations occurred and illustrates them as shown in Figure 1-13.<sup>83,11,48,57</sup> The figure on the right illustrates

polymer-formation proceeding homogeneously inside the monomer crystal starting at randomly distributed points where polymerization has been initiated. The result is that the product is dispersed in the undisturbed monomer matrix so that a solid solution of product and reactant is obtained. Thus coherence between all parts of the crystal, and thus the single-crystal texture, is retained. This is believed to be the mechanism by which several diacetylenes polymerize to give macroscopic single crystals of extended chain polymers. In fact, the polymerization of a diacetylene monomer is the first documented example of a topochemical reaction producing single crystals of product.

Work done by Braun, et al, on the photopolymerization of distyrylpyrazine (DSP)<sup>6,7,10</sup> revealed that its mechanism of polymerization--homogeneous or heterogeneous--could be controlled with irradiation conditions. When the UV-VIS photoactive DSP crystals are irradiated with light of wavelengths for which the chromophore has a large extinction coefficient, most of the light is absorbed at the crystal surface, according to Beer's Law. Thus product formation is isolated at the crystal surface and the interior of the crystal, which receives little intensity, remains unreacted. The product eventually reaches its limit of solubility at the crystal surface and precipitates out. It is the dimensional mismatch between the parent phase and new phase which cause incoherent phase boundaries and disintegration of the crystal into polycrystalline powder.<sup>53,100,11,34,36</sup> Most solid state photoreactions proceed by such a heterogeneous mechanism, illustrated in Figure 1-13 on the left.

However, when DSP crystals are irradiated with wavelengths of light for which the chromophore has a small extinction coefficient, for example, in the absorption tail of the monomer, then the light is absorbed relatively evenly throughout the bulk of the crystal and thus product formation is also randomly distributed throughout the crystal, just as in the diacetylene polymerization. This random product formation results in a single-phase transformation from DSP monomer to oligomer and thus the single-crystal texture of the monomer is preserved.



Conformation of side-groups in solid solutions and structural mimicry. This dissertation provides the first glimpse of the conformational relationships between reactant and product molecules in a crystal in the process of undergoing a topochemical reaction. This is done through the first x-ray crystal structure analysis of a solid solution of reactant and its photoproduct formed through a topochemical reaction.

Here the monomer and dimer structures--for the photodimerization of the styrylpyrylium triflate 1-1c and  $\alpha$ -trans-cinnamic acid--though having different equilibrium conformations, are seen to be constrained to the same lattice positions to form a solid solution. The dimer mimics the monomer at low conversions, whereas the monomer appears to mimic the dimer at high conversions. Because the degree of conversion is kept uniform over the entire crystal and over the course of the reaction through, a single-crystal-to-single-crystal transformation is observed. Throughout the dimensions of the macroscopic single crystal, the monomer and dimer are constrained to resemble one another through the formation of a solid solution. This is achieved through random product formation throughout the crystal via absorption-tail irradiation. Thus the monomer and dimer remain in a single phase throughout the conversion.

However, the photodimerization of BBCP in the solid state is activated with UV-VIS light and occurs with retention of the single-crystal character without specific attention to the irradiation conditions. Assuming the product formation is caused with strongly absorbed wavelengths and is therefore heterogeneous, why is crystal disintegration not observed? In this case, the equilibrium conformation of the monomer and the as-dimerized conformation of the dimer are so similar, that is, they mimic one another so strongly, that no phase separation occurs apparently due to an insufficient difference in their lattice dimensions. On the other hand, in the case of DSP, the styrylpyrylium triflate 1-1c and cinnamic acid, the equilibrium conformation of the monomer and the as-dimerized conformation of the dimer are different enough that they require solid solutions to bridge the gap from reactant to product single crystal. In these solid solutions monomer

and dimer mimic one another in intermediate conformations that are dependent on the degree of conversion.

### Examples of homogeneous and heterogeneous mechanisms

Figure 1-14 summarizes some of the courses documented for the emergence of the product phase in solid state reactions. First, as described originally by Schmidt, product accumulates in the parent crystal in solid solution with the reactant.<sup>53,64,94,93</sup> This is path Ia, in Figure 1-14. As Schmidt and Cohen suggest, this produces a substitutional mixed crystal of reactant and product,  $\begin{bmatrix} R & P \end{bmatrix}$ . Two possible fates await this solid solution as the reaction proceeds and the product concentration increases: continuation of a single-phase transformation, paths I, which are extremely rare, or phase separation, paths II.

Under the category of single-phase transformations, consider the case where the product remains in the solid solution with the reactant until quantitative conversion is reached following the ideal homogeneous mechanism first realized in the laboratories of Wegner and coworkers for the polymerization of the diacetylene 1,6-bis(p-toluene sulfonate) of 2,4-hexadiyne diol (PTS) and the oligomerization of DSP.<sup>16,99,6,7</sup> Ia. A characteristic of the PTS polymerization is the smooth and continuous change in cell parameters from monomer to polymer phase. This is a result of the solid solution of monomer and polymer. The lattice changes to accomodate the gradual increase in concentration of the polymer and decrease in monomer concentration. Other single-crystal-to-single-crystal transformations that have been documented to occur with a smooth, continuous change in lattice parameters are the BBCP photodimerization<sup>12</sup> and the racemization of a coboxalime complex.<sup>18</sup> Cell parameter vs. conversion plots for PTS polymerization and BBCP photodimerization are shown in Figure 1-15.

Before quantitative conversion is reached, however, at some critical concentration, a single-crystal-to-single-crystal structural phase transition may take place, Ib, after which the homogeneous topochemical reaction continues, Ia. This phenomenon has been

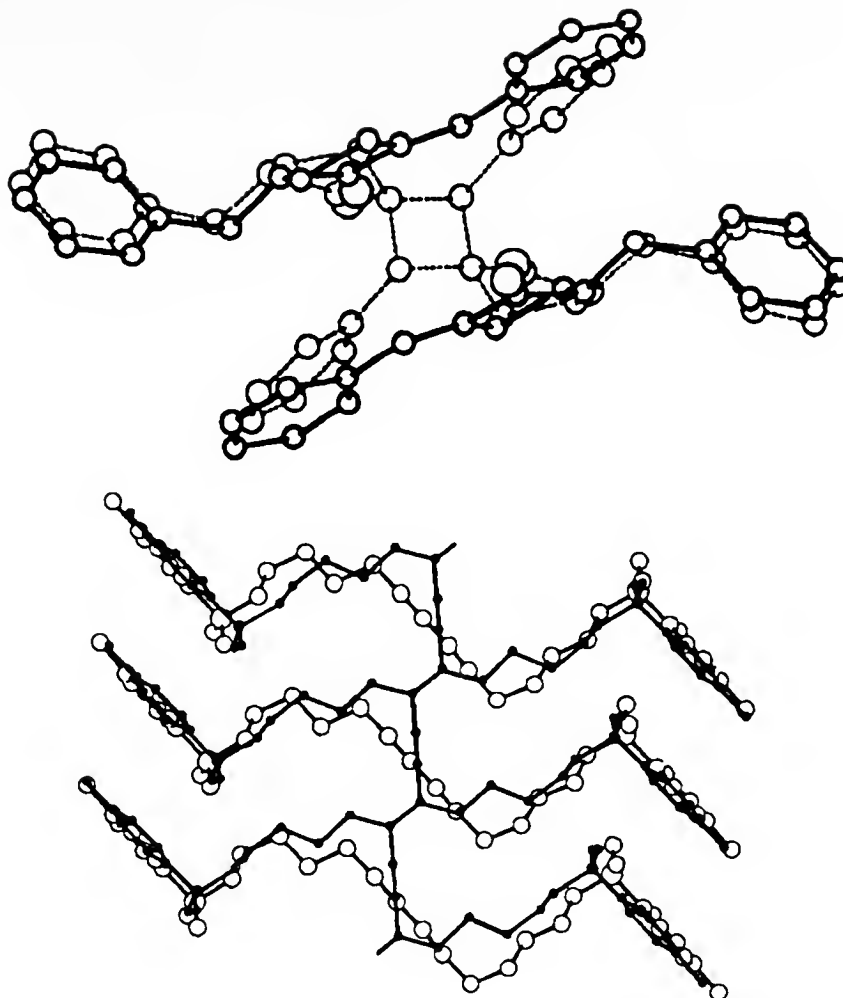


Figure 1-12. Superimposed crystal structures of monomer and photoproduct for the single-crystal-to-single-crystal transformations of BBCP photodimerization (top) and PTS polymerization (bottom).

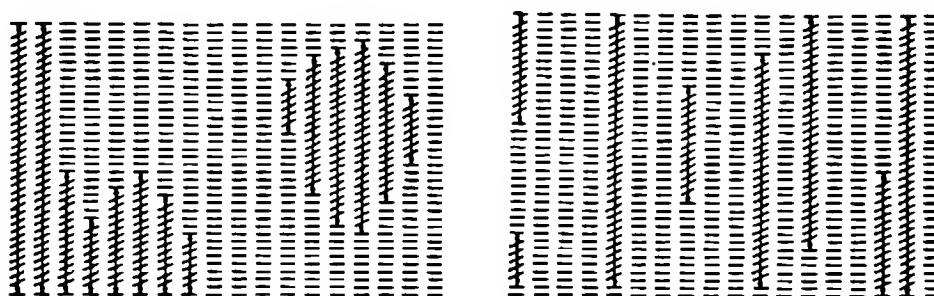


Figure 1-13. A heterogeneous mechanism of topochemical polymerization is pictured on the left, a homogeneous mechanism on the right. In the heterogeneous mechanism, nuclei of the product phase are formed, whereas in the homogeneous case, the product is formed randomly and a solid solution of monomer and polymer is maintained.<sup>11,83,99</sup>

documented for the polymerization of two diacetylene monomers, DCH ( $\text{Cz-CH}_2\text{-C}\equiv\text{C-C}\equiv\text{C-CH}_2\text{-Cz}$ , Cz=carbazolyl) and PTS-12.<sup>82</sup>

The category of phase separation is more complex. Any type of product phase separation, whether this second phase emerges as crystalline or amorphous, has the potential to destroy the parent crystal and lead the reaction into a non-topochemical mode by introducing “defects” or “impurities” into the parent crystal and through this, destroying it. Then the reaction proceeds as if in a melt, that is, by random diffusion of reactants.

However, assuming the parent crystal is not destroyed, the product phase may nucleate in a certain crystalline modification, and proceed with coherent contact between the parent crystal phase and product phase. Or the phase boundaries may be incoherent due to a mismatch in the dimensions of parent and product phases. *Build-up of product such that phase separation occurs across incoherent phase boundaries is the dominant mechanism of product formation in topochemical reactions documented thus far.* This is path IIa in Figure 1-14 and is the established mechanism for most topochemical reactions based on [2+2] photodimerizations which are induced by strongly absorbed irradiation and occur to yield the product as a polycrystalline powder.

It must be emphasized that there is an intimate relationship between paths Ia and IIa in Figure 1-14 for topochemical reactions induced with light in the ultraviolet-visible regions of the spectrum. For example, it is possible to switch from the mechanism of path Ia to the mechanism of path IIa with proper choice of irradiation conditions as described for the oligomerization of DSP and in the studies presented in this dissertation in chapters 3 and 4. How does changing the mechanism change the product identity? To put it another way, how do the as-dimerized products from a homogeneous vs. heterogeneous mechanism compare? Up until now, no comparisons have been possible for topochemical photodimerizations. For the cases reported in this dissertation, however, it has been established that the photodimer of the styrylpyrylium triflate, 1-4c, has the same metastable modification whether produced through a homogeneous or heterogeneous mechanism.

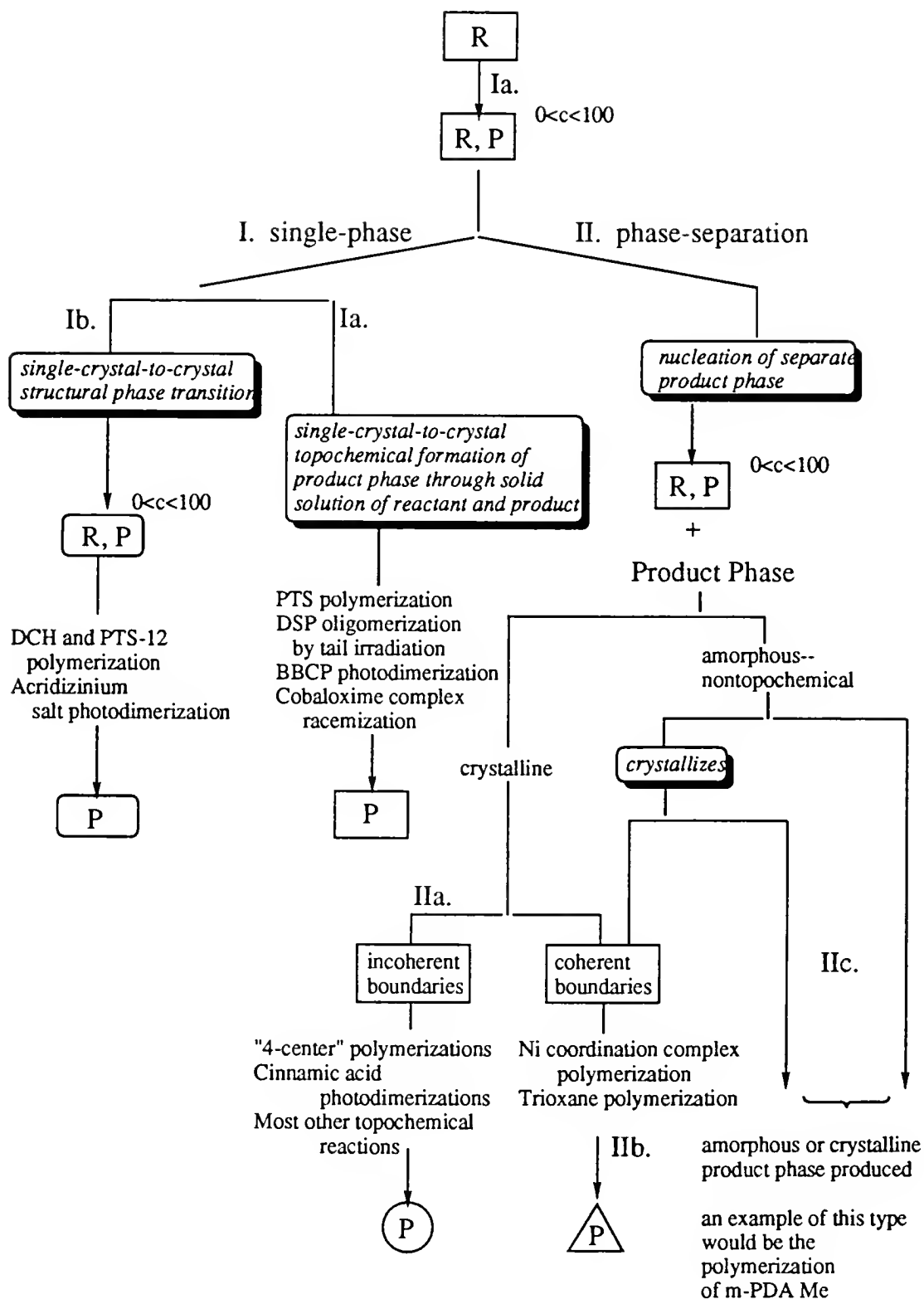


Figure 1-14. A summary of some of the ways in which a product phase may emerge in a solid state reaction. The main mechanisms are homogeneous, Ia, and heterogeneous, IIa.

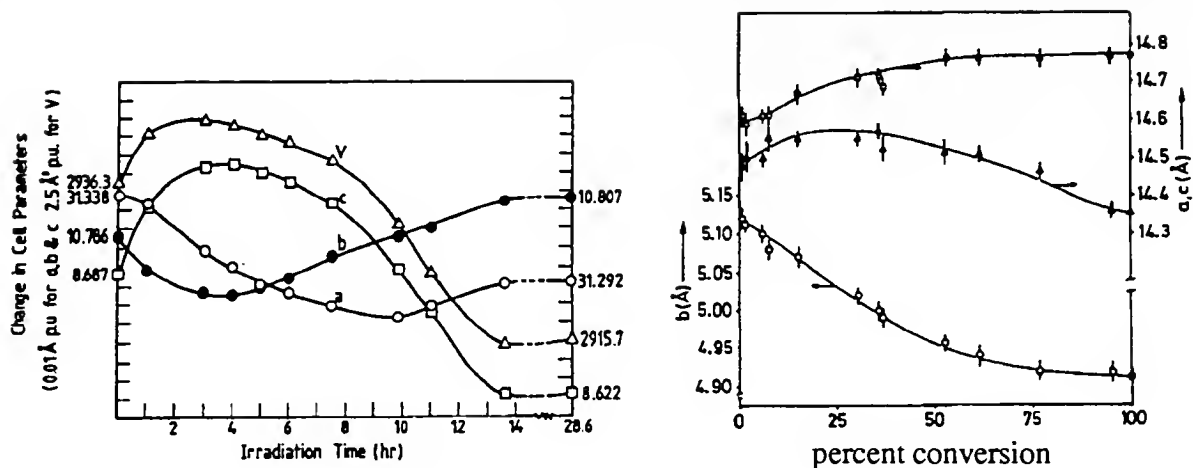


Figure 1-15. Plots of cell parameters vs. conversion for the single-crystal-to-single-crystal transformations of BBCP to photodimer (top)<sup>12</sup> and the diacetylene monomer, PTS to photopolymer (bottom).<sup>82</sup>

However, the styrylpyrylium photodimer, 1-4c, recrystallized from ethanol has a different modification. For cinnamic acid, the homogeneously vs. heterogeneously produced photodimers *are different* as determined X-ray powder diffraction measurements. The crystal structure of the recrystallized cinnamic acid photodimer, that is, truxillic acid, is in progress.

If the product phase emerges as crystalline or amorphous, but in coherent contact with the parent crystal, then a topotactic reaction is possible, path IIb. Figure 1-14 shows that although topochemical control may often lead naturally to topotaxy, the phenomena of topotaxy can occur through an amorphous intermediate and thus have nothing to do with topochemistry. Examples of topotactic reactions in the literature are those reported for trioxane<sup>101</sup> and Ni coordination complex polymerizations.<sup>102</sup>

An example of a nontopochemical reaction, path IIc, in which an amorphous polymer is produced from crystalline monomer is that of [2+2] photopolymerization of the meta-substituted methyl ester of phenylenediacrylic acid, m-PDA Me. For this reaction, Hasegawa reports,<sup>34</sup>

At the initial stage of photoirradiation, the molecules...react topochemically to form the corresponding dimer having a cyclobutane ring with a mirror symmetry. Then, the subsequent reaction between the dimer and its neighbor in the destroyed crystal lattice results in an amorphous oligomer exhibiting more than two kinds of cyclobutane structures.

Figure 1-14 organizes the two principle paths established for the mechanisms of product phase formation in topochemical reactions. The homogeneous mechanism is a single-phase transformation, whereas, the heterogeneous mechanism involves phase separation. In some cases of topochemical photoreactions, these mechanisms can be controlled with irradiation conditions. A few other solid state processes, bearing on the emergence of the product phase, have also been inserted into the scheme as they relate to these two main mechanisms.

### Summary of Results Presented in this Dissertation

In chapter 3, seven crystal structures are reported: the styrylpyrylium triflate monomer, 1-1c, at a higher and lower temperature, the styrylpyrylium triflate photodimer, 1-4c, the monomer crystals obtained when the photodimer is thermally treated, the recrystallized photodimer, and two single crystals of monomer and dimer formed by the partial reaction of monomer through a single-crystal-to-single-crystal photodimerization. The crystal structures of monomer and as-dimerized dimer confirmed topochemical control of the reaction but also revealed large changes in the side-group conformations. Consequently, the crystal structures of the monomer-dimer solid solutions formed from the irradiation of a monomer crystal were of keen interest. They revealed that the side groups occupied the same position in the lattice, whether they were attached to a product or reactant molecule. This results in bond angle deformation involving the ring  $sp^2$  carbon linking the double bond or cyclobutane to the rest of the side-ring. The two crystal structures done on crystals at intermediate conversions catch the side groups in two stages of a smooth rotation from monomer to product structure. Photos of the crystals in the process of photodimerizing and thermally reversing show no second phase emerging in the

crystals during either process. Furthermore, the crystal structure of the monomer crystal obtained from thermal reversion was identical to that of the original and provided the first documentation of a single-crystal-to-single-crystal back reaction. The crystal structure of the recrystallized dimer proved that the as-dimerized and recrystallized dimer were in different modifications. The recrystallized dimer single crystals were resistant to thermal cycloreversion under the same conditions that caused this reaction in the as-dimerized crystals. Calculated and measured powder diffractograms of the homogeneously and heterogeneously-formed photodimers indicate that these products are identical.

Six full crystal structures are reported in chapter 4. Five are of  $\alpha$ -trans-cinnamic acid and photodimer single crystals at 0%, 28%, 40%, 67% and 100% conversion. A crystal structure of an ammonium salt of cinnamic acid was also performed. The ability to achieve a single-crystal-to-single-crystal phototransformation on cinnamic acid indicates that the method of tail irradiation may have some general applicability to topochemical photoreactions. Again, the side groups in this photodimerization occupy the same location in the lattice regardless of whether they are attached to an olefin or cyclobutane. In both the styrylpyrylium triflate and cinnamic acid, the phenyl ring rotates approximately  $20^\circ$  from the reactant to product structure. The same type of bond angle deformation is seen in both cases as well. The main difference in the two cases comes from X-ray powder diffraction measurements on the heterogeneously formed dimer. In the case of cinnamic acid, the X-ray powder diffraction measurements for the heterogeneously produced dimer do not match that calculated from the crystal structure of the homogeneously-produced photodimer single crystal.

Eight full crystal structures are reported in chapter 5: the  $\text{BF}_4^-$ ,  $\text{ReO}_4^-$ ,  $\text{ClO}_4^-$ ,  $\text{SnCl}_5^-$ , and  $\text{AuCl}_2^-$  salts of the styrylpyrylium monomer, discussed in chapter 3, as well as the photodimers of the first two, plus the bis(styrylpyrylium triflate) created by linking two styrylpyrylium triflate chromophores, 1-1c, by replacing the methyls of their methoxy groups with a four carbon methylene bridge. The first three salts are isomorphous with



one another, the lattice adjusting slightly from the smaller  $\text{BF}_4^-$  and  $\text{ClO}_4^-$  counterions to accomodate the larger  $\text{ReO}_4^-$ . Time vs. conversion curves showed the perrhenate salt to have a slower rate once higher conversions were reached. The method for obtaining single-crystal-to-single-crystal conversions by tail-irradiation succeeded with these salts as well and the crystal structures of the photodimers allows comparison of the counterion conformation from the reactant to product structure. The other salts, except for the tin counterion, were photoinactive.

In chapter 6, evidence is presented of a holographic grating written into a styrylpyrylium triflate, 1-1c, single crystal by two interfering laser beams. Besides a photograph of the grating, diffraction efficiency vs. time curves for the writing and thermal erasing of the grating were obtained. Once the  $\sin^2$  dependence of the grating growth was established, the diffraction efficiency vs. time curves could be related to rate of product formation. Then gratings were written and erased at various temperatures to obtain rate constants at various temperatures which were used to construct Arrhenius plots which yielded energies of activation for crystalline-state photodimerization and thermal cycloreversion of the styrylpyrylium salt, 1-1c, and its photodimer, 1-4c.

Preparative work for the styrylpyrylium triflate, 1-1c, was begun at the University of Florida (UF), Gainesville, Florida. All of the absorption-tail irradiations and crystallographic analyses were performed at the Max-Planck-Institut für Polymerforschung (MPI-P), Mainz, Germany. The work on the bis(styrylpyrylium triflates) was begun at UF with the synthesis of compounds 2-25, 2-29 and 2-33. The balance of the bis(styrylpyrylium salts) were synthesized at MPI-P. All of the work reported in Chapters 4 and 6 was done at MPI-P. All of the mass spectral, nuclear magnetic resonance, and infrared analyses were performed at MPI-P.

## CHAPTER 2 EXPERIMENTAL

### Instrumentation and Analysis

#### General Information

All reagents were purchased from Aldrich and Fluka chemical Co. and used without further purification. Melting points were determined from DSC traces done on a Mettler DSC 30 at a heating rate of 5°C / minute. Routine NMR spectra were recorded on a Bruker AC 300 spectrometer ( $^1\text{H}$ : 300 MHz;  $^{13}\text{C}$ : 75.5 MHz) or a Varian Gemini 200 Fourier NMR spectrometer. The residual  $^1\text{H}$  peak of the deuterated solvent is used as an internal standard ( $\text{CHCl}_3$ :  $^1\text{H}$ ,  $\delta = 7.24$ ;  $^{13}\text{C}$ ,  $\delta = 77.00$ ). Elemental analyses were carried out by the Analytische Laboratorien in Engelskirchen, Germany. Infrared measurements were performed with KBr pellets on a Nicolet 730 FT-IR Spectrometer. The photographs in Figures 3-10, 11, 16 and 6-6 were taken on a Zeiss Photomicroscope III with a high pressure halogen lamp. Mass spectra were obtained using a Varian MAT 7A (70 eV).

#### X-ray Structure Analysis

All of the x-ray structure analyses were performed by Dr. habil. Volker Enkelmann, Privat Dozent, at the MPI-P, with an Enraf-Nonius CAD-4 four circle diffractometer with graphite monochromated Cu-K $\alpha$  radiation. Lattice parameters were obtained by least-squares fits to the setting angles of 25 reflections with  $\theta > 20^\circ$ . The intensity data collection was performed by  $\theta$ -2 $\theta$  scans. The intensities of three control reflections were measured at regular intervals to check the stability of the crystals. The raw data were corrected for Lorentz and polarization effects. The structures were solved by direct methods and refined

by full matrix least squares analyses with anisotropic temperature factors for all atoms except H. Positions of the H atoms were calculated using the known molecular geometry and refined in the riding mode with fixed isotropic temperature factors. Empirical absorption corrections were applied to the data and unit weights were used throughout the refinements.

X-ray powder diffractograms were recorded using a Philips PW1820 powder diffractometer with Ni filtered Cu-K $\alpha$  radiation and a secondary graphite monochromator.

Further details of the crystal structure analyses for the crystal structures reported in chapter 3 are available upon request as described in *Angewandte Chemie*.<sup>118</sup> Those reported in chapter 4 are available from the *Journal of the American Chemical Society*.<sup>117</sup>

### Solid State C-13 Measurement

The solid state C-13 NMR measurements referred to in chapters 3 and 4 were performed by Dr. Jeremy Tittman at the MPI-P on a Bruker MSL 300 at 75.47IR measurements were performed on a Bruker MSL 300 at 75.47 MHz. The MAS (Magic Angle Spinning) speed was 3 kHz, and the Cross Polarization time was 2 msec. A Total Suppression of Spinning Side Bands (TOSS) pulse sequence was used. The signal acquisition was done over 35 msec., the 90° pulse length was 4.5  $\mu$ msec., and the spectral width was 29,411 Hz. 2048 Data points were collected.

### Crystal Preparation

Tables 2-1 - 2-6 list the series of compounds which were synthesized as part of this work. Reference numbers are given to each compound. A series of ammonium salts from 3 types of cinnamic acids were prepared and are listed in Table 2-6. Two classes of styrylpyrylium salts were synthesized: simple p-methoxy-substituted styrylpyrylium salts, shown in Table 2-3, and diolefins involving the styrylpyrylium group. The diolefins fall into two categories: Hasegawa-type diolefins, shown in Table 2-4, which are fully

conjugated with one another through sharing a styryl moiety and diolefins linked together with a methylene bridge, shown in Table 2-5.

Pyrylium salts were required for the syntheses of all classes. These are shown with their numbering scheme for the dissertation in Table 2-1 below. Methylene bridged dialdehydes, shown in Table 2-2, were synthesized in order to prepare the methylene-bridged diolefins.

Table 2-1. 2,6-Di-*tert*-butyl-4-methylpyrylium salts

counterion, X <sup>-</sup>	compound
BF <sub>4</sub> <sup>-</sup>	2-1
ReO <sub>4</sub> <sup>-</sup>	2-2
ClO <sub>4</sub> <sup>-</sup>	2-3
SnCl <sub>6</sub> <sup>=</sup>	2-4
AuCl <sub>4</sub> <sup>-</sup>	2-5
SbF <sub>6</sub> <sup>-</sup>	2-6

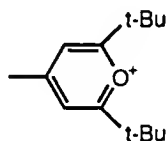


Table 2-2. 4,4'-(Alkylenedioxy)dibenzaldehydes

n	compound
2	2-7
3	2-8
4	2-9
6	2-10
10	2-11

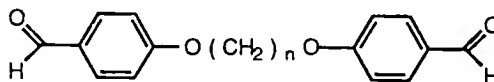


Table 2-3. (*E*)-2,6-Di-*tert*-butyl-4-[2-(4-methoxyphenyl)-ethenyl]pyrylium salts and their photodimers, 4,4'-*c*-2,*t*-4-Bis(4-methoxyphenyl)-*r*-1,*t*-3-cyclobutandiyl]bis(2,6-di-*tert*-butylpyrylium-bis salts

counterion, X <sup>-</sup>	compound
BF <sub>4</sub> <sup>-</sup>	2-12a
photodimer	2-12b
ReO <sub>4</sub> <sup>-</sup>	2-13a
photodimer	2-13b
ClO <sub>4</sub> <sup>-</sup>	2-14a
photodimer	2-14b
SnCl <sub>5</sub> <sup>-</sup>	2-15a
photodimer	2-15b
AuCl <sub>2</sub> <sup>-</sup>	2-16
SbF <sub>6</sub> <sup>-</sup>	2-17

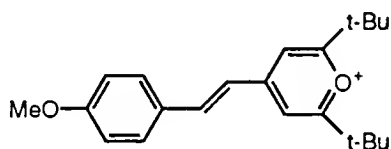
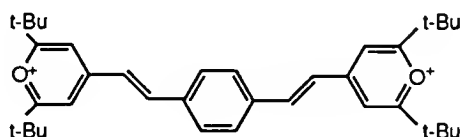


Table 2-4. *p*-Bis[(*E*)-2,6-di-*tert*-butyl-4-(2-ethenyl)-pyrylium]benzene salts

counterion, X <sup>-</sup>	compound
BF <sub>4</sub> <sup>-</sup>	2-18
ReO <sub>4</sub> <sup>-</sup>	2-19
ClO <sub>4</sub> <sup>-</sup>	2-20
CF <sub>3</sub> SO <sub>3</sub> <sup>-</sup>	2-21

Table 2-5.  $\alpha,\omega$ -(Alkylenedioxy)bis[(*E*)-2,6-Di-*tert*-butyl-4-[2-(4-phenyl)-ethenyl]pyrylium] salts

counterion, X <sup>-</sup>	n=2	n=3	n=4	n=6	n=10
BF <sub>4</sub> <sup>-</sup>	2-22	2-26	2-30	2-34	2-38
ReO <sub>4</sub> <sup>-</sup>	2-23	2-27	2-31	2-35	2-39
ClO <sub>4</sub> <sup>-</sup>	2-24	2-28	2-32	2-36	2-40
CF <sub>3</sub> SO <sub>3</sub> <sup>-</sup>	2-25	2-29	2-33	2-37	2-41

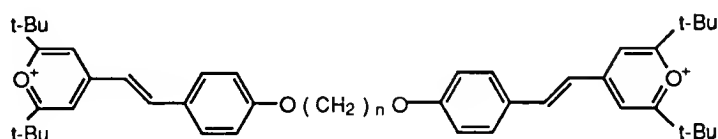


Table 2-6. Ammonium salts of cinnamic acids

<u>amine</u> <u>portion</u>	<u>cinnamic acid portion</u>		
	$\alpha$ - <i>trans</i> -cinnamate	<i>p</i> -methyl- $\alpha$ - <i>trans</i> -cinnamate	<i>p</i> -methoxy- $\alpha$ - <i>trans</i> -cinnamate
piperazinium	2-42	2-46	2-50
piperidinium	2-43	2-47	2-51
benzylammonium	2-44	2-48	2-52
<i>t</i> -butylammonium	2-45	2-49	2-53

## Syntheses

### Pyrylium salt syntheses (Table 2-1)

The following syntheses are adapted from syntheses reported by Balaban and Nenitzescu<sup>103</sup> and Dimroth.<sup>104</sup>

Pyrylium salt 2-4 ( $\text{SnCl}_6^{2-}$ ) 20.24 g (0.16 mol) pivaloyl chloride was stirred with 21.92 g  $\text{SnCl}_4$  (0.084 mol) under Argon. 7.77g (0.084 mol) t-Butyl chloride was added dropwise to that mixture. The mixture was stirred for 16 hours resulting in an orange, viscous reaction mixture. This mixture was poured into 300ml of distilled water where it forms a partially solidified oil. Ether (200ml) was added to this heterogeneous mixture to dissolve the solidified oil, then the ether layer removed and the water layer further extracted with ether until the ether layer remains clear (3 times with 200ml of ether each time). Water (150ml) was removed and the water layer cooled to give 20g of a white solid. The solid was filtered and the filtrate (mother liquor) used in the preparation of additional pyrylium salts described below. The white solid was dried to give 20g of white crystals which were recrystallized in water. Proton and carbon NMR of this substance indicate a pyrylium cation. Elemental analysis revealed that the counteranion contained tin and was mostly  $\text{SnCl}_6^{2-}$ , though  $\text{SnCl}_5^-$  was present as well.

Pyrylium salts 2-1 - 2-3, 2-5 and 2-6. Aqueous solutions of each of the following acids were added to a portion of the mother liquor from the tin-containing pyrylium salt synthesis to give pyrylium salts with the corresponding counterion:  $\text{HBF}_4$ ,  $\text{HClO}_4$ ,  $\text{HReO}_4$ ,  $\text{HSbF}_6$ . White precipitates are seen immediately in the case of  $\text{ClO}_4^-$ ,  $\text{ReO}_4^-$  and  $\text{SbF}_6^-$  pyrylium salts. The  $\text{BF}_4^-$  pyrylium salt crystallizes slowly out of solution as colorless needles.  $\text{HAuCl}_4$  was added to a portion of the mother liquor from the tin-containing pyrylium salt synthesis; the gold-containing pyrylium salt emerges from the solution as orange crystals. Proton and carbon NMR of this substance indicate a pyrylium cation. Elemental analysis revealed that the counteranion was mostly  $\text{AuCl}_4^-$ , however,

$\text{AuCl}_2^-$  was present as well. Each of these pyrylium salts may be recrystallized from methanol.

Miscellaneous pyrylium salts. Attempts were made to obtain other pyrylium salts of the type found in Table 2-1 as described below.

For the counterion  $\text{PF}_6^-$ , an aqueous solution of the acid  $\text{HPF}_6$  was added to the mother liquor from the synthesis of the 2-4 to yield a white precipitate. Elemental analysis indicated that a pyrylium salt of the type found in Table 2-1 with a  $\text{PF}_6^-$  counterion had precipitated out, but this compound could not be converted to a styrylpyrylium salt with a phosphorous-containing counterion.

For the counterions  $\text{PtCl}_6^-$ ,  $\text{IrCl}_6^-$ , and  $\text{OsCl}_6^-$ , aqueous solutions of the acids,  $\text{H}_2\text{PtCl}_6$ ,  $\text{H}_2\text{IrCl}_6$ ,  $\text{H}_2\text{OsCl}_6$ , were added to the mother liquor from the synthesis of the tin-containing pyrylium salts. However, no precipitates were observed.

For the counterion  $\text{CH}_3(\text{CH}_2)_n\text{SO}_3^-$ , the synthesis of the pyrylium salt with a triflate counterion<sup>105</sup> was repeated using  $\text{CH}_3\text{SO}_3\text{H}$  instead of triflic acid in an attempt to synthesize a pyrylium methanesulfonate; however, only starting materials could be recovered. Addition of methane sulfonic acid to an aqueous solution of the pyrylium tin hexachloride yielded no precipitate. An equimolar solution of the styrylpyrylium triflate, 1-1c, in methane sulfonic acid was subjected to vacuum distillation to remove the triflic acid; however, under these conditions the pyrylium cation decomposed. Further attempts to obtain this compound via ion-exchange columns from Fluka's Amberlyst resins also failed.

#### Methylene-bridged dialdehydes (Table 2-2)

The series of dialdehydes in Table 2-2, as well as dialdehydes bridged with 7 and 11 methylene units, were prepared as follows. A solution of sodium ethanolate was freshly prepared by dissolving 5.75g Na in 150ml anhydrous ethanol from a freshly opened bottle. The residual moisture from a 3-necked round bottom flask fitted with a reflux condenser was driven off with a heat gun. The apparatus was flushed with argon via a connection at the top of the condenser and freshly cut Na was added to the round

bottom flask. Dry ethanol (150ml) was quickly added with a funnel through one of the necks and the apparatus resealed and allowed to stand until all the sodium had dissolved. p-Hydroxy benzaldehyde was dissolved under argon in dry ethanol and quickly pipetted into the sodium ethanolate solution along with the dialkylbromide. The reaction mixture was stirred under reflux for 4 hours. After 1 hour a precipitate emerged.

The reaction mixture was then cooled and the ethanol removed with a rotovap. 100ml of 5% NaOH solution was added to the reaction residue and the dialdehyde extracted with diethylether. This organic layer was washed repeatedly with fresh portions of water until the water layer tested neutral for pH. The ether layer was then dried for 15 minutes over calcium chloride, filtered and the ether layer removed with a rotovap to yield a dull white flaky residue in the case of  $n=2, 3, 6$  and  $10$ .  $n=4$  gave shiny, translucent flakes. Raw yields in each of these cases were around 100%. The yields reported are the yields obtained after recrystallization. Very low raw yields in the case of  $n=7$  and  $n=11$  were obtained probably due to an insufficient amount of sodium ethanolate. White powders were obtained in those cases. They were not recrystallized or used further.

Table 2-7. Synthesis data for methylene-bridged dialdehydes (Table 2-2)

	p-hydroxy benzaldehyde	dialkylbromide	sodium ethanolate	yield
$n=2$	30g(250mmoles)	9.4g(50mmoles)	150ml x 1.7M (255mmoles)	2.0g 15%
$n=3$	15.4g(124mmoles)	10.0g(50mmoles)	150ml x 0.83M (124mmoles)	6.3g 16%
$n=4$	"	10.7g(50mmoles)	150ml x 1.7M	4.8g 27%
$n=6$	"	12.1g(50mmoles)	150ml x 1.7M	4.0g 25%
$n=7$	49g(400mmoles)	8.6g(33mmoles)	50ml x 0.83M (40mmoles)	50mg 4%
$n=10$	30g(250mmoles)	14.9g(50mmoles)	150ml x 1.7M	4.5g 24%
$n=11$	49g(400mmoles)	10.5g(33mmoles)	50ml x 0.83	50mg 4%

For  $n=2, 4, 6$  and  $10$  dialdehydes were recrystallized in ethanol,  $n=3$  in methylene dichloride, and used in Knoevenagel condensations with the  $\text{ReO}_4^-$ ,  $\text{BF}_4^-$  and  $\text{ClO}_4^-$  pyrylium salts as well as the triflate pyrylium in the cases of  $n=3$  and  $n=4$ .



### Styrylpyrylium salt syntheses (Tables 2-3 - 2-5)

p-Methoxy-substituted styrylpyrylium salts (Table 2-3) Each of the styrylpyrylium salts in Table 2-3, was synthesized by Knoevenagel condensation of the corresponding pyrylium salt described above (for 1-1c, the synthesis of the pyrylium salt was carried out as described previously in the literature<sup>105</sup>) with p-anisaldehyde via a procedure directly analogous with that reported by Hünig for the p-methoxy substituted styrylpyrylium triflate, 1-1c. Each of the pyrylium salts was refluxed for 16 hours in glacial acetic acid (5ml/1g pyrylium salt) with 3 molar equivalents of p-anisaldehyde (MW=136, density=1.119 g/ml). The reaction mixture is then poured into an equivalent volume of ether to yield the photoactive crystals. The crystals are sucked dry and washed repeatedly with ether to remove the acetic acid. Typical reaction data is given below. These syntheses were repeated as often as further product was required. The yields were in the range 70-90%.

Table 2-8. Synthesis data for p-methoxy styrylpyrylium salts (Table 2-3)

styrylpyrylium salt	pyrylium salt	aldehyde	AcOH	Yield
BF <sub>4</sub> <sup>-</sup>	0.20g(0.70mmoles)	0.25ml(2.0mmoles)	5ml	0.25g 85%
ClO <sub>4</sub> <sup>-</sup>	0.26g(0.85mmoles)	0.31ml(2.5mmoles)	5ml	0.35g 95%
ReO <sub>4</sub> <sup>-</sup>	2.10g(4.6mmoles)	1.67ml(14.8mmoles)	12ml	1.90g 70%
AuCl <sub>2</sub> <sup>-</sup>	1.63g(3.0mmoles)	1.09ml(9.0mmoles)	10ml	1.30g ~75%
SnCl <sub>5</sub> <sup>-</sup>	2.0g(5.4mmoles)	2.0ml(16.5mmoles)	12ml	2.70g ~80%
SbF <sub>6</sub> <sup>-</sup>	0.60g(1.1mmoles)	0.50ml(4.0mmoles)	7ml	0.50g 85%

Hasegawa-type diolefins (Table 2-4) The salts in Table 2-4 were prepared in a manner similar to those in Table 2-3 except in these cases, an excess of the pyrylium salt was used. Acetic acid solutions of the pyrylium were refluxed with terephthaldehyde for 16 hours. However, each of the products begin to precipitate out of the reaction mixture after several hours of refluxing. The hot reaction mixtures were vacuum filtered to isolate in each case a yellow powder which was washed with hot glacial acetic acid repeatedly until

<sup>1</sup>H NMR analysis indicated that all the mono-functionalized terephthaldehyde as well as the excess pyrylium salt had been removed.

Table 2-9. Synthesis data for Hasegawa-type diolefins (Table 2-4)

	terephthaldehyde	pyrylium salt	AcOH	yield
BF <sub>4</sub> <sup>-</sup>	0.268g (2.0mmoles)	1.8g(6mmoles)	12ml	0.9g 70%
ClO <sub>4</sub> <sup>-</sup>	0.268g(2.0mmoles)	1.8g(6mmoles)	12ml	1.0g 70%
ReO <sub>4</sub> <sup>-</sup>	0.134g(1.0mmoles)	1.4g(3mmoles)	10ml	0.7g 70%
CF <sub>3</sub> SO <sub>3</sub> <sup>-</sup>	0.268g(2.0mmoles)	2.0g(6mmoles)	12ml	1.1g 70%

Methylene-bridged diolefins (Table 2-5) Styrylpyrylium salts linked by an alkyl chain were prepared by refluxing the corresponding dialdehyde with the appropriate pyrylium salt. Reaction data is given below. Each pyrylium salt was refluxed with each dialdehyde in 15ml of acetic acid for 16 hours to give the yields indicated. After 8 hours yellow or orange precipitates were observed in each of the reaction mixtures except those of the n=3 materials. The hot reaction mixtures were vacuum filtered to isolate the precipitates which were then dissolved in trifluoroacetic acid and reprecipitated in acetic acid.

Table 2-10. Synthesis data for methylene-bridged diolefins (Table 2-5)

		BF <sub>4</sub> <sup>-</sup> 1.92g (6.53mmoles)	ClO <sub>4</sub> <sup>-</sup> 2.00g (6.53mmoles)	ReO <sub>4</sub> <sup>-</sup> 2.98g (6.53mmoles)
n=2	0.594g (2.2mmoles)	1.3g	0.9g	1.4g
n=3	0.625g	oil	0.7g	oil
n=4	0.660g	1.5g	0.9g	1.8g
n=6	0.717g	0.7g	1.2g	1.2g
n=10	0.840g	0.8g	1.1g	1.3g

#### Ammonium salts of cinnamic acids (Table 2-6)

The ammonium salts of the cinnamic acids in Table 2-6 were formed by first dissolving the acid in 20ml of methanol, then equimolar amounts of the t-butylamine, benzylamine, and piperidine were added to the solution. The methanol was then removed by evaporation to give the acid ammonium salt. Equimolar portions of piperazine were

dissolved in methanol and added to a methanolic solution of each acid. The piperazinium salts precipitated out immediately.

Table 2-11. Synthesis data for cinnamic acid ammonium salts

cinnamic acid	amine
$\alpha$ -trans-cinnamic acid 1.48g (10mM)	piperazine 0.43g (5mM)
<i>p</i> -methyl-cinnamic acid 1.62g (10mM)	piperidine 0.85g (10mM)
<i>p</i> -methoxy-cinnamic acid 1.78g (10mM)	<i>t</i> -butyl amine 0.73g (10mM)
	benzylamine 1.07g(10mM)

### Recrystallizations

#### Styrylpyrylium triflate monomer (1-1c) and dimer (1-4c)

Micrographs. The styrylpyrylium triflate, 1-1c, crystals for the photographs in Figures 3-10, 11 and 16 were formed by evaporation of ethanolic solutions of the monomer on a glass slide. A clean glass slide was boiled in HMDS for 30 minutes to make it hydrophobic, then rinsed in ethanol. 10mg of styrylpyrylium salt, was warmed in 1ml of ethanol until dissolved. The solution was cooled to room temperature then several drops applied to the prepared glass slide. Slow evaporation of the ethanol left styrylpyrylium crystals of various sizes and optical quality adhered to the glass slide. The crystals were loosened from the slide surface with ether. This preparation was repeated until at least 3 crystals at least 0.2-0.3mm in size and of sufficient optical quality were found in the proximity of one another for photographic purposes.

Time vs. conversion vs. cell parameters. The styrylpyrylium triflate crystals for these experiments were prepared from room temperature ethanolic solutions of the styrylpyrylium triflate. 50Mg of styrylpyrylium triflate were dissolved in 50ml of ethanol

and allowed to cool to room temperature overnight. The crystals that formed were filtered and 50 ml of ether was added to the mother liquor. 0.2mm-0.5mm single crystals of excellent optical quality emerged from this solution overnight.

Photodimer, 1-4c. The cyclobutane dimer formed from the irradiation of styrylpyrylium triflate was recrystallized by solvent diffusion. 10mg of the dimer is dissolved in 0.5 ml of trifluoroacetic acid. A layer of ether is carefully applied over this acid solution. After several hours, orange cyclobutane dimer crystals are formed at the acid / ether interface . They must be quickly rinsed with ether when removed from the solution. Repeated attempt sto recrystallize the cyclobutane dimer by cooling in methanol failed.

p-Methoxy-substituted styrylpyrylium salts (Table 2-3)

The recrystallizations of these compounds are summarized in Table 2-12.

Table 2-12. Recrystallization data for p-methoxy-substituted styrylpyrylium salts (Table 2-3)

		recrystallization solvent	color / crystal habit
2-12	BF <sub>4</sub> <sup>-</sup>	acetic acid	gold / platy
2-13	ReO <sub>4</sub> <sup>-</sup>	acetic acid	gold / platy
2-14	ClO <sub>4</sub> <sup>-</sup>	acetic acid	gold / platy
2-15	SnCl <sub>5</sub> <sup>-</sup>	acetic acid	orange / bladed
2-16	AuCl <sub>2</sub> <sup>-</sup>	formic acid	orange / bladed
2-17	SbF <sub>6</sub> <sup>-</sup>	acetic acid	gold / platy and red / prismatic

Slow cooling in acetic acid of 2-12 - 2-14 gives crystals of sufficient quality for x-ray structure analysis. Michael Steiert at the Max-Planck-Institut für Polymerforschung performed many of these recrystallizations. Normal cooling in acetic acid of 2-15 through 2-17 gives crystals of sufficient quality for x-ray structure analysis. Addition of ether to room temperature acetic acid solutions of 2-12 and 2-13 sometimes produces excellent gold tabular crystals of those products. Cooling of hot acetic acid/ether, ethanolic and ethanol/ether solutions, and solvent evaporation from ethanolic solutions are further possible methods for recrystallization for compounds 2-12 - 2-17. The apparent

chromoisomerism of  $\text{SbF}_6^-$  styrylpyrylium salt may be actually due to the formation of a mixed salt of Sb and Sn-containing counterions. This phenomenon was observed for the  $\text{ReO}_4^-$  salt, 2-12, where in addition to the usual gold platelets, red bladed crystals were obtained from the crude reaction mixture. Crystallographic analysis revealed that a mixed salt had been formed with Re and Sn-containing counterions.

#### Hasegawa-type diolefins (Table 2-4)

The recrystallization of these compounds is summarized in Table 2-13.

Table 2-13. Recrystallization data for Hasegawa-type diolefins

		solvent	crystal / habit
2-18	$\text{BF}_4^-$	*	
2-19	$\text{ReO}_4^-$	*	
2-20	$\text{ClO}_4^-$	acetic acid	orange / bladed
2-21	Triflate	formic acid	orange / bladed

Acetonitrile, trifluoroacetic acid / acetic acid, trifluoroacetic acid / ether, chloroform / carbon tetrachloride, ethanol / ether and solvent evaporation from ethanolic solutions yielded only finely divided precipitates for 2-18 and 2-19.

#### Methylene-bridged diolefins (Table 2-5)

Of the distyrylpyrylium salts with the alkyl chain, crystals from only 2-33 ( $\text{BF}_4^-$ ,  $n=6$ ) and 2-34 (tyfriflate,  $n=4$ ) could be obtained. Crystals of 2-33 were reached by slow evaporation of an acetonitrile solution. A 20ml vial of the acetonitrile solution was capped with a perforated lid. After 2 weeks, red blade-like crystals were observed to be growing in the direction of the receding acetonitrile solution. Crystallographic analysis revealed trifluoroacetic acid solvent molecules incorporated into the crystal lattice. Crystals of 2-34 were obtained from cooling a hot, saturated acetic acid solution of the salt.

### Ammonium salts of cinnamic acid (Table 2-6)

All of the ammonium salts of cinnamic acid were recrystallized by cooling hot isopropanol solutions to give white needles, blades and platelets as described below. Only the piperidinium salts failed to recrystallize.

Table 2-14. Recrystallization data for cinnamic acid ammonium salts (Table 2-6)

<u>acid portion</u>	<u>amine portion</u>			
	t-butyl- ammonium	benzyl ammonium	piperidinium	piperazinium
$\alpha$ -trans-cinnamic acid	bladed	acicular	--	platy
p-methyl- cinnamic acid	platy	bladed	--	acicular
p-methoxy- cinnamic acid	acicular	--	--	platy

$\alpha$ -trans-cinnamic acid itself was recrystallized by slow evaporation of an ether solution to form colorless platy crystals.

### Irradiation

#### Photodimer Single-Crystal Preparation

Preparative irradiations for single crystals of 1-4c, 2-12b, 2-13b, 2-14b and  $\alpha$ -trans-cinnamic acid were performed with a 450 Watt Xenon lamp from Photon Technology International Inc., Mod. A 5000 (spectral output shown in Figure 2-1). A quartz diffusor was placed in the beam focus, 17cm from the lamp housing. The filter used for each irradiation was air-cooled and placed at 21cm from the lamp housing.

In the case of the styrylpyrylium salts, a silver mirror was used to direct the light emerging from the filter onto a covered petri dish containing the crystals. For 1-1c, a band-pass filter at 570.4 nm (HW= 54.0 nm) was used. A significant number of the crystals were converted to photodimer in 4 hours. The reaction was complete after 24 h of irradiation under these conditions. For 2-12 - 2-14, a band-pass filter at 548.5 nm (HW=

54.0 nm) was used. Styrylpyrylium salts 2-12 and 2-14 were completely photodimerized within 36 h, while 2-13 required 48 h of irradiation.

For the cinnamic acid, the crystals were irradiated in an NMR tube as follows: The 28% dimer crystals were obtained after irradiation in an NMR tube of 10mm diameter, with Schott long-pass filter WG345 (transmission spectra for Schott long-pass filters shown in Figure 2-2) after 100 h. The degree of conversion was determined by integration of the cyclobutane and vinyl proton signals in the  $^1\text{H}$ -NMR and was consistent with the percent conversion derived from the population parameters in the crystallographic analysis. The 40%, 67% mixed monomer-dimer single crystals and photodimer crystals were obtained from irradiation of a batch of  $\alpha$ -trans-cinnamic acid monomer crystals in an NMR tube of 5mm diameter with long-pass filter WG360 for 100 h.  $^1\text{H}$  NMR sampling of this batch indicated an average conversion of over 90%. The percent conversions of the individual crystals were derived from the population parameters of the crystallographic analysis. The UV-VIS absorption spectrum of a polycrystalline film of cinnamic acid is shown in Figure 2-3.

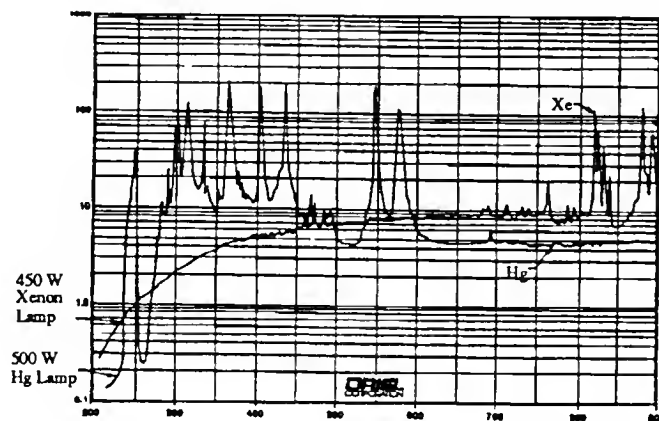


Figure 2-1. Spectral output for the 450W Xenon lamp used in the photodimerizations of the styrylpyrylium salts and cinnamic acid.

### Micrographs

The photodimer crystals pictured in Figures 3-10 and 3-11 were formed with radiation from a Coherent Innova 90-K Krypton Laser with the 568.19 nm line as

described below under "Kinetic Studies". The crystals were exposed to 33.1 mWatts / cm<sup>2</sup> and were completely photodimerized in 30 minutes.

The photodimer crystals pictures in Figure 3-16 were dimerized with radiation from a Xenon lamp passing through the 570.4 nm band-pass filter. The monomer crystals were formed on a glass slide as described above under "Recrystallizations" and the slide mounted on the microscope stage of a Zeiss Photomicroscope in Dr. rer. nat. Günter Lieser's laboratory at the Max-Planck-Institut für Polymerforschung. The lamp was brought as close as possible to the stage and the beam from the lamp reflected off a mirror next to the microscope objective and onto the slide. A photo--not included in this dissertation--of the original monomer crystals for Figure 3-16 was taken. (The microscope was then focused on another group of crystals also on the slide. Photographs of the photodimerization of these crystals were then taken over a period of 24 hours. These photographs have also not been included in the dissertation.) After the photodimerization was complete, a photo of the dimer crystals with cross-polarized light was made. This is the top photo in Figure 3-16. The subsequent thermal treatment of the crystals was done by removing the glass slide to a hot plate set at 100° C until a color change was noted then reinserting it on the stage for photographing.

### Kinetic Studies

#### Styrylpyrylium salts 2-12 - 2-14

Compounds 2-12 - 2-14 were irradiated in their absorption maxima (thus heterogeneous conversions were effected) under identical conditions and their conversion to photodimer measured with time. Table 2-7 lists the times and conversions of each substance for each trial. The irradiations were done with the 450W Xenon lamp described above with a pyrex filter ( $\lambda > 270$  nm). 50ml suspensions of each of these compounds were prepared in dry hexane and degassed for 5 minutes with bubbling Ar. The same 100ml flask was used for each preparation and placed in the center of the radiating beam, 29.5 cm



from the lamp housing. Table 2-15 lists the specific amounts of the substances used for each trial as well as the sampling volume throughout the irradiation. The samples were rapidly stirred during irradiation and sampling. After the sample was withdrawn, the hexane was removed under vacuum and a  $^1\text{H}$  NMR run in 3:1  $\text{CDCl}_3:\text{CF}_3\text{CO}_2\text{H}$ . The signals from the protons on the p-methoxy as well as t-butyl groups were integrated to determine the percent conversion. Figure 2-4 shows a typical  $^1\text{H}$  NMR for a partially dimerized styrylpyrylium salt.

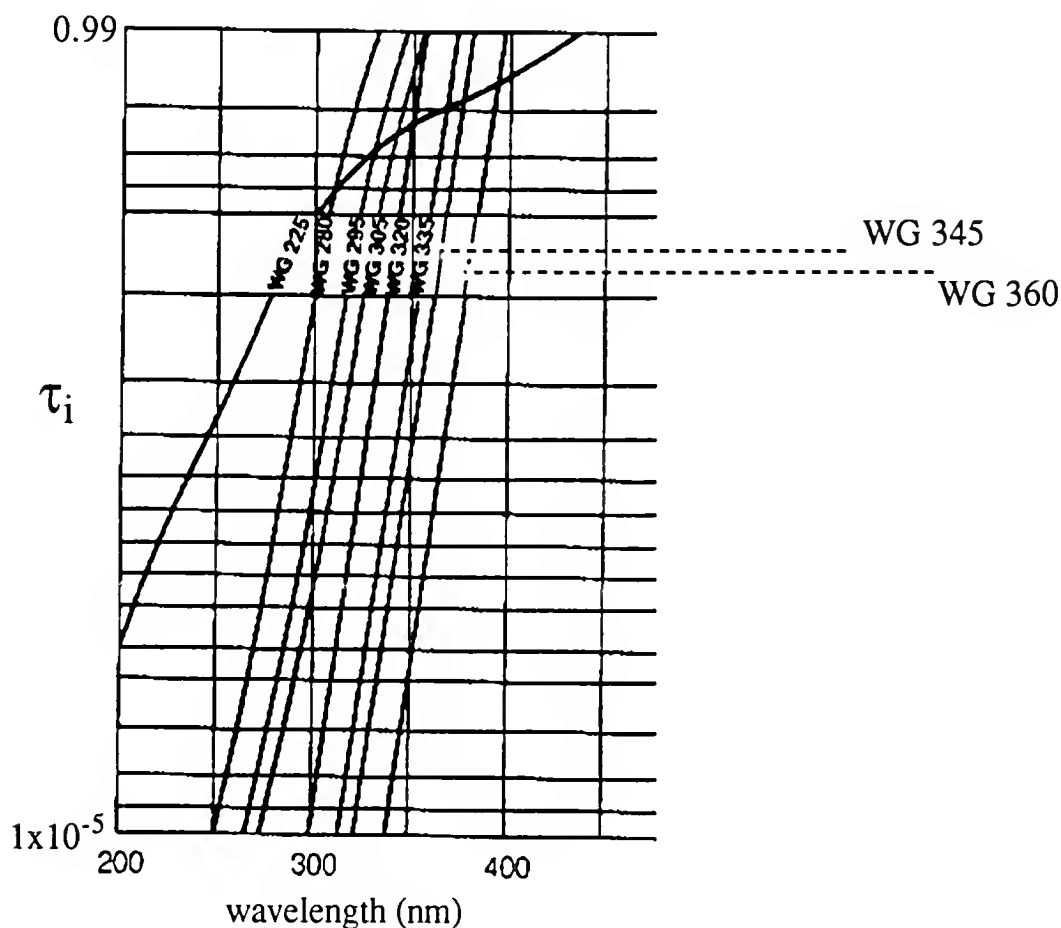


Figure 2-2. Transmission spectra of Schott long-pass filters WG345 and WG360 used in the cinnamic acid irradiation.

$$\tau_i = \frac{(\text{transmitted photon flux})\lambda}{(\text{incident photon flux})\lambda}$$

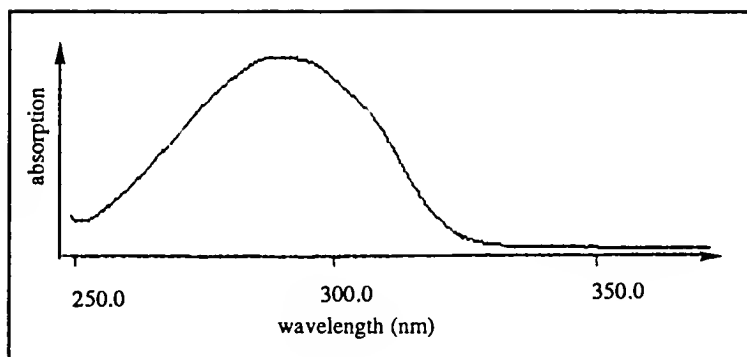


Figure 2-3. UV-VIS absorption spectrum of a polycrystalline film of a cinnamic acid.

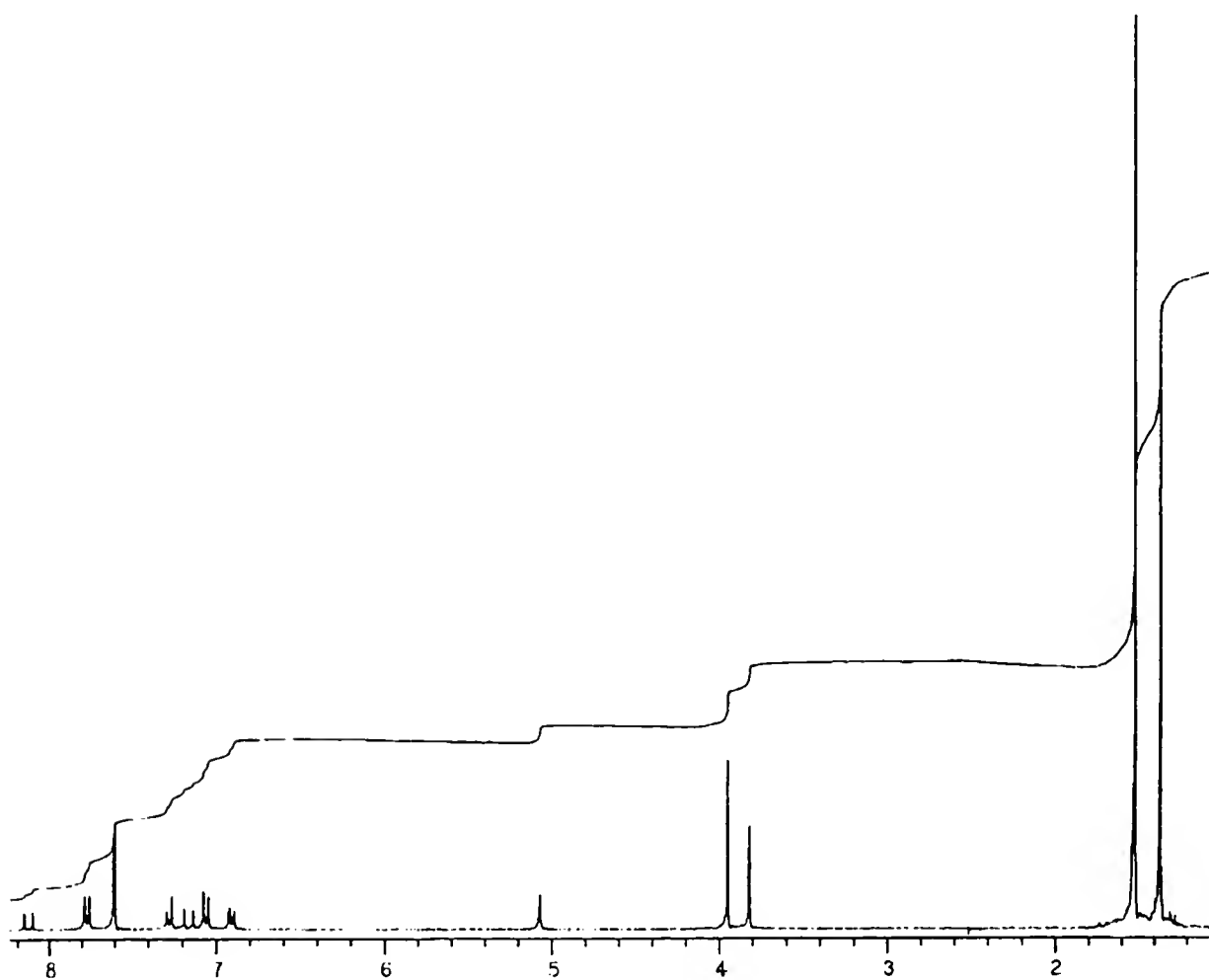


Figure 2-4.  $^1\text{H}$  NMR of a partially dimerized styrylpyrylium triflate, 1-1c and 1-4c..

Table 2-15. Time (left-hand column) vs. conversion data for the photoirradiation of 2-12 (left-hand column under percent conversion), 2-13 (right-hand column under percent conversion) and 2-14 (middle column under percent conversion). The sampling volume as well as the mass of each salt used is indicated for each trial.

<u>Trial 1</u> sampling volume=2ml			
0.217g 2-12	0.223g 2-14	0.303g 2-13	
seconds	percent conversion		
10	13	11	9
20	19	20	13
30	25	25	20
40	34	29	26
60	47	40	34
80	53	55	36
100	62	60	38
140	78	--	48
180	83	55	
220	86	88	60
320	95	98	75
420	97	99	86

<u>Trial 2</u> sampling volume=3ml			
0.179g 2-12	0.183g 2-14	0.250g 2-13	
seconds	percent conversion		
10	9	5	14
40	13	10	16
100	24	21	33
140	37	28	29
180	46	34	38
220	56	42	38
320	76	62	52
420	91	70	65
620	94	86	78
820	100	96	83

<u>Trial 3</u> sampling volume=1ml			
0.360g 2-12	0.360g 2-14	0.500g 2-13	
seconds	percent conversion		
20	--	15	12
40	12	11	11
60	13	16	14
80	12	30	13
100	14	17	16
140	35	25	19
180	25	25	--
220	26	27	32
320	34	39	--
420	46	56	41
620	63	63	--
1020	84	88	62
1620	100	100	85
2420	100	--	99

<u>Trial 4</u> sampling volume=not recorded			
0.100g 2-12	0.100g 2-14	0.100g 2-13	
seconds	percent conversion		
0	3	5	2
100	17	18	16
200	28	28	19
400	43	37	30
600	57	52	49
800	65	66	60
1000	76	77	59
1500	84	91	68
2000	90	95	80
3000	100	100	87
4000	--	100	92

### Styrylpyrylium triflate, 1-1c

The goal was to monitor the time-dependence of the single-crystal-to-single crystal homogeneous conversion of styrylpyrylium triflate, 1-1c, and also obtain substitutionally mixed single crystals of known conversion for crystallographic analysis.

Initial experiments. Initially, a dye laser was chosen for the irradiation. Forty to sixty monomer crystals 0.3-0.5 mm in length were irradiated with light at approximately 570 nm over a 1 cm<sup>2</sup> area of uniform intensity created with a pin-hole and beam expander.

It is possible that the monomer crystals have different absorptivities, depending on the orientation of their crystallographic axes with respect to the plane polarized light from the laser. Therefore, a Soleil-Babinet plate (a quarter lambda plate tunable for various wavelengths) was used to circularly polarize the beam. The power of the dye laser was such that the crystals received  $0.16 \text{ mWatts} / \text{cm}^2$ . At this power, the time required for complete conversion was 24 h. However, the optics involving the pin-hole were not stable over this time period. Figure 2-5 shows the beam profile at the conclusion of the irradiation. Thus the crystals were unevenly irradiated and no useful data could be gathered.

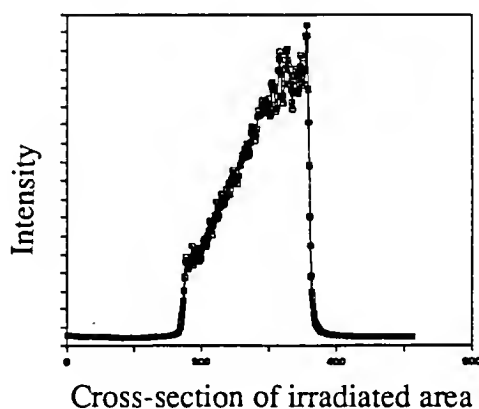


Figure 2-5. Beam profile after 24 h. Crystals in an area corresponding to the left side of the cross-section would receive much less intensity than those on the right.

In the second type of experiment designed to acquire the desired kinetic data, single crystals of the monomer were individually rotated in the laser beam to reduce the area required for uniform intensity. This was done by mounting each crystal on a glass fiber which was in turn placed in a goniometer head rotated by an adapted stirring apparatus. During these experiments it was discovered that the power of the dye laser steadily decreased with time. In addition, the Soleil-Babinet plate was no longer available and two of the crystal faces were indistinguishable from each other, one of which had to be chosen for mounting the crystal: if the crystal has different absorptivities depending on its orientation, 2 conversion curves are possible. Most problematic was that a crystal small

enough for crystallographic analysis was not large enough for percent conversion analysis by IR methods; that is, an individual crystal was too small for making KBr pellets of sufficient concentration for reliable data, but was too thick for single-crystal IR analysis.

Final experiment. The following method finally gave reproducible data: For each conversion, 8-9 crystals, 0.3-0.5 mm in length, were aligned along one optical axis using the crystal habit as a guide. The crystals, lying on their one easily identified face ( this was the [100] face which corresponds to the plane of the bc cell axes as shown in Figure 2-6), were then rotated in a beam from a Krypton laser in an area of uniform intensity created with a beam expander. After each dosage, 2-3 of the crystals were submitted for crystallographic study while the balance of the crystals were taken for IR percent conversion analysis. The time vs. conversion data collected is listed below in Table 2-16. The power from the Krypton laser was such that the optics were steady over the time required for the conversions. Furthermore the power from the Krypton laser was steady with time.

Table 2-16. Time vs. conversion data for the single-crystal to single-crystal conversion of the styrylpyrylium triflate, 1-1c. The conversion in italics are those of uncracked crystals; those underlined are conversions of cracked crystals.

time (s)	trial 1	trial 2	trial 3
840	96	87	<u>83</u>
780	<u>84</u>	86	89
720	89	82	78
630	77	<u>61</u>	83
540	62	<u>51</u>	65
450	49	<u>42</u>	57
360	47	<u>35</u>	35
270	32	<u>30</u>	31
180	23	<u>23</u>	27
90	8	<u>12</u>	10
30	0	<u>1</u>	-2

The Krypton laser was a Coherent Innova 90-K, with a range of 350.7-799.3 nm, 800mW. The 568.19 nm line was used for this work. A beam splitter directed a portion of the beam to the head of a Coherent 210 Power Meter hooked up to a 5000 Digital

Multimeter by Prema. This in turn was connected to a personal computer installed with software that transferred the power data from the multimeter to a file. For each conversion, a file containing the power vs. time data was created and integrated with Lotus Symphony software to give the total relative energy dosage for each time period. A plot of time vs. dosage was linear. The beam not collected for power analysis was passed through a #8 Oriel beam expander and then onto a mirror which directed the beam onto the rotating crystals. The power of the beam was  $21.7 \text{ mW/cm}^2$ . The laser setup was constructed by Bernhard Zimmer at the Max-Planck-Institut für Polymerforschung.

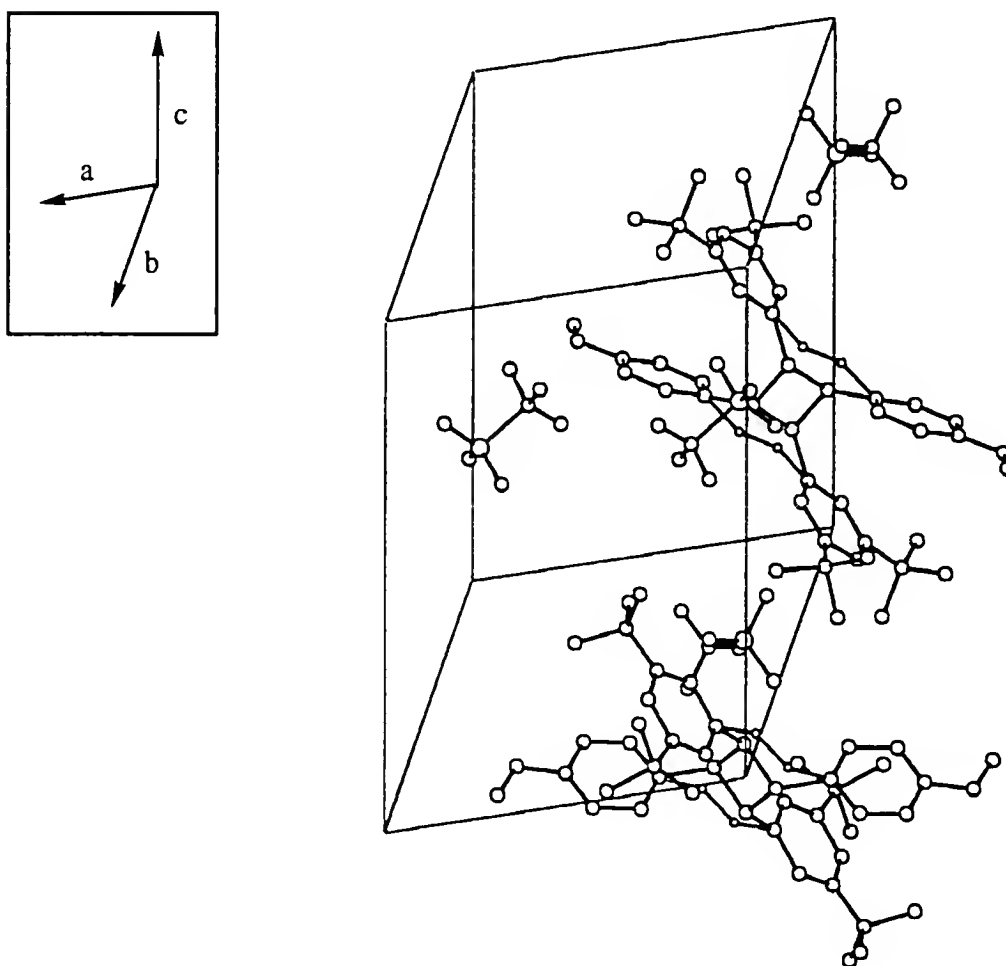


Figure 2-6. This projection of the crystal structure of the 67% monomer-dimer substitutional mixed crystal shows the orientation of the styrylpyrylium salt, 1-1c, in its unit cell. The [100] face, or bc plane of the unit cell was perpendicular to the radiation beam.

Calibration curve. The percent conversion for each batch of crystals was determined by integrating the C=C-H out-of-plane bend absorption band between 920 and 967  $\text{cm}^{-1}$  and referencing it to an internal standard, the -SO<sub>2</sub>- absorption band of the counterion at 1030  $\text{cm}^{-1}$ . The calibration curve shown in Figure 2-7 was created by irradiating suspensions of the monomer with the Xenon lamp, no filter, and determining percent conversion of a given sample by <sup>1</sup>H NMR. IRs of samples of known conversions could then be measured and the ratio of the peaks described above determined for each conversion. Initially, the large C=C stretching peak at 1583  $\text{cm}^{-1}$  was chosen as the peak to monitor for conversion analysis but identically handled monomer crystals repeatedly failed to give the same ratios for this peak area to that of the internal standard. Figure 2-8 shows the IR spectra for the 0, 20, 40, 60, 80 and 100% conversion points on the curve.

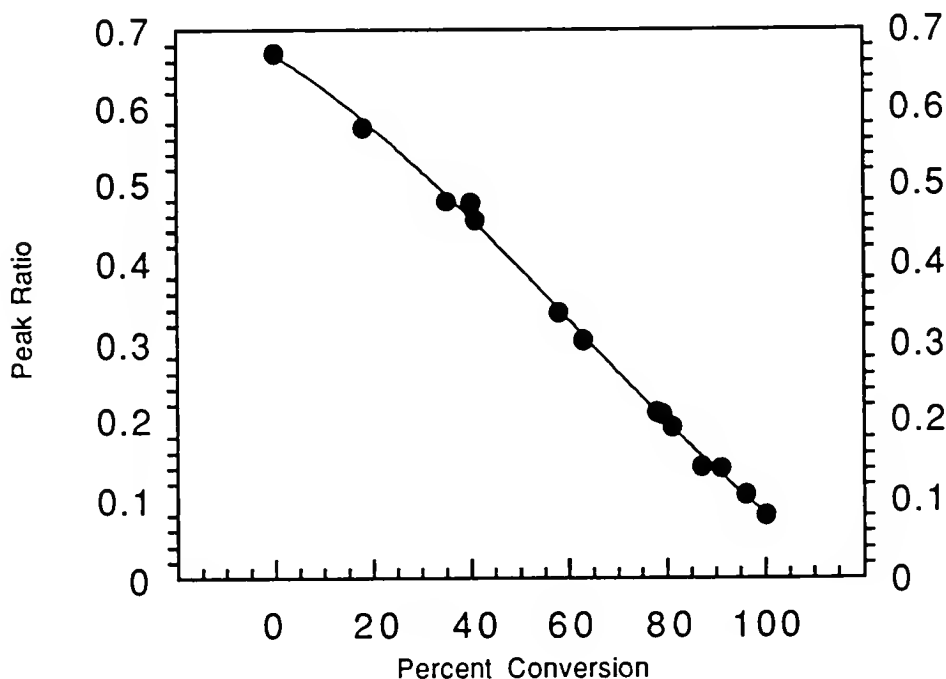


Figure 2-7. Calibration curve for IR analysis of single-crystal-to-single-crystal conversion of 1-1c.  $y=0.668-3.84\times10^{-3}-4.60\times10^{-5}+2.58\times10^{-7}$ ,  $r=0.999$ . The peak ratio is the ratio of the C=C-H absorption at 954  $\text{cm}^{-1}$  to the -SO<sub>2</sub>- absorption at 1030  $\text{cm}^{-1}$ .

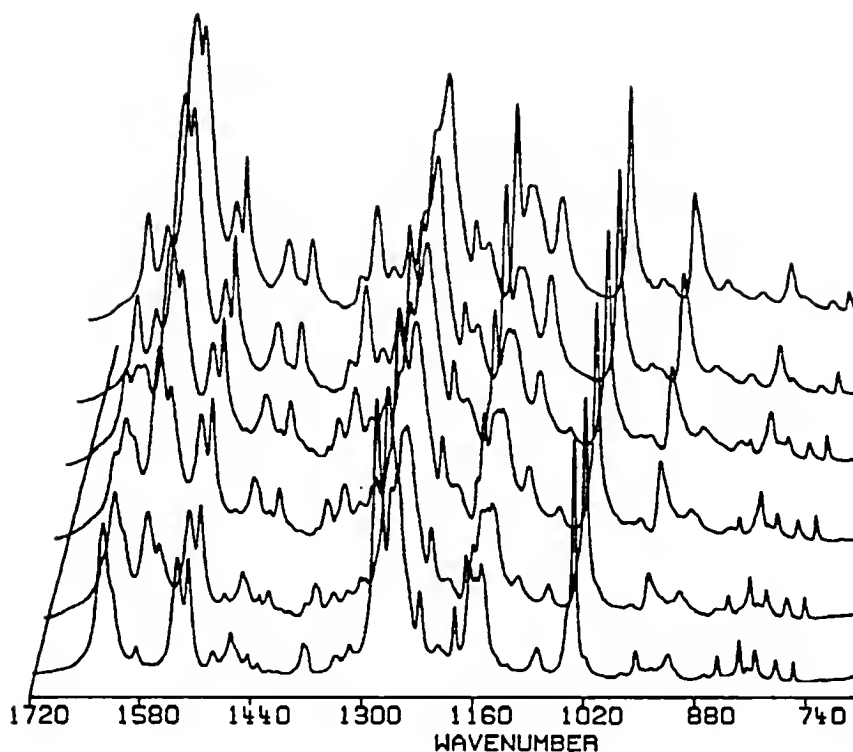


Figure 2-8. Series of IR spectra for the conversion of 1-1c to 1-4c. The rearmost spectrum is 1-1c unirradiated while the foremost spectrum is photodimer 1-4c. The intermediate percent conversions are 20, 40, 60 and 80%.

### Characterization

Selected elemental, infrared, mass spectral and nmr analyses for the compounds in Tables 2-1 - 2-6 are presented in the balance of this chapter as follows. Tables 2-17 through 2-22 list elemental analyses for all the compounds reported in this dissertation. Tables 2-23 through 2-26 present infrared spectral analyses for all the compounds except the methylene-bridged diolefins. Tables 2-27 through 2-28 contain data from the mass spectral analyses of the pzzlium and ammonium salts. Tables 2-29 through 2-33 report the NMR analyses.



Elemental Analyses

The leftmost column is the carbon analysis and the adjacent column is hydrogen.

Table 2-17. Elemental analyses for Table 2-1 compounds

2-4	exp.	31.95	6.30	Cl 26.07	Sn 17.25
	SnCl <sub>5</sub> <sup>-</sup> theo.	33.41	4.61	Cl 35.22	Sn 23.58
	SnCl <sub>6</sub> <sup>2-</sup> theo.	45.08	6.21	Cl 28.51	Sn 15.91
2-5	exp.	30.62	4.21	Cl 26.22	Au 36.35
	AuCl <sub>2</sub> <sup>-</sup> theo.	35.39	4.88	Cl 14.92	Au 41.45
	AuCl <sub>4</sub> <sup>-</sup> theo.	30.76	4.21	Cl 26.00	Au 36.07

2-6	exp.	37.86	5.11	F 25.46	Sb 27.70
	theo.	37.95	5.23	F 25.73	Sb 27.48

Table 2-18. Elemental analyses for Table 2-2 compounds

2-7	exp.	70.83	5.29	2-10	exp.	73.42	6.96
	theo.	71.10	5.22		theo.	73.60	6.79
2-8	exp.	55.25	4.41	2-11	exp.	75.20	7.92
	theo.	71.82	5.67		theo.	75.36	7.91
2-9	exp.	72.25	6.16				
	theo.	72.47	6.08				

Table 2-19. Elemental analyses for Table 2-3 compounds

2-12	exp.	64.02	6.99	F 18.22	B 2.80				
	theo.	64.09	7.09	F 18.43	B 2.62				
2-13	exp.	45.79	5.06	Re 32.45	2-14	exp.	62.28	6.87	Cl 8.34
	theo.	45.90	5.08	Re32.35		theo.	62.19	6.88	Cl 8.34
2-15	exp.	44.08	4.93	Cl 23.25	Sn 19.60				
	SnCl <sub>5</sub> <sup>-</sup> theo.	42.52	4.70	Cl 38.53	Sn 19.10				
	SnCl <sub>6</sub> <sup>2-</sup> theo.	53.80	5.95	Cl 21.65	Sn 12.08				
2-16	exp.	42.06	4.67	Cl 19.97	Au 28.30				
	AuCl <sub>2</sub> <sup>-</sup> theo.	44.53	4.93	Cl 11.95	Au 33.20				
	AuCl <sub>4</sub> <sup>-</sup> theo.	39.76	4.37	Cl 21.39	Au 29.67				
2-17	exp.	47.23	5.11	F 20.23	Sb 21.75				
	theo.	47.08	5.21	F 20.31	Sb 21.69				

Table 2-20. Elemental analyses for Table 2-4 compounds

2-18 $\text{BF}_4^{-1}$	exp.	59.25	6.37	2-20 $\text{ClO}_4^{-1}$	exp.	55.37	5.96	Cl 8.71
	theo.	63.00	7.05		theo.	60.76	6.80	Cl 9.96
2-19 $\text{ReO}_4^{-1}$	exp.	41.60	4.69	2-21 Triflate	exp.	56.07	5.87	F=13.83 S=7.75
	theo.	42.68	4.78		theo.	56.29	5.97	F=14.06 S=7.91

Table 2-21. Elemental analyses for Table 2-5 compounds

2-22	exp.	63.40	6.57	2-33	exp.	58.41	6.14
	theo.	64.25	6.86		theo.	59.12	6.20
2-23	exp.	43.95	4.57	2-34	exp.	64.44	7.03
	theo.	45.98	4.91		theo.	65.62	7.34
2-24	exp.	61.17	6.30	2-35	exp.	47.38	5.35
	theo.	62.33	6.66		theo.	47.83	5.35
2-28	exp.	61.74	6.43	2-36	exp.	63.33	6.85
	theo.	62.71	6.78		theo.	63.78	7.14
2-29	exp.	51.86	5.08	2-38	exp.	66.04	7.45
	theo.	58.74	6.08		theo.	66.82	7.76
2-30	exp.	62.96	6.67	2-39	exp.	48.66	5.47
	theo.	64.96	6.99		theo.	49.51	5.75
2-31	exp.	46.65	5.07	2-40	exp.	64.46	7.39
	theo.	46.93	5.14		theo.	65.06	7.56

Table 2-22. Elemental analyses for Table 2-6 compounds

2-42	exp.	68.91	6.79	7.25	2-48	exp.	75.76	7.15	5.10
	theo.	69.09	6.85	7.32		theo.	75.81	7.11	5.20
2-43	exp.	68.24	8.31	5.75	2-49	exp.	71.61	8.86	5.86
	theo.	72.07	8.21	6.00		theo.	71.46	8.99	5.95
2-44	exp.	75.36	6.74	5.46	2-50	exp.	65.02	6.83	6.26
	theo.	75.27	6.71	5.49		theo.	65.14	6.83	6.33
2-45	exp.	70.58	8.55	6.24	2-51	exp.	65.60	7.76	4.66
	theo.	70.56	8.65	6.33		theo.	68.42	8.04	5.32
2-46	exp.	70.06	7.32	6.73	2-52	exp.	71.46	6.76	4.78
	theo.	70.22	7.37	6.82		theo.	71.56	6.71	4.91
2-47	exp.	69.34	8.46	5.14	2-53	exp.	66.78	8.34	5.47
	theo.	72.84	8.56	5.66		theo.	66.91	8.42	5.57

## Infrared Analyses

Many of the following IR analyses were performed by Frau Elke Muth at the Max-Planck-Institut-für Polymerforschung.

### Ammonium salts of cinnamic acids (Table 2-6)

On making the ammonium salt from the free acid, the shifts listed in Table 2-23 are observed.

Table 2-23. Prominent shifts in the IR absorption spectra of cinnamic acid ammonium salts compared to the free acid.

#### cinnamic acid

C=O shifts from	to	C=C shifts from	to
2-45	1680	1529	1381
2-44		1530	1355
2-43		1548	1376
2-42		1534	1379
		1628	1643
			1639
			1639
			1641

#### p-methoxy-cinnamic acid

C=O shifts from	to	C=C shifts from	to
2-53	1686	1532/1513	1381
2-52		1512	1383/1373
2-51		1562	1401
2-50		1511	1374
		1624/1598	1641
			1643
			1637
			1640

#### p-methyl-cinnamic acid

C=O shifts from	to	C=C shifts from	to
2-49	1681	1530	1361
2-48		≈1530/1500	1360
2-47		1555	1374
2-46		1512/1490	1372
		1622/1605	1643
			1641
			1641
			1642

All the ammonium salts of the p-methoxy cinnamic acid also shows an absorption at  $1605\text{ cm}^{-1}$ . The ammonium salts of the primary amines, benzyl amine and t-butyl amine, each show absorption at approximately  $2200\text{ cm}^{-1}$ .

Table 2-24 lists the strongest IR absorption bands for the cinnamic acids and their ammonium salts (Table 2-6).

Table 2-24. IR absorption bands for cinnamic acid ammonium salts (Table 2-6)  
 The numbers listed are wavenumbers and have the units  $\text{cm}^{-1}$ . The absorptions are arranged in columns with the use of italics for easier comparison.

<b>cinnamic acid</b>		1577	1494	1449	1313	1284		1222	1098/1072
	979	943	875	846		768	709	682	588 541
<b>2-45</b>			1497	1450		1285	1250	1228	1073
	994 968			883		775	717	689	584 534
<b>2-44</b>		1577	1496	1450	1324	1286	1249		1102/1071
	991 964			882	847	778	718	690	586 535
<b>2-43</b>			1495	1447			1247		1087/1072
	1034 979	953	879	841		774	724	685	585 532
<b>2-42</b>			1494	1446	1313	1295	1248		1095/1073
	1032 980	963	880	844		776	721	687	584 537
<b>p-methoxy cinnamic acid</b>		1429	1314	1255			1171	1028	
	975	944	828	773			566	528	
<b>2-53</b>		1607	1422	1306	1257/1242		1174	1030	
	983/974		832	775		705	555		
<b>2-52</b>		1606	1418	1302	~1255		1170	1025	
	993/970	934	835	775	728	705	552		
<b>2-51</b>		1607	1424	1305	1258/1239		1174	1032	
	977		825	774		710	553		
<b>2-50</b>		1605	1419	1305	1251/1241		1173	1038	1009
	983/964		829	776		706	554		
<b>p-methyl cinnamic acid</b>		1511	1421	1311	1284	1222	1176	1115	1040
	941	877	812	771	735	685	547		988
<b>2-48</b>		1453	1284	1251	1220	1175	1116	1069	982
	966	897 884		814		752	704	542	
<b>2-49</b>			1284	1249	1225	1180	1117		990
	968	883	854	817	778	742	705	544	
<b>2-46</b>		1313	1292	1254		1182	1096	1033	1010 987
	961	885	854	818	774	741	706	540	
<b>2-47</b>	1512		1283	1250		1178	1083	1033	987
	952	883		817	775	740	705	551	

Compound 2-50 has a prominent absorption at  $620\text{ cm}^{-1}$ .  $\alpha$ -trans-Cinnamic acid has a prominent absorption at  $1419\text{ cm}^{-1}$ , not seen in its ammonium salts. 2-42 has a prominent absorption at  $622\text{ cm}^{-1}$ . p-Methyl cinnamic acid has a prominent absorption at  $1421\text{ cm}^{-1}$ , not seen in its ammonium salts. 2-46 has a prominent absorption at  $621\text{ cm}^{-1}$ .

### Pyrylium and styrylpyrylium salts

Table 2-25 is grouped by counterion. Pyrylium salts, p-methoxy-styrylpyrylium salts and selected Hasegawa-type diolefins were subjected to analysis. The counterion is indicated and the compound number is underlined. The strongest absorption bands are listed as wavenumbers in units of  $\text{cm}^{-1}$  and have been arranged roughly in columns for easier comparison. Bands due to counterions as well as double bonds have been indicated. In each of the p-methoxy-substituted compounds, a C-O-C aromatic ether absorption around  $1022\text{ cm}^{-1}$  (in the case of 2-16, the gold-containing counterion it is at  $1036\text{ cm}^{-1}$ ) can be seen except for the compounds with a triflate counterion. In these cases the  $-\text{SO}_2$ -absorption falls in this region.

Table 2-25. IR absorption bands for pyrylium and styrylpyrylium salts. The numbers listed are wavenumbers and have the units  $\text{cm}^{-1}$ . The absorptions are arranged in columns with the use of italics for easier comparison.

---

ReO<sub>4</sub><sup>-</sup>

2-2

3050	2974	2873	1633						
1538	1498	1463	1445	1369	1241	1200			1036

910 (ReO<sub>4</sub><sup>-</sup>)

2-13

3064	2976	2841	1638	1613					
1525	1514	1459	1428	1366	1311	1256	1174	1113	1022
	981	949	831		528				

900 (ReO<sub>4</sub><sup>-</sup>) 1588 1567 (C=C)

photodimer 2-13b

3051	2974	2837	1623						
1527	1514	1462	1431	1368	1306	1255	1176	1117	1032

450

909 (ReO<sub>4</sub><sup>-</sup>)

Table 2-25--continued.

---

 $\text{BF}_4^-$  $\boxed{2-1}$ 

3065	2982	2882	1633							
1538	1499	1469	1452	1373	1244	1201			1097	1034

1052 ( $\text{BF}_4^-$ ) $\boxed{2-12}$ 

3071	2975	2846		1615						
1530	1515	1462	1429	1370	1312	1258	1176	1118		1025
	978	949	830		521					

1058 ( $\text{BF}_4^-$ ) 1589 1568 (C=C) $\boxed{\text{photodimer 2-12b}}$ 

	2973	2842	1626							
		1464		1370		1251	1180			1033
	450									

1057 ( $\text{BF}_4^-$ )

---

 $\text{ClO}_4^-$  $\boxed{2-3}$ 

3061	2980	2880	1631							
1536	1500	1467	1449	1372		1244	1200			

622 1092 ( $\text{ClO}_4^-$ ) $\boxed{2-14}$ 

3070	2975	2844	1640	1614						
1529	1515	1460	1429	1367	1312	1257	1176	1118	1097	1022
	977	949	831		521					

622 1081 ( $\text{ClO}_4^-$ ) 1589 1568 (C=C) $\boxed{2-20}$ 

	2976	2875	1638							
1526		1463	1428		1313	1369				
			949							

623 1595 (C=C) miscellaneous bands: 1781, 1741, 1556, 690

---

 $\text{CF}_3\text{SO}_3^-$  $\boxed{2-21}$ 

3059	2975	2875	1642							
1529			1429		1313	1262		1122		
			954			517				
			1556	1351	1278	1220	1156	1029 (-SO <sub>2</sub> -)	636	

1608 (C=C)

 $\boxed{1-1c}$ 

			1639	1615						
1528	1515	1460	1430	1350	1309	1259	1174	1116		
			950							

1294 1155 1030 (-SO<sub>2</sub>-) 638

1579 1568 (C=C)

Table 2-25--continued.

---

SbF<sub>6</sub><sup>-1</sup>

2-6

3099	2983	2880	1633						
1536	1497	1465		1374	1238	1198			1034
	874								

658 (SbF<sub>6</sub><sup>-</sup>)

2-17

	2978	2875	1641	(2845)					
1522	1516	1462	1431	1306		1264	1175	1109	1024
	979	946	836		527				

658 (SbF<sub>6</sub><sup>-</sup>)

1580 1556 (C=C)

---

SnCl<sub>6</sub><sup>=</sup>

2-4

3048	2971	2870	1629						
1533	1491	1461	1448	1372	1240	1200			1030

SnCl<sub>5</sub><sup>-</sup>

2-15

3064	2973	2871	1638	1615	(2837	1693)			
1529	1514	1463	1429	1307		1261	1172	1113	1025
	983	947	836		523				

1583 1567 (C=C)

---

AuCl<sub>4</sub><sup>-</sup>

2-5

3048	2971	2870	1629						
1533	1491	1461	1448	1372	1240	1200			1030

AuCl<sub>2</sub><sup>-</sup>

2-16

	2973	2871	1641	(2837)					
1537	1486	1460	1442	1368	1314	1258	1173	1116	1036
		949	852		528				

1588 1563 (C=C)

Methylene-bridged dialdehydes (Table 2-2)

Table 2-26. IR absorption bands for methylene-bridged dialdehydes 2-7 - 2-11. Note that the data in Table 2-26 are not arranged in a columnar fashion, rather they are simply listed as wavenumbers, in units of  $\text{cm}^{-1}$ .

2-7:	3046 1508	2954 1247	2943 1222	2922 1212	2852 1156	2810 832	2758 655	1697 625	1681	1601	1579
2-8:	3074 1265	2952 1247	2882 1215	2842 1159	2810 1049	2756 828	1696 616	1601	1580	1510	1314
2-9:	3040 1248	2956 1216	2933 1155	2888 1045	2861 972	2843 833	2757 651	1683	1605	1577	1509
2-10:	3071 1214	2945 1156	2916 1010	2855 833	2842 614	2805	2755	1687	1598	1309	1255
2-11	3052 1155	2942 836	2922 615	2870	2852	2737	1687	1596	1316	1274	1265

Mass Spectral Analyses

Mass spectra were obtained using a Varian MAT 7A with EI ionization (70 eV) for compounds in Tables 2-1 and 2-6. The compound number is underlined and the mass to charge ratio listed with the intensity of the peak relative to the base peak:  $m/z$  (rel. int., %).

Table 2-27. Mass spectral analyses for pyrylium salts (Table 2-1)

2-2

206.20 ( $M^+$ -HReO<sub>4</sub>, 100), 191.17 (40.29,  $M^+$ -CH<sub>3</sub>), 91.11 (15.29,  $M^+$ -2xtBu), 57.18 (34.47, -tBu)

2-3

206.00 ( $M^+$ -HClO<sub>4</sub>, 100), 191.17 (39.88), 91.00 (14.14), 57.00 (41.67)

2-1

206.20 ( $M^+$ -HBF<sub>4</sub>, 100) 191.00 (41.67), 91.00 (12.21), 57.18 (37.07)

2-6

206.19 ( $M^+$ -HSbF<sub>6</sub>, 100), 191.14 (44.87,  $M^+$ -CH<sub>3</sub>), 169.12 (26.28), 105.06 (9.78), 91.09 (10.82,  $M^+$ -2xtBu), 69.12 (10.98), 57.16 (29.17, -tBu)

2-4

206.17 ( $M^+$ -H<sub>2</sub>SnCl<sub>6</sub>, 100), 191.13 (42.21,  $M^+$ -CH<sub>3</sub>), 91.08 (10.76  $M^+$ -2xtBu), 69.09 (11.68), 57.16 (29.51, -tBu)

2-5

276.12 (24.22), 274.11 (38.02), 240.13 (30.21), 206.14 ( $M^+$ -HAuCl<sub>2</sub> 41.41), 191.17 (19.53,  $M^+$ -CH<sub>3</sub>), 91.03 (19.01  $M^+$ -2xtBu), 69.08 (30.47), 57.17 (100, -tBu)



Table 2-28. Mass spectral analyses for ammonium salts of cinnamic acids (Table 2-6)

2-45

148.00 ( $M^*$  -  $\text{NH}_2\text{tBu}$ , 71.55), 147.00 ( $M^*$  -  $\text{NH}_3^+\text{tBu}$ , 100), 103.00 (148 -  $\text{CO}_2\text{H}$ ),  
 91.00 (20.47), 77.00 (34.27, Ph), 51.00 (32.33)  
 58.00 ( $\text{NH}_2\text{tBu}$  -  $\text{CH}_3$ , 76.72)

2-44

148.00 ( $M^*$  -  $\text{NH}_2\text{CH}_2\text{Ph}$ , 50.82), 147.00 ( $M^*$  -  $\text{NH}_3^+\text{CH}_2\text{Ph}$ , 71.43), 103.00 (35.99),  
 91.00 (30.22), 77.00 (42.31), 51.00 (33.24)  
 107.00 (59.62,  $\text{NH}_2\text{CH}_2\text{Ph}$ ), 106.00 (100)

2-43

148.00 ( $M^*$  -  $\text{NH}_2\text{C}_5\text{H}_{10}$ , 70.35), 147.00 ( $M^*$  -  $\text{NH}_3^+\text{C}_5\text{H}_{10}$ , 100), 103.00 (48.84),  
 91.00 (23.11), 77.00 (35.47), 51.00 (32.41)  
 84.00 ( $\text{NH}_2\text{C}_5\text{H}_{10}$ , 90.12), 57.00 (21.80), 56.00 (84.00 -  $\text{C}_2\text{H}_4$ , 29.65)

2-42

148.00 ( $M^*$  -  $\text{NH}_2\text{C}_4\text{H}_8\text{NH}_2$ , 70.43), 147.00 ( $M^*$  -  $\text{NH}_3^+\text{C}_4\text{H}_8\text{NH}_3^+$ , 100), 103.00  
 (47.17), 91.00 (24.13), 77.00 (39.57), 51.00 (35.22)  
 44.00 ( $\text{NH}_2\text{C}_2\text{H}_4$ , 37.61)

2-49

162 ( $M^*$  -  $\text{NH}_2\text{tBu}$ , 52.31), 161 ( $M^*$  -  $\text{NH}_3^+\text{tBu}$ , 31.54), 147 (162- $\text{CH}_3$ , 22.69), 115  
 (33.27), 91.00 (19.62)  
 58.00 ( $\text{NH}_2\text{tBu}$  -  $\text{CH}_3$ , 100)

2-48

162 ( $M^*$  -  $\text{NH}_2\text{CH}_2\text{Ph}$ , 33.23), 161.00 ( $M^*$  -  $\text{NH}_3^+\text{CH}_2\text{Ph}$ , 19.94), 147 (15.43), 115  
 (20.57), 91.00 (24.37)  
 107 (56.96,  $\text{NH}_2\text{CH}_2\text{Ph}$ ), 106.00 (100),

2-47

162.00 ( $M^*$  -  $\text{NH}_2\text{C}_5\text{H}_{10}$ , 64.47), 161.00 ( $M^*$  -  $\text{NH}_3^+\text{C}_5\text{H}_{10}$ , 40.10), 147.00 (30.08),  
 115 (45.69), 91.00 (26.65)  
 84 ( $\text{NH}_2\text{C}_5\text{H}_{10}$ , 100), 57.00 (27.41), 56.00 (84 -  $\text{C}_2\text{H}_4$ , 32.99)

2-46

162.00 ( $M^*$  -  $\text{NH}_2\text{C}_4\text{H}_8\text{NH}_2$ , 100), 161.00 ( $M^*$  -  $\text{NH}_3^+\text{C}_4\text{H}_8\text{NH}_3^+$ , 63.36), 147.00  
 (47.52), 115.00 (74.81), 91.00 (24.13)  
 44.00 ( $\text{NH}_2\text{C}_2\text{H}_4$ , 51.91)

2-53

178.00 ( $M^*$  -  $\text{NH}_2\text{tBu}$ , 38.07), 177.0 ( $M^*$  -  $\text{NH}_3^+\text{tBu}$ , 12.27), 161.00 (14.11), 89.00  
 (12.56), 77.00 (12.84), 63.00 (11.35)  
 58.00 ( $\text{NH}_2\text{tBu}$  -  $\text{CH}_3$ , 100)

2-52

178.00 ( $M^*$  -  $\text{NH}_2\text{tBu}$ , 49.65), 177.0 ( $M^*$  -  $\text{NH}_3^+\text{tBu}$ , 14.96), 161.00 (17.25), 89.00  
 (17.08), 77.00 (36.97), 63.00 (14.26)  
 107 (63.03,  $\text{NH}_2\text{CH}_2\text{Ph}$ ), 106.00 (100),

2-51

178.00 ( $M^*$  -  $\text{NH}_2\text{tBu}$ , 100), 177.0 ( $M^*$  -  $\text{NH}_3^+\text{tBu}$ , 31.08), 161.00 (44.14), 89.00  
 (21.28), 77.00 (15.77), 63.00 (11.71)  
 84.00 ( $\text{NH}_2\text{C}_5\text{H}_{10}$ , 19.26)

2-50

178.00 ( $M^*$  -  $\text{NH}_2\text{tBu}$ , 100), 177.0 ( $M^*$  -  $\text{NH}_3^+\text{tBu}$ , 29.69), 161.00 (33.33), 89.00  
 (21.61), 77.00 (21.09), 63.00 (16.67)  
 44.00 ( $\text{NH}_2\text{C}_2\text{H}_4$ , 30.21)

NMR Analyses

Table 2-29. NMR analyses of pyrylium salts (Table 2-1)

Proton-CDCl<sub>3</sub>

2-6

1.492 (s; 18H, C<sub>4</sub>H<sub>9</sub>), 2.759 (s; 3H, -CH<sub>3</sub>), 7.683 (s; 2H, pyrylium ring-H)

2-3

1.492 (s; 18H, C<sub>4</sub>H<sub>9</sub>), 2.773 (s; 3H, -CH<sub>3</sub>), 7.716 (s; 2H, pyrylium ring-H)

2-1

1.487 (s; 18H, C<sub>4</sub>H<sub>9</sub>), 2.760 (s; 3H, -CH<sub>3</sub>), 7.715 (s; 2H, pyrylium ring-H)

2-4

1.495 (s; 18H, C<sub>4</sub>H<sub>9</sub>), 2.889 (s; 3H, -CH<sub>3</sub>), 7.781 (s; 2H, pyrylium ring-H)

2-5

1.543 (s; 18H, C<sub>4</sub>H<sub>9</sub>), 2.760 (s; 3H, -CH<sub>3</sub>), 7.715 (s; 2H, pyrylium ring-H)

2-2

1.509 (s; 18H, C<sub>4</sub>H<sub>9</sub>), 2.800 (s; 3H, -CH<sub>3</sub>), 7.747 (s; 2H, pyrylium ring-H)Carbon CDCl<sub>3</sub>

2-5

25.08 (-CH<sub>3</sub>), 28.15 (-C(CH<sub>3</sub>)<sub>3</sub>), 39.23 (-C(CH<sub>3</sub>)<sub>3</sub>), 120.53 (pyrylium ring C-H), 176.55 (pyrylium ring C-CH<sub>3</sub>), 186.90 (pyrylium ring C-tBu)

2-4

24.62 (-CH<sub>3</sub>), 27.84 (-C(CH<sub>3</sub>)<sub>3</sub>), 39.05 (-C(CH<sub>3</sub>)<sub>3</sub>), 120.09 (pyrylium ring C-H), 176.78 (pyrylium ring C-CH<sub>3</sub>), 186.85 (pyrylium ring C-tBu)

2-1

24.00 (-CH<sub>3</sub>), 27.68 (-C(CH<sub>3</sub>)<sub>3</sub>), 39.04 (-C(CH<sub>3</sub>)<sub>3</sub>), 119.91 (pyrylium ring C-H), 176.77 (pyrylium ring C-CH<sub>3</sub>), 187.10 (pyrylium ring C-tBu)

2-3

24.10 (-CH<sub>3</sub>), 27.73 (-C(CH<sub>3</sub>)<sub>3</sub>), 39.07 (-C(CH<sub>3</sub>)<sub>3</sub>), 119.97 (pyrylium ring C-H), 176.69 (pyrylium ring C-CH<sub>3</sub>), 187.04 (pyrylium ring C-tBu)

2-6

24.05 (-CH<sub>3</sub>), 27.73 (-C(CH<sub>3</sub>)<sub>3</sub>), 39.05 (-C(CH<sub>3</sub>)<sub>3</sub>), 119.92 (pyrylium ring C-H), 176.81 (pyrylium ring C-CH<sub>3</sub>), 186.97 (pyrylium ring C-tBu)

2-2

24.12 (-CH<sub>3</sub>), 27.77 (-C(CH<sub>3</sub>)<sub>3</sub>), 39.18 (-C(CH<sub>3</sub>)<sub>3</sub>), 119.83 (pyrylium ring C-H), 176.65 (pyrylium ring C-CH<sub>3</sub>), 187.42 (pyrylium ring C-tBu)

Table 2-30. NMR analyses of p-methoxy styrylpyrylium salts (Table 2-3)

Proton-CDCl<sub>3</sub>/CF<sub>3</sub>CO<sub>2</sub>H

2-16

1.527 (s; 18H, C<sub>4</sub>H<sub>9</sub>), 3.942(s; 3H, -OCH<sub>3</sub>), AA' BB' -signal ( $\delta_A=7.047$   $\delta_B=7.811$  4H, C<sub>6</sub>H<sub>4</sub>), 7.636 (s, 2H, pyrylium -H), AB-signal ( $\delta_A=7.21$   $\delta_B=8.18$ , J<sub>AB</sub>=16Hz; 2H, ethylene-H)

2-12

1.493 (s; 18H, C<sub>4</sub>H<sub>9</sub>), 3.921(s; 3H, -OCH<sub>3</sub>), AA' BB' -signal ( $\delta_A=7.028$   $\delta_B=7.753$  4H, C<sub>6</sub>H<sub>4</sub>), 7.597 (s, 2H, pyrylium -H), AB-signal ( $\delta_A=7.153$   $\delta_B=8.118$ , J<sub>AB</sub>=16Hz; 2H, ethylene-H)

photodimer, 2-12b

Table 2-30--continued.

1.348 (s; 18H, C<sub>4</sub>H<sub>9</sub>), 3.794(s; 3H, -OCH<sub>3</sub>), AA' BB' -signal ( $\delta_A=7.271$   $\delta_B=6.872$  4H, C<sub>6</sub>H<sub>4</sub>), 7.644 (s, 2H, pyrylium -H), 5.06 (m; 4H, cyclobutane ring-H)

## 2-14

1.492 (s; 18H, C<sub>4</sub>H<sub>9</sub>), 3.914(s; 3H, -OCH<sub>3</sub>), AA' BB' -signal ( $\delta_A=7.018$   $\delta_B=7.764$  4H, C<sub>6</sub>H<sub>4</sub>), 7.609 (s, 2H, pyrylium -H), AB-signal ( $\delta_A=7.166$   $\delta_B=8.125$ , J<sub>AB</sub>=16Hz; 2H, ethylene-H)  
photodimer, 2-14b

1.352 (s; 18H, C<sub>4</sub>H<sub>9</sub>), 3.795(s; 3H, -OCH<sub>3</sub>), AA' BB' -signal ( $\delta_A=7.304$   $\delta_B=6.880$  4H, C<sub>6</sub>H<sub>4</sub>), 7.632 (s, 2H, pyrylium -H), 5.110 (m; 4H, cyclobutane ring-H)

## 2-17

1.490 (s; 18H, C<sub>4</sub>H<sub>9</sub>), 3.919(s; 3H, -OCH<sub>3</sub>), AA' BB' -signal ( $\delta_A=7.019$   $\delta_B=7.764$  4H, C<sub>6</sub>H<sub>4</sub>), 7.598 (s, 2H, pyrylium -H), AB-signal ( $\delta_A=7.156$   $\delta_B=8.097$ , J<sub>AB</sub>=16Hz; 2H, ethylene-H)

## 2-13

1.502 (s; 18H, C<sub>4</sub>H<sub>9</sub>), 3.926(s; 3H, -OCH<sub>3</sub>), AA' BB' -signal ( $\delta_A=7.039$   $\delta_B=7.748$  4H, C<sub>6</sub>H<sub>4</sub>), 7.589 (s, 2H, pyrylium -H), AB-signal ( $\delta_A=7.138$   $\delta_B=8.128$ , J<sub>AB</sub>=16Hz; 2H, ethylene-H)  
photodimer, 2-13b

1.348 (s; 18H, C<sub>4</sub>H<sub>9</sub>), 3.794(s; 3H, -OCH<sub>3</sub>), AA' BB' -signal ( $\delta_A=7.242$   $\delta_B=6.908$  4H, C<sub>6</sub>H<sub>4</sub>), 7.589 (s, 2H, pyrylium -H), 5.06 (m; 4H, cyclobutane ring-H)

## 2-15

1.508 (s; 18H, C<sub>4</sub>H<sub>9</sub>), 3.922(s; 3H, -OCH<sub>3</sub>), AA' BB' -signal ( $\delta_A=7.027$   $\delta_B=7.806$  4H, C<sub>6</sub>H<sub>4</sub>), 7.611 (s, 2H, pyrylium -H), AB-signal ( $\delta_A=7.194$   $\delta_B=8.131$ , J<sub>AB</sub>=16Hz; 2H, ethylene-H)  
photodimer, 2-15b

1.362 (s; 18H, C<sub>4</sub>H<sub>9</sub>), 3.824(s; 3H, -OCH<sub>3</sub>), AA' BB' -signal ( $\delta_A=7.242$   $\delta_B=6.598$  4H, C<sub>6</sub>H<sub>4</sub>), 7.544 (s, 2H, pyrylium -H), 5.160 (m; 4H, cyclobutane ring-H)

Carbon-CDCl<sub>3</sub>/CF<sub>3</sub>CO<sub>2</sub>H

## 2-13

27.80 (-C(CH<sub>3</sub>)<sub>3</sub>), 38.70 (-C(CH<sub>3</sub>)<sub>3</sub>), 55.84 (-OCH<sub>3</sub>), 112.36 (pyrylium ring C-H), 115.70 (phenyl ring C-H), 119.73 (ethylene CH), 127.19 (phenyl C-OMe), 133.10 (phenyl ring C-H), 151.99 (ethylene CH), 164.64 (phenyl ring C-CH=), 164.85 (pyrylium ring C-CH=), 184.36 (pyrylium ring C-tBu)

## photodimer of 2-13

27.57 (-C(CH<sub>3</sub>)<sub>3</sub>), 39.25 (-C(CH<sub>3</sub>)<sub>3</sub>), 46.68, 49.23 (cyclobutane ring C), 55.82 (-OCH<sub>3</sub>), 115.29 (pyrylium ring C-H), 118.46 (phenyl ring C-H), 128.64 (phenyl C-OMe), 129.45 (phenyl ring C-H), 159.12 (phenyl ring C-CH=), 176.31 (pyrylium ring C-CH=), 187.23 (pyrylium ring C-tBu)

## 2-15

27.95 (-C(CH<sub>3</sub>)<sub>3</sub>), 38.71 (-C(CH<sub>3</sub>)<sub>3</sub>), 55.89 (-OCH<sub>3</sub>), 112.72 (pyrylium ring C-H), 115.59 (phenyl ring C-H), 120.20 (ethylene CH), 127.39 (phenyl C-OMe), 133.31

Table 2-30--continued.

(phenyl ring C-H), 151.90 (ethylene CH), 164.64 (phenyl ring C-CH=), 164.85 (pyrylium ring C-CH=), 184.18 (pyrylium ring C-tBu)  
 photodimer, 2-15b  
 27.79 (-C(CH<sub>3</sub>)<sub>3</sub>), 39.27 (-C(CH<sub>3</sub>)<sub>3</sub>), 46.68, 49.31 (cyclobutane ring C), 55.89 (-OCH<sub>3</sub>), 115.37 (pyrylium ring C-H), 118.76 (phenyl ring C-H), 129.0 (phenyl C-OMe), 130.24 (phenyl ring C-H), 159.1 (phenyl ring C-CH=), 176.5 (pyrylium ring C-CH=), 186.92 (pyrylium ring C-tBu)

2-14

27.79 (-C(CH<sub>3</sub>)<sub>3</sub>), 38.67 (-C(CH<sub>3</sub>)<sub>3</sub>), 55.80 (-OCH<sub>3</sub>), 112.64 (pyrylium ring C-H), 115.54 (phenyl ring C-H), 120.07 (ethylene CH), 127.40 (phenyl C-OMe), 133.06 (phenyl ring C-H), 151.76 (ethylene CH), 164.57 (phenyl ring C-CH=), 164.96 (pyrylium ring C-CH=), 184.22 (pyrylium ring C-tBu)

photodimer, 2-14b

27.56 (-C(CH<sub>3</sub>)<sub>3</sub>), 39.19 (-C(CH<sub>3</sub>)<sub>3</sub>), 48.95, 46.07 (cyclobutane ring C), 55.80 (-OCH<sub>3</sub>), 115.09 (pyrylium ring C-H), 118.66 (phenyl ring C-H), 129.11 (phenyl C-OMe), 129.67 (phenyl ring C-H), 158.72 (phenyl ring C-CH=), 176.68 (pyrylium ring C-CH=), 186.91 (pyrylium ring C-tBu)

2-12

27.76 (-C(CH<sub>3</sub>)<sub>3</sub>), 38.68 (-C(CH<sub>3</sub>)<sub>3</sub>), 55.82 (-OCH<sub>3</sub>), 112.51 (pyrylium ring C-H), 115.61 (phenyl ring C-H), 120.05 (ethylene CH), 127.33 (phenyl C-OMe), 133.06 (phenyl ring C-H), 151.87 (ethylene CH), 164.98 (phenyl ring C-CH=), 164.73 (pyrylium ring C-CH=), 184.33 (pyrylium ring C-tBu)

photodimer, 2-12b

27.50 (-C(CH<sub>3</sub>)<sub>3</sub>), 39.18 (-C(CH<sub>3</sub>)<sub>3</sub>), 45.99, 48.44 (cyclobutane ring C), 55.82 (-OCH<sub>3</sub>), 115.10 (pyrylium ring C-H), 118.61 (phenyl ring C-H), 127.33 (phenyl C-OMe), 129.60 (phenyl ring C-H), 158.75 (phenyl ring C-CH=), 176.9 (pyrylium ring C-CH=), 186.97 (pyrylium ring C-tBu)

2-16

28.06 (-C(CH<sub>3</sub>)<sub>3</sub>), 38.79 (-C(CH<sub>3</sub>)<sub>3</sub>), 55.94 (-OCH<sub>3</sub>), 112.94 (pyrylium ring C-H), 115.68 (phenyl ring C-H), 120.02 (ethylene CH), 127.5 (phenyl C-OMe), 133.37 (phenyl ring C-H), 152.21 (ethylene CH), 164.8 (phenyl ring C-CH=), 164.8 (pyrylium ring C-CH=), 184.13 (pyrylium ring C-tBu)

2-17

27.79 (-C(CH<sub>3</sub>)<sub>3</sub>), 38.68 (-C(CH<sub>3</sub>)<sub>3</sub>), 55.83 (-OCH<sub>3</sub>), 112.50 (pyrylium ring C-H), 115.54 (phenyl ring C-H), 120.19 (ethylene CH), 127.50 (phenyl C-OMe), 133.06 (phenyl ring C-H), 151.60 (ethylene CH), 164.45 (phenyl ring C-CH=), 165.07 (pyrylium ring C-CH=), 184.29 (pyrylium ring C-tBu)

Table 2-31. NMR analyses of styrylpyrylium salts (Table 2-5)

Proton-CDCl<sub>3</sub>/CF<sub>3</sub>CO<sub>2</sub>H

2-22

1.493 (s; 36H, C<sub>4</sub>H<sub>9</sub>), 4.485 (t; 4H, -OCH<sub>2</sub>-), AA' BB' -signal ( $\delta_A=7.060$   $\delta_B=7.758$ H, C<sub>6</sub>H<sub>4</sub>, 9Hz), 7.607 (s, 4H, pyrylium -H), AB-signal ( $\delta_A=7.161$   $\delta_B=8.116$ , J<sub>AB</sub>=16Hz; 4H, ethylene-H)

Table 2-31--continued.

2-24

1.496 (s; 36H, C<sub>4</sub>H<sub>9</sub>), 4.484 (t; 4H, -OCH<sub>2</sub>-), AA' BB' -signal ( $\delta_A=7.054$   $\delta_B=7.768$ H, C<sub>6</sub>H<sub>4</sub>, 9Hz), 7.618 (s, 4H, pyrylium -H), AB-signal ( $\delta_A=7.179$   $\delta_B=8.049$ , J<sub>AB</sub>=16Hz; 4H, ethylene-H)

2-23

1.505 (s; 36H, C<sub>4</sub>H<sub>9</sub>), 4.497 (s; 4H, -OCH<sub>2</sub>-), AA' BB' -signal ( $\delta_A=7.078$   $\delta_B=7.756$ H, C<sub>6</sub>H<sub>4</sub>, 9Hz), 7.601 (s, 4H, pyrylium -H), AB-signal ( $\delta_A=7.153$   $\delta_B=8.127$ , J<sub>AB</sub>=16Hz; 4H, ethylene-H)

2-30

1.489 (s; 36H, C<sub>4</sub>H<sub>9</sub>), 2.036 (t; 4H, methylene-H, alkyl chain), 4.184 (t; 4H, -OCH<sub>2</sub>-), AA' BB' -signal ( $\delta_A=7.003$   $\delta_B=7.745$  8H, C<sub>6</sub>H<sub>4</sub>, 8Hz), 7.585 (s, 4H, pyrylium -H), AB-signal ( $\delta_A=7.147$   $\delta_B=8.118$ , J<sub>AB</sub>=15Hz; 4H, ethylene-H)

2-32

1.492 (s; 36H, C<sub>4</sub>H<sub>9</sub>), 2.037 (t; 4H, methylene-H, alkyl chain), 4.189(t; 4H, -OCH<sub>2</sub>-), AA' BB' -signal ( $\delta_A=6.991$   $\delta_B=7.751$  8H, C<sub>6</sub>H<sub>4</sub>, 9Hz), 7.594 (s, 4H, pyrylium -H), AB-signal ( $\delta_A=7.160$   $\delta_B=8.121$  J<sub>AB</sub>=16Hz; 4H, ethylene-H)

2-31

1.499 (s; 36H, C<sub>4</sub>H<sub>9</sub>), 2.044 (t; 4H, methylene-H, alkyl chain), 4.190 (t; 4H, -OCH<sub>2</sub>-), AA' BB' -signal ( $\delta_A=7.020$   $\delta_B=7.740$  8H, C<sub>6</sub>H<sub>4</sub>, 8Hz), 7.579 (s, 4H, pyrylium -H), AB-signal ( $\delta_A=7.133$   $\delta_B=8.127$ , J<sub>AB</sub>=16Hz; 4H, ethylene-H)

2-33

1.491 (s; 36H, C<sub>4</sub>H<sub>9</sub>), 2.042 (t; 4H, methylene-H, alkyl chain), 4.186 (t; 4H, -OCH<sub>2</sub>-), AA' BB' -signal ( $\delta_A=7.018$   $\delta_B=7.737$  8H, C<sub>6</sub>H<sub>4</sub>, 9Hz), 7.565 (s, 4H, pyrylium -H), AB-signal ( $\delta_A=7.137$   $\delta_B=8.103$ , J<sub>AB</sub>=16Hz; 4H, ethylene-H)

2-29

1.496 (s; 36H, C<sub>4</sub>H<sub>9</sub>), 2.355 (m; 2H, methylene-H, alkyl chain, 6Hz), 4.305 (t; 4H, -OCH<sub>2</sub>-, 6Hz), AA' BB' -signal ( $\delta_A=7.036$   $\delta_B=7.730$  8H, C<sub>6</sub>H<sub>4</sub>, 9Hz), 7.561 (s, 4H, pyrylium -H), AB-signal ( $\delta_A=7.127$   $\delta_B=8.092$ , J<sub>AB</sub>=16Hz; 4H, ethylene-H)

2-28

1.486 (s; 36H, C<sub>4</sub>H<sub>9</sub>), 2.337 (m; 2H, methylene-H, alkyl chain, 6Hz), 4.294 (t; 4H, -OCH<sub>2</sub>-, 6Hz), AA' BB' -signal ( $\delta_A=7.019$   $\delta_B=7.750$  8H, C<sub>6</sub>H<sub>4</sub>, 9Hz), 7.595 (s, 4H, pyrylium -H), AB-signal ( $\delta_A=7.156$   $\delta_B=8.115$  J<sub>AB</sub>=16Hz; 4H, ethylene-H)

2-34

1.492 (s; 36H, C<sub>4</sub>H<sub>9</sub>), 1.577 (m; 4H, methylene-H, alkyl chain) 1.870 (m; 4H, methylene-H, alkyl chain), 4.128 (t; 4H, -OCH<sub>2</sub>-), AA' BB' -signal ( $\delta_A=7.015$

Table 2-31--continued.

$\delta_B=7.745$  8H, C<sub>6</sub>H<sub>4</sub>), 7.581 (s, 4H, pyrylium -H), AB-signal ( $\delta_A=7.143$   $\delta_B=8.118$ ,  $J_{AB}=16\text{Hz}$ ; 4H, ethylene-H)

2-36

1.491 (s; 36H, C<sub>4</sub>H<sub>9</sub>), 1.564 (m; 4H, methylene-H, alkyl chain) 1.867 (m; 4H, methylene-H, alkyl chain), 4.121 (t; 4H, -OCH<sub>2</sub>-), AA' BB' -signal ( $\delta_A=7.005$   $\delta_B=7.757$  8H, C<sub>6</sub>H<sub>4</sub>), 7.592 (s, 4H, pyrylium -H), AB-signal ( $\delta_A=7.157$   $\delta_B=8.123$ ,  $J_{AB}=16\text{Hz}$ ; 4H, ethylene-H)

2-35

1.500 (s; 36H, C<sub>4</sub>H<sub>9</sub>), 1.514 (m; 4H, methylene-H, alkyl chain) 1.875 (m; 4H, methylene-H, alkyl chain), 4.126 (t; 4H, -OCH<sub>2</sub>-), AA' BB' -signal ( $\delta_A=7.027$   $\delta_B=7.738$  8H, C<sub>6</sub>H<sub>4</sub>), 7.571 (s, 4H, pyrylium -H), AB-signal ( $\delta_A=7.126$   $\delta_B=8.124$ ,  $J_{AB}=16\text{Hz}$ ; 4H, ethylene-H)

2-38

1.345 (m; 12H, methylene-H, alkyl chain), 1.492 (s; 36H, C<sub>4</sub>H<sub>9</sub>), 1.827 (m; 4H, methylene-H, alkyl chain), 4.105 (t; 4H, -OCH<sub>2</sub>-), AA' BB' -signal ( $\delta_A=7.019$   $\delta_B=7.739$  8H, C<sub>6</sub>H<sub>4</sub>), 7.573 (s, 4H, pyrylium -H), AB-signal ( $\delta_A=7.132$   $\delta_B=8.112$ ,  $J_{AB}=16\text{Hz}$ ; 4H, ethylene-H)

2-40

1.350 (m; 12H, methylene-H, alkyl chain), 1.490 (s; 36H, C<sub>4</sub>H<sub>9</sub>), 1.823 (m; 4H, methylene-H, alkyl chain), 4.101 (t; 4H, -OCH<sub>2</sub>-), AA' BB' -signal ( $\delta_A=7.013$   $\delta_B=7.751$  8H, C<sub>6</sub>H<sub>4</sub>), 7.585 (s, 4H, pyrylium -H), AB-signal ( $\delta_A=7.150$   $\delta_B=8.119$ ,  $J_{AB}=16\text{Hz}$ ; 4H, ethylene-H)

2-39

1.371 (m; 12H, methylene-H, alkyl chain), 1.499 (s; 36H, C<sub>4</sub>H<sub>9</sub>), 1.830 (m; 4H, methylene-H, alkyl chain), 4.105 (t; 4H, -OCH<sub>2</sub>-), AA' BB' -signal ( $\delta_A=7.027$   $\delta_B=7.736$  8H, C<sub>6</sub>H<sub>4</sub>), 7.569 (s, 4H, pyrylium -H), AB-signal ( $\delta_A=7.123$   $\delta_B=8.124$ ,  $J_{AB}=16\text{Hz}$ ; 4H, ethylene-H)

Carbon-CDCl<sub>3</sub>/CF<sub>3</sub>CO<sub>2</sub>H

2-22

1.493 (s; 36H, C<sub>4</sub>H<sub>9</sub>), 4.485 (t; 4H, -OCH<sub>2</sub>-), AA' BB' -signal ( $\delta_A=7.060$   $\delta_B=7.758$  8H, C<sub>6</sub>H<sub>4</sub>, 9Hz), 7.607 (s, 4H, pyrylium -H), AB-signal ( $\delta_A=7.161$   $\delta_B=8.116$ ,  $J_{AB}=16\text{Hz}$ ; 4H, ethylene-H)

2-24

1.496 (s; 36H, C<sub>4</sub>H<sub>9</sub>), 4.484 (t; 4H, -OCH<sub>2</sub>-), AA' BB' -signal ( $\delta_A=7.054$   $\delta_B=7.768$  8H, C<sub>6</sub>H<sub>4</sub>, 9Hz), 7.618 (s, 4H, pyrylium -H), AB-signal ( $\delta_A=7.179$   $\delta_B=8.049$ ,  $J_{AB}=16\text{Hz}$ ; 4H, ethylene-H)

Table 2-31--continued.

2-23

1.505 (s; 36H, C<sub>4</sub>H<sub>9</sub>), 4.497 (s; 4H, -OCH<sub>2</sub>-), AA' BB' -signal ( $\delta_A=7.078$   $\delta_B=7.756$ H, C<sub>6</sub>H<sub>4</sub>, 9Hz), 7.601 (s, 4H, pyrylium -H), AB-signal ( $\delta_A=7.153$   $\delta_B=8.127$ , J<sub>AB</sub>=16Hz; 4H, ethylene-H)

2-30

1.489 (s; 36H, C<sub>4</sub>H<sub>9</sub>), 2.036 (t; 4H, methylene-H, alkyl chain), 4.184 (t; 4H, -OCH<sub>2</sub>-), AA' BB' -signal ( $\delta_A=7.003$   $\delta_B=7.745$  8H, C<sub>6</sub>H<sub>4</sub>, 8Hz), 7.585 (s, 4H, pyrylium -H), AB-signal ( $\delta_A=7.147$   $\delta_B=8.118$ , J<sub>AB</sub>=15Hz; 4H, ethylene-H)

2-32

1.492 (s; 36H, C<sub>4</sub>H<sub>9</sub>), 2.037 (t; 4H, methylene-H, alkyl chain), 4.189(t; 4H, -OCH<sub>2</sub>-), AA' BB' -signal ( $\delta_A=6.991$   $\delta_B=7.751$  8H, C<sub>6</sub>H<sub>4</sub>, 9Hz), 7.594 (s, 4H, pyrylium -H), AB-signal ( $\delta_A=7.160$   $\delta_B=8.121$  J<sub>AB</sub>=16Hz; 4H, ethylene-H)

2-31

1.499 (s; 36H, C<sub>4</sub>H<sub>9</sub>), 2.044 (t; 4H, methylene-H, alkyl chain), 4.190 (t; 4H, -OCH<sub>2</sub>-), AA' BB' -signal ( $\delta_A=7.020$   $\delta_B=7.740$  8H, C<sub>6</sub>H<sub>4</sub>, 8Hz), 7.579 (s, 4H, pyrylium -H), AB-signal ( $\delta_A=7.133$   $\delta_B=8.127$ , J<sub>AB</sub>=16Hz; 4H, ethylene-H)

2-33

1.491 (s; 36H, C<sub>4</sub>H<sub>9</sub>), 2.042 (t; 4H, methylene-H, alkyl chain), 4.186 (t; 4H, -OCH<sub>2</sub>-), AA' BB' -signal ( $\delta_A=7.018$   $\delta_B=7.737$  8H, C<sub>6</sub>H<sub>4</sub>, 9Hz), 7.565 (s, 4H, pyrylium -H), AB-signal ( $\delta_A=7.137$   $\delta_B=8.103$ , J<sub>AB</sub>=16Hz; 4H, ethylene-H)

2-29

1.496 (s; 36H, C<sub>4</sub>H<sub>9</sub>), 2.355 (m; 2H, methylene-H, alkyl chain, 6Hz), 4.305 (t; 4H, -OCH<sub>2</sub>-, 6Hz), AA' BB' -signal ( $\delta_A=7.036$   $\delta_B=7.730$  8H, C<sub>6</sub>H<sub>4</sub>, 9Hz), 7.561 (s, 4H, pyrylium -H), AB-signal ( $\delta_A=7.127$   $\delta_B=8.092$ , J<sub>AB</sub>=16Hz; 4H, ethylene-H)

2-28

1.486 (s; 36H, C<sub>4</sub>H<sub>9</sub>), 2.337 (m; 2H, methylene-H, alkyl chain, 6Hz), 4.294 (t; 4H, -OCH<sub>2</sub>-, 6Hz), AA' BB' -signal ( $\delta_A=7.019$   $\delta_B=7.750$  8H, C<sub>6</sub>H<sub>4</sub>, 9Hz), 7.595 (s, 4H, pyrylium -H), AB-signal ( $\delta_A=7.156$   $\delta_B=8.115$  J<sub>AB</sub>=16Hz; 4H, ethylene-H)

2-34

1.492 (s; 36H, C<sub>4</sub>H<sub>9</sub>), 1.577 (m; 4H, methylene-H, alkyl chain) 1.870 (m; 4H, methylene-H, alkyl chain), 4.128 (t; 4H, -OCH<sub>2</sub>-), AA' BB' -signal ( $\delta_A=7.015$   $\delta_B=7.745$  8H, C<sub>6</sub>H<sub>4</sub>), 7.581 (s, 4H, pyrylium -H), AB-signal ( $\delta_A=7.143$   $\delta_B=8.118$ , J<sub>AB</sub>=16Hz; 4H, ethylene-H)

2-36

1.491 (s; 36H, C<sub>4</sub>H<sub>9</sub>), 1.564 (m; 4H, methylene-H, alkyl chain) 1.867 (m; 4H, methylene-H, alkyl chain), 4.121 (t; 4H, -OCH<sub>2</sub>-), AA' BB' -signal ( $\delta_A=7.005$

Table 2-31--continued.

$\delta_B=7.757$  8H, C<sub>6</sub>H<sub>4</sub>), 7.592 (s, 4H, pyrylium -H), AB-signal ( $\delta_A=7.157$   $\delta_B=8.123$   $J_{AB}=16\text{Hz}$ ; 4H, ethylene-H)

2-35

1.500 (s; 36H, C<sub>4</sub>H<sub>9</sub>), 1.514 (m; 4H, methylene-H, alkyl chain) 1.875 (m; 4H, methylene-H, alkyl chain), 4.126 (t; 4H, -OCH<sub>2</sub>-), AA' BB' -signal ( $\delta_A=7.027$   $\delta_B=7.738$  8H, C<sub>6</sub>H<sub>4</sub>), 7.571 (s, 4H, pyrylium -H), AB-signal ( $\delta_A=7.126$   $\delta_B=8.124$ ,  $J_{AB}=16\text{Hz}$ ; 4H, ethylene-H)

2-38

1.345 (m; 12H, methylene-H, alkyl chain), 1.492 (s; 36H, C<sub>4</sub>H<sub>9</sub>), 1.827 (m; 4H, methylene-H, alkyl chain), 4.105 (t; 4H, -OCH<sub>2</sub>-), AA' BB' -signal ( $\delta_A=7.019$   $\delta_B=7.739$  8H, C<sub>6</sub>H<sub>4</sub>), 7.573 (s, 4H, pyrylium -H), AB-signal ( $\delta_A=7.132$   $\delta_B=8.112$ ,  $J_{AB}=16\text{Hz}$ ; 4H, ethylene-H)

2-40

1.350 (m; 12H, methylene-H, alkyl chain), 1.490 (s; 36H, C<sub>4</sub>H<sub>9</sub>), 1.823 (m; 4H, methylene-H, alkyl chain), 4.101 (t; 4H, -OCH<sub>2</sub>-), AA' BB' -signal ( $\delta_A=7.013$   $\delta_B=7.751$  8H, C<sub>6</sub>H<sub>4</sub>), 7.585 (s, 4H, pyrylium -H), AB-signal ( $\delta_A=7.150$   $\delta_B=8.119$ ,  $J_{AB}=16\text{Hz}$ ; 4H, ethylene-H)

2-39

1.371 (m; 12H, methylene-H, alkyl chain), 1.499 (s; 36H, C<sub>4</sub>H<sub>9</sub>), 1.830 (m; 4H, methylene-H, alkyl chain), 4.105 (t; 4H, -OCH<sub>2</sub>-), AA' BB' -signal ( $\delta_A=7.027$   $\delta_B=7.736$  8H, C<sub>6</sub>H<sub>4</sub>), 7.569 (s, 4H, pyrylium -H), AB-signal ( $\delta_A=7.123$   $\delta_B=8.124$ ,  $J_{AB}=16\text{Hz}$ ; 4H, ethylene-H)

Table 2-32. NMR analyses of styrylpyrylium salts (Table 2-4)

Proton-CDCl<sub>3</sub>/CF<sub>3</sub>CO<sub>2</sub>H

2-21

1.559 (s; 36H, C<sub>4</sub>H<sub>9</sub>), 7.880 and 7.842 (s; 4H, C<sub>6</sub>H<sub>4</sub>; 4H, pyrylium -H), AB-signal ( $\delta_A=7.48$   $\delta_B=8.15$ ,  $J_{AB}=16\text{Hz}$ ; 4H, ethylene-H)

2-19

1.533 (s; 36H, C<sub>4</sub>H<sub>9</sub>), 7.812 and 7.867 (s; 4H, C<sub>6</sub>H<sub>4</sub>; 4H, pyrylium -H), AB-signal ( $\delta_A=7.442$   $\delta_B=8.147$ ,  $J_{AB}=16\text{Hz}$ ; 4H, ethylene-H)

2-18

1.519 (s; 36H, C<sub>4</sub>H<sub>9</sub>), 7.810 and 7.852 (s; 4H, C<sub>6</sub>H<sub>4</sub>; 4H, pyrylium -H), AB-signal ( $\delta_A=7.437$   $\delta_B=8.129$ ,  $J_{AB}=16\text{Hz}$ ; 4H, ethylene-H)

2-20

1.523 (s; 36H, C<sub>4</sub>H<sub>9</sub>), 7.821 and 7.839 (s; 4H, C<sub>6</sub>H<sub>4</sub>; 4H, pyrylium -H), AB-signal ( $\delta_A=7.442$   $\delta_B=8.133$ ,  $J_{AB}=16\text{Hz}$ ; 4H, ethylene-H)



Table 2-32--continued.

Carbon-CDCl<sub>3</sub>/CF<sub>3</sub>CO<sub>2</sub>H

2-20

28.10 (-C(CH<sub>3</sub>)<sub>3</sub>), 39.05 (-C(CH<sub>3</sub>)<sub>3</sub>), 114.32 (pyrylium ring C-H), 124.91 (ethylene CH), 130.75 (phenyl ring C-H), 137.96 (phenyl ring C-CH=) 148.9 (ethylene CH), 165.08 (pyrylium ring C-CH=), 186.19 (pyrylium ring C-tBu)

2-18

27.74 (-C(CH<sub>3</sub>)<sub>3</sub>), 39.06 (-C(CH<sub>3</sub>)<sub>3</sub>), 114.17 (pyrylium ring C-H), 124.80 (ethylene CH), 130.75 (phenyl ring C-H), 137.97 (phenyl ring C-CH=) 148.95 (ethylene CH), 165.14 (pyrylium ring C-CH=), 186.35 (pyrylium ring C-tBu)

2-19

27.80 (-C(CH<sub>3</sub>)<sub>3</sub>), 39.11 (-C(CH<sub>3</sub>)<sub>3</sub>), 114.10 (pyrylium ring C-H), 124.78 (ethylene CH), 130.80 (phenyl ring C-H), 137.97 (phenyl ring C-CH=) 148.94 (ethylene CH), 165.01 (pyrylium ring C-CH=), 186.48 (pyrylium ring C-tBu)

2-21

28.03 (-C(CH<sub>3</sub>)<sub>3</sub>), 39.19 (-C(CH<sub>3</sub>)<sub>3</sub>), 120.03 (pyrylium ring C-H), 125.06 (ethylene CH), 131.08 (phenyl ring C-H), 138.0 (phenyl ring C-CH=) 149.23 (ethylene CH), 164.9 (pyrylium ring C-CH=), 186.3 (pyrylium ring C-tBu)

Table 2-33. NMR analyses of methylene-bridged dialdehydes

Proton-CDCl<sub>3</sub>

2-7

4.412 (s; 4H, -OCH<sub>2</sub>CH<sub>2</sub>O-), 7.023 (m; 4H, aromatic), 7.816 (m; 4H, aromatic), 9.859 (s; 2H, aldehyde)

2-8

2.313 (p; 2H, -OCH<sub>2</sub>CH<sub>2</sub>-), 4.234 (t; 4H, -OCH<sub>2</sub>-), 6.987 (m; 4H, aromatic), 7.618 (m; 4H, aromatic), 9.848 (s; 2H, aldehyde)

2-10

1.502 (m; 4H, -OCH<sub>2</sub>CH<sub>2</sub>CH<sub>2</sub>-), 1.795 (m; 4H, -OCH<sub>2</sub>CH<sub>2</sub>-), 3.992(t; 4H, -OCH<sub>2</sub>-), 6.919 (m; 4H, aromatic), 7.753 (m; 4H, aromatic), 9.804 (s; 2H, aldehyde)

2-11

1.335 and 1.465 (m; 12H, alkyl chain), 1.808 (p; 4H, -OCH<sub>2</sub>CH<sub>2</sub>-), 4.027(t; 4H, -OCH<sub>2</sub>-), 6.979 (m; 4H, aromatic), 7.814 (m; 4H, aromatic), 9.867 (s; 2H, aldehyde)

Carbon-CDCl<sub>3</sub>

2-11

25.87 (methylene C, alkyl chain), 28.97, 29.22, 29.36 (methylene C, alkyl chain), 68.33 (-OCH<sub>2</sub>-), 114.68 (phenyl ring C-H), 129.72 (phenyl C-OCH<sub>2</sub>-), 131.89 (phenyl ring C-H), 164.19 (phenyl ring C-CH=O), 190.66 (CH=O)

2-10

25.67 (methylene C, alkyl chain), 28.88 (methylene C, alkyl chain), 68.10 (-OCH<sub>2</sub>-), 114.66 (phenyl ring C-H), 129.75 (phenyl C-OCH<sub>2</sub>-), 131.87 (phenyl ring C-H), 164.06 (phenyl ring C-CH=O), 190.64 (CH=O)

Table 2-33--continued.

2-8

28.92 (methylene C, alkyl chain), 64.51 (-OCH<sub>2</sub>-), 114.72 (phenyl ring C-H), 130.08 (phenyl C-OCH<sub>2</sub>-), 131.95 (phenyl ring C-H), 163.75 (phenyl ring C-CH=O), 190.67 (CH=O)

2-7

66.47 (-OCH<sub>2</sub>-), 114.84 (phenyl ring C-H), 130.35 (phenyl C-OCH<sub>2</sub>-), 131.93 (phenyl ring C-H), 163.35 (phenyl ring C-CH=O), 190.64 (CH=O)

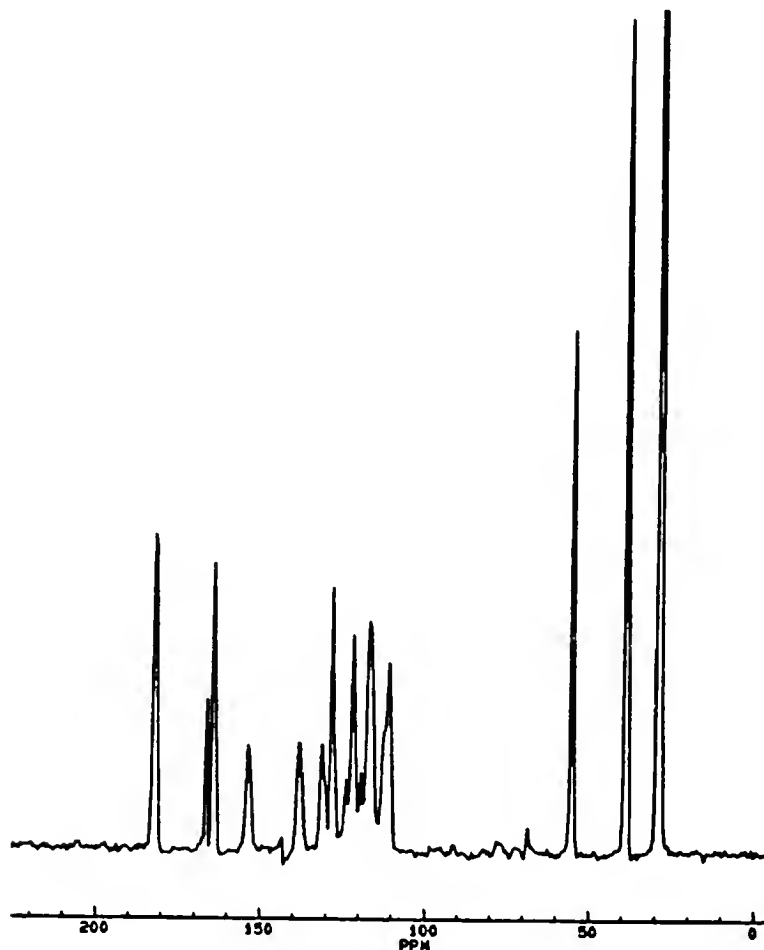


Figure 2-9. C-13 Solid state NMR of styrylpyrylium triflate, 1-1c. Note that the spectrum has been expanded so the top of the t-butyl signal near 30 ppm is cut off.

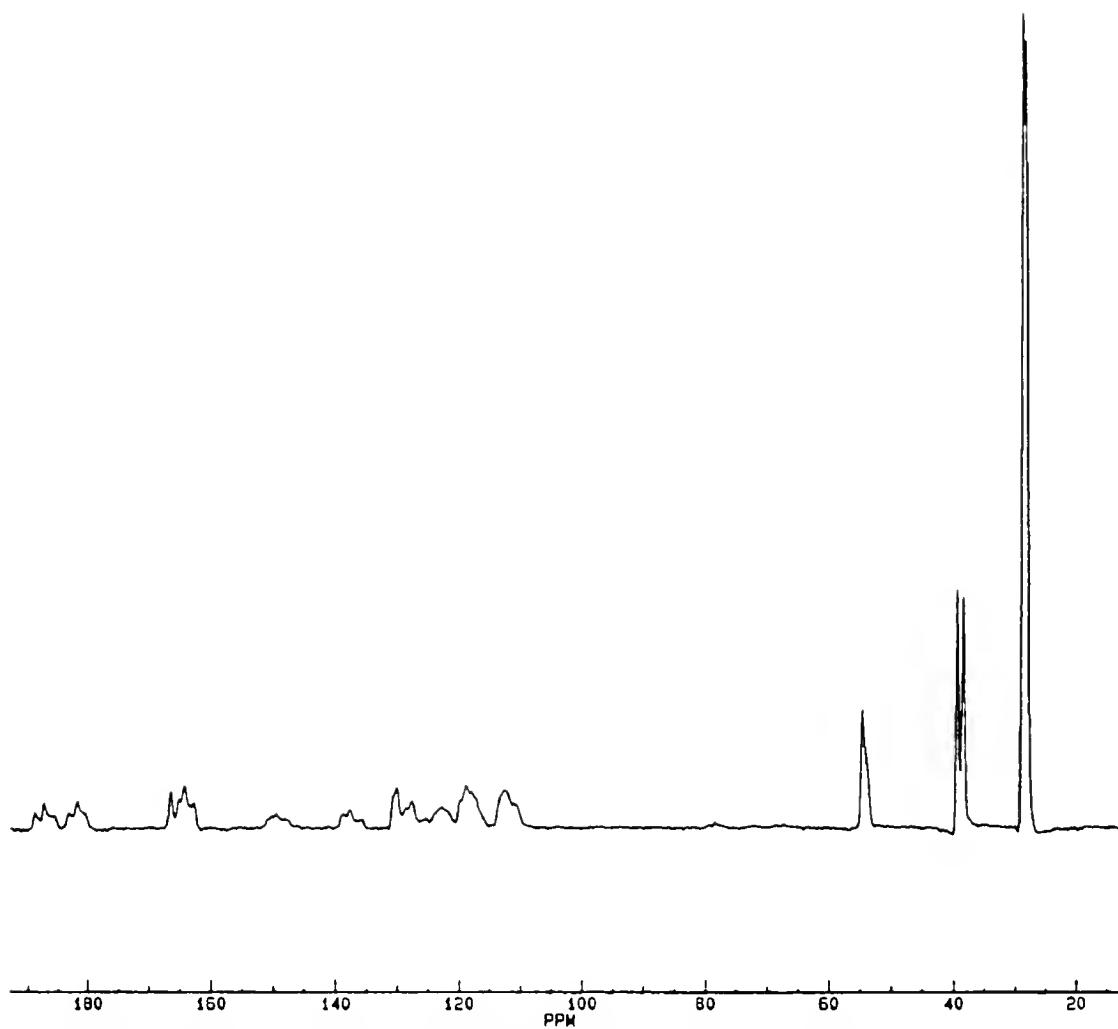


Figure 2-10. C-13 Solid state NMR of styrylpyrylium perchhenate, 2-13a.

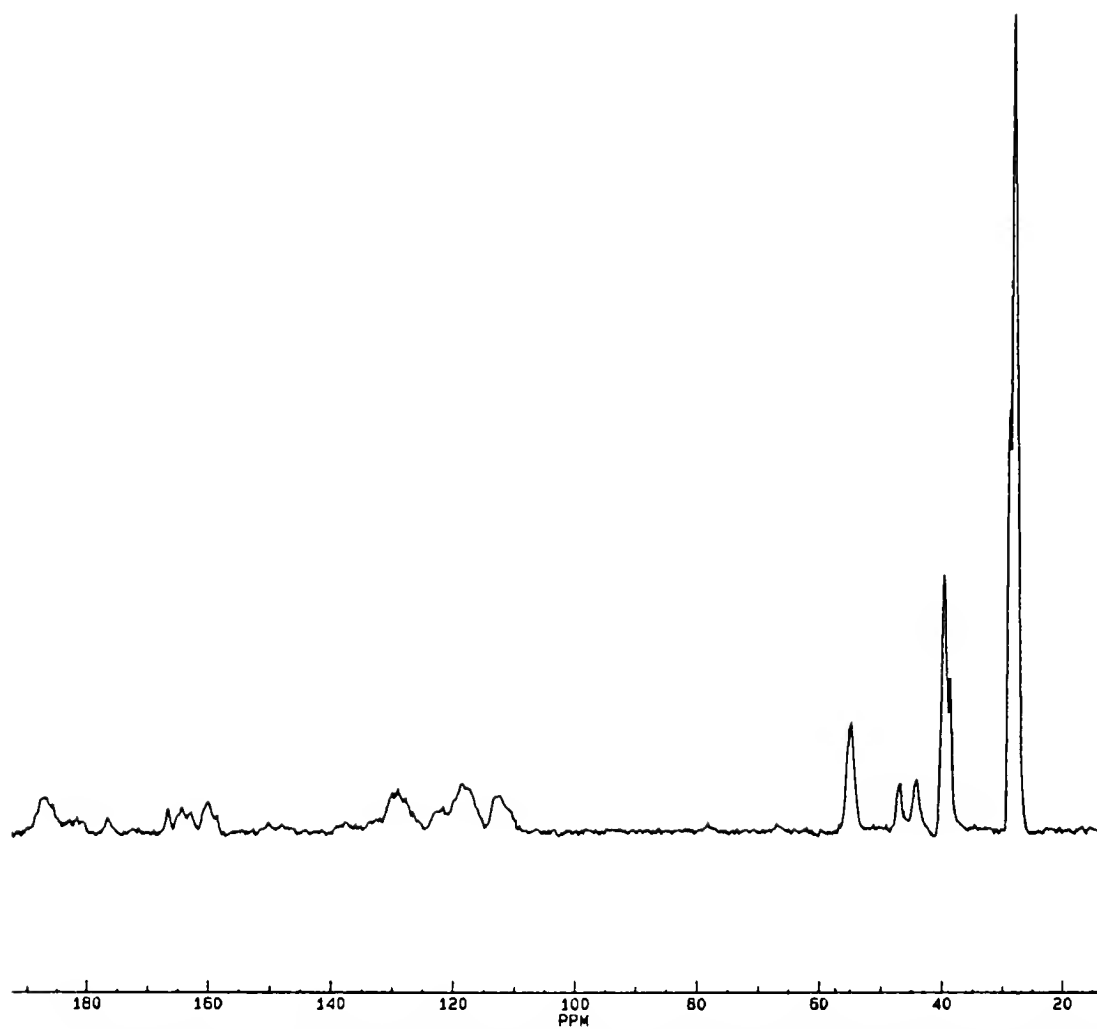


Figure 2-11. C-13 Solid state NMR of irradiated styrylpyrylium perchhenate monomer, 2-13a. The two small signals between 40 and 50 ppm are from the cyclobutane carbons

### CHAPTER 3 CRYSTALLINE-STATE PHOTODIMERIZATION OF A STYRYLPYRYLIUM TRIFLATE

#### Introduction

This chapter is concerned with the topochemical photodimerization of a styrylpyrylium salt. The introduction to this chapter describes how a topochemical reaction may be viewed as a special type of phase transition. If this phase transition occurs simultaneously over the full dimensions of a single crystal, the transformation is said to be single-phase or homogeneous. It is then explained how homogeneous product formation within a topochemically reacting single crystal is believed to lead in turn to single crystals of the product. The significance of this is discussed as well as a method to induce such transformations in UV-VIS-photoreactive crystals.

The results reported in the balance of the chapter offer the first proof of a single-crystal-to-single crystal topochemical reaction that undergoes a single crystal-to-single crystal back reaction. The forward photodimerization reaction is demonstrated to proceed through the formation of a solid solution of monomer and dimer molecules in the reacting crystal over the entire range of conversion of the monomer crystal to the dimer crystal. That is, the photodimerization is shown to occur homogeneously throughout the crystal to produce substitutional mixed crystals of the monomer and dimer. By full crystal structure analysis of the as-reacted dimer crystal and single crystals of intermediate conversion, it is proven that the photodimerization under investigation proceeds under strict control of the crystal lattice. The crystal structures are the first direct proof of the verity of Schmidt's Topochemical Principle. The irradiation conditions are the key to inducing the homogeneous mechanism in this photoreaction.

### Topochemical Reactions: A Type of Phase Transition

A phase is a region of uniform chemical potential, that is, uniform chemical composition and uniform physical properties and phase transitions are driven by applying some type of gradient. For example, Figure 3-1 shows how a phase change may be driven by a temperature gradient. In a certain temperature range, phase 1 has a lower potential and is therefore the stable phase that is observed, at a higher temperature range, the potential of phase 2 is lower and therefore this is the phase observed. There is a distinct transition temperature at which this transformation takes place. Figure 3-1a is an example of a first order transition because its first derivative,  $(dG/dT)_P$ , entropy, is discontinuous at the transition temperature. An example of a first order transition is the phase change undergone in  $H_2O$  at  $0^\circ C$  and atmospheric pressure.

Figure 3-1b shows the temperature dependence of the chemical potential for a second order conversion. In this kind of transition, the first derivative of the potential with respect to temperature changes continuously. While no sudden change in the entropy of the system at the transition temperature is observed, there is a sudden change in the second derivative, that is, the heat capacity.

Another measure of the order of a transition is the order parameter. Figure 3-2 shows how the order parameter of a system varies as the system undergoes a second order transition. The order parameter changes continuously below the transition temperature and then vanishes at the transition. An example of an order parameter would be a certain crystallographic dimension describing the packing in the unit cell. In these types of transitions, though the dimensions describing the unit cell change continuously, the symmetry of the crystal changes discontinuously.

To illustrate this type of second order phase transition, consider the behavior of  $SrTiO_3$ , a perovskite characterized by an oxygen octahedra.<sup>106,107</sup> Below the phase

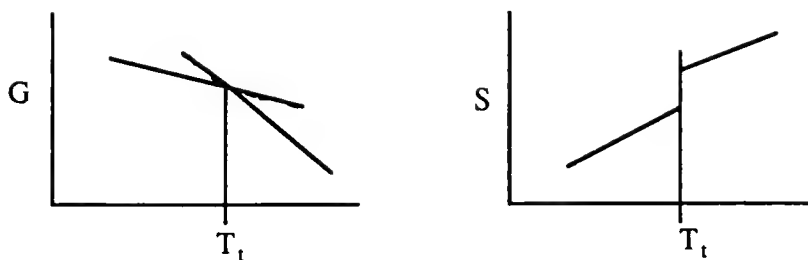


Figure 3-1a.

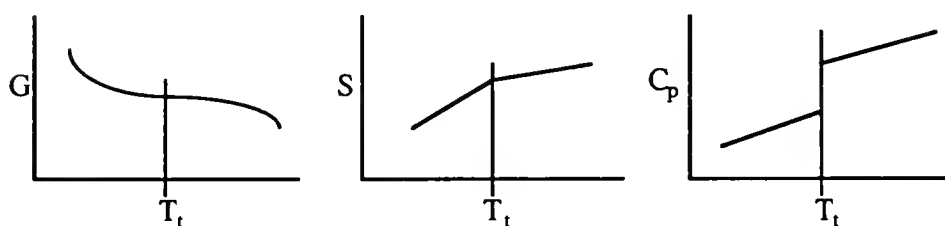


Figure 3-1b.

Figure 3-1. Behavior of thermodynamic parameters with temperature during classic phase transitions.

a) A first order transition is discontinuous in the first derivatives of the Gibbs free energy, that is, entropy, enthalpy and volume.

b) Second order transition continuous in the first derivatives but discontinuous in the second derivatives of the Gibbs free energy, for example, heat capacity.

transition temperature,  $\text{SrTiO}_3$  is tetragonal; call the unequal cell parameters,  $x$  and  $y$ ,  $x > y$ . As the transition temperature is approached, the oxygen octahedra rotate which leads to a corresponding change in the cell parameters. In this case, the angle of rotation of the oxygen octahedra is the order parameter. The cell parameters change such that the rate of expansion of  $y$  with increasing temperature is greater than the rate of expansion of  $x$ . Thus as the temperature increases,  $y$  will become equal to  $x$ . At that point the symmetry of the crystal suddenly changes to cubic, even though the configuration of the atoms have been changing continuously.

A similar situation is observed for the phase transition of the  $\text{AsF}_6^-$  radical cation salt of fluoranthene. At the transition temperature, the symmetry of the crystal changes corresponding to a rotation of the fluoranthenyl cation as shown in Figure 3-2b.<sup>108</sup> In both cases, the continuous change in the atom configurations results in a continuous change in the first derivatives of the free energy of the system. But because the change in symmetry is discontinuous, they are second order transitions. These types of symmetry changes are characterized by a group-subgroup relationship; that is, the transition is between phases of related symmetry. For example, in the case of the fluoranthenyl cation, the high-symmetry, high temperature phase is  $A2/m$  and the low-temperature, low-symmetry phase is  $P2_1/c$ .

Among the best investigated examples of crystalline-state reactions are the [2+2] photodimerizations of cinnamic acid derivatives.<sup>66,92,13</sup> G.M.J. Schmidt noted in his landmark studies on the photodimerizations of cinnamic acids that the only dimers formed in the crystal are those whose symmetry is already present in the monomer packing.<sup>55</sup> This observation led to the proposal that there is a distinct type of crystalline-state reaction which is characterized by the following: the atoms involved in bond formation approach one another by well-defined rotations of the reacting molecules on their lattice sites and in such a way that the smallest atomic displacements prevail. Hence the product is always crystalline, and also, will have the same type of crystal packing (symmetry) as the parent crystal. The reaction is controlled by the parent-lattice. Such reactions are known as topochemical reactions, and this "least motion" rule is Schmidt's Topochemical Principle.

To contrast a topochemical reaction with other types of crystalline state reactions, consider the following. Reactions of crystals may occur, instead, by *diffusion* of the reactants to centers of reactivity or initial product formation may destroy the parent lattice. In addition, the parent lattice may act as a template for the oriented growth of product nuclei leading to a crystal modification with axes having a certain orientation with respect to the crystallographic axes of the parent crystal (topotactic). Although other types of



organic solid state reactions involve two or more phases, topochemical reactions may be single-phase.

Thus a topochemical reaction may be viewed as a special type of phase transition. According to the definition that a phase is a region of uniform chemical potential, a solution of two substances is also a single phase. Consider substance *m* constituting a mother phase *M* reacting to form substance *d*, constituting a daughter phase *D*. If the two substances are miscible to form a single phase, the system may be converted from phase *M* to phase *D* by the conversion of substance *d* to substance *m*. In this case, the gradient that drives the phase transition is concentration. The behavior of the free energy with the gradient, concentration, can be roughly estimated as the curve shown in Figure 3-3.<sup>109</sup> The first derivative of this function with respect to the gradient is continuous throughout the transformation as in a typical second order transition.

Now consider that this conversion of *M* to *D* may take place in the crystalline state through a topochemical reaction. Thus superimposed on the chemical transformation of phase *M* to *D*, is a type of second order structural phase transition such that we may write, crystal *C<sub>M</sub>* is converted to crystal *C<sub>D</sub>* through a continuous series of crystals *C<sub>MD</sub>* which are solid solutions of the reactant and product (in the case of a photodimerization, monomer and dimer). In a topochemical reaction, the reaction proceeds through the rotation of molecules on their lattice sites and thus there is no diffusion or displacement of the molecule from the lattice site. Although the center of mass of the molecule is not shifted from its lattice site, side groups projecting from the reacting centers, become reoriented accounting for the continuous shift in lattice parameters throughout the conversion. The continuous changes in cell parameters that have been observed for topochemical systems due to side group reorientations as the system proceeds from the reactant phase to the product phase, strongly recalls the second order transitions of SrTiO<sub>3</sub> and the fluoranthyl radical cation salt discussed above. However, in contrast to these types of second order

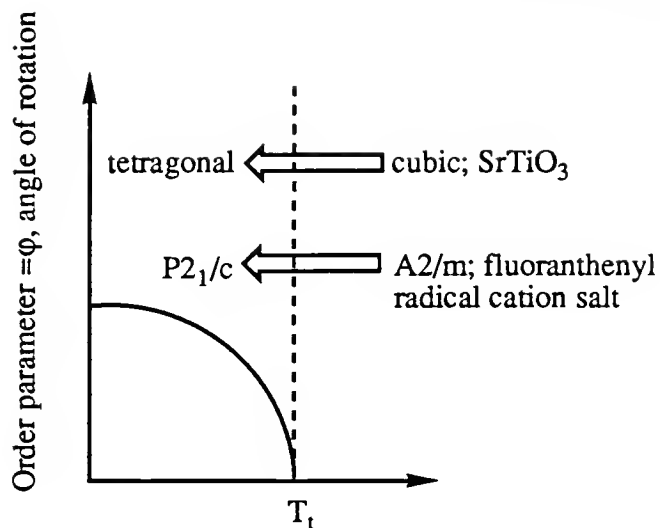


Figure 3-2a.

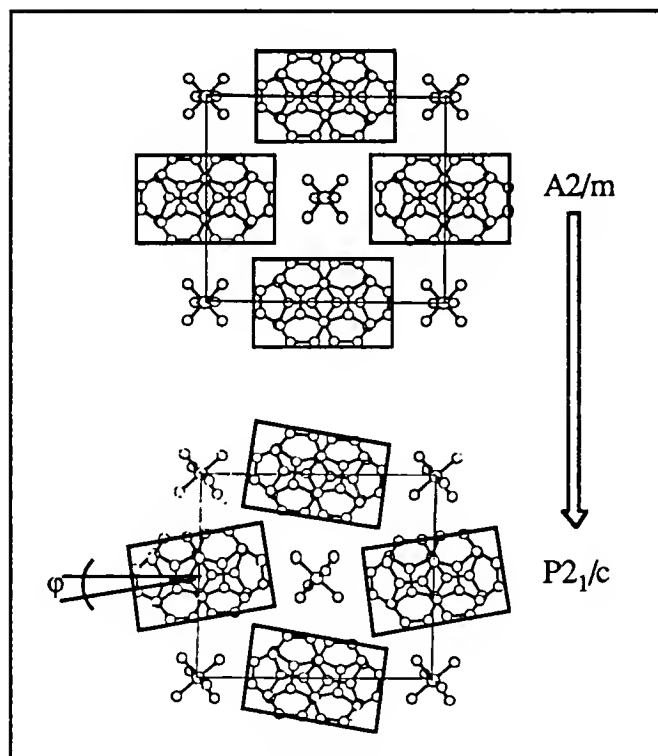


Figure 3-2b.

Figure 3-2. The rotation of fluoranthenyl radical cations during a phase transition.

a) The change in order parameter in a second order transition is continuous. One example of an order parameter might be an angle of rotation of defined in relation to the unit cell.

b) The top projection shows the crystal structure of the fluoranthenyl radical cation  $T > T_t$ . The bottom projection shows the structure at  $T < T_t$ . Note the angle of rotation,  $\phi$ , in the low temperature structure.

structural phase transitions, the symmetry of the system is never changed in a topochemical reaction. The symmetry in the reactant crystal is identical to that in the product crystal.

An interesting system highlighting the difference between a structural phase transition which involves the displacement of molecules from their lattice sites and a phase transition characterized only by side group reorientation, is the polymerization of the diacetylene, 1,6-Di-(*n*-Carbazoyl)-2,4-hexadiyne (DCH).<sup>82</sup> This system proceeds through the series: *CM* to *CMO*, which is a phase transition of a monomer crystal reacting to form a mixed crystal of monomer and oligomer; then *CMO* to *CMO*<sup>\*</sup> which is a displacive structural phase transition where the concentrations of monomer and oligomer do not change; and finally from *CMO*<sup>\*</sup> to *CP*<sup>\*</sup> which is a continuation of the topochemistry to form a polymer. The cell parameters vs. conversion curves show that up until a conversion of approximately 25%, a topochemical reaction proceeds in the crystal as evidenced by the smooth change in lattice parameters. Then a concentration driven phase transition takes place which is manifested by an abrupt change in the lattice parameters (as seen in Figure 3-4) and a large increase in the rate of the reaction. Thus the strictly structural phase transition in the crystal results in a monomer packing that favors the continued topochemical phase transition.

### Homogeneous vs. Heterogeneous Product Formation

Viewed at the macroscopic level, topochemical reactions may be seen as occurring heterogeneously or homogeneously within a single crystal.<sup>83,11,7,57</sup> For example, with one exception up until now,<sup>12</sup> topochemical [2+2] photodimerizations of olefin crystals, have been observed to proceed with disintegration of the crystal. No single crystal of the product could be obtained. In the cases where the crystal disintegrates upon reaction, it is believed that the product forms heterogeneously within the crystal, that is, the spatial distribution of product within the crystal is not uniform.

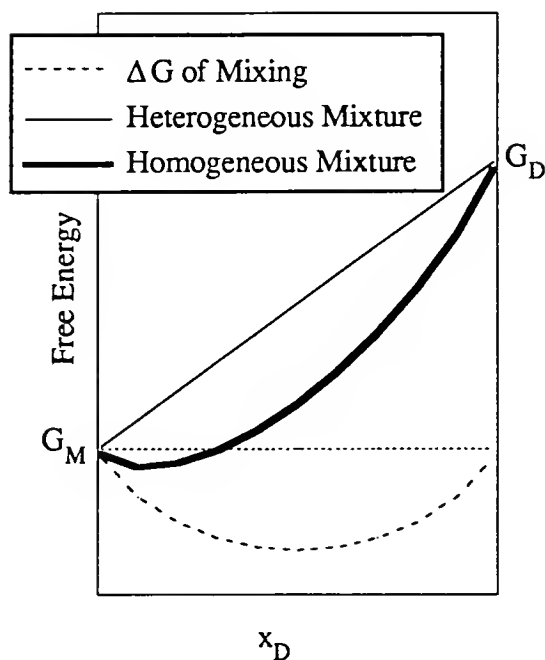


Figure 3-3. Free energy of the system as a function of dimer percentage.

The reason a crystal disintegrates during heterogeneous product formation is the following. When a reactant molecule converts to product molecule, van-der-Waals contacts are converted to comparatively shorter chemical bonds. Thus there will be a difference in the dimensions between the reactant and product lattices. As the concentration of product builds up locally in the monomer crystal, a new daughter lattice, characteristic of the product concentration, evolves. Eventually this daughter lattice reaches its limit of solubility in the mother lattice and nucleation of a new phase occurs. Phase boundaries between discrepant phases causes the disintegration of the single crystal into polycrystalline particles.

However, a homogeneous transformation--that is, a single-phase transformation--produces single crystals of product. When the product is formed homogeneously, a solid solution of the reactant and product is formed over the entire dimensions of the crystal. Thus, the product and reactant form a mixed

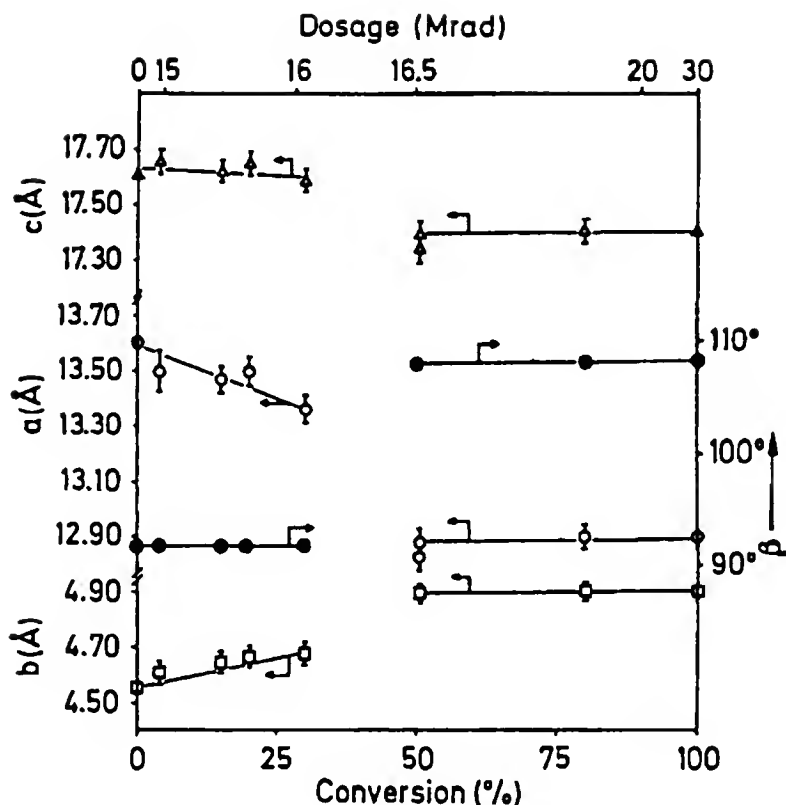


Figure 3-4. Cell parameters vs. conversion for the crystalline-state polymerization of DCH.

macroscopic single crystal in which both statistically occupy the same lattice sites. Thus the crystal must house only one lattice at any given moment throughout the conversion. Therefore there is never a dimensional discrepancy between lattices. Only one phase exists at a given moment, and the crystal remains intact.

There is evidence that the mechanism of phase transition in a topochemical reaction, whether it be homogeneous or heterogeneous, has no influence on the morphology of the final product. For example, the diacetylene, DCH polymerizes homogeneously by gamma radiation and heterogeneously by thermal polymerization. The lattice parameters of the products from each mechanism are identical. This has also been observed for the [2+2] photodimerization discussed in this chapter. The same atomic displacements occur in both mechanisms: either simultaneously over the entire bulk of the crystal or within various

spatial dimensions of the single crystal along the time coordinate of the conversion. Thus the disintegration of a crystal in a topochemical reaction is simply a morphological phenomenon arising from temporal conditions, as opposed to a chemical or crystallographic, phenomenon.

#### Tail irradiation: a method for inducing homogeneous reactions in photoactive crystals

The key to the homogeneous conversion in [2+2] photodimerizations is the irradiation in the absorption tail of the chromophore. This same effect has been observed in the photopolymerization of distyrylpyrazine (DSP)<sup>7</sup> and can be explained by considering the light intensity gradient through a cross-section of an irradiated crystal. When the crystal is exposed to light for which it has a high absorptivity, the light intensity will be high at the incident surface and will drop off quickly through the inner bulk of the crystal according to Beer's Law. This is shown schematically in Figure 3-5.<sup>110</sup> Thus product accumulates quickly at the surface, precipitating out as a separate phase due to dimensional mismatch between the product and reactant lattices.

However, when the crystal is exposed to light for which it has a low absorptivity, the light intensity will be comparatively even from the surface throughout the bulk of the crystal. Thus product is formed evenly throughout the crystal, and the distribution of the product is homogeneous. At low conversions the lattice is most similar to the parent lattice, thus the product can be viewed as a guest in the parent. At higher conversions the situation is reversed and the reactant is seen as the guest in the daughter lattice. The crystal is then a solid solution of the product and reactant. This leads to intact single crystals of the product. The importance of this is that the full power of x-ray crystallography may now be engaged as a tool for investigating the topochemistry.

#### Homogeneous transformations and the investigation topochemical reactions

The importance of the homogeneous mechanism of phase transition for crystalline-state reactions is that it produces single crystals of the topochemical products which may be studied thoroughly by x-ray crystallography. Table 3-1 contains the unit cell parameters

for the most well-investigated topochemical reactions, as well as the percent changes that occur in these cell dimensions during the conversion of the crystal from the parent to the daughter phase. Although suggested by Schmidt,<sup>55</sup> the detailed atomic movements responsible for these changes have been unexplored up until now. Equivalently, one may wonder how the lattice accommodates the considerable atomic displacements that must occur for bond formation.

This work presents the first full x-ray crystal structures of substitutional mixed crystals formed during the topochemical reactions of photoreactive crystals. It will be shown for the photodimerization of the styrylpyrylium salt under investigation, that the photoactive molecules in the lattice can be divided into two parts: the atoms directly involved in bond breaking and formation, that is, the reacting centers, and the side groups or substituents on these atoms. The Van der Waals contacts among these side groups form a fixed matrix that, over the course of the conversion to product, flexes in response to the changing interatomic distances of the reacting centers. That means that these “contact” groups have the same (fixed) lattice positions whether they are part of a reacted or unreacted species. Yet these groups shift and rotate (flex) as the lattice evolves to accommodate more product.

#### Single-Crystal-to-Single-Crystal Topochemical Reactions: Phase “Transitions” Involving Dimensionally Similar Lattices

The transformations in Table 3-1 cover the single-crystal-to-single-crystal transformations that have been reported in the literature. They are divided into those that are induced by UV-VIS irradiation and  $\gamma$  irradiation. One would expect homogeneous product formation for all reactions involving  $\gamma$  irradiation and this explains why they are seen to proceed with retention of single crystalline character, despite large changes in lattice dimensions. The UV-VIS induced topochemistry should lead to heterogeneous product formation as described above and thus disintegration of the single crystal. The fact that it

does not in the case of DSP (a diolefin undergoing a [2+2] photopolymerization) is because here the irradiation was in the tail of absorption.

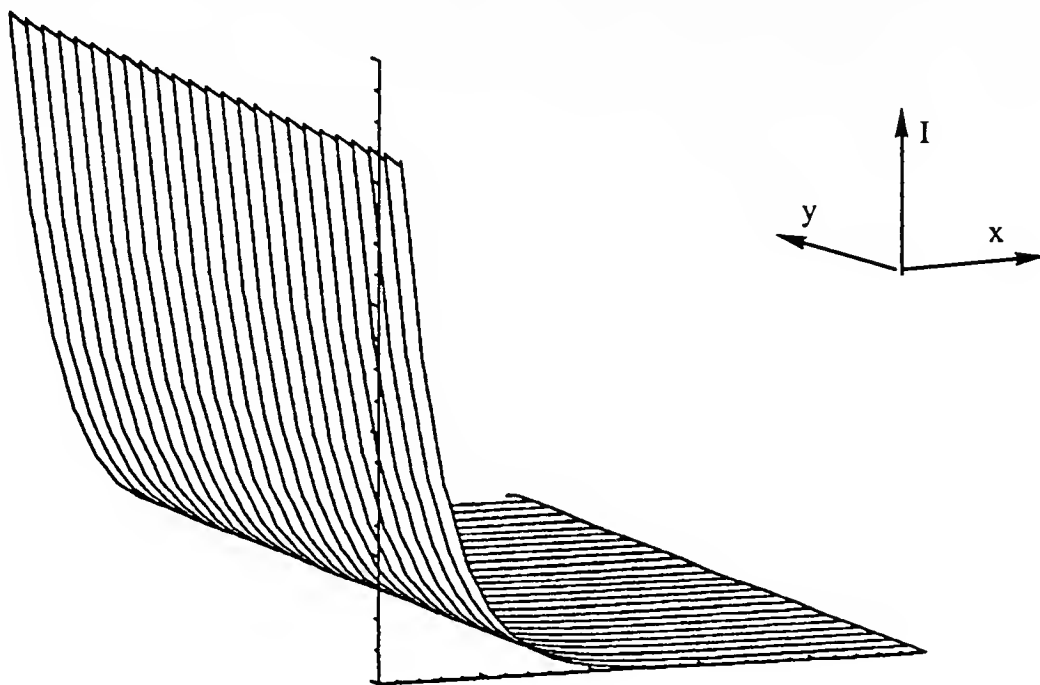


Figure 3-5a.

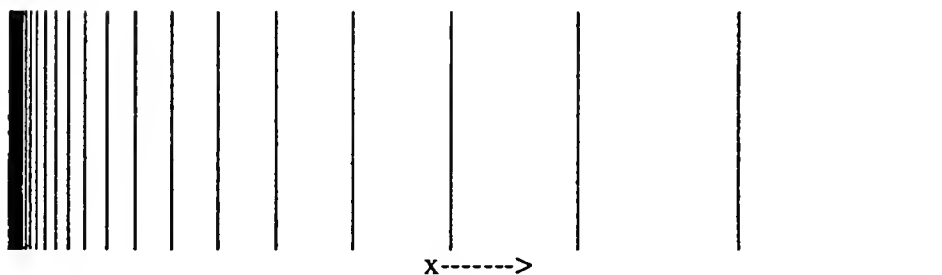


Figure 3-5b.

Figure 3-5. Absorption of radiation at the crystal surface.

- a) According to Beer's Law, the intensity of radiation,  $I$ , passing through a sample of molar absorptivity,  $\epsilon$ , and uniform concentration,  $c$ , will fall off exponentially through the bulk of the sample according to  $I = I_0 10^{-\epsilon c x}$ , where  $I_0$  is the intensity of the incident radiation and  $x$  is the distance through the sample. This plot shows the intensity of radiation,  $I$ , vs.  $x$ , for such behavior, where  $x$  is a dimension of a crystal parallel to the incident radiation and the  $xy$  plane is a cross section of the crystal.
- b) This plot is a diagram of the  $xy$  plane divided into sections containing equal amounts of photoproduct after a given period of exposure. The incident radiation is perpendicular to the  $y$  axis and from the direction where the lines are most closely spaced.



But why does the photodimerization of 2-benzyl-5-benzylidenecyclopentanone (BBCP) and the photoaddition of deoxycholic acid (DCA) to p-fluoroacetophenone proceed single-crystal-to-single-crystal? It has not known by which mechanism these transformations occur because the irradiation conditions were either not carefully controlled or fully described. But the difference in lattice parameters between the parent and final daughter phase are typically 1% or below. So even if product formation in the crystal is not homogeneous, it is possible that the dimensional discrepancy between the parent and daughter lattices is not significant enough at the phase boundary for a mechanical disruption of the molecular cohesion.

Table 3-1. "Before and After" lattice parameters of single crystals in which a topochemical reaction has occurred to give a single crystal of the product.

Reaction (Symmetry)	lattice parameter			% change in parameter
<hr/>				
UV-VIS Induced				
BBCP photodimerization <sup>12</sup>				
(Pbca)	a	31.302	31.321	<0.1%
	b	10.784	10.811	<1%
	c	8.678	8.629	<1%
	V	2932	2922	<0.1%
DCA-p-fluoroacetophenone photoaddition <sup>17</sup>				
(P2 <sub>1</sub> 2 <sub>1</sub> 2 <sub>1</sub> )	a	25.27	25.155	<1%
	b	13.579	13.679	<1%
	c	7.198	7.135	<1%
DSP <sup>7</sup> photopolymerization				
(Pbca)	a	2.056	2.034	1%
	b	0.959	1.043	9%
	c	0.763	0.731	4%
styrylpyrylium triflate (this work)				
photodimerization				
P2 <sub>1</sub> /c	a	10.39	10.86	5%
	b	14.79	14.14	4%
	c	16.49	16.40	<1%
	β	103	106	3%

Table 3-1--continued.

 $\alpha$ -trans-cinnamic acid (this work)

photodimerization

(P2 <sub>1</sub> /n)	a	7.716	7.67	<1%
	b	17.61	18.231	4%
	c	5.57	5.60	<1%
	$\beta$	96	106	9%

acridizinium salt

photodimerization<sup>20</sup>

(P2 <sub>1</sub> /a to P2 <sub>1</sub> )	a	9.996	7.737	22%
	b	13.065	17.075	31%
	c	10.186	9.942	2%
	$\beta$	119.10	99.15	17%

(P1)

a	7.632	7.938	4%
b	9.651	9.785	1%
c	10.253	9.931	3%
$\alpha$	118.54	103.24	13%
$\beta$	111.33	110.33	<1%
$\gamma$	74.01	98.96	34%

 $\gamma$ - Irradiation Inducedcobaloxime complex<sup>18</sup>

racemization

(P2 <sub>1</sub> to P2 <sub>1</sub> /n)	a	16.036	15.824	1.3%
	b	12.606	12.704	<1%
	c	9.634	9.559	<1%
	$\beta$	94.4	92.8	

diacetylene (PTS)<sup>82</sup>

photopolymerization

(P2 <sub>1</sub> /c)	a	14.61	14.77	1%
	b	5.11	4.91	4%
(also thermally induced)	c	25.56	25.34	<1%

6-amino-2,4-trans, trans-hexadienoic acid<sup>19</sup>

butadiene photopolymerization

(P1)	a	10.52	9.67	8%
	b	10.84	10.70	1.3%
	c	17.03	17.79	4.5%

The [4+4] photodimerization of acridizinium salts is a case where spectacularly large changes in lattice parameters are observed. Here water molecules are known to play a large, but as yet, undetermined role in the reactions of these crystals. It is also possible these dramatic changes in lattice parameters are due to an additional phase transition superimposed on the topochemistry of the system as in the case described above for DCH.

## Results

### Crystal Modifications of a Styrylpyrylium Triflate and its Photoproducts: The Overall Scheme

The photodimerization of the styrylpyrylium triflate, (1-1c) and thermal cycloreversion of its photodimer (1-4c) investigated in this work is shown in Figure 3-6.<sup>4</sup>

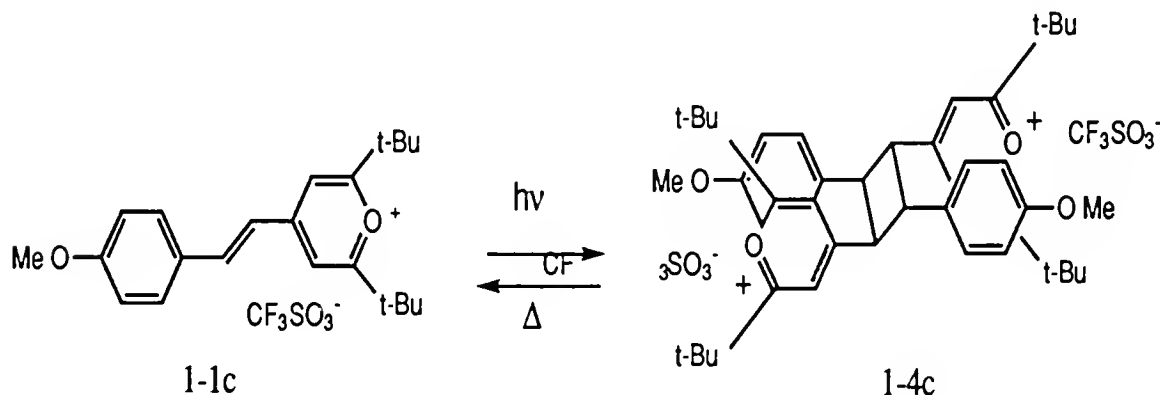


Figure 3-6. The photodimerization and thermal cycloreversion of the styrylpyrylium triflate and its photodimer.

The conversions among crystal modifications involved in the [2+2] photodimerization of a styrylpyrylium triflate are summarized in Figure 3-7. An asterisk, C\*, denotes a crystal modification with an orthrhombic unit cell, space group Pbca, whereas C means monoclinic, P2<sub>1</sub>/c. C<sub>M</sub> is the crystal modification of the monomer (1-1c) obtained from solvent recrystallization. Crystals of the dimer (1-4c), C<sub>D</sub>, symmetry P2<sub>1</sub>/c, have been obtained from the topochemical photodimerization of the monomer, C<sub>M</sub>.

These dimer crystals are the final result of a continuous series of substitutional mixed crystals of monomer and dimer with  $P2_1/c$  symmetry,  $C_{MD}$ , which were formed through the topochemical photodimerization of the monomer. Substitutional mixed crystals of the monoclinic type formed from annealing have not been investigated crystallographically but have been observed visually (see the middle photograph in Figures 3-11 and 3-12).

A second form of dimer crystals,  $C^*_D$ , with symmetry  $Pbca$ , have been isolated through solvent recrystallization of the as-dimerized dimer. Although the as-dimerized dimer crystals,  $C_D$ , may be annealed to form monomer crystals,  $C_M$ , dimer crystals formed from recrystallization,  $C^*_D$ , are stable under the same conditions. Table 3-2 contains the crystallographic data on the monomer, monomer formed from heating the dimer, photodimer, recrystallized dimer and two mixed crystals. Thus if it is possible to obtain dimer crystals with “monomer symmetry” ( $P2_1/c$ ), monomer crystals with “dimer symmetry” ( $Pbca$ ) are also conceivable,  $C^*_M$ , as well as substitutional mixed crystals  $C^*_{MD}$ . This is represented in the inset of Figure 3-7.

Since the recrystallized dimer crystals are not thermally reversible, other routes to  $C^*_{MD}$  must be considered. Figure 3-8 shows how  $C^*_{MD}$  and  $C_{MD}$  may be obtained through solvent recrystallization. From solutions of monomer and dimer, two types of crystal structures are possible: orthrhombic, that is, “dimer symmetry” and monoclinic, “monomer symmetry”. The relative concentrations of monomer and dimer from the starting solution will determine not only their relative content in the mixed, but also the type of crystal. It is possible that at some concentrations both types of crystals will form, or neither will form as indicated by the gray region in Figure 3-8.

When a 2:1 molar ratio of the monomer and dimer were recrystallized from a trifluoroacetic acid solution by addition of ether, two types of crystals were recovered. The data on these crystals is summarized in Table 3-3.  $^1H$  NMR indicated that the yellow crystals contained 13% monomer, whereas the orange crystals contained 43% dimer. This

agrees with the argument that due to entropy considerations, it would be easier to pack dimer molecules into a monomer-type crystal, than monomer into a dimer-type crystal. In

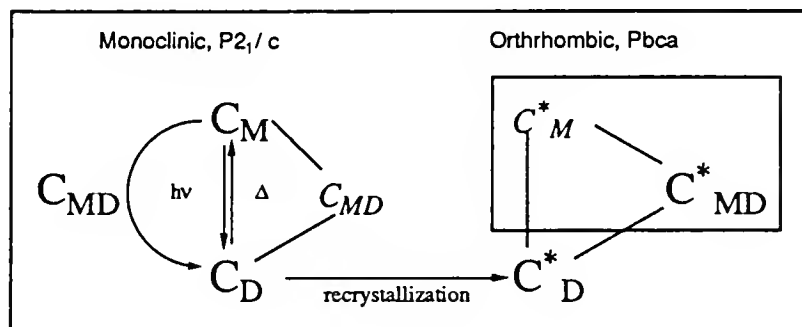


Figure 3-7. This diagram shows the relationship between the various crystal modifications that exist through topochemistry and solvent recrystallization for a styrylpyrylium triflate, its photodimer and mixed crystals of both. The conversion  $C_D$  to  $C_{MD}$  via annealing has not yet been investigated crystallographically. The conversion  $C^*_D$  to  $C^*_MD$  does not occur thermally. Evidence exists that crystals of type  $C_{MD}$  and  $C^*_MD$  have been obtained through solvent recrystallization from a solution of monomer and dimer.

Table 3-2. Crystallographic data on the styrylpyrylium triflate crystals. The first six rows measure the edges of the unit cell in Å and the angles between the edges. A \* indicates 90°. V is the volume of the unit cell, while Z indicates the number of molecules per unit cell.  $D_x$  is the density. “#Refl.” and “#obs.” stand for the number of reflections and number observed. R is the residual index.

	C <sub>M</sub> monoclinic monomer			C <sub>D</sub> monoclinic photo- dimer	C <sup>*</sup> <sub>D</sub> orthrhombic recrystal- lized dimer	C <sub>MD</sub> monoclinic mixed crystal	C <sub>MD</sub> monoclinic mixed crystal
		monomer	monomer				
		T=165	T=165			67% T=165	13% T=165
a	10.3873(8)	10.3377(9)	10.2845(10)	10.8603(6)	14.3055(8)	10.7497(12)	10.2941(14)
b	14.7855(8)	14.7763(7)	14.7491(27)	14.1449(35)	16.2259(9)	14.2531(13)	14.7400(12)
c	16.4929(16)	16.0772(12)	16.1026(18)	16.4046(8)	21.5090(15)	16.4773(15)	16.0874(16)
α	*	*	*	*	*	*	*
β	103.147(8)	102.162(9)	102.210(9)	106.324(4)	*	105.267(7)	102.328(8)
γ	*	*	*	*	*	*	*
V	2466.5	2393.8	2387.3	2418.5	4992.7	2435.5	2385
Z	4	4	4	4	8	4	
$D_x$	1.272	1.311	1.320	1.298	1.257	1.294	1.322
space group	P2 <sub>1</sub> /c	P2 <sub>1</sub> /c	P2 <sub>1</sub> /c	P2 <sub>1</sub> /c	Pbca	P2 <sub>1</sub> /c	P2 <sub>1</sub> /c
# refl.	3256	2859	3294	3759	3203	3215	2820
# obs.	2071	1589	2440	2744	1369	1863	2088
R	0.090	0.073	0.031	0.056	0.077	0.090	0.068
R <sub>w</sub>	0.099	0.088	0.034	0.053	0.071	0.082	0.080

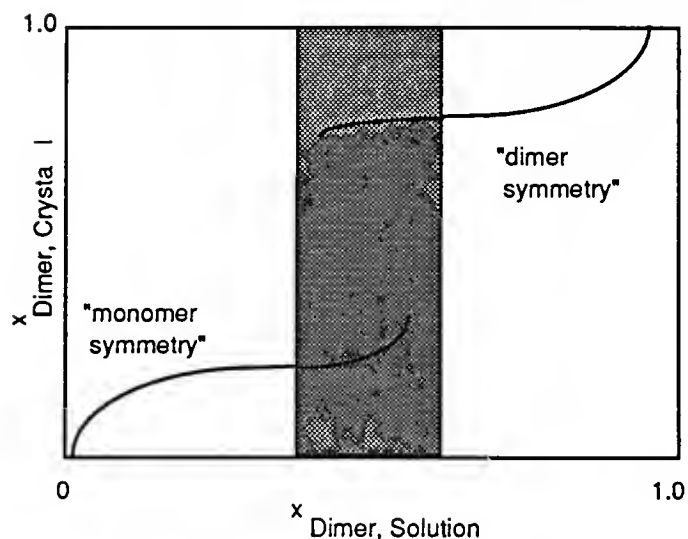


Figure 3-8. Solvent composition versus crystal composition and crystal type for the formation of mixed crystals of monomer and dimer.

the latter case, the monomer has to pair with itself for an effective substitution into the dimer lattice.

Initial crystallographic analysis indicated that the red crystals were monoclinic and had cell parameters that matched substitutional mixed crystals formed directly from photodimerization, CMD, with a composition of 50-80% dimer (compare the cell parameters in Table 3-3 for the monoclinic crystals with those in Table 3-4). The yellow crystals had cell parameters very close to those of recrystallized dimer,  $C^*D$  (compare the cell parameters in Table 3-3 for the orthorhombic crystals with those in Table 3-2). These crystals are also resistant to cycloreversion on annealing. Full X-ray structure analysis on this crystal may definitively reveal a crystal of type  $C^*MD$ . Crystals of this type with increasing dimer content may be obtained by adjusting the monomer/dimer feed ratio in the solution recrystallization as shown in Figure 3-8. Finally, photocleavage of the cyclobutane moiety in the recrystallized dimer has yet to be tested as a route to  $C^*MD$ .

Table 3-3. Structural and composition data on the crystals obtained from a solution of monomer and dimer.

crystal type	composition by $^1\text{H}$ NMR monomer:dimer	cell parameters	
red (monoclinic)	57:43	a=10.684 b=14.310 c=16.5525 $\beta$ =106.198 V=2430.3	
			after annealing
yellow (orthrhombic)	13:87	a=14.3220 b=16.2189 c=21.4943 V=4992.9	a=14.3028 b=16.2152 c=21.5066 V=4987.9

## [2+2] Photodimerization: The Forward Reaction

### Broad band irradiation

Figure 3-9 shows the UV-VIS spectra of the styrylpyrylium chromophore (3-1). When the photodimerization shown in Figure 3-6 is done in the maximum absorption of the chromophore, the typical heterogeneous reaction is observed. The surface of the originally red crystals first become covered with a fine yellow powder, and the crystal eventually breaks down into microcrystalline particles. The crystals at the top of the photographs in Figures 3-10 and 3-11 show styrylpyrylium crystals irradiated for several seconds with a Xenon lamp and no filter. The top layer of the styrylpyrylium crystal has absorbed most of the light, as illustrated schematically in Figure 3-5. As dimer (1-4c) accumulates in this part of the crystal's volume, a new phase evolves with dimensions incompatible with those of the bulk of styrylpyrylium crystal. The differences in lattice parameters between the monomer and dimer can be seen in Table 3-1. At some point the dimensional mismatch is so great, and a phase boundary develops. The steeper the light gradient in the crystal, the smaller the macroscopic dimensions of the new phase. Thus when the wavelength of the

irradiation is moved into the shoulder of the chromophore's absorption curve, the crystal still breaks up but it breaks up into bigger pieces. The limiting case is when the wavelength of the irradiation is moved far into the tail of the absorption curve and the crystal remains intact.

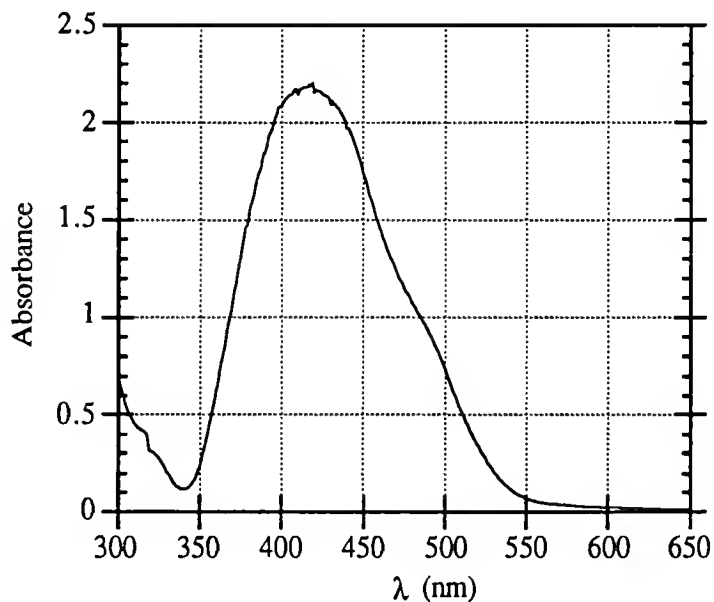


Figure 3-9. The UV-VIS absorption spectrum of a polycrystalline film of the styrylpyrylium triflate monomer cast from an ethanol solution and corrected for light scattering.

### Tail irradiation

UV-VIS reflection measurements made by Professor Dr. Geserich at the Universität Stuttgart, Institut für Physik, on the (100) face of a styrylpyrylium crystal in the region of its absorption tail revealed the following: “the spectra showed a steep absorption tail starting near 640nm. At longer wavelength no absorption is observed. At 620 nm the absorption coefficient  $\alpha$  is about  $7\text{cm}^{-1}$  and it increases at 570 nm to  $62\text{cm}^{-1}$ .” Crystals formed from irradiation of the styrylpyrylium monomer on this face with the 568nm line of a Kr laser are shown in the lower half of the top photos of Figures 3-10 and 3-11. The photos show perfect single crystals of the yellow photodimer.



### X-ray structures of the monomer and as-dimerized dimer

The full x-ray crystal structure of a styrylpyrylium monomer crystal and an as-dimerized cyclobutane crystal are shown in Figure 3-12 and 3-13, respectively. Additional crystallographic data on these two structures are found in Table 3-2. The monomer exhibits disorder in the counterion and t-butyl group. Two statistically occupied orientations for each of those moieties are observed at room temperature of which only one is shown in Figure 3-12. The fact the solid state C-13 MAS spectrum of the monomer showed only one t-butyl signal suggests that this is a dynamic process. This is also confirmed by the observation that when the crystal structure is determined at 165K, this disorder vanishes and only one orientation for each moiety is found. Surprisingly, this disorder is absent at room temperature in the as-dimerized dimer, indicating that the shapes of the original cavities that permitted these rotations in the monomer evolve in such a way so as to prevent these rotations in the dimer. However, no significantly shorter interatomic contacts can be detected in the as-reacted dimer.

### Product comparison

The reflection angles and intensities of the experimental powder x-ray diffractogram of the heterogeneously formed dimer matches that calculated from the crystal structure of the dimer formed from tail-irradiation as shown in Figure 3-14. Thus a single-phase, homogeneous transformation and a heterogeneous transformation, where phase separation is observed, form products of identical crystallographic structure. Because the crystal modification of the dimer formed is independent of the wavelength used for the photoreaction, it is likely that the mechanisms of the two transformations are the same. For example, in Figure 3-5, a length of the cross-section,  $\Delta x$ , may be chosen such that the phase in that region is homogeneous and that phase may be identical to a macroscopic phase observed in the single-phase homogeneous transformation. This should be true for  $\Delta x$  at any point along the cross-section. To put this another way, the continuous phase change undergone by a homogeneously converting crystal with time is identical to

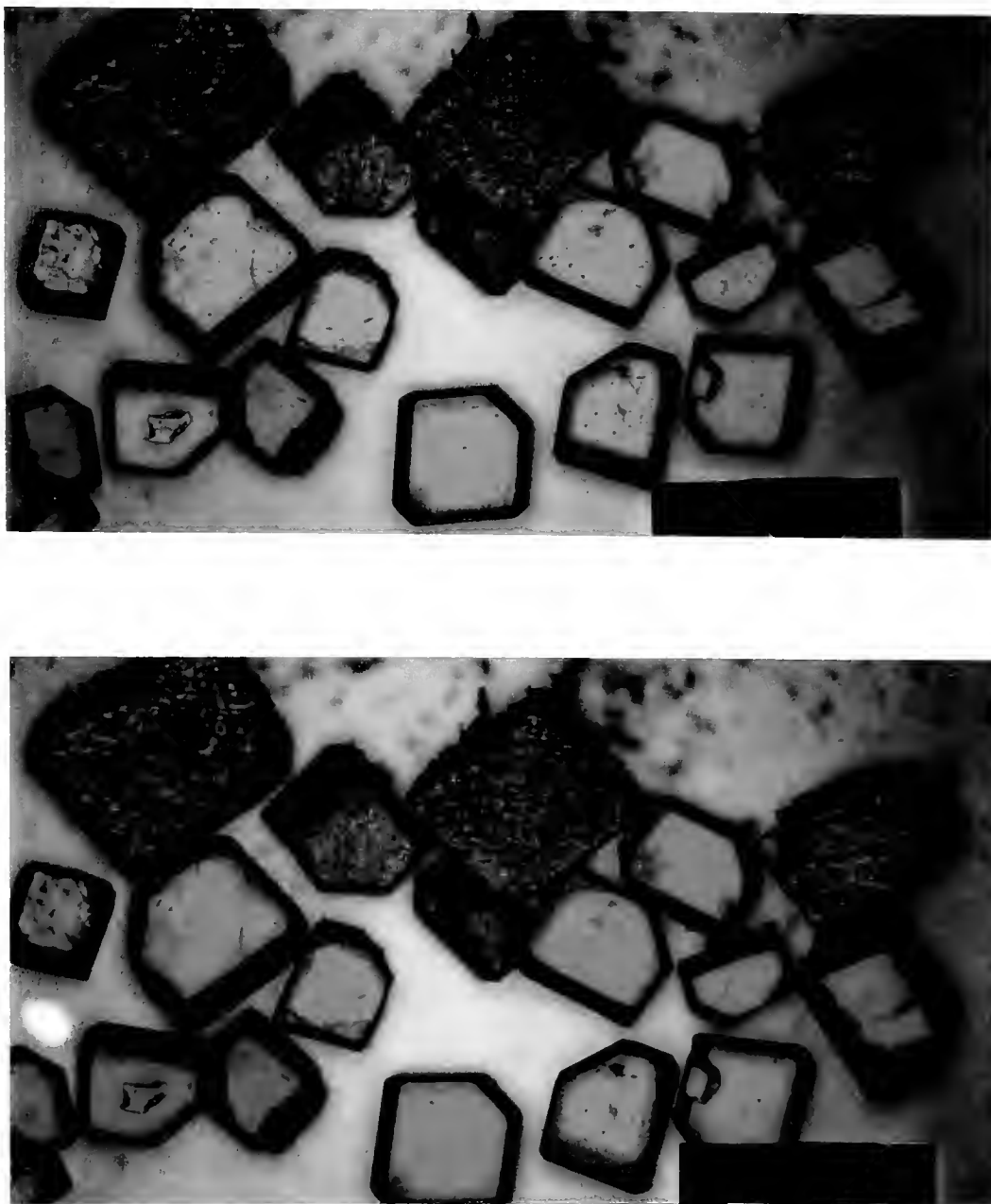


Figure 3-10. The top photo shows styrylpyrylium crystals that have been irradiated in two different ways; here the crystals are viewed with transmitted light. The crystals at the top of each photo are monomer crystals that have been irradiated with unfiltered radiation from a Xenon lamp. They have started to disintegrate into microcrystalline aggregates of photodimer and therefore scatter the light making them appear dark. The clear, yellow crystals in the top photo are photodimer single crystals formed from monomer crystals irradiated with monochromatic light from a laser in the absorption tail of the monomer. The clear, orange crystals in the bottom photo are monomer single crystals formed from heating the photodimer single crystals in the top photo. The crystals are in the range of 0.3 - 0.5 mm in length.

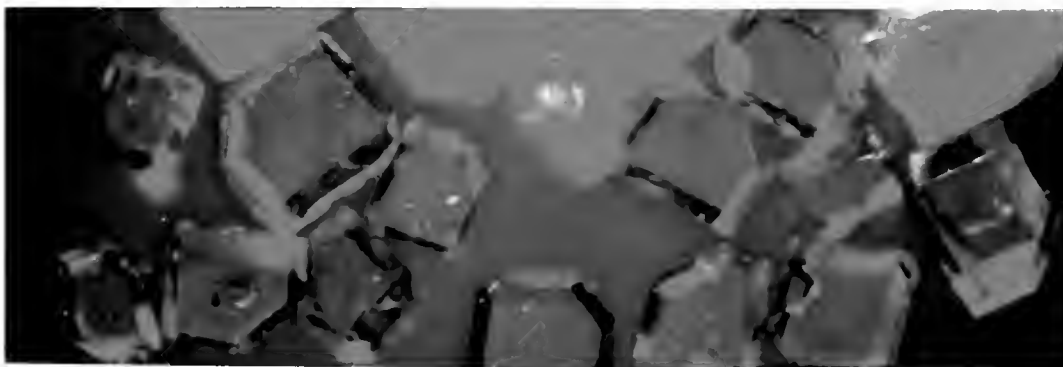
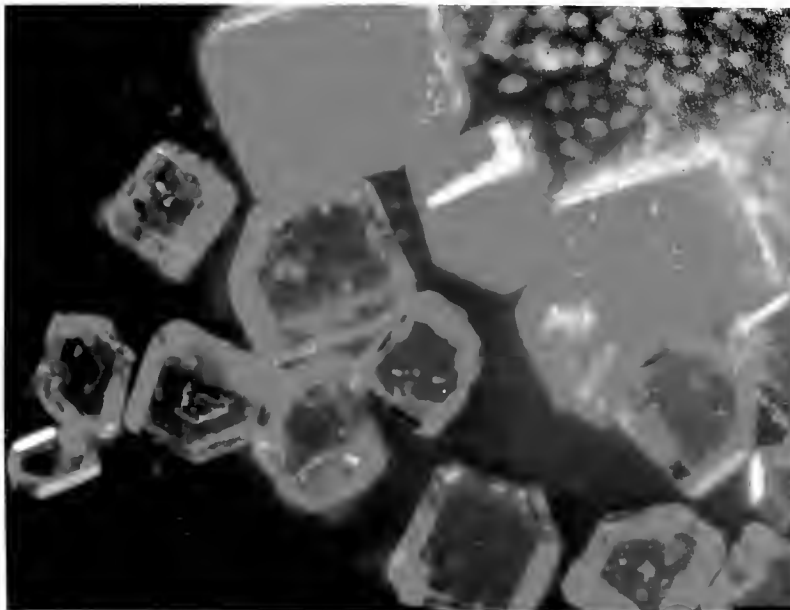


Figure 3-11. The top photo in this figure is of the same subject in the top photo of Figure 3-10 only viewed with light reflected from the side as opposed to transmitted light. Here the yellow microcrystalline aggregates of the heterogeneously formed dimer are visible. The bottom photo corresponds to the bottom photo of Figure 3-10 in an identical manner. The middle photo shows the crystals at an intermediate stage of heating. Note how the single crystals in each photo change from yellow (top) to orange (middle) to red (bottom), with retention of their single crystal character.

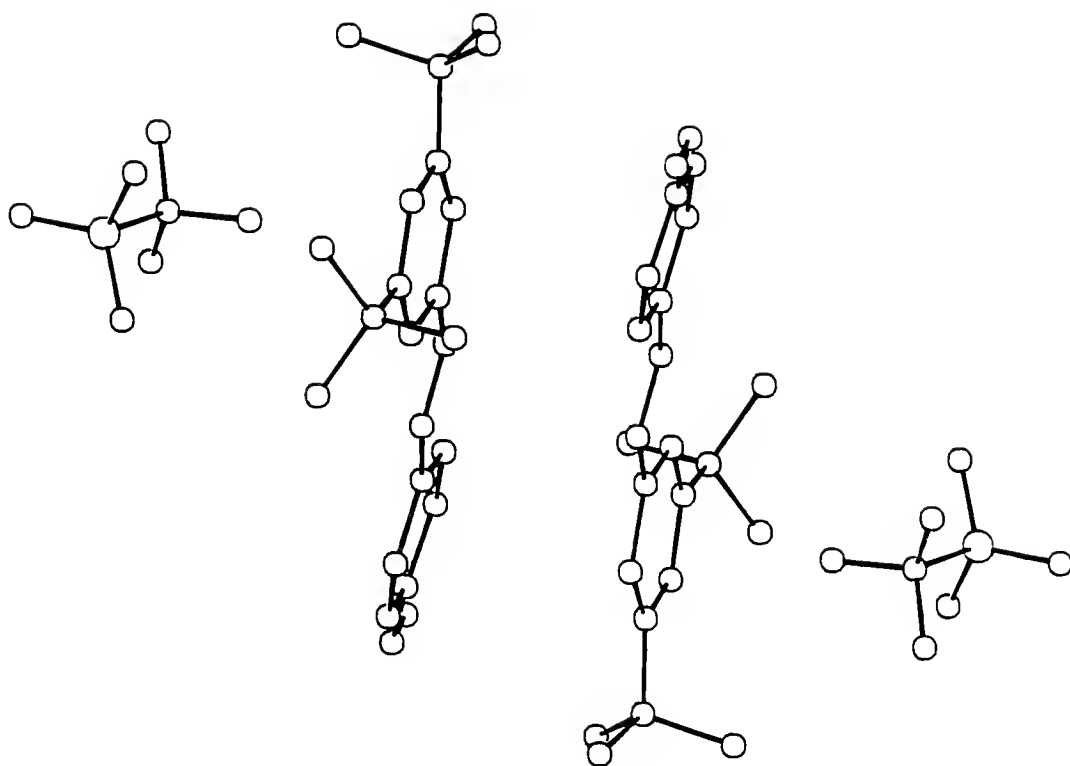


Figure 3-12. Projection of the crystal structure of the styrylpyrylium triflate monomer (1-1c). Crystallographic data is in Table 3-2.

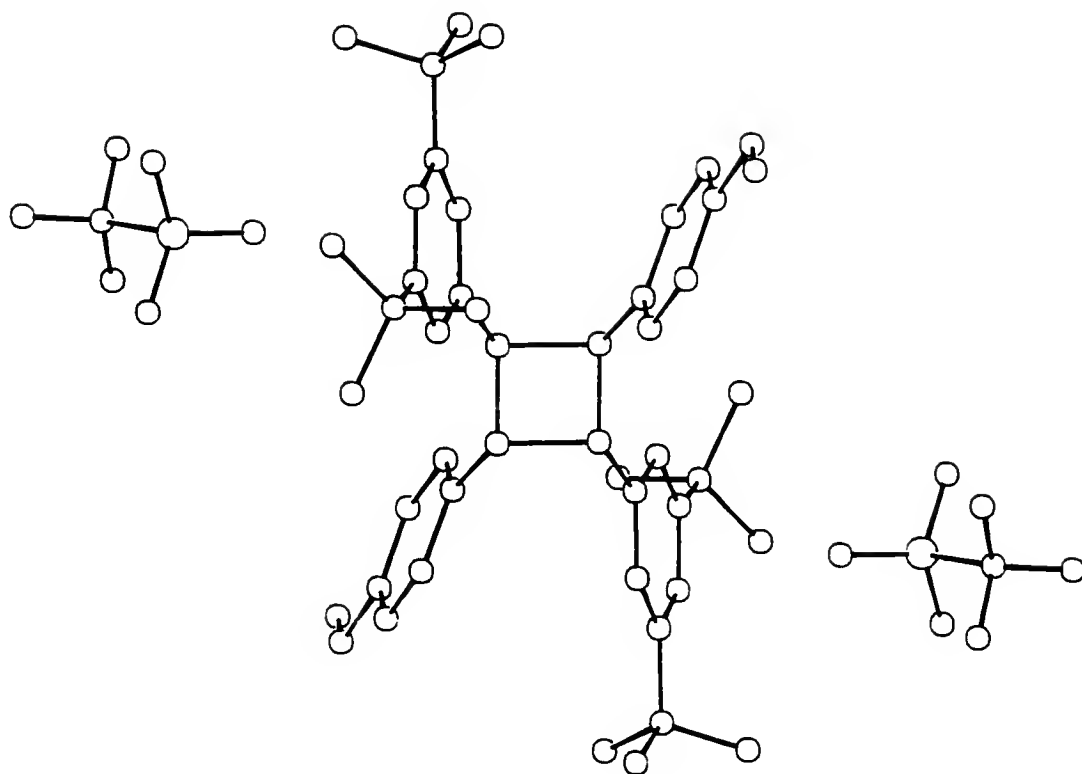


Figure 3-13. Projection of the crystal structure of the styrylpyrylium triflate photodimer (1-4c). The single crystal of photodimer used for this analysis was obtained from irradiation of 1-1c at 568 nm, in the tail of its absorption. Crystallographic data is in Table 3-2.

the phase change seen through a cross-section of a heterogeneously converting crystal (perpendicular to the surface exposed to the irradiation) at any given moment.

### Thermal Cycloreversion: The Backward Reaction

#### As-dimerized dimer

The thermal cycloreversion of the as-dimerized dimer occurs at 110°C with an unusually low enthalpy of reaction of 1.8 kcal mol<sup>-1</sup> as shown in Figure 3-15. (The heat of cyclobutane cleavage in amorphous poly-DSP has been measured at 5.39 kcal mol<sup>-1</sup>.)<sup>9</sup> The thermal cycloreversion of the styrylpyrylium photodimer is a single-crystal-to-single-crystal conversion that produces crystals of the original monomer. The photo series in Figure 3-11 and 3-16 show the transformation of photodimer crystals back to monomer crystals with increasing exposure to heat. The red crystals at the bottom of the lower photo in Figure 3-10 shows monomer crystals viewed with transmitted light, obtained from annealing dimer crystals. A full crystal structure analysis of the thermally regenerated monomer was performed and within experimental error gave identical atomic parameters. This is the first reversible system demonstrated to be a single-crystal-to-single-crystal in both directions. Cycling these monomer and dimer states homogeneously is explored in chapter 6. It should be noted that the crystal quality of the irradiated and subsequently thermally treated crystals as judged by the width of the reflections during crystallographic analysis and the R values (see Table 3-2) is better than that of the monomer crystals formed from recrystallization. This may be due simply to differences in recrystallization batches or there may be a type of annealing effect.

#### Recrystallized dimer

The crystal structure of the recrystallized dimer is shown in Figure 3-17a. When the dimer is recrystallized from organic solvents, crystals of another modification are

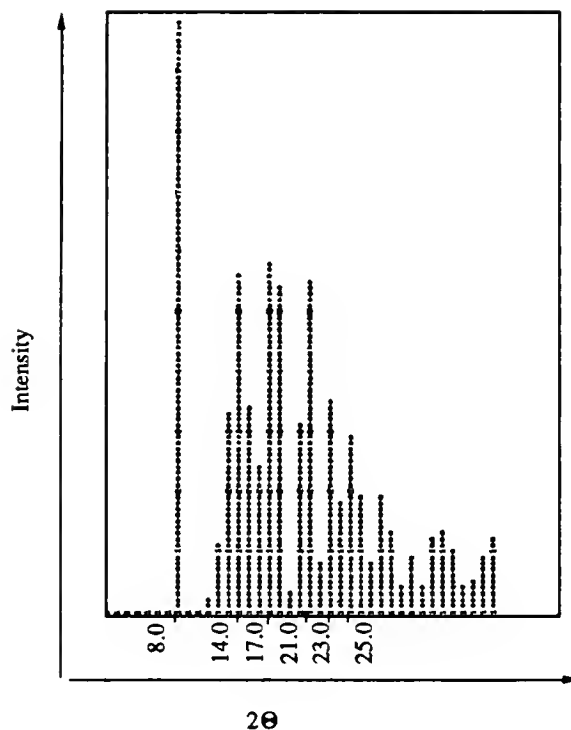


Figure 3-14a.

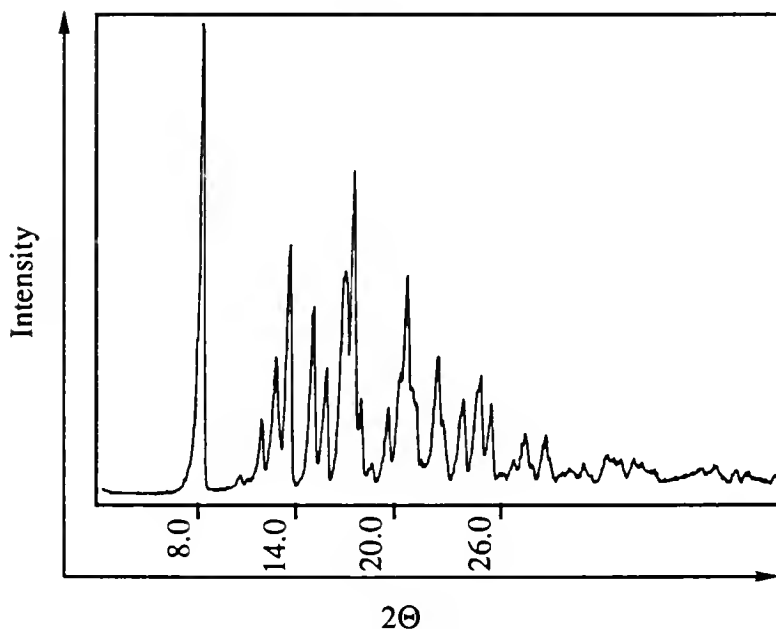


Figure 3-14b.

Figure 3-14. Powder diffractograms from heterogeneous vs. homogeneous photodimerizations of 1-1c.

a) This graph is the calculated powder diffractogram based on the full X-ray crystal structure analysis of a cyclobutane as-dimerized single crystal. (Projection of crystal structure shown in Figure 3-13.)

b) This graph is the measured powder diffractogram of the powder obtained when a styrylpyrylium salt is irradiated with a Xenon lamp without filters.

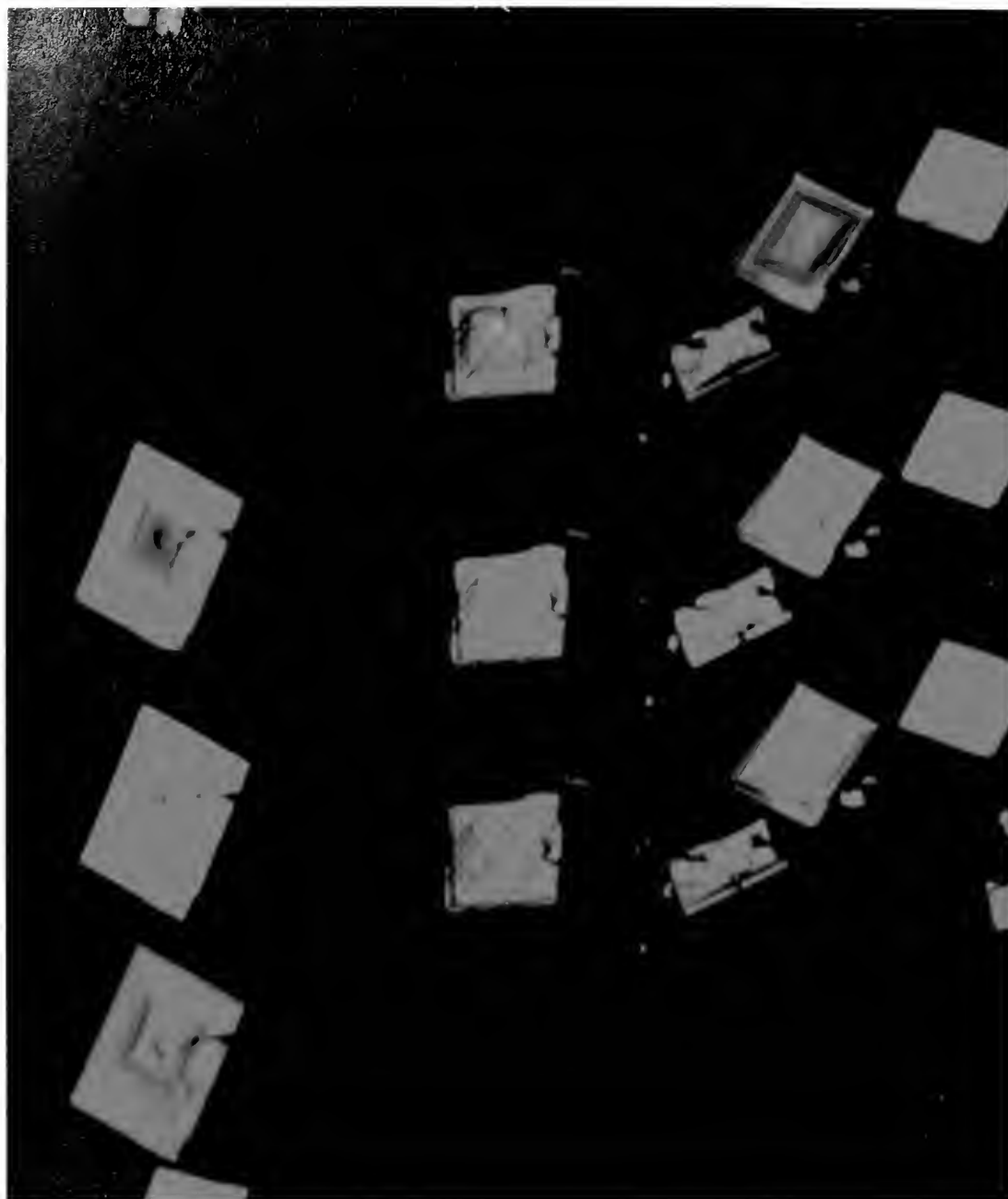


Figure 3-16. This series of photos show the single-crystal-to-single-crystal thermal cycloreversion of photodimer crystals viewed with polarized light. Note that some crystals have cracked during irradiation, but none suffer damage during the thermal treatment. These crystals are 0.10 - 0.20 mm in length.



obtained which, under the same conditions for the thermal reversion of the as-dimerized form, do not convert thermally to the monomer. At room temperature it exhibits the same disorder present in the monomer. Thus the as-dimerized form is apparently in a metastable state, that is, its as-dimerized conformation is not its equilibrium conformation. The consequence of this is a lattice strain which facilitates the back reaction. In the recrystallized dimer, assumed to be much closer to the equilibrium conformation, this lattice strain is absent and consequently the cyclobutane dimer does not cleave. Projections

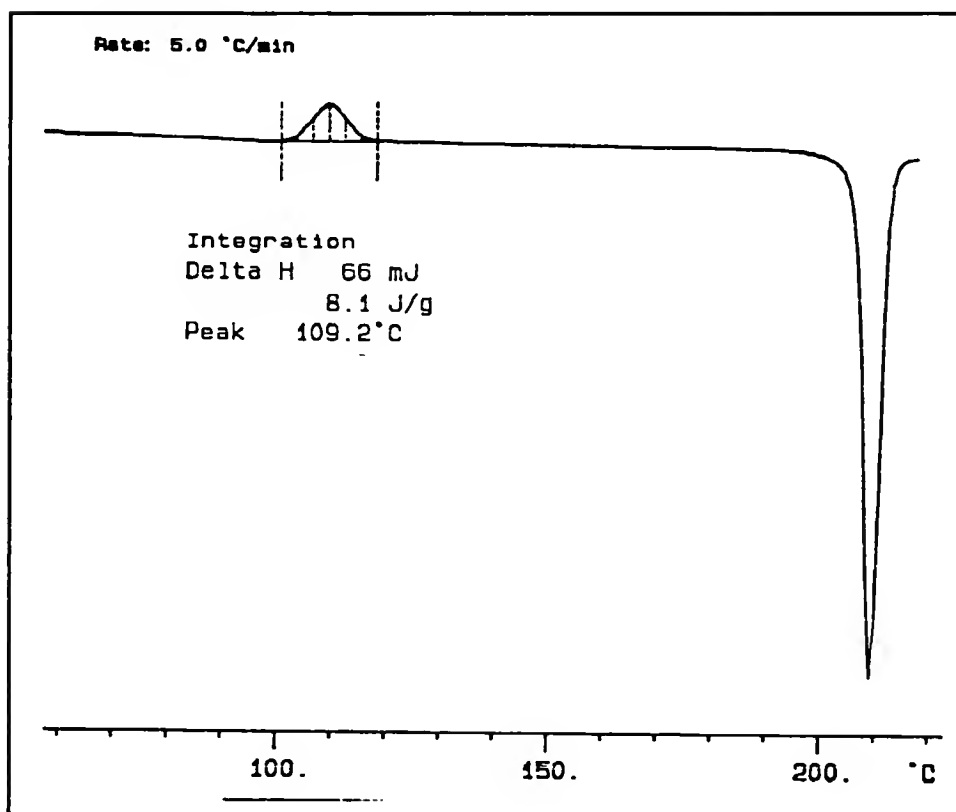


Figure 3-15. The enthalpy of reaction for the thermal cycloreversion of the cyclobutane in the as-dimerized modification is measured by differential scanning calorimetry at  $1.8 \text{ kcal mol}^{-1}$  as shown in the graph above.  $^1\text{H}$  NMR taken of the sample after the exotherm at  $108^\circ\text{C}$  but before the endotherm at  $209^\circ\text{C}$ , indicates an exclusive back reaction to monomer. The area and position of the melting exotherm matches the exotherm obtained when monomer is subjected to thermal analysis.

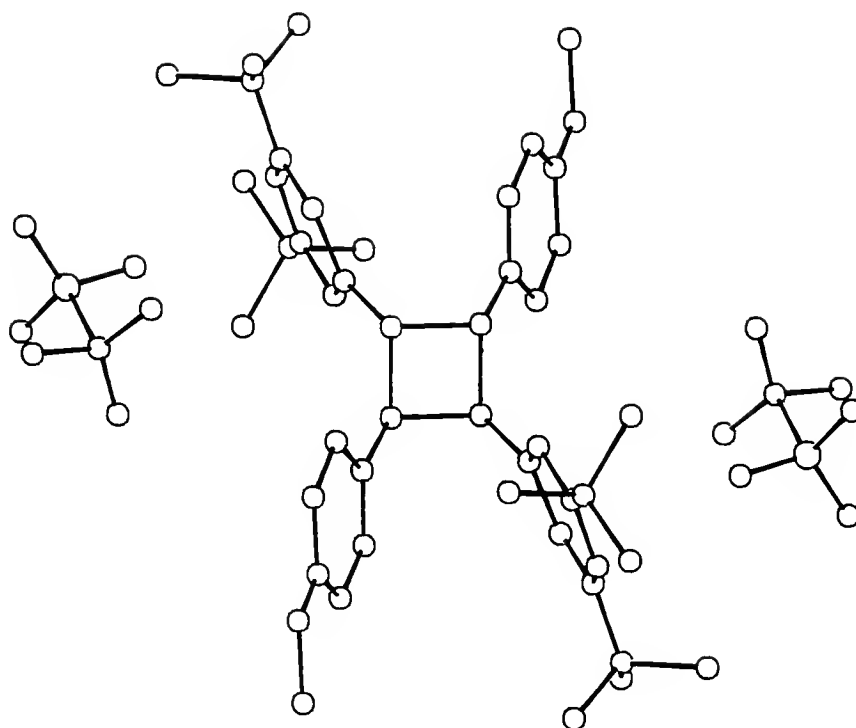


Figure 3-17a.

- Figure 3-17. Projections of the crystal structures of styrylpyrylium photodimer.
- Projection of the crystal structure of the styrylpyrylium triflate photodimer (1-4c) that has been recrystallized from trifluoroacetic acid and ether. Crystallographic data is in Table 3-2.
  - Comparison of the recrystallized and as-dimerized photodimers of styrylpyrylium triflate 1-4c. The as-dimerized dimer maintains the space group of the monomer ( $P2_1/c$ ) whereas the recrystallized dimer has the  $Pbca$  space group.

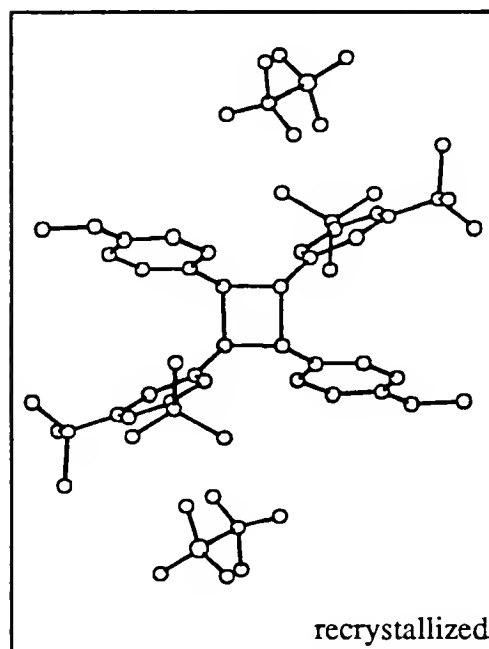
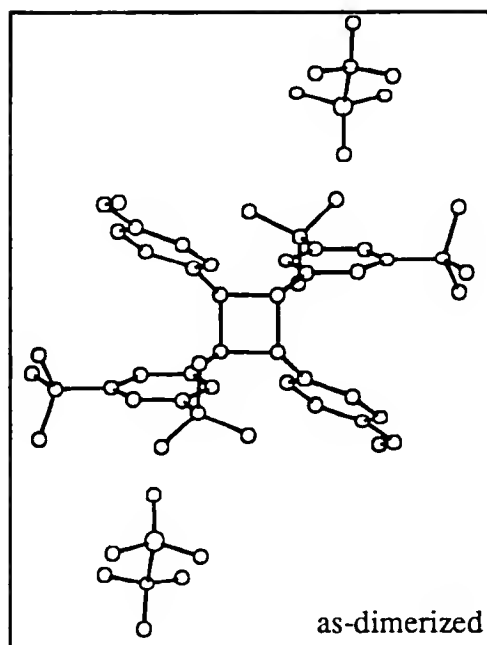


Figure 3-17b.

of the crystal structures of both types of dimers are shown together in Figure 3-17b. This makes an interesting comparison to the case of the thermal depolymerization of DSP. In this case, the superior thermal stability of as-reacted crystalline poly-DSP as compared to that of amorphous poly-DSP prompted the authors to suggest that “the crystal lattice ...protects the cyclobutane cleavage by restricting the local movement of the polymer chain.”<sup>9</sup>

### Substitutional Mixed Crystals: What Happens “In-Between”

#### Time vs. conversion vs. cell parameters

Single crystals of styrylpyrylium monomer were exposed to increasing doses of 568 nm light from a Kr laser to form single crystals containing various amounts of dimer. The power output from the laser was monitored throughout each trial and found to be constant, thus the dosage is directly proportional to the time of exposure. The conversion of the crystals at various times for three trials were measured by IR and the average conversion plotted in Figure 3-18. It was noticed that for certain dosages, among the three trials, the crystals formed cracks or remained intact. The conversions for these two cases are plotted below as well. Cracking led to light scattering and a less efficient conversion. The plot of the average dimer content is linear with time through at least 80% of the conversion. The cell parameters of certain single crystals from the above trials were measured and are shown in Table 3-4. Plots of cell parameters versus conversion are shown in Figure 3-19.

In homogeneous topochemical reactions the overall volume change is often low. However, the changes in lattice parameters can be fairly large since in certain directions van der Waals contact are transformed into chemical bonds. This is the case here, as can be seen in Figure 3-19 where, though the volume change is on the order of 2%, the changes in cell parameters go up to over twice that amount (see Table 3-1). This is truly a homogeneous reaction since these large changes of the cell parameters are nevertheless

continuous. Thus at any point in the conversion, a perfect single crystal exists which can be used for a crystal structure analysis.

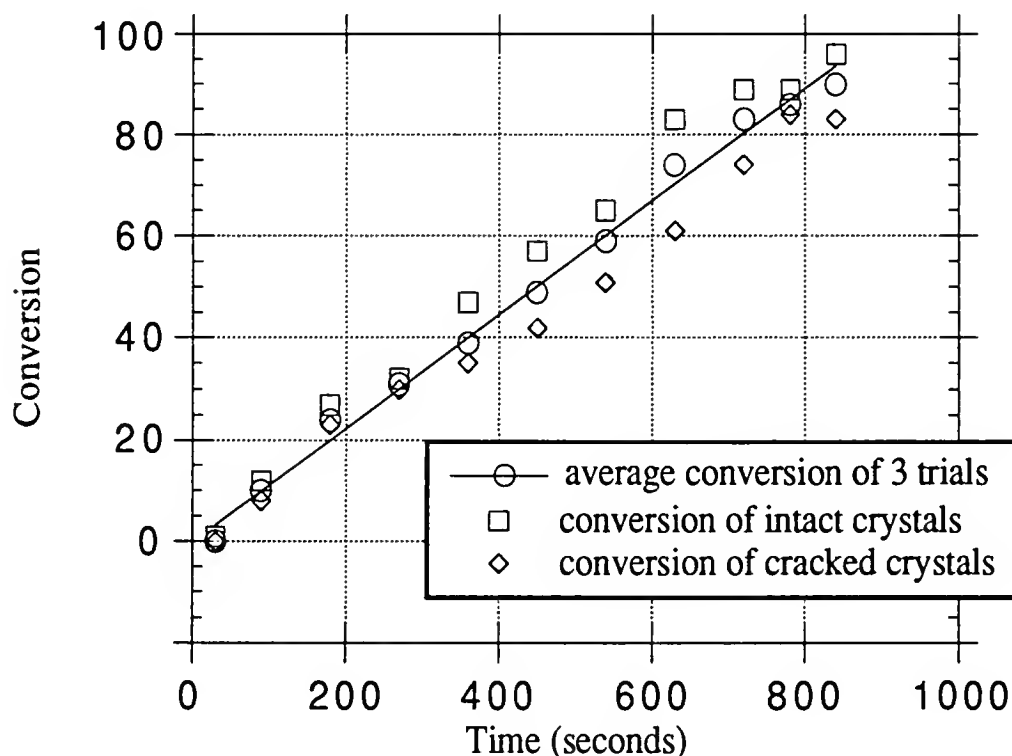


Figure 3-18. Conversion versus time curve for the homogeneous topochemical conversion of styrylpyrylium triflate.

Table 3-4. Unit cell parameters  $a$ ,  $b$  and  $c$  as well as the monoclinic angle,  $\beta$  and the cell volume for substitutional mixed crystals with increasing dimer fraction.

% dimer	$a$ (Å)	$b$ (Å)	$c$ (Å)	$\beta$ (°)	$V$ (Å <sup>3</sup> )
0	10.387	14.785	16.493	103.147	2466.6
8	10.404	14.754	16.519	103.161	2469.0
12	10.416	14.712	16.545	103.092	2469.6
23	10.443	14.641	16.580	103.175	2468.1
49	10.584	14.411	16.605	104.177	2455.6
66	10.750	14.253	16.477	105.266	2435.5
77	10.856	14.155	16.411	106.280	2420.7
89	10.864	14.155	16.413	106.334	2422.2
96	10.863	14.154	16.413	106.321	2421.8
100	10.860	14.145	16.405	106.325	2418.4

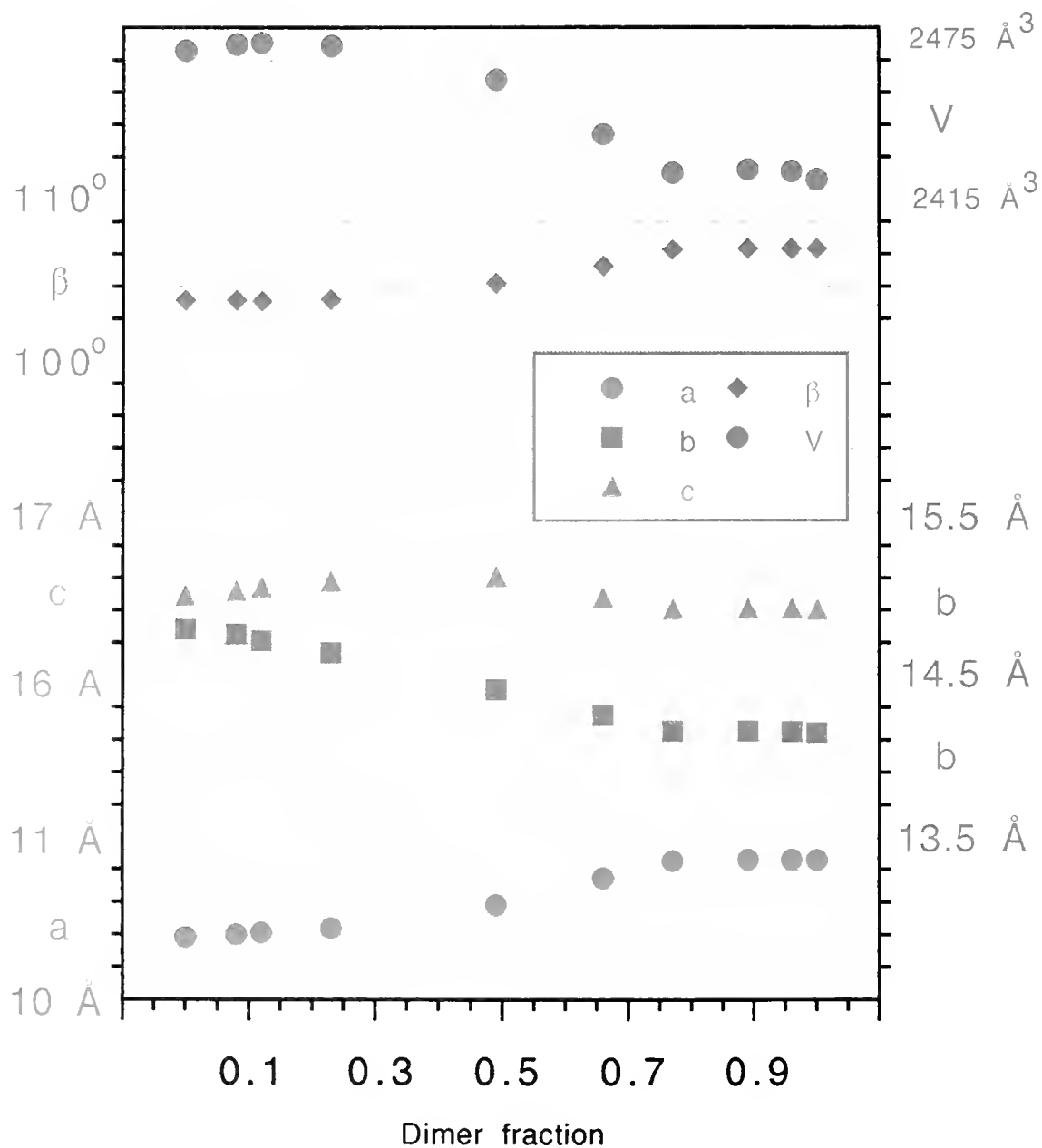


Figure 3-19. This plot shows the continuous change in cell parameters of a series of substitutional mixed single crystals of styrylpyrylium monomer and dimer with increasing dimer content effected with radiation in the absorption tail of the monomer.

### Full x-ray structure analyses

Such crystal structure analyses were performed on crystals at 13% and 67% conversion. These are shown in Figure 3-20 and 3-21. In these crystals, separate atomic coordinates are observed only for the two C atoms which are directly involved in the cyclobutane formation. All other atoms occupy identical positions within the error of analysis. The population parameters have been included in the structure refinement and match the values determined by IR spectroscopy. Thus the states at intermediate conversions can be described as mixed crystals in which the monomer and dimer molecules statistically occupy the same lattice sites.

Figure 3-22 displays projections of the crystal structures of the monomer (Figure 3-12), dimer (Figure 3-13) and substitutional mixed crystals of intermediate conversion (Figure 3-20 and 3-21) for comparison. Consider the conformational reorientation the phenyl rings are expected to undergo for dimerization. The reacting olefin bond can be viewed as a crankshaft: when it rotates into the dimer position, the stiff arm of the phenyl substituent is driven out away from the reacting partner. The phenyl substituent pivots on the connecting  $sp^2$  ring carbon. Thus in a partially reacted crystal, the phenyl substituents should have two orientations: unreacted and reacted. The same argument follows for the pyrylium ring.

However, as mentioned above, two distinct sets of atomic coordinates are observed only for the C atoms which are directly involved in the cyclobutane formation. They correspond to the monomer and dimer positions of those reacting carbons. Only one electron density maximum for each of the atoms in the side groups are observed for each crystal. That is, the positions of the atoms in the phenyl ring and the pyrylium side groups are the same, within the positional error of the crystal structure analysis, regardless of whether those groups are part of a reacted or unreacted molecule.

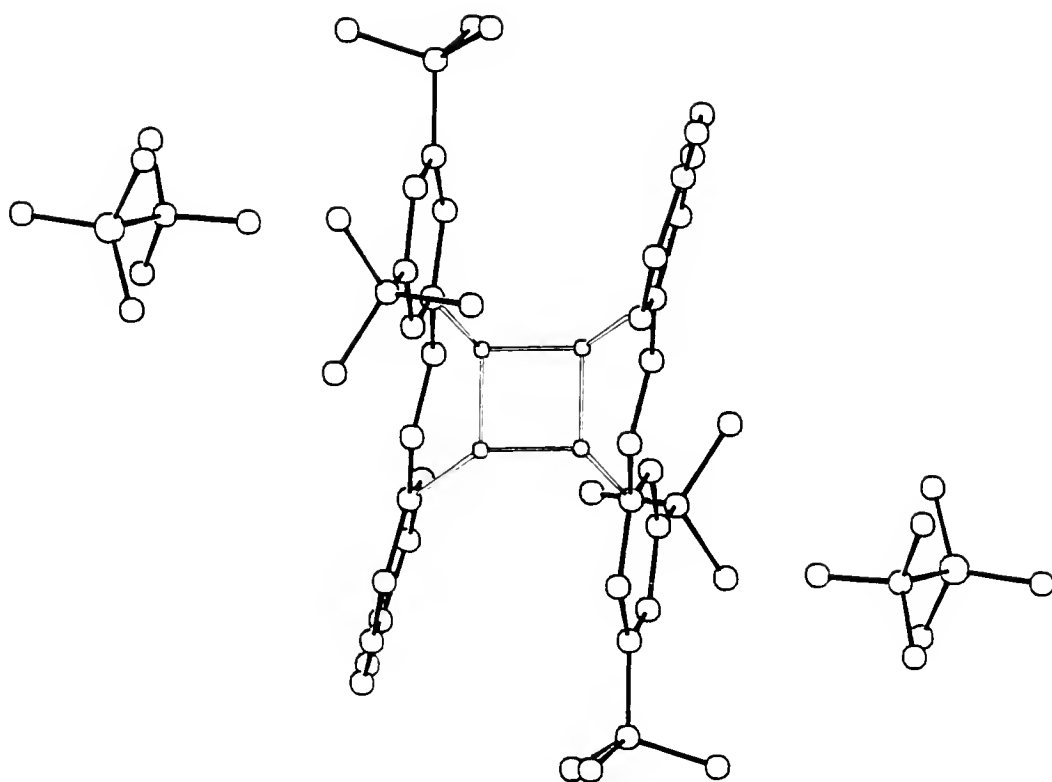


Figure 3-20. Projection of the crystal structure of a styrylpyrylium triflate monomer-dimer substitutional mixed single crystal with a dimer content of 13%. Crystallographic data is in Table 3-2.



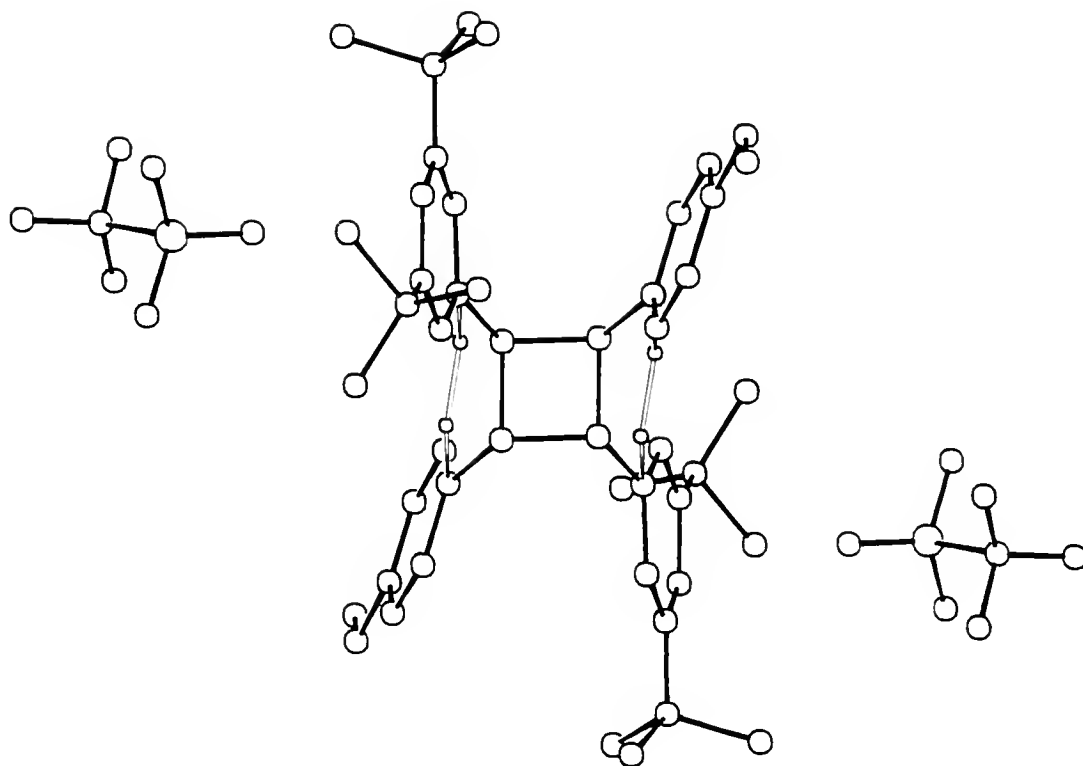


Figure 3-21. Projection of the crystal structure of a styrylpyrylium triflate monomer-dimer substitutional mixed single crystal with a dimer content of 67%. Crystallographic data is in Table 3-2.

It is concluded that two structures with different equilibrium conformations are constrained to the same lattice positions to form a substitutional mixed crystal, the structure of which is established by the intermolecular contacts between the side groups. The consequence of the single orientation for each side group in these structures is bond angle deformation. Note that the deformation observed for the phenyl carbon attached to the cyclobutane ring is greater than that for the phenyl carbon attached to the unreacted double bond. Thus the crystal structure may be viewed as a compromise between the conformations of the monomer and dimer, with the expected result that the species of higher concentration in the lattice is less deformed. This deformation can be measured as the angle between the plane of the phenyl ring and the axis corresponding to the bond linking the phenyl ring to the cyclobutane carbon or the unreacted olefin carbon. Table 3-5 summarizes these values for the phenyl ring and the pyrylium ring and Figure 3-23 shows a plot of these values versus percent conversion.

#### Side-group rotation

As the dimer lattice evolves, the side groups also rotate along the axes of the bonds which connect them to the reacting centers. The rotational conformation of the phenyl rings, as well as the pyrylium groups, as seen in Figure 3-22, shows significant differences in the 13% dimerized mixed crystal compared to the 67%. For example, in the crystal with 13% dimer content, the view of the phenyl substituent, behind the plane of the cyclobutane ring, is to the side of the phenyl ring which faces the reacting partner. Whereas for the crystal with 67% dimer content, the view is on the opposite side. The phenyl ring rotates by  $18^\circ$  in the conversion from monomer to dimer. The rotation of the phenyl ring, as measured as the dihedral angle between the plane of the

Table 3-5. A measure of bond angle deformation in the styrylpyrylium substitution mixed crystals.

% dimer	phenyl ring tilt <sup>a</sup> monomer	dimer	total <sup>b</sup>
0	3.8°	(37.3°)	40.4
13	6.2°	34.7°	40.3
67	21.0°	13.7°	34.4
100	(31.2°)	5.1°	35.5

	pyrylium ring tilt <sup>a</sup> monomer	dimer	total <sup>b</sup>
0	2.4°	(26.4°)	27.9
13	3.4°	25.2°	28.3
67	12.8°	13.0°	24.7
100	(18.3°)	6.6°	23.9

<sup>a</sup> Angle between plane of phenyl ring and the axis along the bond linking the phenyl or pyrylium ring to the double bond or cyclobutane ring. Note that in the undimerized crystal, this axis is defined using the coordinates for the cyclobutane ring in the 13% dimerized crystal. In the fully dimerized crystal, this axis was defined using the coordinates for the double bond in the 67% converted crystal. <sup>b</sup> This is the total angle between the olefin-phenyl/pyrylium ring bond and the cyclobutane-phenyl/pyrylium ring bond.

Table 3-6. Phenyl ring rotation with increasing conversion to dimer.

% dimer	phenyl ring rotation <sup>a</sup>
0	94.49°
13	93.62°
67	79.78°
100	77.36°

<sup>a</sup> Dihedral angle the plane of the phenyl ring makes with the plane of the cyclobutane ring. For the undimerized crystal, the cyclobutane plane for the dihedral angle was defined using the atomic coordinates of the cyclobutane rings in the 13% dimer crystals.

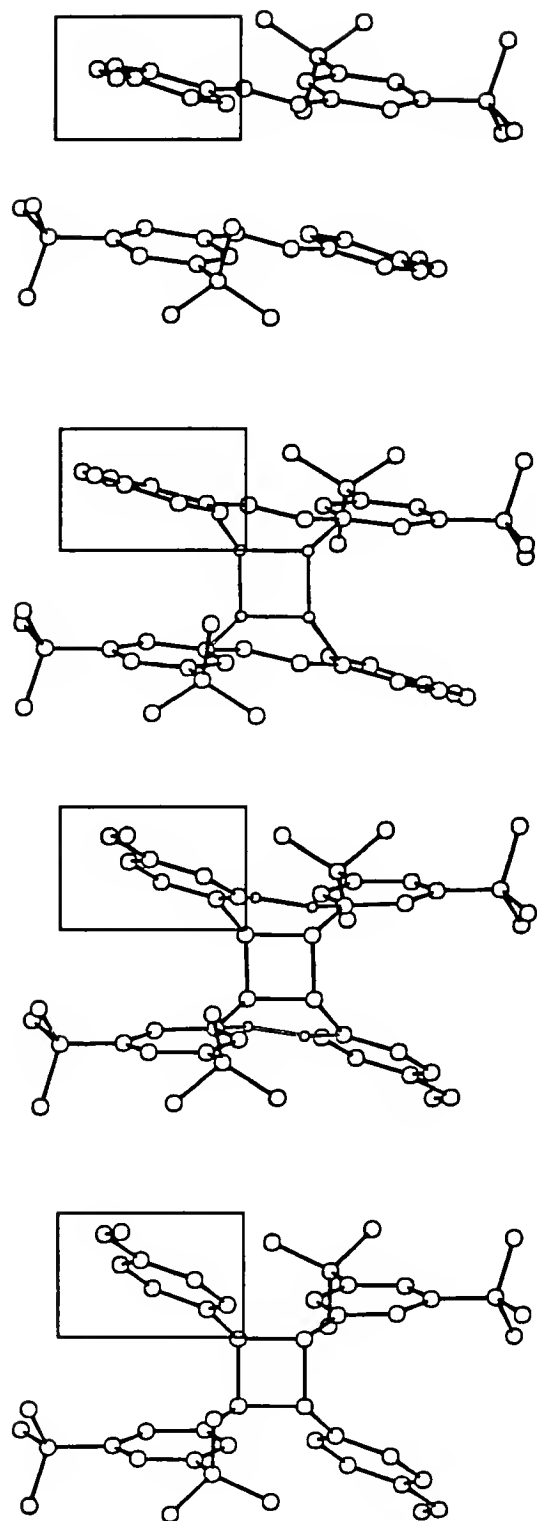


Figure 3-22. This Figure shows projections of the crystal structures shown in Figures 12, 13, 20 and 21 combined, that is from 0 to 100% conversion, omitting the triflate counterion. Note the movement of phenyl ring as the lattice of each single crystal adapts to accomodate more dimer.

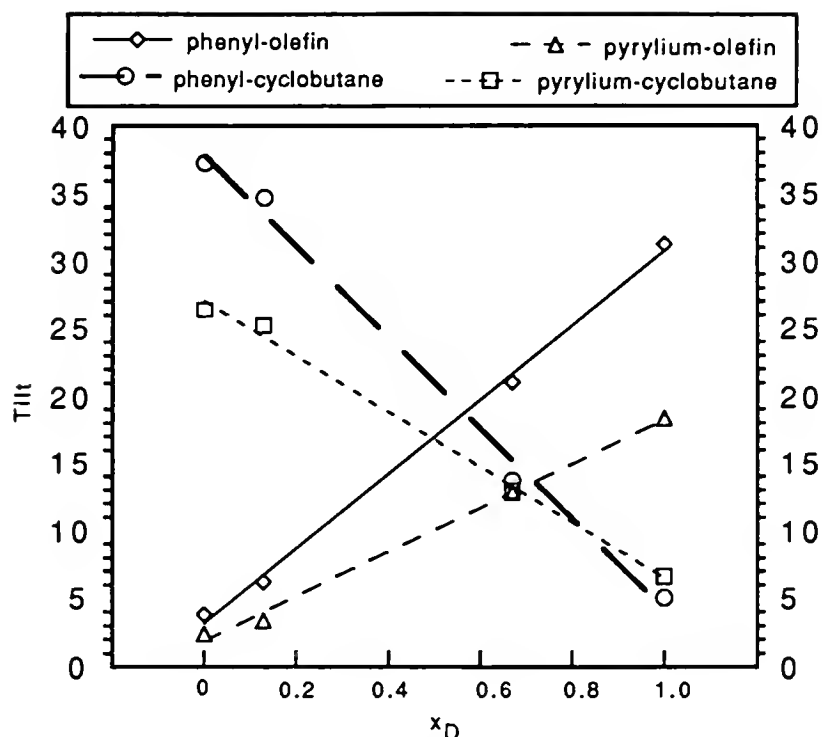


Figure 3-23. Dimer fraction,  $x_D$  versus ring “tilt,” ie., bond angle deformation for the values in Table 3-5.

cyclobutane ring and the plane of the phenyl ring, is listed for each structure in Table 3-6. Similar but smaller conformational changes can be seen for the pyrylium ring and the counterion as well. These rotations seem to be continuous since the rotation angles found in the mixed crystals are between the limiting values of monomer and dimer. See Figure 4-9 for a comparison of the phenyl ring rotation in this styrylpyrylium salt photodimerization and that of  $\alpha$ -trans-cinnamic acid photodimerization.

In summary, two types of conformational changes are observed in the side groups with respect to bonds connecting them to the reacting centers: rotation along the axis of the bond and tilt, that is, the angle the bond makes with the planes of the side groups. In the continuous evolution to the dimer lattice, the side groups reorient themselves to become increasingly planar with the  $sp^3$  bond off the cyclobutane ring as it increases in concentration. The extent to which a side group plane and connecting bond are nonplanar

is a measure of bond angle deformation for the  $sp^2$  carbon. This deformation is the geometrically necessary response to the large displacement of the reacting C atoms in a stiff lattice defined by the intermolecular contacts of these groups.

Thus the side groups serve two functions in a topochemical reaction: one involves an “anchoring” effect, the other involves conformational mobility. The side groups can be seen as anchors in that they determine the intermolecular contacts existing in the crystal lattice. During the course of the conversion, the atomic displacements in these side groups are not large since they are removed from the reacting centers. Thus the side groups preserve the overall packing, stabilizing the evolving lattice changes, and making the continuous shift in lattice parameters possible. On the other hand, the side groups provide the conformational flexibility required such that the reacting centers may approach each other.

#### C=C atom reorientation

It is interesting to note that the position of an unreacted C atom shifts relative to its reacting partner by 0.35 Å from the monomer to the 67% converted crystal. This is explained by considering the monomer is becoming constrained to a structure which accommodates more dimer.

#### Future Studies

Full x-ray structure analysis on substitutional mixed crystals produced from the thermal back reaction of the as-dimerized styrylpyrylium triflate dimer would round out these investigations. It would be expected that the cell parameters from such a study would fall directly on the curves represented by the points in Figure 3-19. Studies similar to the those described in this chapter might also be performed on styrylpyrylium triflates with other substituents besides alkoxy on the phenyl ring. For example, 1-1b and 1-1d photodimerize and thermally reverse as well with the added interesting feature that the monomer undergoes a thermal phase transition. In addition, full x-ray crystal structure on

a crystal of type C\*<sub>MD</sub> in Figure 3-7 would be fascinating to study. This might be achieved by solvent recrystallization or by irradiating a recrystallized dimer with wavelengths of high enough energy to cleave the dimer. It would be important to do this homogeneously, however. Finally, it has been noticed that the styrylpyrylium triflate exhibits chromoisomerism; that is, it crystallizes in two different colored forms: red and gold. The gold platelets rapidly turn red when removed from the acetic acid solution from which they are recrystallized. A crystal structure analysis of this gold form is planned.

## CHAPTER 4 CINNAMIC ACID: A REPRISÉ

### Introduction

Schmidt's investigations on cinnamic acids laid the foundation for the science of topochemical organic solid state reactions. At that time, it was proposed that the dimer goes into solid solution in the monomer lattice until its concentration exceeds the limit of solubility, at which time it precipitates. This is due to the large difference in the crystal structures of the monomer and dimer. Thus the ability of the product to conformationally mimic the monomer in the lattice was thought to control its solubility. The first example of a reaction in which the product never loses its solubility in the monomer lattice was that of the polymerization of diacetylenes. But at some point, for most topochemical reactions and every photodimerization reaction, except BBCP, the photodimer has been observed to precipitate out; that is, nucleate and crystallizes in a second phase. In the case of cinnamic acids it was believed that the strong hydrogen bonding made the lattice too rigid to accomodate dimer.

In his classic treatise on topochemistry based on the cinnamic acid studies, Schmidt predicted that single-crystal transitions would be possible "where two structures are closely related". For example, see Figure 1-11. The view may be taken that the following results show how it is possible to cause a reaction in a crystal so that the *lattice forces* two structures which are not naturally similar, to be similar. On the other hand, it is the intermolecular contacts among the component structures themselves that determine the lattice. Thus one could imagine the preservation of these contacts, likewise, *forcing the lattice* to evolve.



## Results

### t-Butyl Amine Salt of trans-Cinnamic Acid

Tail-absorption irradiation had been successful in producing single crystals of photoproduct in the case of the polymerization of distyrylprazine and in the case of a styrylpyrylium salt. In order to test the generality of this method, the single-crystal-to-single-crystal [2+2] photodimerization of a cinnamic acid derivative was sought.

However, up until now, the few known single-crystal-to-single-crystal topochemical photoreactions had been characterized by centers of unsaturation bearing large side groups, for example, the diacetylene, bis(p-toluene sulfonate) diyne (PTS) and benzyl benzyliidenecyclopentanone (BBCP).<sup>16,94,93,12</sup> Species with a molecular weights over 250 a.m.u. comprise all examples of single-crystal-to-single-crystal reactions in the literature.<sup>16,12,17,18,7,6,10,19,20</sup>

Bulky side groups are thought to be important for single-crystal-to-single-crystal reactions by stabilizing the crystal lattice through intermolecular contacts, in other words, acting as anchors for the reacting atoms which underwent comparatively much more movement. They are also thought to be important for such reactions by reducing the relative amount of cell volume taken up by the reacting centers during bond formation. In other words, large peripheral groups are necessary for a single-crystal-to-single-crystal reaction because the smaller the percentage of reacting components in the monomer, the more the product will resemble the monomer.

The single-crystal-to-single-crystal photodimerization of a cinnamic acid had never been achieved: cinnamic acid has a molecular weight of approximately 150 a.m.u. and, furthermore, it was believed that the hydrogen bonding made the monomer lattice too rigid to permit incorporation of dimer molecules.<sup>13</sup>

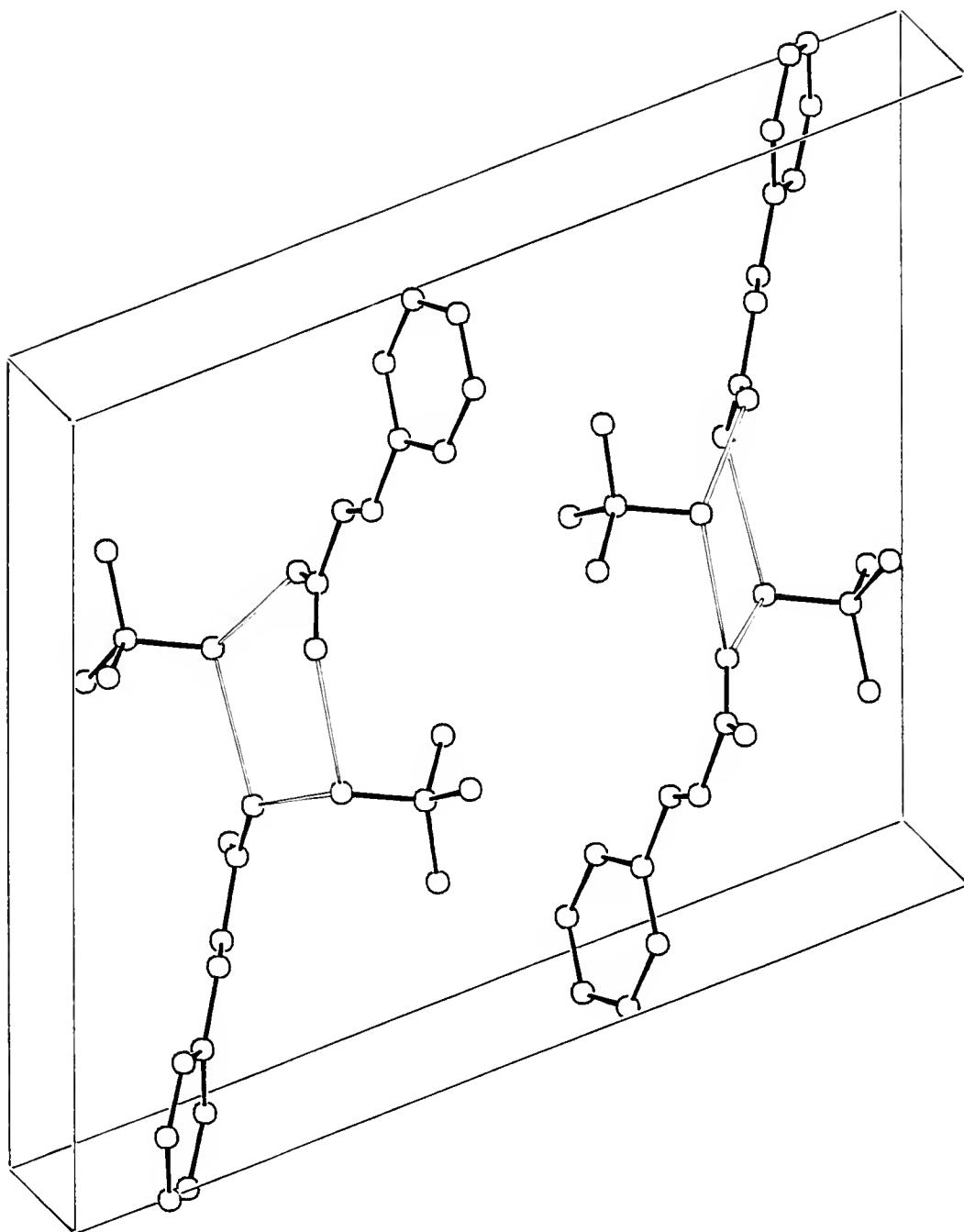


Figure 4-1. t-butyl amine salt of  $\alpha$ -trans-Cinnamic acid

Therefore the compounds in Table 2-6 were synthesized. However they each proved to be photostable, that is, do not undergo a photoreaction. A crystal structure of the t-butyl amine salt of cinnamic acid is shown in Figure 4-1. Each cinnamic acid is isolated from the others through hydrogen bonding with the ammonium salt.

### $\alpha$ -trans-Cinnamic Acid

Focus was redirected to  $\alpha$ -trans-cinnamic acid itself, a known photoactive substance. Single crystals of cinnamic acid monomer were exposed to wavelengths in the tail of their absorption. Since the long-wavelength absorption maximum of cinnamic acid lies around 290nm, the irradiation was performed using a Xenon lamp and an edge filter, which cut off most of the irradiation below wavelengths of 350 nm.

Projections of crystal structures of crystals isolated from this experiment are shown in Figure 4-2 through Figure 4-6, and summarized for comparison in Figure 4-7. Crystallographic data is found in Table 4-1. Figure 4-1 shows the cinnamic acid monomer pair before irradiation while Figure 4-6 shows a projection of the crystal structure of as-dimerized cinnamic acid, truxillic acid. Figures 4-3 through 4-5 show partially dimerized structures.

Table 4-1. Crystallographic data for crystal structures from  $\alpha$ -trans-cinnamic acid photodimerization and the photostable t-butyl amine salt of cinnamic acid.

	0%	100%	28%	40%	67%	2-45
a	7.7163	7.668	7.658	7.625	7.593	13.9630
b	17.6101	18.231	18.217	18.283	18.322	6.3769
c	5.5655	5.595	5.533	5.550	5.594	16.3366
$\beta$	96.396°	106.24°	100.68°	102.41°	104.42°	109.76°
V	751.6Å <sup>3</sup>	750.9Å <sup>3</sup>	758.5Å <sup>3</sup>	755.5Å <sup>3</sup>	753.8Å <sup>3</sup>	1369Å <sup>3</sup>
space group	P2 <sub>1</sub> /n	P2 <sub>1</sub> /n	P2 <sub>1</sub> /n	P2 <sub>1</sub> /n	P2 <sub>1</sub> /n	P2 <sub>1</sub> /c
density	1.307	1.311	1.302	1.300	1.306	1.074
Z	4	4	4	4	4	4
#refl.	985	983	993	917	984	2100
#obs.	775	746	547	575	616	1371
R	0.066	0.040	0.100	0.080	0.073	0.070
R <sub>w</sub>	0.074	0.077	0.077	0.073	0.074	0.040

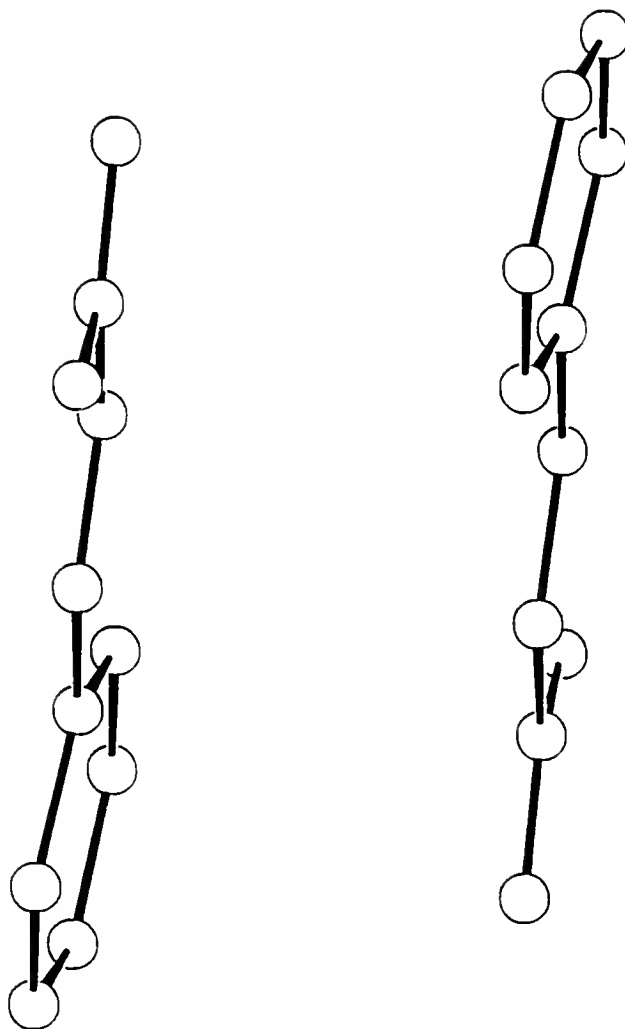


Figure 4-2.  $\alpha$ -trans-Cinnamic acid monomer pair.

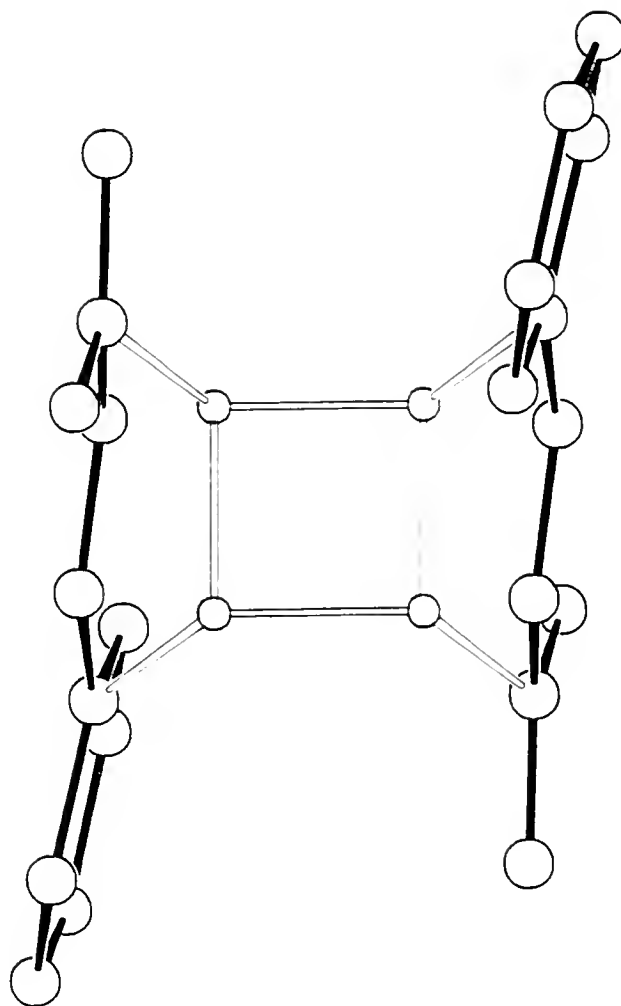


Figure 4-3.  $\alpha$ -trans-Cinnamic acid / truxillic acid substitutional mixed crystal at 28% conversion.

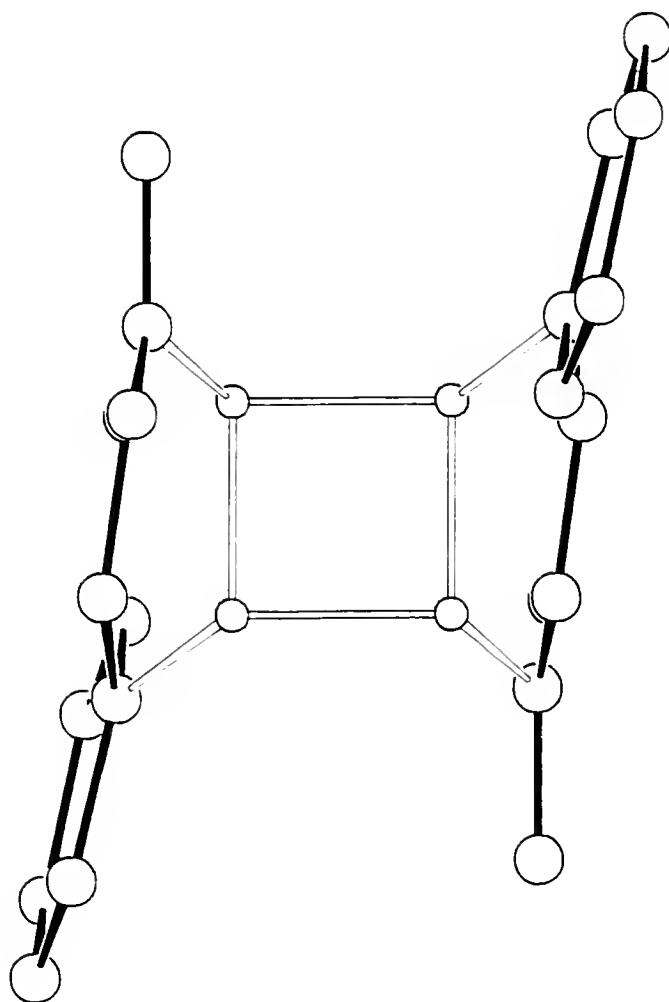


Figure 4-4.  $\alpha$ -trans-Cinnamic acid / truxillic acid substitutional mixed crystal at 40% conversion.

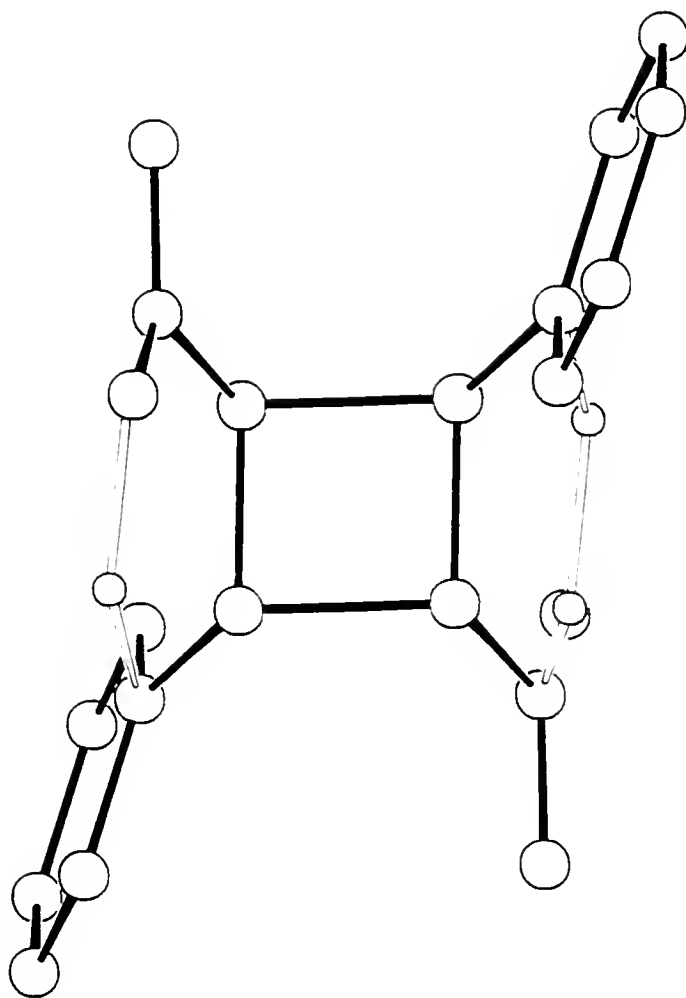


Figure 4-5.  $\alpha$ -trans-Cinnamic acid / truxillic acid substitutional mixed crystal at 67% conversion.

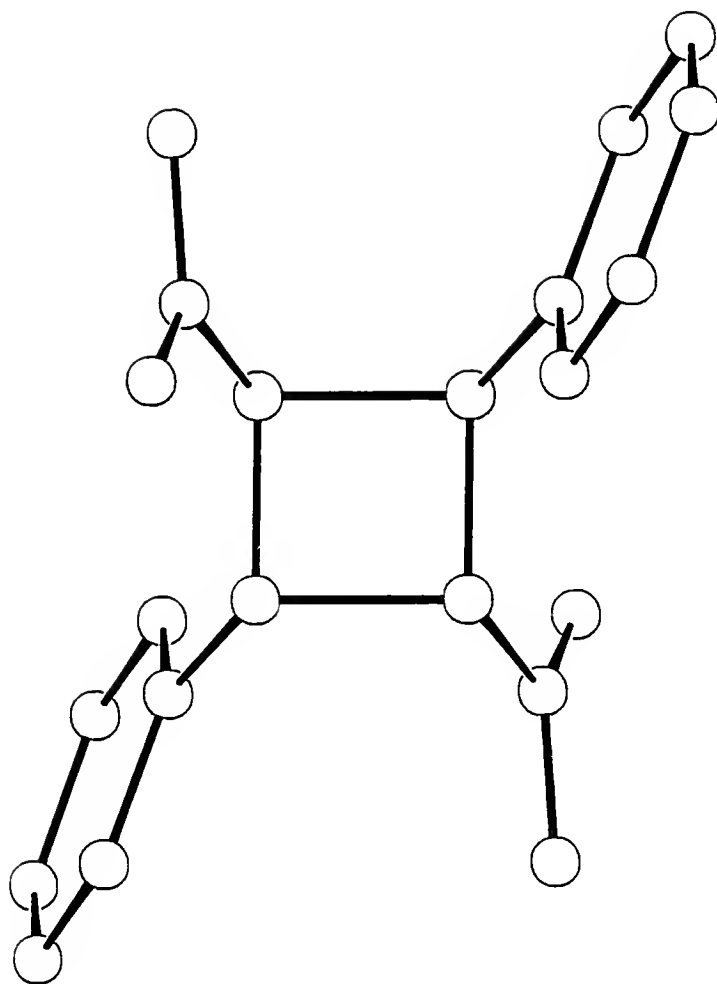


Figure 4-6. As-dimerized truxillic acid.



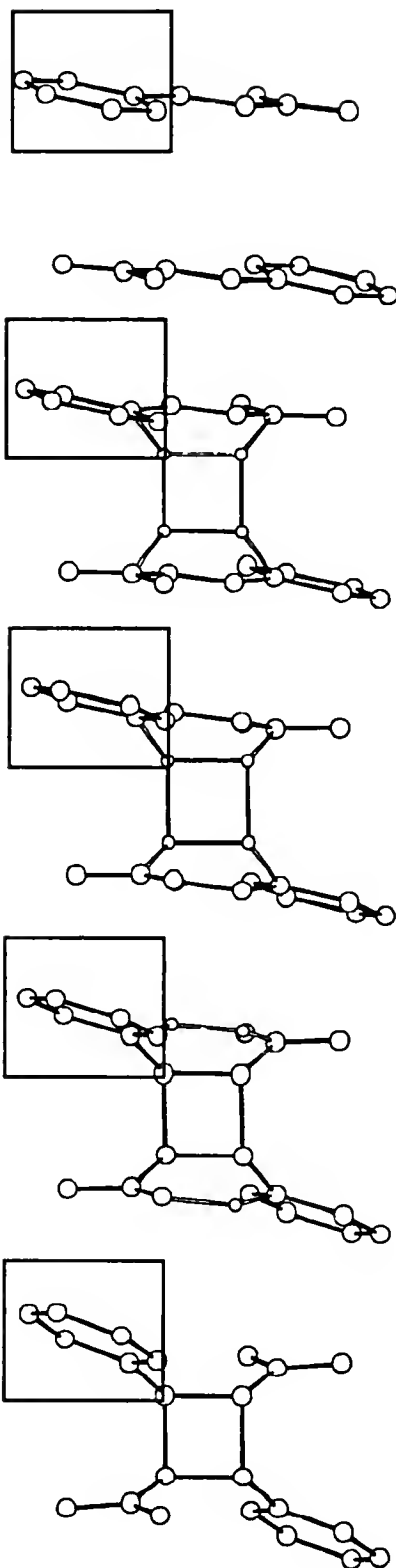


Figure 4-7. Comparison of Figures 6-2 through 6-6:  $\alpha$ -trans-cinnamic acid photodimerization to truxillic acid.

As with the styrylpyrylium salt described in chapter 3, to compare the structures, consider the conformational changes the side groups are expected to undergo during dimerization. When the olefin carbons move toward one another in assuming their new positions as cyclobutane carbons, the side groups move outward and away from the reacting centers. The side groups should have an unreacted orientation, coplanar with the olefin carbon to which they are attached and a reacted position, coplanar with the cyclobutane carbon to which they are attached.

But this is not the case in a partially reacted crystal. Only one set of positions are observed for each side group. All the phenyl groups have the same conformation in a crystal and all the carboxyl groups as well; it is not possible to distinguish side groups attached to olefins or cyclobutane rings. As described above, there are two preferred orientations for the side groups, that is, one in which there is no bond angle deformation for the cyclobutane structure and likewise for the olefin. Which is observed? Neither, rather intermediate conformations are seen depending on the concentration of each species in the crystal, in other words, depending upon how far the dimerization has proceeded. When the olefin concentration is higher, that species has more control over the packing and less deformation is observed in the olefin structure than in that of the cyclobutane. As the olefin concentration decreases, it assumes more deformation. Finally, when the cyclobutane has a higher concentration in the crystal, that species has more control over the packing and most of the deformation lies in the olefin structure. Figure 4-8 shows clearly the preference of the phenyl ring for the conformation coplanar with the olefin and the bond angle deformation suffered by the cyclobutane structure in a 28% dimerized substitutional mixed crystal. In this structure the deformation between the plane of the phenyl ring and the bond connecting the phenyl ring with the cyclobutane ring (hollow line) is  $32.7^\circ$ . The phenyl ring is out of the olefin plane by  $8.2^\circ$ . Table 4-2 contains values for this phenyl ring "tilt". The side groups also rotate along the axes of the bonds which connect them to the reacting centers. Consider the boxed phenyl ring in Figure 4-7. In the monomer

structure the view of the phenyl ring is to the side facing away from the reacting partner or the "top-side". In the next structure, at 28% conversion, the view is nearly parallel to the plane of the ring. At 40% conversion, the ring has continued to rotate so that the view is now to the "under-side" or the side facing the reacting partner. Even more of the "under-side" is seen in the next structure at 67%. Table 4-2 list values for the rotation of the

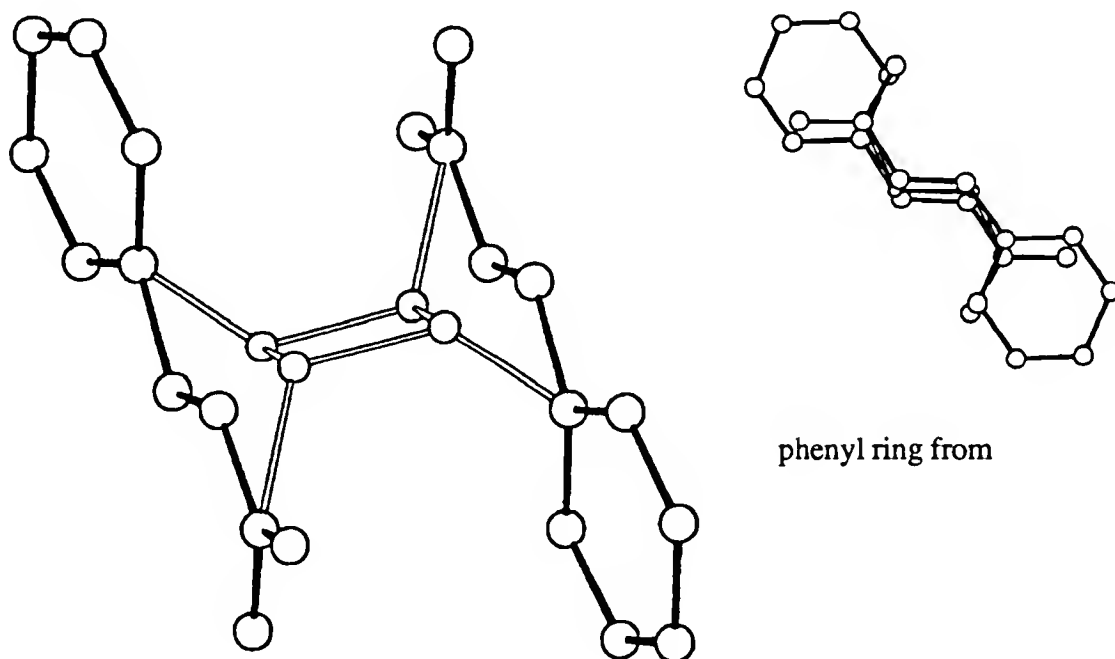


Figure 4-8. Projections of the crystal structure of a 28% substitutional mixed crystal of cinnamic and truxillic acid obtained from the tail-irradiation of a single crystal of cinamic acid. The left-hand projection shows the bond angle deformation in the cyclobutane ring. The right-hand projection is parallel to the plane of the cyclobutane ring.

its starting conformation in the monomer lattice to its final conformation in the dimer lattice and Figure 4-9 graphs the degree of rotation undergone by the phenyl ring from its starting position in the monomer lattice to the dimer lattice in comparison with p-methoxy substituted phenyl ring in the styrylpyrylium salt (see Table 3-6).

These shifts in conformation occur continuously as the relative concentrations of monomer and dimer change. Since these concentration changes occur evenly throughout

the entire bulk of the crystal, the intermolecular contacts among the side group which determine the lattice, are maintained throughout the crystal. Thus throughout the evolution of the lattice, the single crystal is preserved.

Table 4-2. Selected dimensions from crystal structures of  $\alpha$ -trans-cinnamic acid single crystals at various degrees of dimerization.

% dimer	phenyl ring	
	tilt <sup>a</sup> monomer / dimer	rotation <sup>a</sup>
0	--	81.5°
28	8.2° / 32.7°	86.2°
40	15.2° / 25.7°	94.4°
67	25.5° / 13.6°	96.9°
100	---	100.9°

<sup>a</sup> as defined in chapter 3 for Tables 3-5 and 3-6

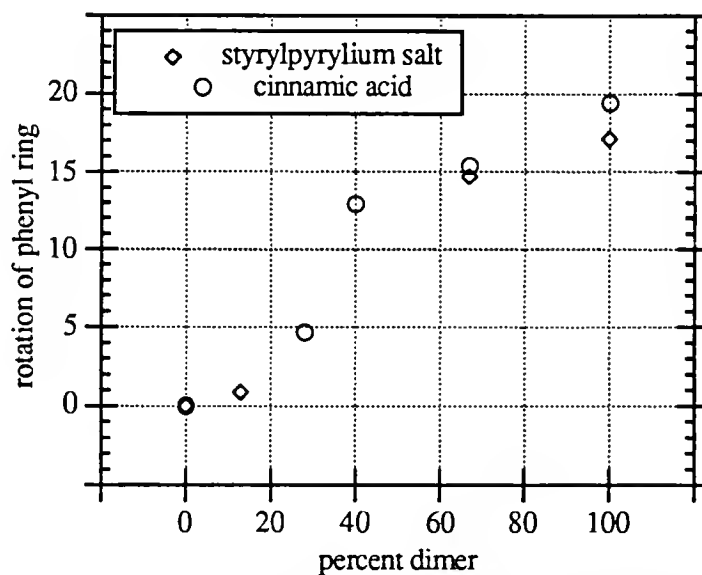


Figure 4-9. This plot shows the amount the phenyl ring rotates from its starting position in the monomer lattice to its final position in the dimer lattice for the cinnamic acid and styrylpyrylium salt photodimerization.

### Future Studies

Figure 1-13 shows a variety of ways in which the product phase may evolve in a solid state reaction. In chapter 3, it was revealed that the product phase obtained from homogeneous evolution,  $\boxed{\text{P}}$  was identical to that formed heterogeneously, P (circled). However, when cinnamic acid is irradiated without a filter, the crystal modification obtained for the truxillic acid is different from that obtained homogeneously as determined by a comparison of x-ray powder diffraction measurements. Investigations directed at determining whether or not the recrystallized truxillic acid represents yet another modification of truxillic acid are underway.

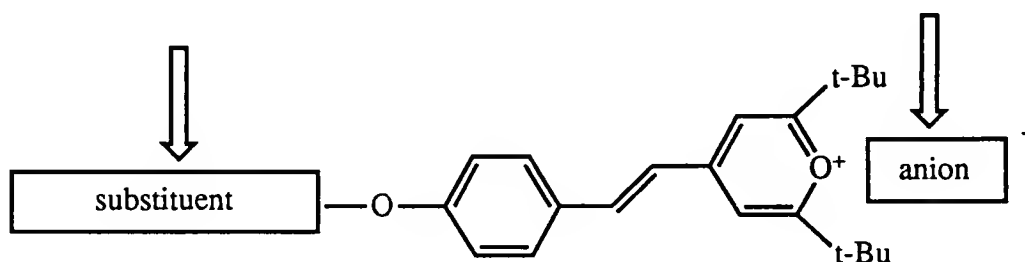
The crystal structure of the recrystallized truxillic acid is being determined.<sup>111</sup> An interesting comparison will then be possible between the as-dimerized and recrystallized truxillic acid structures. If the heterogeneously dimerized truxillic acid does not match the two mentioned above, then three modifications of truxillic acid will have been proven. But what causes this third modification in the broad-band irradiation? A study might be done in which samples of the monomer are irradiated with a series of edge-filters backing into the monomer absorption. X-ray powder diffraction measurements of each irradiated sample might reveal a certain wavelength cut-off which corresponds to a phase transition from the homogeneously as-dimerized truxillic acid to the heterogeneously formed acid. Furthermore, the single-crystal-to-single photodimerization of a  $\beta$  cinnamic acid and a coumarin ("too rigid" to undergo a single-crystal-to-single-crystal reaction) would be further examples of the generality of tail-irradiation for producing such transformations.

## CHAPTER 5 STYRYLPYRYLIUM SALTS: VARIATIONS ON A THEME

### Introduction

#### Crystal Packing

Investigations on a styrylpyrylium salt with a p-methoxy substituent on the phenyl ring and a triflate counterion are reported in chapter 3. This chapter concerns itself with the effects of variations on the basic structure involving counterion as well as phenyl ring substituent replacement as shown below:



Namely, the compounds 2-12 through 2-14 in Table 2-3 and 2-18 through 2-20 in Table 2-4 were synthesized in a step toward crystal engineering to investigate the effects of changing the counterion size, in an isomorphous manner, on the crystal packing and reactivity. This type of investigation has been reported in the literature for acridizinium salts, a [4+4] anthracene-type photodimerization,<sup>20</sup> as well as styrylpyridinium salts.<sup>21</sup>

For example, Williams and coworkers found that although the methiodide salts of certain styrylpyridines were photostable, replacing the iodide with a sulfate resulted in quantitative solid state dimerization.<sup>21</sup> Williams writes "substitution and the nature of the anion might control the crystal parameters and therefore the ease of dimerization" More

recently, Jones and Wang, found the photoreactivity for a series of acridizinium salts followed the order:  $I^- > Br^- > Cl^- > ClO_4^- \approx \text{picrate} \approx \text{oxalate}$ .<sup>20</sup> Cell parameters for each structure are measured and a full structure analysis done on the bromide salt, which, in addition to the iodide undergoes one of the rare single-crystal-to-crystal conversions listed in Table 3-1.

Another study involving N-heteroaromatic quaternary salts is that by Quina and Whitten<sup>22</sup> who also investigated the photodimerization of styrylpyridinium salts. Here the quaternizing group was not a methyl, as used in the study by Williams, but rather an eighteen-carbon aliphatic chain. Four counterions were tested including bromide, tetrafluoroborate, chlorosulfonate and bromosulfonate; only the sulfonates were reactive. Although a head-to-tail alignment of the chromophore would minimize steric and like-charge repulsion (as is seen in the styrylpyrylium salts discussed in this Thesis), the product has a head-to-head orientation. No crystallographic measurements were made but the authors speculate that a "preferential association of hydrophilic zones and of hydrophobic zones occurs" due to a "crystal packing phenomenon in which molecular shape such as the regular structure of the hydrocarbon chain plays a major role." They note that interchain spacing of hydrocarbons is approximately 4.2 Å. Thus such packing could bring attached olefins within the distance typically necessary for reactivity. Thus the methylene-bridged salts in Table 2-5 were synthesized in a search for [2+2] photopolymerizable crystals.

### Kinetic Investigations on [2+2] Photodimerizations

Investigators in the field of organic solid state chemistry have often noted that quantitative mechanistic studies on molecular solid state reactions are few and often sketchy. It has been pointed out that an assumption of first-order kinetics may not always be valid because solid state kinetics is often complicated in comparison to solution kinetics by induction periods and mid-reaction changes in mechanism. For example, Heyes and

coworkers<sup>59</sup> have investigated the photodimerization of  $\alpha$ -trans-cinnamic acid and its o-methoxy derivative by solid state NMR spectroscopy.

Sharp-Hancock plots,  $\ln(-\ln(1-\text{conversion}))$  vs.  $\ln(\text{time})$ , were made on the time vs conversion data collected for the photodimerization of each of these compounds performed with broad-band irradiation. From 5 to 25% and 30 to 75% a slope of 1.0 was observed, with a shallow changeover slope connecting the two regions. Over 75% the slope was 2.0. It has been empirically determined that a slope of 1.0 corresponds to a random first order nucleation mechanism, whereas a slope of 2.0 indicates a 2-dimension nucleation and growth mechanism is controlling the rate.

Thus the following interpretation was made: At 25 to 30% the initial first order reaction mechanism is replaced by a second first-order reaction mechanism. It was suggested that this might be due to a change in the phonon mode assisting the reaction, due in turn to the change in lattice parameters that occurs as the lattice accomodates more cyclobutane. Both first order plots intersect the origin, indicating they are sequential processes. When the conversion reaches 75% the authors state that "This is the point at which reaction at random lattice sites gives way to nucleation and growth. At this stage in the reaction, phase separation occurs and the reactant lattice loses its physical significance..."

Time vs. conversion curves and the corresponding Sharp-Hancock plots for the styrylpyrylium salts 2-12 through 2-14 are presented below

## Results

### Crystal Structures

Imagine two chromophores packed parallely in a lattice with a certain double-bond-center to double-bond-center, separation distance,  $d$ , as shown in Figure 5-1. How is the reactivity of the these double bonds affected as  $d$  is changed? Altering  $d$  can be likened to the action of a vise comprising two jaws, the olefin planes, held together by a threaded



shaft, the lattice. Rotating the shaft draws the planes closer or pulls them apart. Might this type of action be realized in the crystal lattice of a styrylpyrylium salt by substituting the counteranion? The styrylpyrylium salts, 2-12 through 2-17, were synthesized in an effort to answer this question.

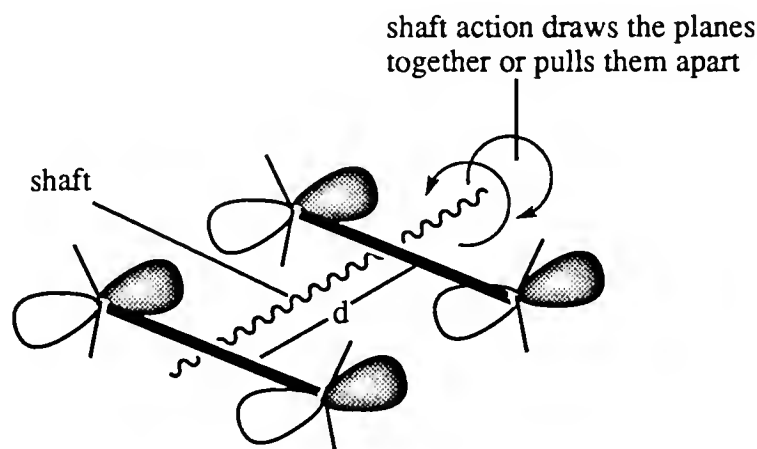


Figure 5-1. The crystal lattice holds two olefin planes apart by a distance,  $d$ , like a vise separates the planes of two adjustable jaws with a threaded shaft.

#### Gold dichloride and tin pentachloride counterions

The pyrylium salt, 2-4, with the tin hexachloride counterion was synthesized as an intermediate to the isomorphous series, 2-12 through 2-14. As an incidental experiment, 2-4 was also refluxed with *p*-anisaldehyde to give a styrylpyrylium salt with a new counterion. The salt picture in Figure 5-2 was expected; however, the relatively unknown tin pentachloride counterion was created instead. A projection of the crystal structure, roughly parallel to the plane of conjugation is shown in Figure 5-3. The counterion is disordered as is indicated by the hollow bonds connecting the tin atom to the two partially occupied chlorine positions. Figure 5-4 shows a projection of the crystal structure perpendicular to the plane of the *p*-methoxy-substituted ring. These two projections show that  $\theta_1$ ,  $\theta_2$ , and  $\theta_3$  (see chapter 1, Background section) are nearly ideal for

photodimerization and, indeed, this structure is photoactive; its cell parameters and other crystallographic data are listed in Table 5-1.

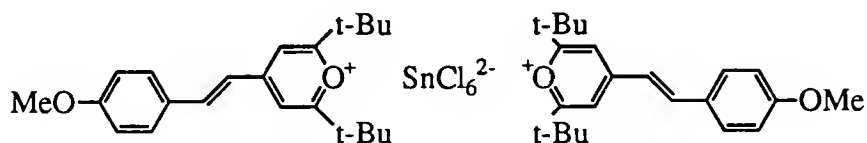


Figure 5-2. Expected product from the reaction of 2-4 with p-anisaldehyde. Crystal structure of obtained salt, tin pentachloride counterion, shown in Figure 5-3 and 5-4.

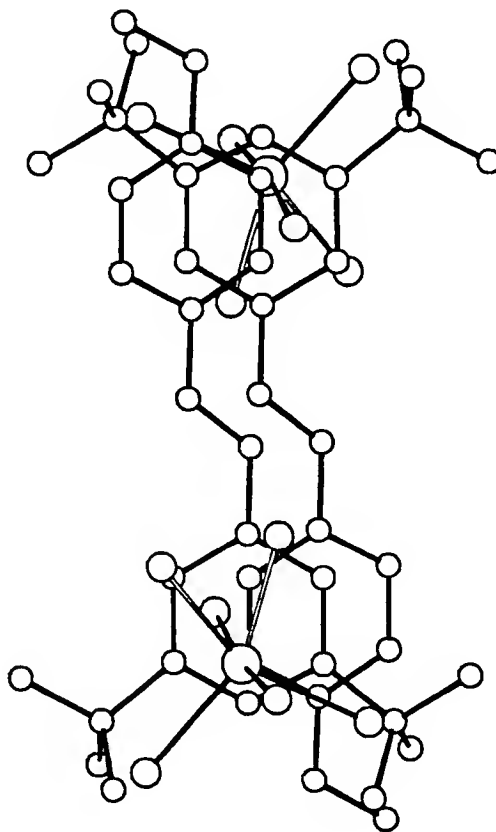


Figure 5-4. Projection of crystal structure of  $\text{SnCl}_5^-$  styrylpyrylium salt perpendicular to phenyl ring plane.

As part of a  $\text{BF}_4^-$ ,  $\text{ClO}_4^-$ ,  $\text{ReO}_4^-$  series (2-12 through 2-14), the synthesis of the  $\text{AuCl}_4^-$  styrylpyrylium salt was attempted by refluxing the  $\text{AuCl}_4^-$  pyrylium salt, 2-5, with p-anisaldehyde. Instead, the  $\text{AuCl}_2^-$  salt was obtained. A projection of the crystal structure including cell axes is shown in Figure 5-5; see Table 5-1 for crystallographic data.

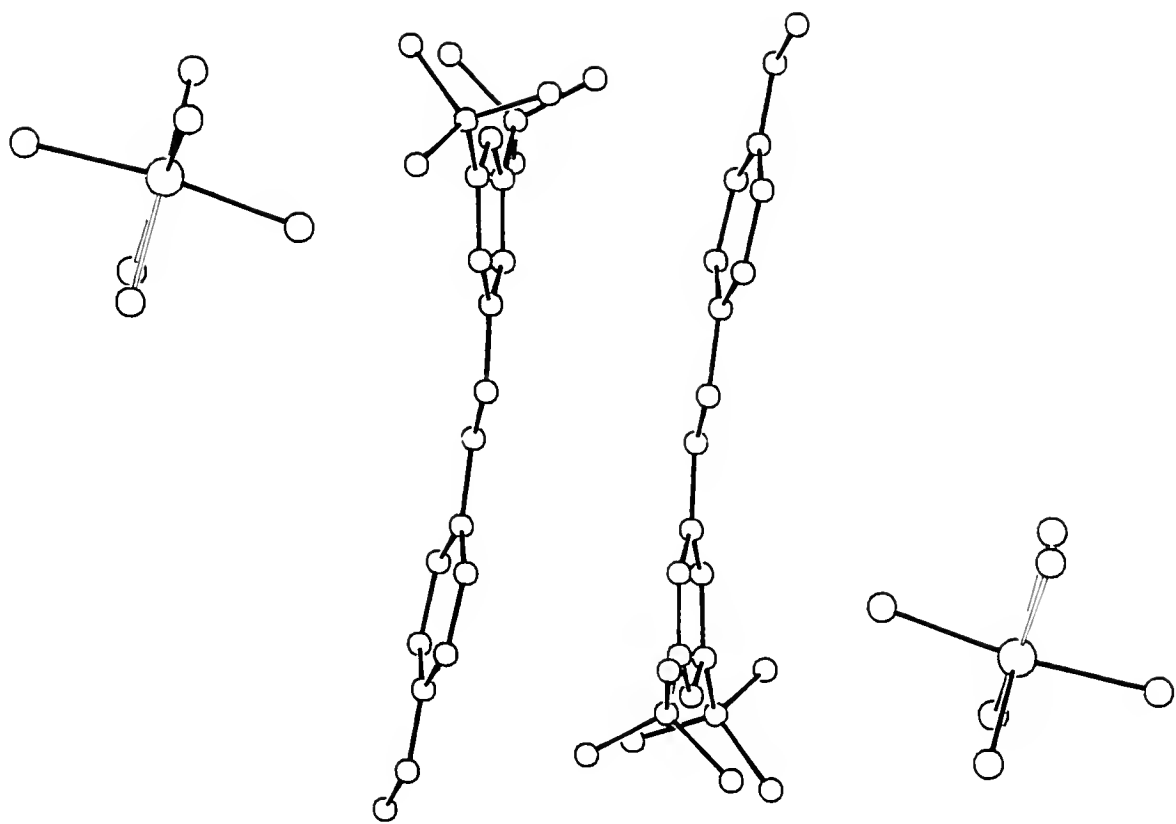


Figure 5-3. Projection of the crystal structure of styrylpyrylium salt 2-15,  $\text{SnCl}_5^-$  counterion. The two hollow bonds indicate that there is disorder in the counterion and these two positions are statistically occupied in the crystal by the fifth chlorine atom.

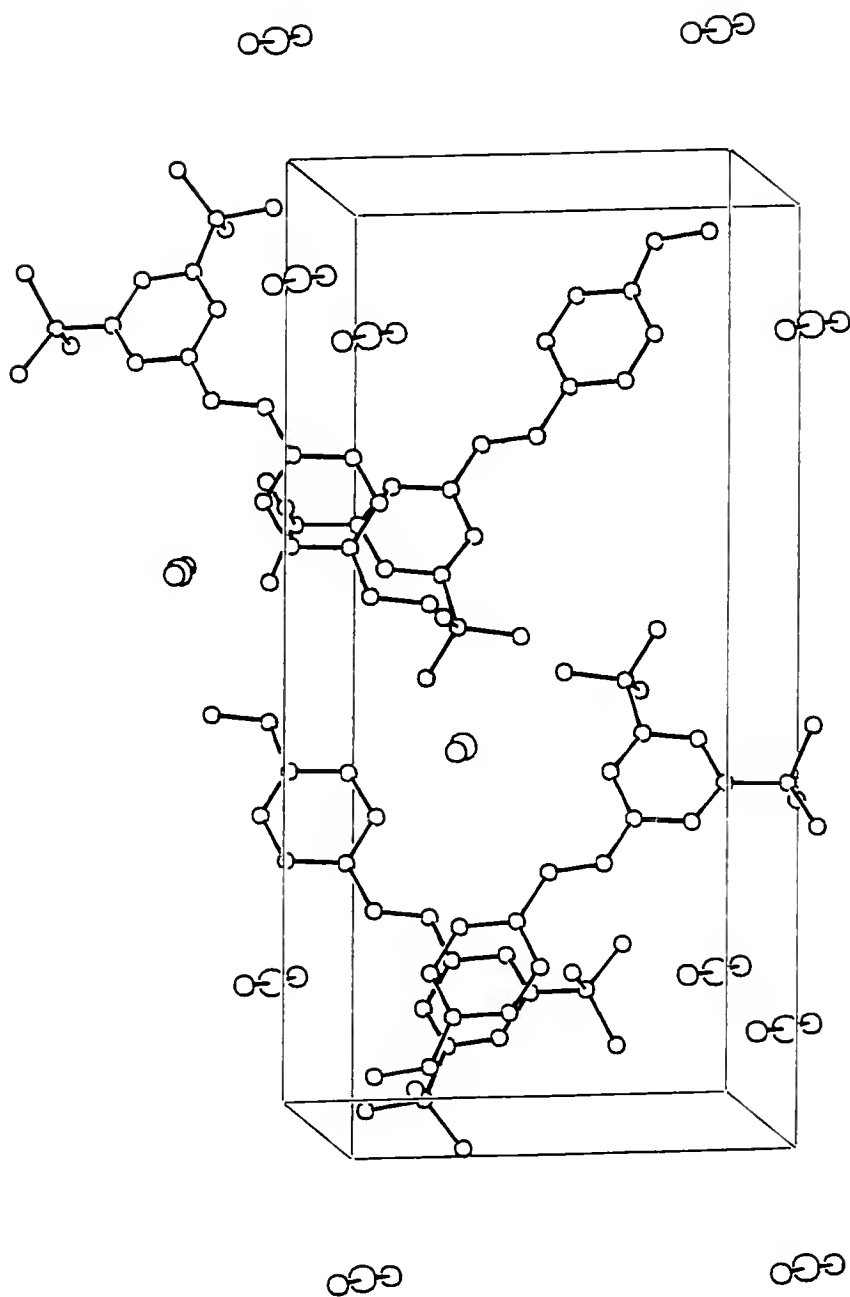


Figure 5-5. Projection of the crystal structure of styrylpyrylium salt 2-16, AuCl<sub>2</sub><sup>-</sup> counterion with cell axes.

Of the five  $\alpha$ -styrylpyrylium salts whose crystal structures have been determined, 2-16, the  $\text{AuCl}_2^-$  counterion structure is strikingly different from the others. Immediately evident is the lack of ion pairing in this structure as compared to that of the styrylpyrylium triflate (chapter 3), tin pentachloride, Figure 5-3 and Figure 5-4, and the tetrahedral counterion series, 2-12 through 2-14, whose crystal structures are shown below. The pyrylium ring of the salt does not “know” its counterion. In this respect the lattice is comparable to the lattice of an inorganic salt. Note that the other counterions can be roughly pictured geometrically as spheres or ellipsoids, whereas the  $\text{AuCl}_2^-$  counterion is, in comparison, shaped like a stick. This difference in geometry may account for the radical difference in packing: the  $\text{AuCl}_2^-$  anions stack in channels in a homoseric fashion with the styrylpyrylium backbones rotated approximately  $90^\circ$  with respect to one another in a criss-cross pattern.

Though the two styrylpyrylium salts, 2-15 and 2-16, differ only in their counterions, the  $\text{AuCl}_2^-$  styrylpyrylium salt, 2-16, is photostable, providing another example of topochemistry: chemically similar compounds may show markedly different chemical behavior in the solid state. Thus, reactivity is controlled by lattice packing and not by the intrinsic reactivity of species comprising the lattice.

#### Tetrahedral counterion series

The series of salts, 2-12 through 2-14, were synthesized in order to observe what effect varying the double bond separation distance has on the photoactivity of the lattice. In the ideal case, the replacement of the counterion results in an isomorphous structure so that only the intermolecular double bond distance would be fine-tuned as the size of the counterion is varied. Thus, the counterions are assumed to be merely space-fillers, making no electronic contributions to the photodimerization. One might compare this to a thermal expansion of the crystal but without the heat.

Table 5-1. Crystallographic data for styrylpyrylium salts 2-15, 2-16 and the bis(styrylpyrylium triflate), 2-33.

counterion	2-33 CF <sub>3</sub> SO <sub>3</sub> <sup>-</sup>	2-15 SnCl <sub>5</sub> <sup>-</sup> monomer	2-16 AuCl <sub>2</sub> <sup>-</sup> monomer
a	9.563(4)	9.7307(8)	9.4884
b	11.746(13)	12.3642(7)	10.7194
c	12.126(6)	12.6983(4)	22.8517
α	72.585(6)	102.511(4)	*
β	83.5642	97.341(4)	91.718
γ	75.914(7)	95.982(5)	*
V	--	1465.5	2323.2
Z	2	2	4
density	1.286	1.408	1.696
space group	P $\overline{1}$	P $\overline{1}$	P2 <sub>1</sub> /c
#refl.	3747	3678	3661
#obs.	2993	3032	2414
R	0.067	0.072	0.048
R <sub>w</sub>	0.066	0.082	0.056

This synthetic goal has been largely fulfilled for the BF<sub>4</sub><sup>-</sup>, ClO<sub>4</sub><sup>-</sup> and ReO<sub>4</sub><sup>-</sup> series. With regard to possible electronic effects of the counterion, Table 2-30 in chapter 2 may be consulted for the solution <sup>1</sup>H and C-13 NMR measurements for the series BF<sub>4</sub><sup>-</sup>, ClO<sub>4</sub><sup>-</sup> and ReO<sub>4</sub><sup>-</sup>. No significant shift in the ring current on changing the counteranion is observed. Due to possible solvent effects, NMR measurements in the solid state would be more persuasive and a comparison of the solid state C-13 NMR of the styrylpyrylium triflate with the styrylpyrylium perrhenate reveals identical shifts in the p-methoxy, and t-butyl carbon signals for these two compounds, with the carbons in the conjugated backbone in both cases falling between 110 and 190 ppm. Thus the monopole-monopole interaction between the carbon backbone and counteranion as measured by NMR does not appear to significantly effect the electronic nature of the reacting double bond.

As to the question of geometrically isomorphous structures, compare the crystallographic data for the monomers listed in Table 5-2. Note that they all crystallize in

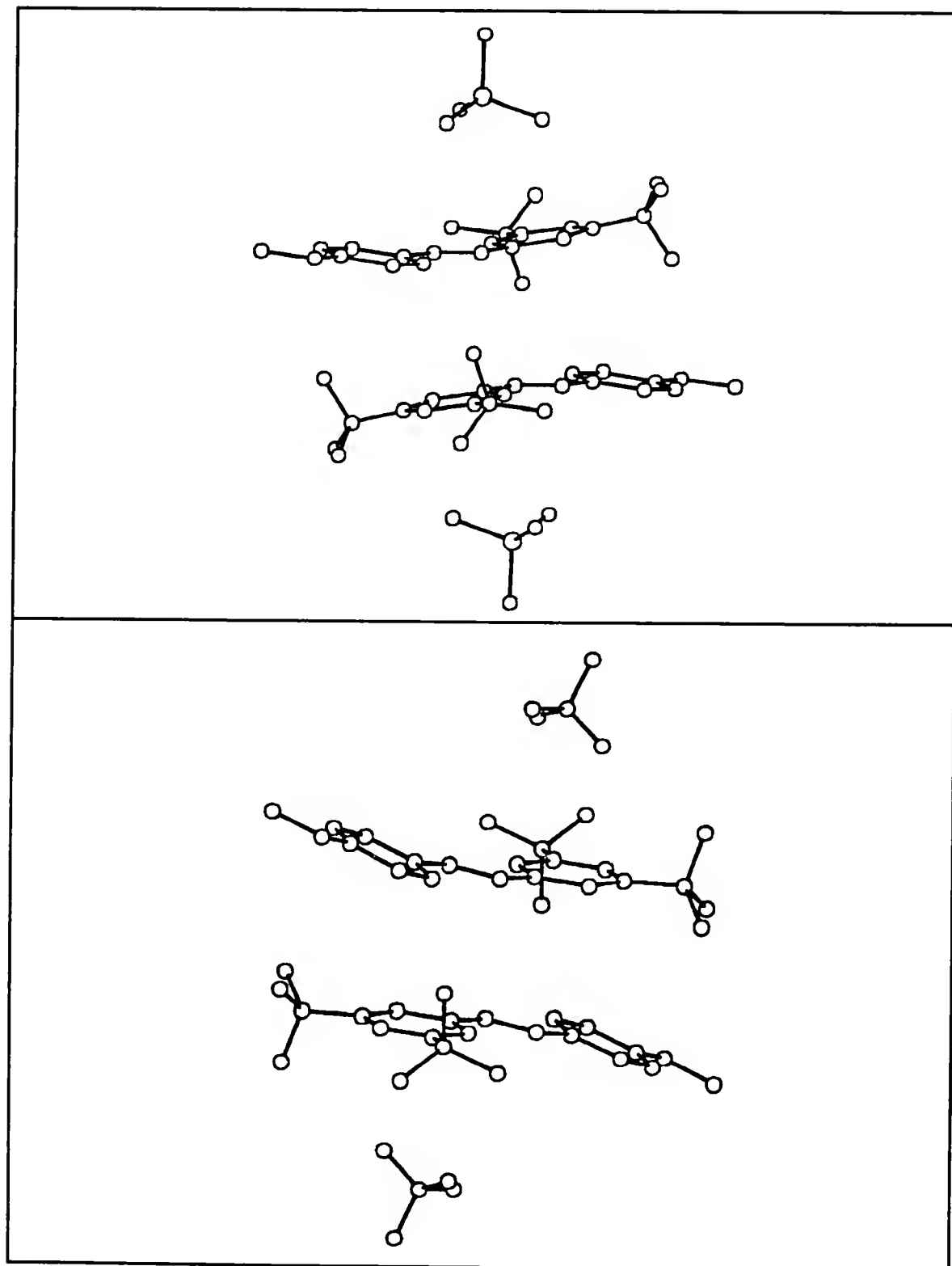


Figure 5-6. Projections of the crystal structures of monomer pairs for 2-13,  $\text{ReO}_4^-$  (top) and 2-12,  $\text{BF}_4^-$  (bottom).

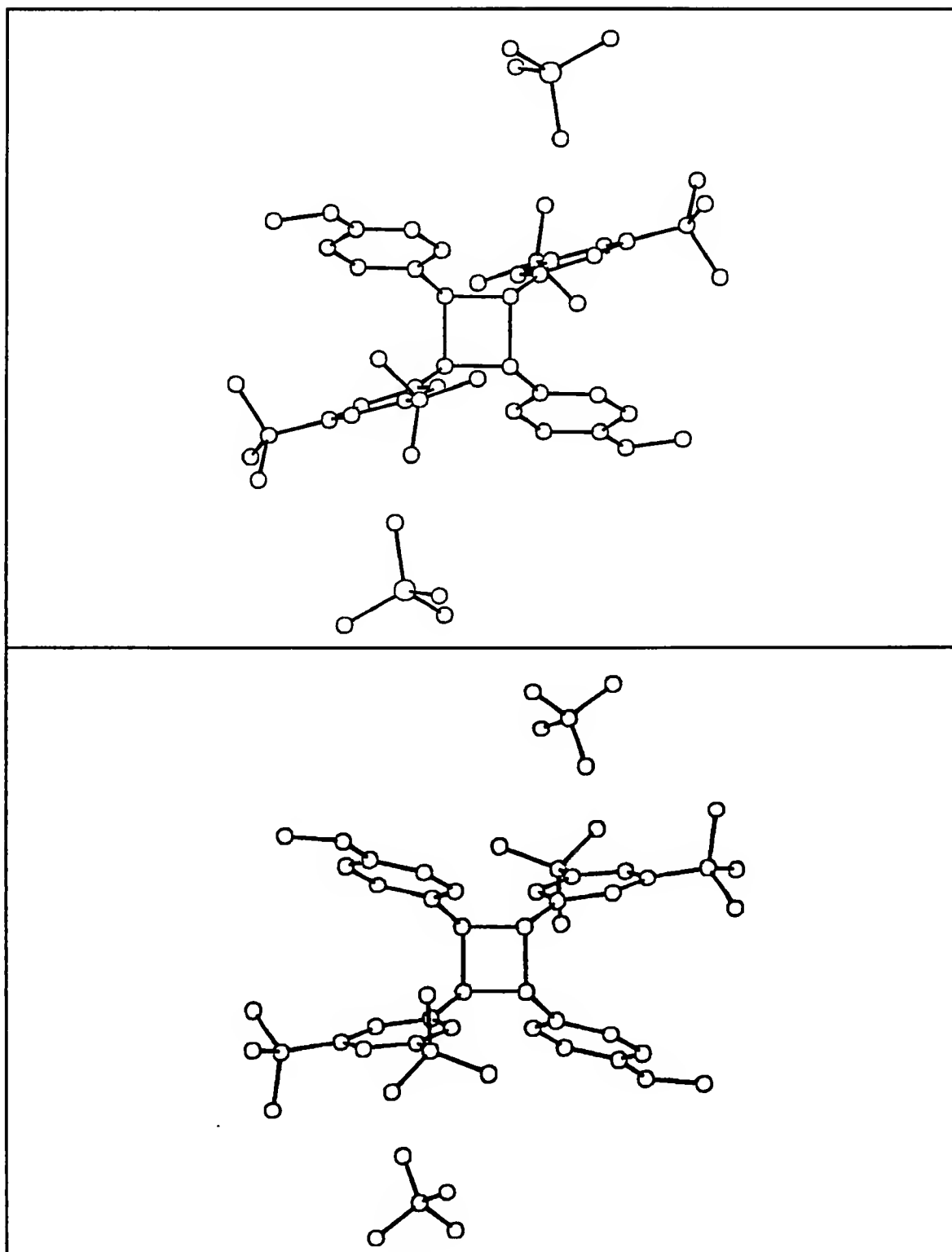


Figure 5-7. Projections of the crystal structures of the dimers of 2-13,  $\text{ReO}_4^-$  (top) and 2-12,  $\text{BF}_4^-$  (bottom).



the same space group,  $P2_1/c$ , and their lattice parameters are different but within a few percent of one another. Qualitatively, what is expected is observed: the structures are all similar with the  $\text{ReO}_4^-$  styrylpyrylium salt lattice cell occupying the largest dimensions. Full x-ray crystal structures on the three monomers were done; projections of  $\text{BF}_4^-$  and  $\text{ReO}_4^-$  salts are presented in Figure 5-6 and Figure 5-8. The  $\text{BF}_4^-$  and  $\text{ClO}_4^-$  structures are nearly identical.

When these crystals are irradiated with wavelengths in the tail of their absorption spectra via a transmission filter,  $\lambda_{\text{max}} = 550\text{nm}$  with a half-width of 50nm, single-crystal-to-single-crystal transformations are observed. This allows the determination of the x-ray structures of the photodimers, projections of which are presented in Figure 5-7 and Figure 5-9 for the  $\text{BF}_4^-$  and  $\text{ReO}_4^-$  salts. The crystallographic data is presented in Table 5-2. Certain features of the monomer crystal structures and dimer crystal structures may be compared. In some of the structures, the t-butyl groups and the counterions are spinning (as opposed to a tumbling-type of disorder for the counterions). This disorder is summarized in Table 5-3. This disorder in the triflate salt is discussed in chapter 3 and has been included here for comparison. The most notable observation in Table 5-3 is that there is no disorder in the perrhenate salt monomer even though a t-butyl group and counterion in each of the other two isomorphous salts are disordered. Two reasons can be imagined for this phenomena. The  $\text{ReO}_4^-$  group can be envisioned as inserted into a lattice position or cavity that also accommodates the much smaller  $\text{BF}_4^-$  counterion. Thus it is possible that there are much shorter intermolecular contacts between the oxygen atoms of the perrhenate ion and its neighboring groups, than in the perchlorate or tetrafluoroborate structures. The perrhenate cavity nevertheless must certainly be larger than that for the other counterions which explains the restricted movement of the t-butyl group in the perrhenate monomer. It is also possible that counteranion disorder is not observed in the perrhenate monomer due to the counterion's larger mass and corresponding larger inertia.

Table 5-2. Crystallographic data for 2-12 through 2-14 and photodimers.

	BF <sub>4</sub> <sup>-</sup> monomer	BF <sub>4</sub> <sup>-</sup> <i>dimer</i>	ReO <sub>4</sub> <sup>-</sup> monomer	ReO <sub>4</sub> <sup>-</sup> <i>dimer</i> <i>T=250K</i>	ClO <sub>4</sub> <sup>-</sup> monomer <i>T=180K</i>
a	14.2489 (9)	14.2272 (5)	14.3705 (14)	13.581	14.1390
b	13.1652 (18)	12.6764 (10)	13.683 (9)	13.112	13.2048
c	13.0178( 13)	13.4776 (12)	12.886 (2)	13.7369	12.8311
α	*	*	*	*	*
β	112.929 (6)	111.790 (4)	113.683 (12)	110.406	112.184
γ	*	*	*	*	*
V	2249	2257	2320.5	2292.5	2218
Z	4	4	4	4	4
density	1.218	1.213	1.648	1.671	1.308
space group	P2 <sub>1</sub> /c	P2 <sub>1</sub> /c	P2 <sub>1</sub> /c	P2 <sub>1</sub> /c	P2 <sub>1</sub> /c
#refl.	2972	3000	2521	2421	2766
#obs.	1958	2286	1456	1613	1926
R	0.053	0.065	0.048	0.034	0.054
R <sub>w</sub>	0.048	0.063	0.055	0.037	0.056

Table 5-3. Disorder in the t-butyl groups and counteranions of 2-12 through 2-14.

	Monomer		Dimer	
	room T	low T	as-dimerized	recrystallized
CF <sub>3</sub> SO <sub>3</sub> <sup>-</sup>				
t-Bu	yes	no	no	yes
X <sup>-</sup>	yes	no	no	yes
BF <sub>4</sub> <sup>-</sup>				
t-Bu	1		no	
X <sup>-</sup>	yes		no	
ClO <sub>4</sub> <sup>-</sup>				
t-Bu	yes	1		
X <sup>-</sup>	yes	no		
ReO <sub>4</sub> <sup>-</sup>				
t-Bu	no		no	
X <sup>-</sup>	no		no	

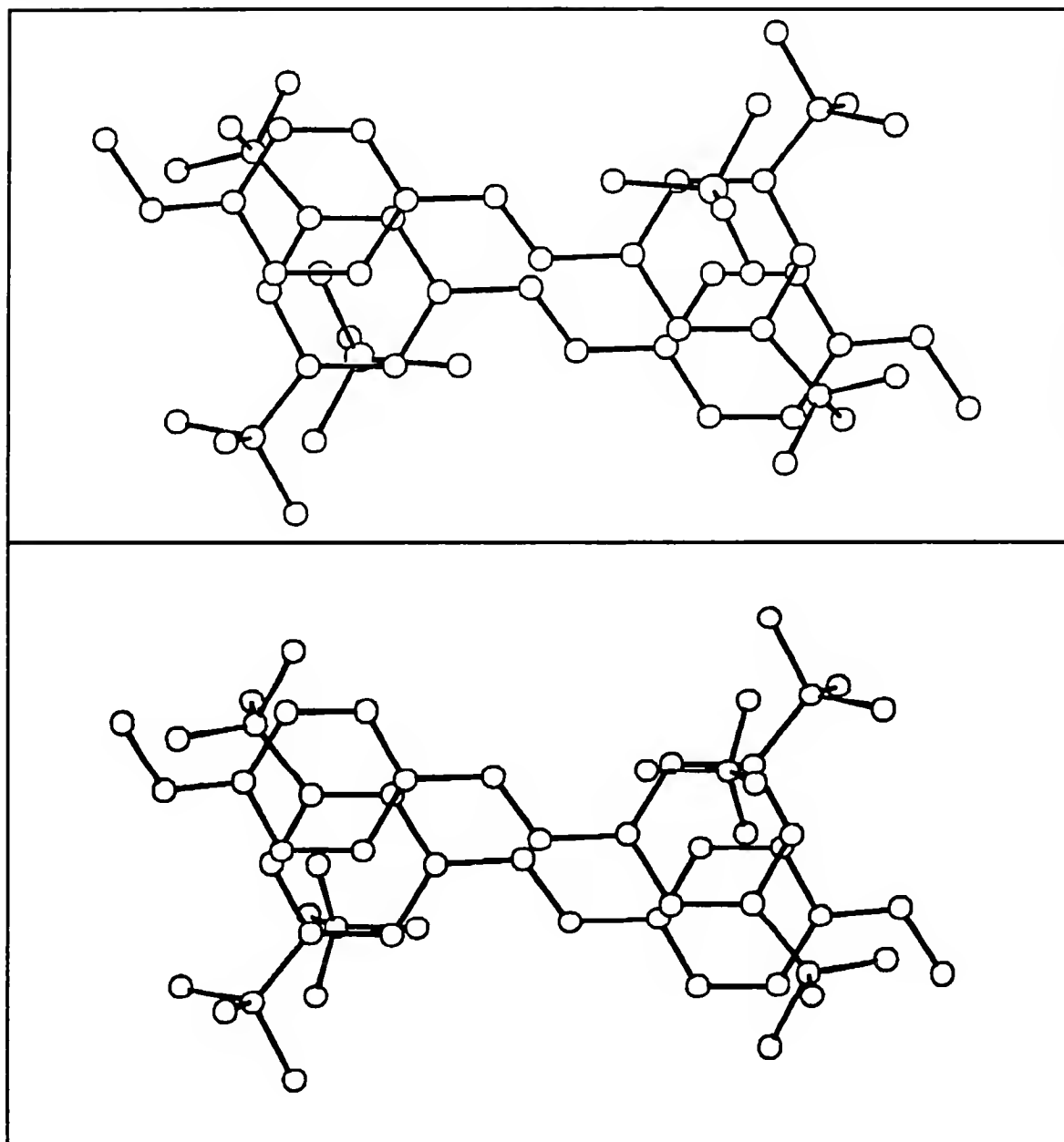


Figure 5-8. Projections of the crystal structures of the monomers of 2-13,  $\text{ReO}_4^-$  (top) and 2-12,  $\text{BF}_4^-$  (bottom) perpendicular to the plane of the chromophore.

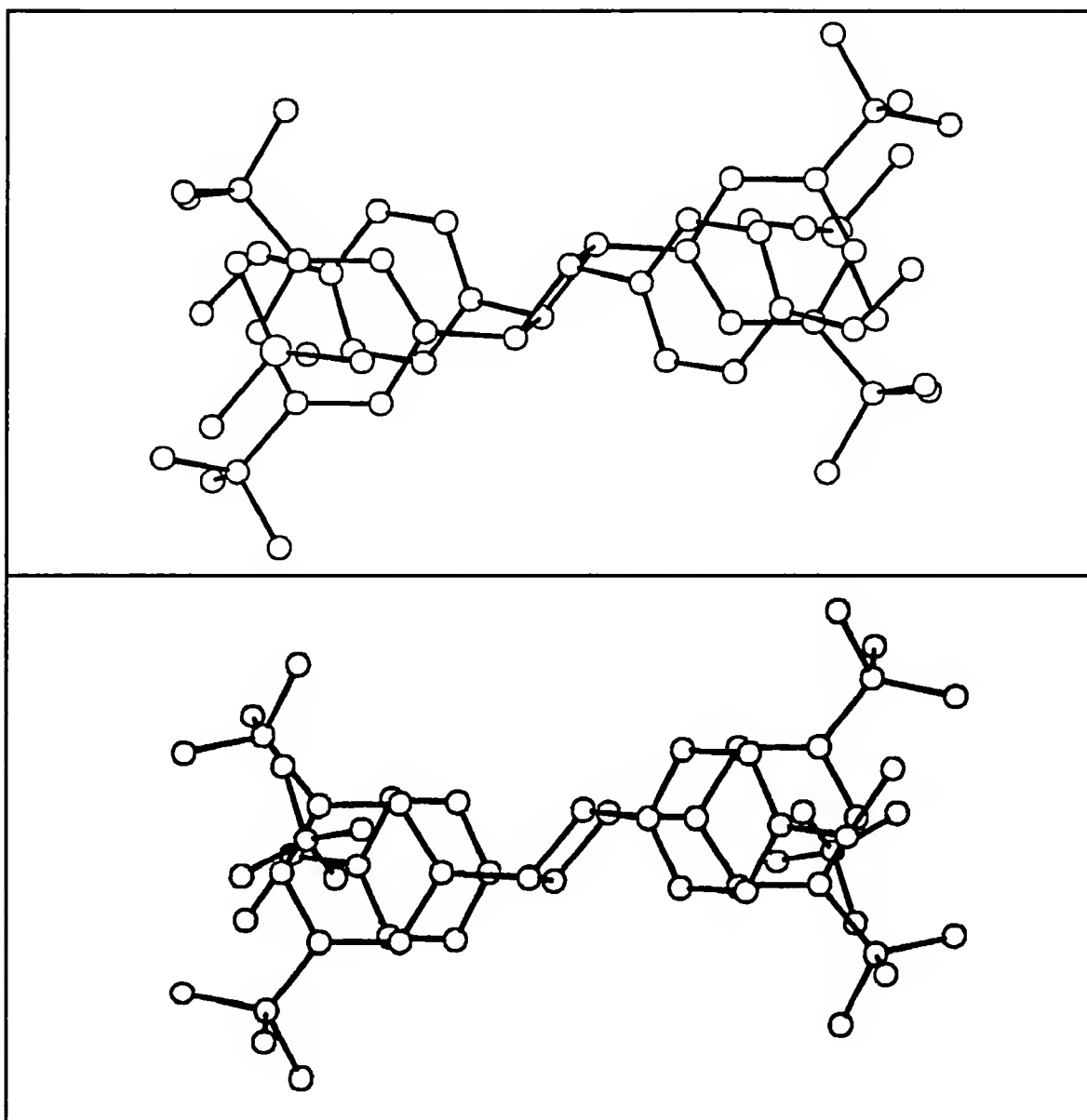


Figure 5-9. Projections of the crystal structures of the dimers of 2-13, ReO<sub>4</sub><sup>-</sup> (top) and 2-12, BF<sub>4</sub><sup>-</sup> (bottom) perpendicular to the plane of the chromophore.

As can be seen from the views in Figure 5-8 and Figure 5-9, the center of mass of each counterion shifts with respect to its projection on the plane of the pyrylium ring from the monomer to dimer. In both cases, each counterion is forced to a position closer to a point midway between the t-butyl groups. For the tetrafluoroborate salt, the action of dimerization appears to draw these spinning groups together until they lock up due to volume restrictions. Figure 5-8 shows one orientation for the tetrafluoroborate tetrahedron: a tetrahedron plane facing the t-butyl-substituted pyrylium ring; however, in Figure 5-9, the final, exclusive orientation of the tetrahedron directs a point toward the ring plane. This may be interpreted as a space-conserving reaction to the new proximity of the bulky t-butyl groups. The final conformation of the perrhenate counterion is similar.

What draws the center of mass of the counterions to a space more directly over the oxygen of the pyrylium ring? Perhaps geometrical constraints from the motion of neighboring groups are responsible. This cannot be determined from these projections. However, it should be considered that the  $\pi$ -conjugation is interrupted through dimerization which results in the previously delocalized positive charge being localized on the pyrylium ring. This is easily seen in the comparison of the  $^1\text{H}$  NMRs of a pyrylium, styrylpyrylium and photodimer salts where the signal from the t-butyl groups shift from 1.4 to 1.5 back to 1.4 ppm, respectively. It is unknown what effect this change in the monopole-monopole interaction might have on the position of the counterion.

Finally, it is interesting to note how little the pyrylium rings change their conformation in comparison with the phenyl rings. This may be related to the argument put forth in chapter 1 that it is the van der Waals contacts among the substituents on the reacting centers that stabilize the lattice during a crystal-to-crystal transformation. However, as can be seen from Figure 5-10, this argument applied to the inertia of the pyrylium ring makes sense only if the t-butyl groups maintain intermolecular contact with molecules in neighboring stacks. Certainly the phenyl ring rotates most dramatically in the perrhenate

salt dimerization and less so in the tetrafluoroborate dimerization, whereas the pyrylium ring appears to move very little in comparison.

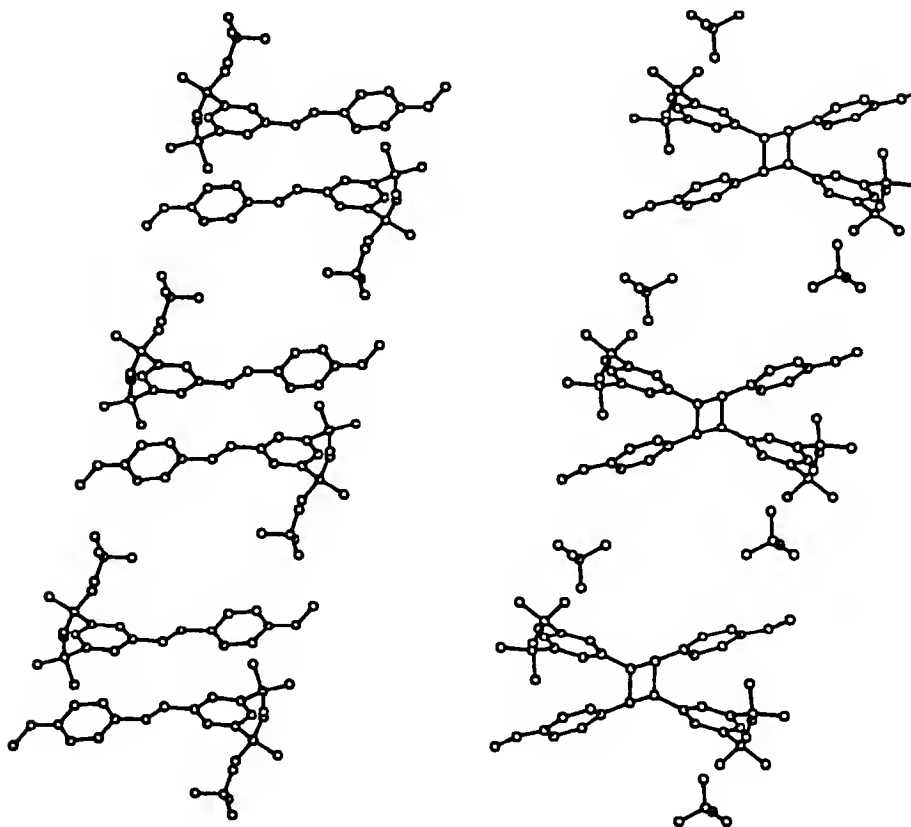


Figure 5-10. Packing of the tetrafluoroborate styrylpyrylium salt monomer pairs, ie., "incipient dimer" and the cyclobutane photoproduct.

### Kinetic Studies

The more pronounced rotation of the phenyl ring seen in Figure 5-6 and Figure 5-7 undergone by the styrylpyrylium perrhenate compared to the tetrafluoroborate salt, is reflected in the more severe change in lattice parameters for perrhenate salt dimerization shown in Table 5-2 and summarized in Table 5-4. This is a direct result of the larger center-to-center double bond distance in the perrhenate than in the tetrafluoroborate salt, values for which are also shown in Table 5-4. The double bond carbons have to travel farther to form the cyclobutane ring in the perrhenate salt than in the others.

Table 5-4 also lists the distances between the olefin carbons attached to the pyrylium rings in each pair under "plane-to-plane": note that because the planes of conjugation for each chromophore pair are roughly parallel and because the double bond overlap is so staggered (see Figure 5-8), the distance between these carbons is a rough measure of the distance between the olefin planes. This is less so in the case of the triflate pyrylium salt due to increased overlap, as can be seen in Figure 5-11 which also shows the interplanar distance between monomer pairs for a stack of monomers for the triflate salt.

Based on the data in Table 5-4, and the greater conformational rigidity of the perrhenate packing as measured by the lack of rotation in the counterion and side groups normally observed, the tetrafluoroborate and perchlorate salts would be expected to react faster than the perrhenate. Indeed, in all four trials, the perrhenate takes significantly longer to reach quantitative conversion. Figure 5-12 and Figure 5-13 show the time vs. conversion curves for the four broad-band irradiation (heterogeneously-formed product) trials run on the three salts, 2-12 through 2-14. Note that for the second trial, the perchlorate salt received a comparatively lower intensity of radiation due to a misplacement of the reaction flask in the beam and therefore exhibits a

Table 5-4. Percent change in lattice parameters for the dimerization of 2-12 and 2-13.

	$\text{BF}_4^-$	$\text{ReO}_4^-$	$\text{ClO}_4^-$	$\text{CF}_3\text{SO}_3^-$
a	<1%	6%	--	5%
b	4%	4%	--	4%
c	4%	7%	--	<1%
B	1%	3%	--	3%
plane-to-plane (Å)	3.54	3.76	3.54	3.37
center-to-center (Å)	3.95	4.26	3.99	3.42

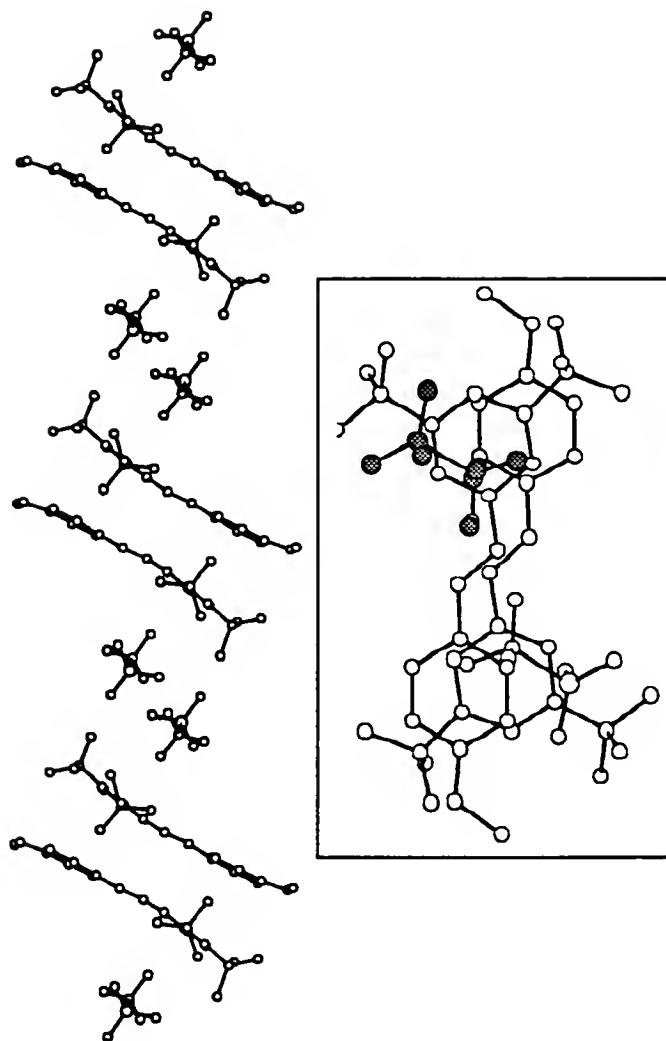


Figure 5-11. Projections of the triflate crystal structure with a view of the monomer stack parallel to the plane of conjugation of showing the plane-to-plane separation distance of less than 3.4 Å. The double bond center-to-center distance is slightly larger because the olefins are slightly staggered as can be seen in the projection on the left. See Table 5-4 for values for salts 2-12 through 2-14.



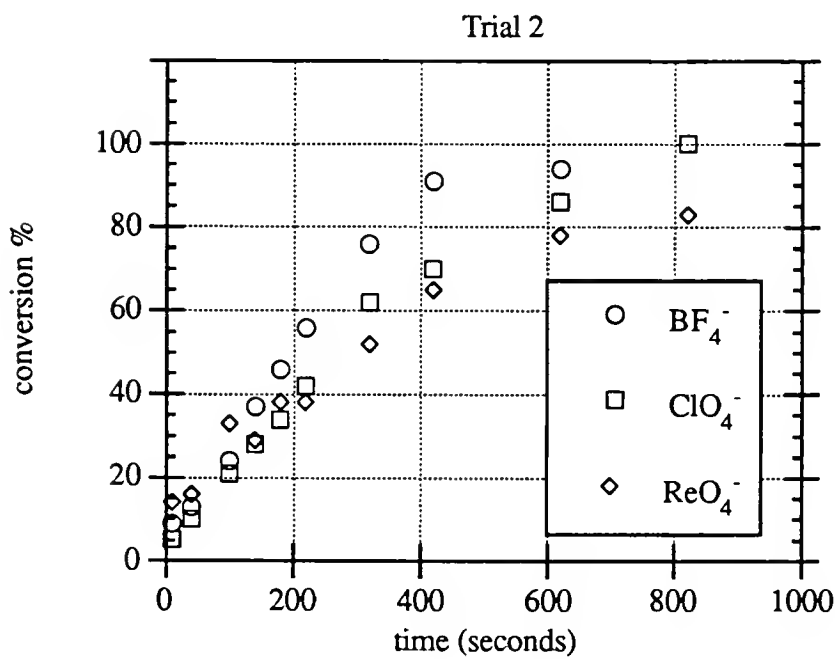
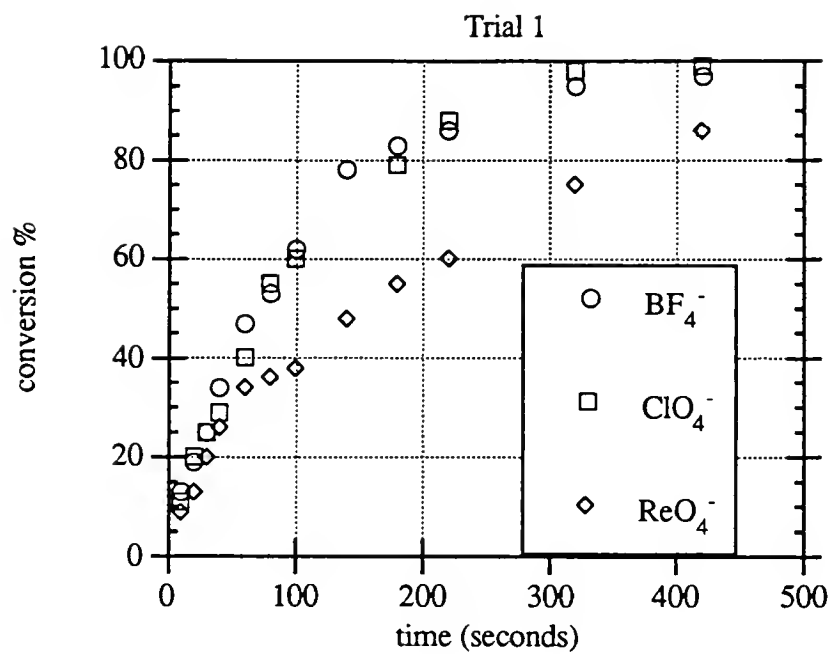


Figure 5-12a.

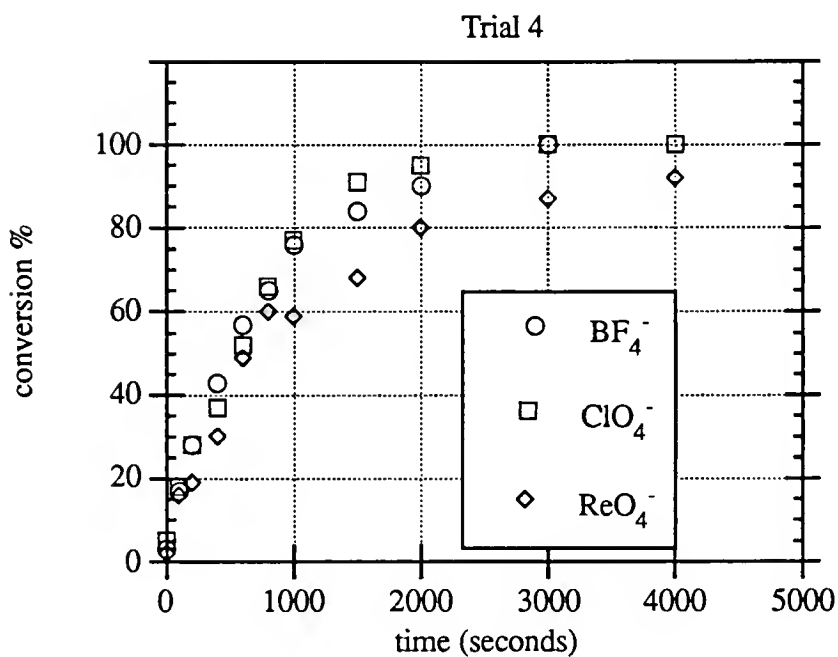
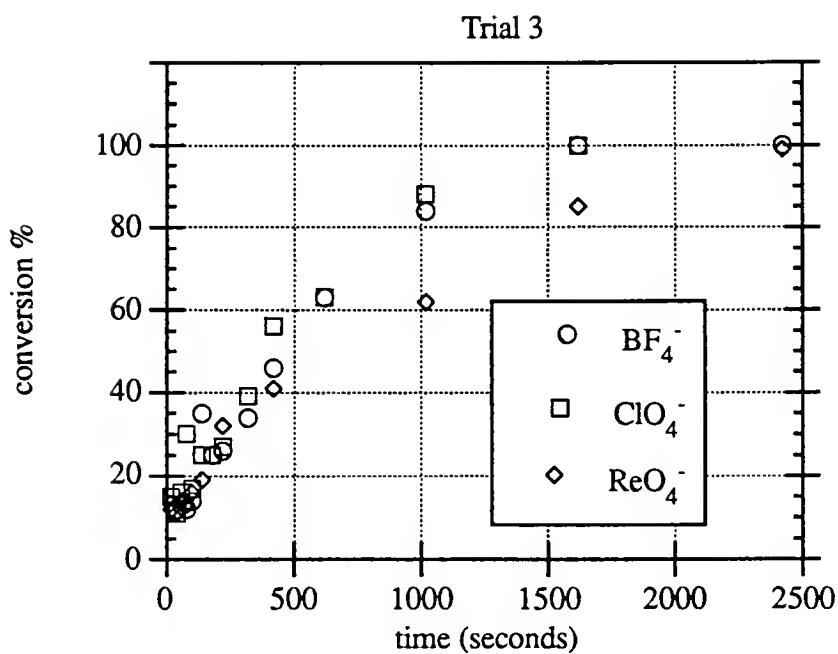


Figure 5-12b.

Figure 5-12. Time vs. conversion curves for the broad-band irradiation of styrylpyrylium salts, 2-12 through 2-14.

- a) Trials 1 and 2  
b) Trials 3 and 4

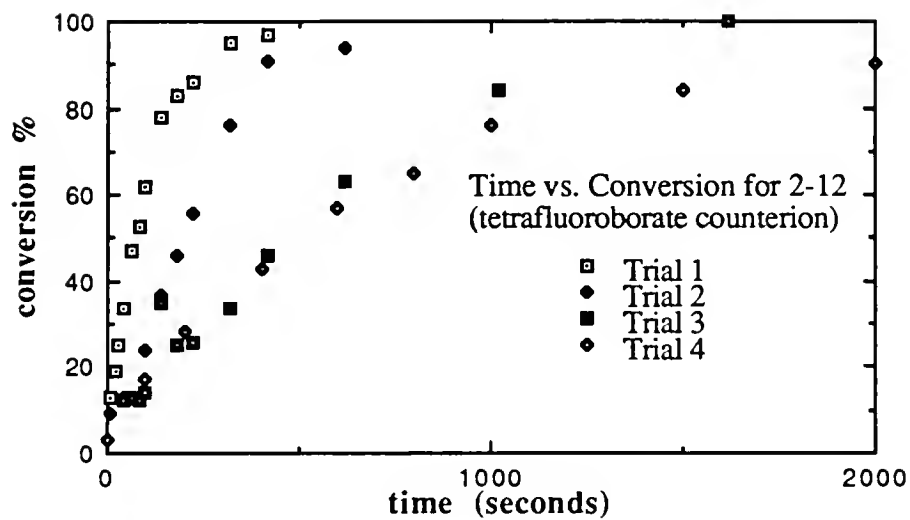


Figure 5-13a.

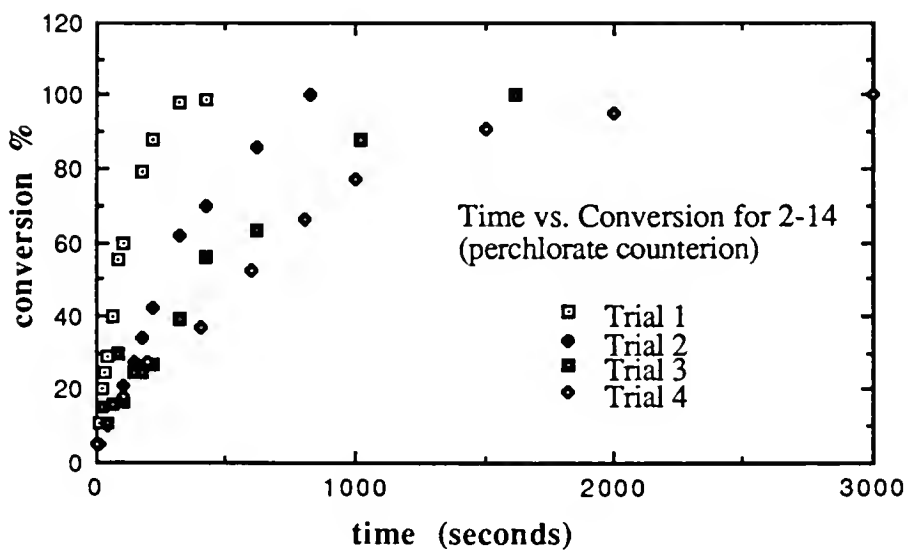


Figure 5-13b.

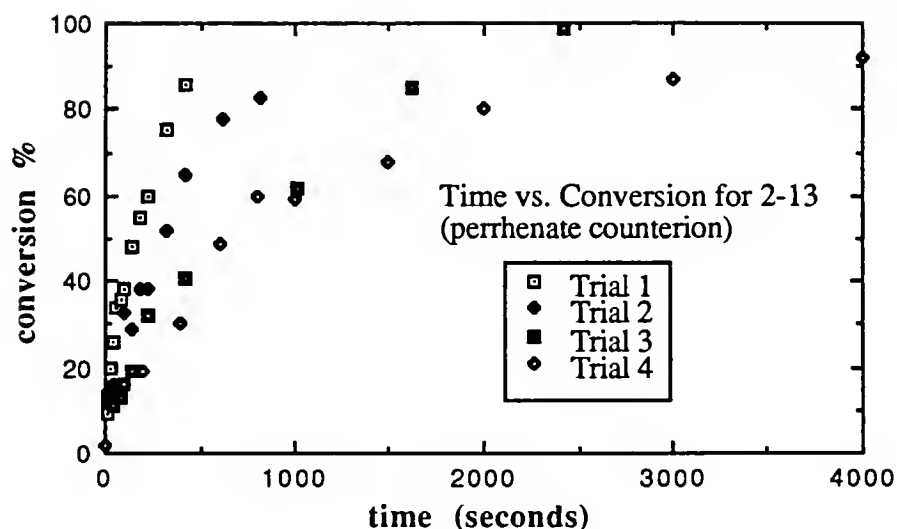


Figure 5-13c.

Figure 5-13. Time vs. conversion trials for each styrylpyrylium salt.  
 a) 2-12,  $\text{BF}_4^-$  b) 2-14,  $\text{ClO}_4^-$  c) 2-13,  $\text{ReO}_4^-$

correspondingly slower rate. Figure 5-14 and Figure 5-15 show the  $\ln(\text{concentration})$  vs. time plots derived from these curves which indicate that these processes obey typical first-order kinetics. Table 5-5 lists the rates obtained from the slopes of these plots. Among the salts within each trial, the perchlorate and tetrafluoroborate are seen to react with roughly the same rate, which is double that of the rate of perrhenate dimerization at mid-conversion ranges. Following research directed by Heyes,<sup>59</sup> Sharp-Hancock plots, shown in Figure 5-16, were made for each trial to reveal slopes averaging around 1.0 at intermediate conversions, indicating a random nucleation mechanism.

In trials 1 and 4, the perrhenate salt is observed to react with rates comparable to those of the other salts at initial conversions. Interestingly, the behavior of the perrhenate in trial 1 is identical to that described for the o-methoxy derivative studied by Heyes: up until a conversion of approximately 35% and then from 40 to 90% Sharp-Hancock slopes

of 1.0 connected by a shallow slope are observed. Furthermore, as with the *o*-methoxy derivative, the first order plots for these two regions both intersect the origin. Thus perhaps, as suggested for *o*-methoxy cinnamic acid, two sequential first order processes were operating in the first trial, the first process having a rate very similar to that of the perchlorate and tetrafluoroborate. Trial 4 also indicates two distinct regions of kinetic behavior. At lower conversion, again, the rate of perrhenate dimerization is comparable to that of the perchlorate and tetrafluoroborate. However, the Sharp-Hancock slope for higher conversions is less than 1.0 and the first order plot for this region does not intersect the origin.

A suggestion for this dual kinetic behavior in trial 4 may be that two modifications of the perrhenate salt can be created on grinding the sample in preparation for irradiation. When these salts are ground extensively, they change from a gold to a bright orange color. Therefore in the trials reported above, grinding was stopped short of this color change and limited to reducing the particle size so as to allow the suspension to be syringed. Thus perhaps a phase transition has been induced in a portion of the perrhenate sample on grinding, not visually detectable. Such phase transitions due to mechanical manipulation of a sample are known; for example, the  $\beta$  to  $\alpha$  phase transition in cinnamic acid may be induced by grinding.

The anomalous behavior of the perrhenate in trials 1 and 4 may also be explained simply by considering that the more dramatic change in lattice parameters suffered by the perrhenate salt when its photoproduct is formed, may lead to a relatively higher incidence of phase boundaries, that is, smaller product particles. If the reactant crystals are too large, or the syringe bore too small, syringe sampling may favor withdrawal of the product at the early stages of the reaction.

In order to distinguish the intrinsic reactivity of each lattice, more sensitive methods focusing on the photodimerization at early conversions are needed. Care must be taken to eliminate effects of product phase evolution. Chapter 6 reports methods for obtaining such

solid state kinetic data. Kinetic studies on the homogeneous photodimerization of these salts over the entire range of conversion, such as that reported in chapter 3 for the triflate counterion, would also provide a useful comparison to the results reported here.

### Thermal Cycloreversion of Photodimers

The photodimers of salts 2-12 through 2-14 cyclorevert quantitatively to the monomers after being held at 190° C for five minutes, as shown by <sup>1</sup>H NMR analysis of the thermally treated powders. Figure 5-17 shows the DSCs of the photodimers. The temperatures at which cycloreversion occur are approximately 30° C higher than that for the styrylpyrylium triflate salt photodimer and the heat released on cycloreversion is over two to three times that for the triflate dimer as shown in Table 5-6.

Table 5-5.<sup>a</sup> Slopes (s<sup>-1</sup>) for first-order plots in Figure 5-14 and Figure 5-15

	ReO <sub>4</sub> <sup>-</sup>	BF <sub>4</sub> <sup>-</sup>	ClO <sub>4</sub> <sup>-</sup>
Trial 1	0.0067 (40%) / 0.0046	0.0086	0.0092
Trial 2	0.0021	0.0052	(0.0034)
Trial 3	0.0011	0.0019	0.0022
Trial 4	0.0011 (60%) / 0.0053	0.0011	0.0015

<sup>a</sup> The decay of lamp power is evident among the trials: the salts convert at increasingly slower rates from trial 1 to trial 4.

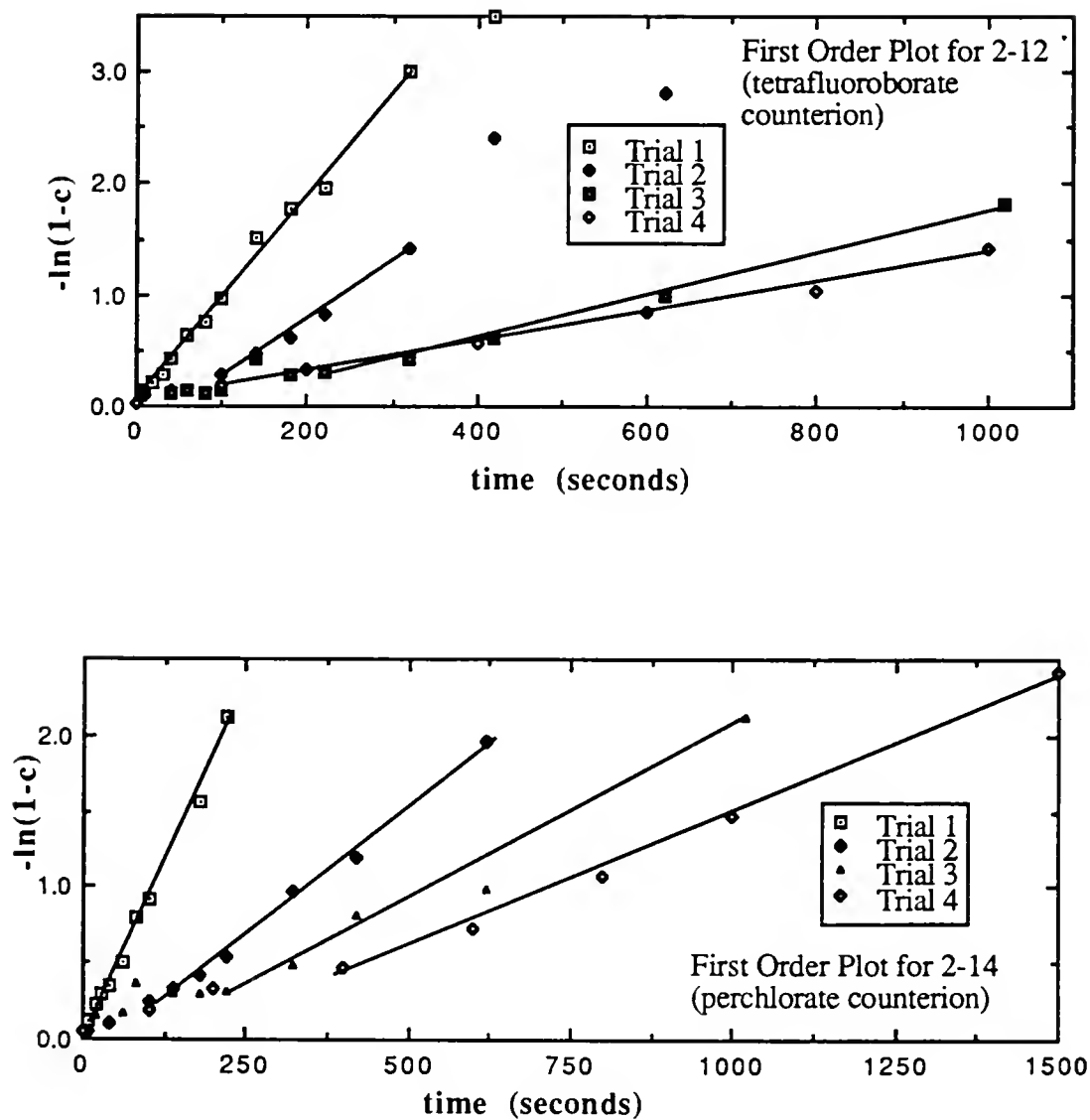


Figure 5-14. First-order plots for the photodimerization of styrylpyrylium salts 2-12, top, and 2-14, bottom.

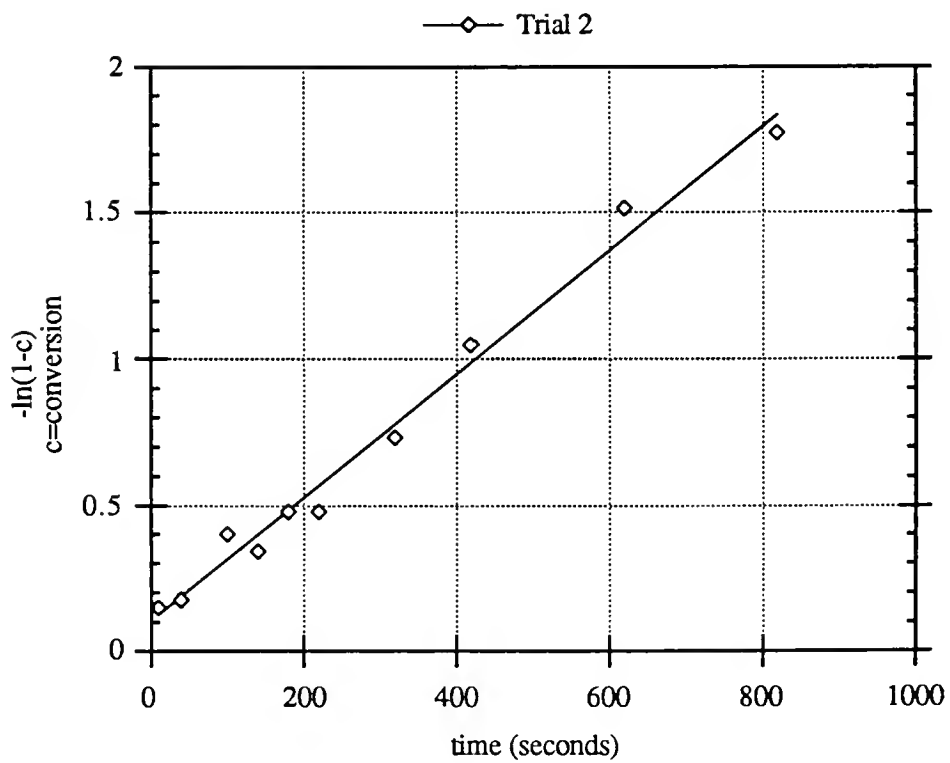
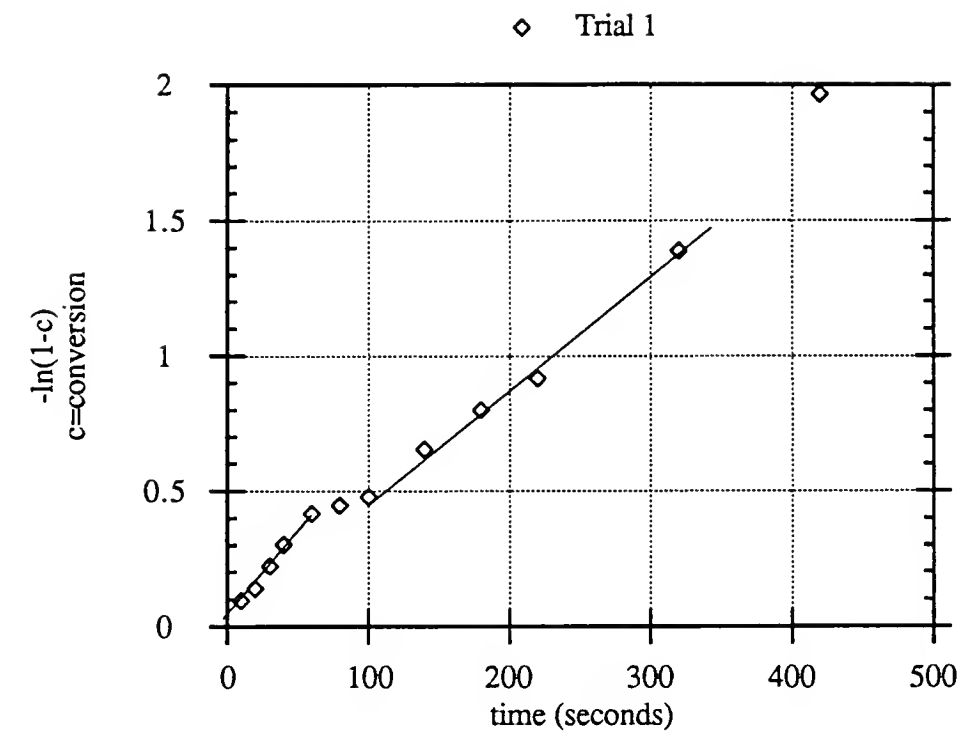


Figure 5-15a.



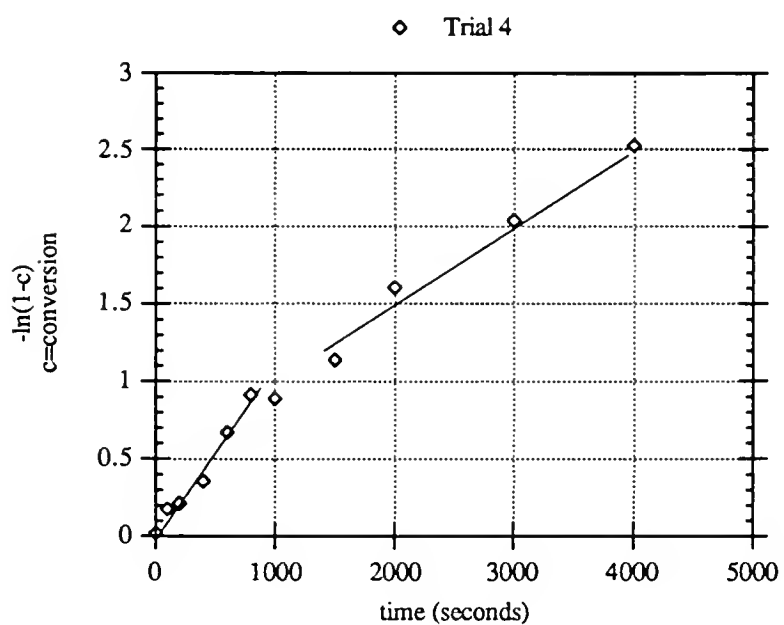
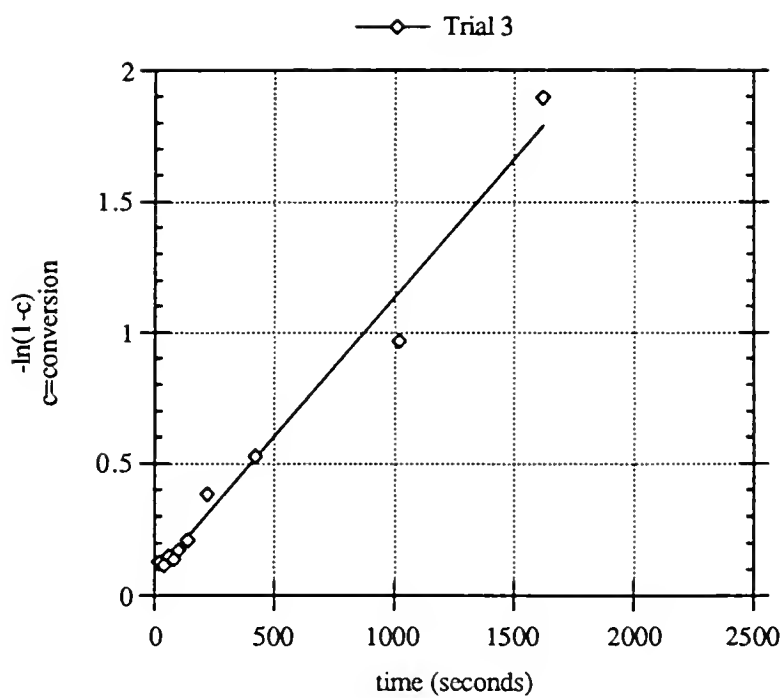


Figure 5-15b.

Figure 5-15. First order plots for the styrylpyrylium perrhenate photodimerization.  
 a) Trials 1 and 2.  
 b) Trials 3 and 4.

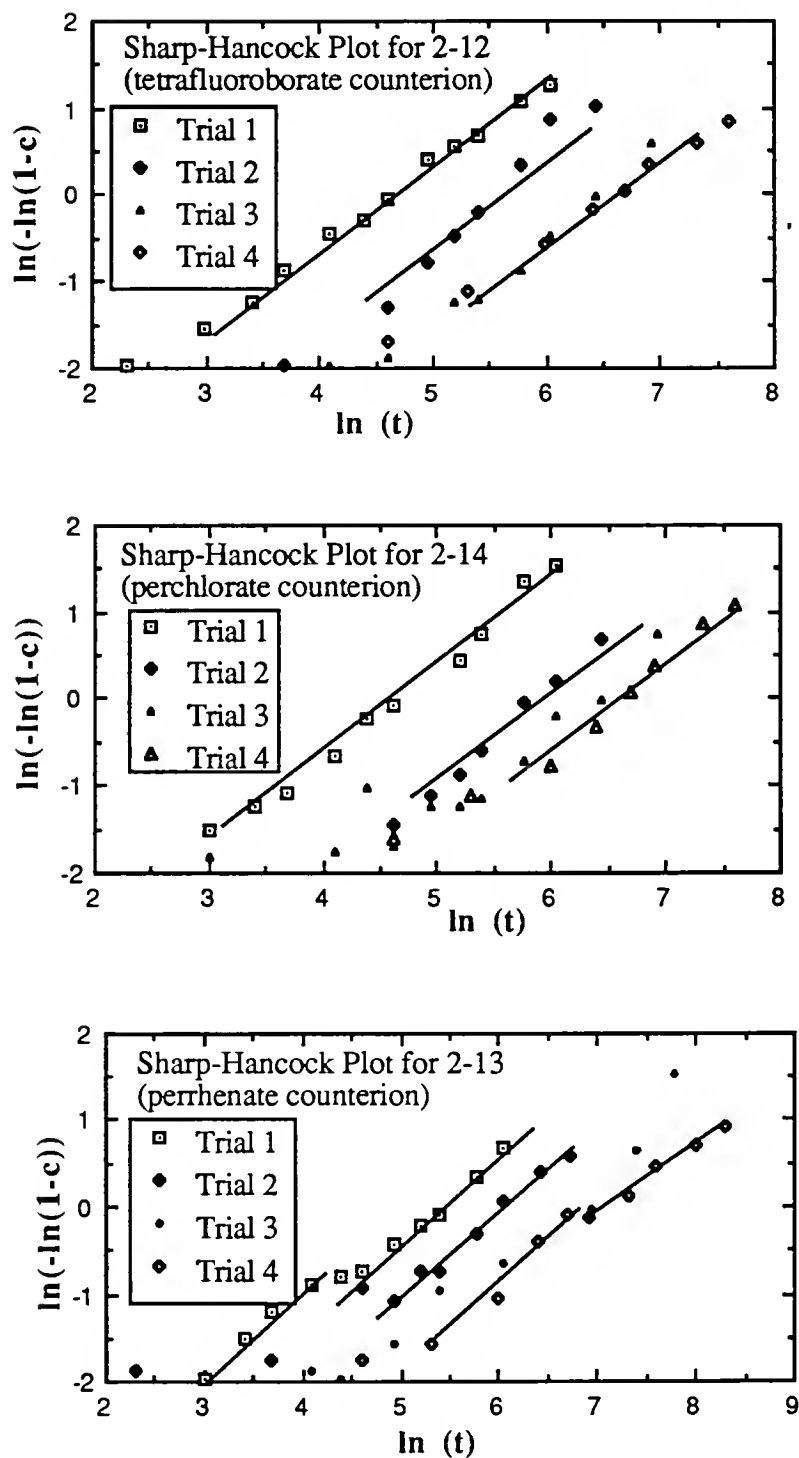
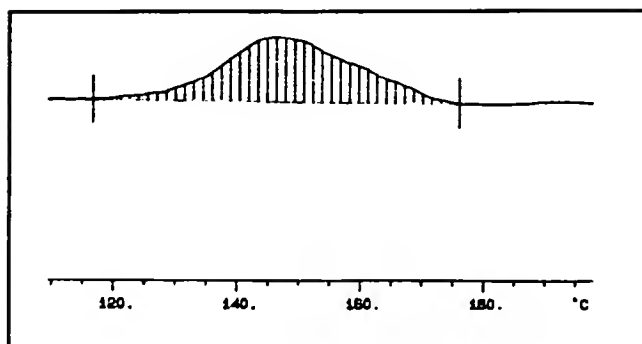
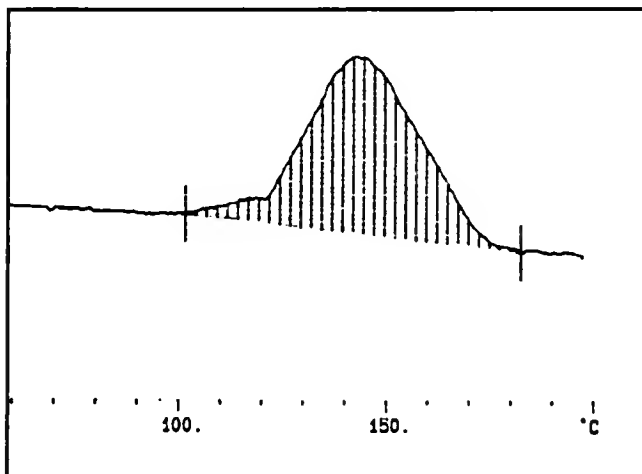


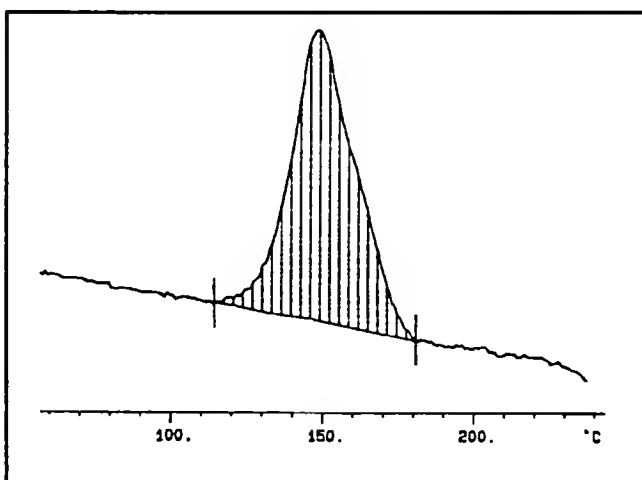
Figure 5-16. Sharp-Hancock plots for the photodimerization time vs. conversion curves of styrylpyrylium salts 2-12 through 2-14. All the lines have a slope of 1, except for the perrhenate, trial 4 at higher conversions.



$\text{ClO}_4^-$   
 peak=146.1 ° C  
 enthalpy= 5.33 kcal/mol



$\text{ReO}_4^-$   
 peak=143.1 ° C  
 enthalpy=6.03 kcal/mol



$\text{BF}_4^-$   
 peak=148.4 ° C  
 enthalpy=4.53 kcal/mol

Figure 5-17. The DSC curves for the thermal cycloreversion of the photodimers from the irradiation of salts 2-14  $\text{ClO}_4^-$  (top), 2-13 (middle)  $\text{ReO}_4^-$  and 2-12  $\text{BF}_4^-$  (bottom).

14. Table 5-6. Enthalpies and temperatures of cycloreversion for salts 2-12 through 2-

	BF <sub>4</sub> <sup>-</sup>	ClO <sub>4</sub> <sup>-</sup>	ReO <sub>4</sub> <sup>-</sup>	CF <sub>3</sub> SO <sub>3</sub> <sup>-</sup>
kcal/mol	4.53	5.33	6.03	1.83
kJ/mol	18.9	22.3	25.2	7.68
T ° C	148.4	146.1	143.1	109.2

#### A bis(Styrylpyrylium Triflate)

Table 2-4 and 2-5 list the styrylpyrylium diolefins that have been synthesized with an interest in observing how the alkyl chains may affect monomer packing in the crystalline state and in their polymer-forming potential. Because the [2+2] cycloadditions required to link these monomers is a type of step polymerization, very high conversions would be required to achieve anything more than low molecular weight oligomers. Without the lattice as a template, that is, in solution, such conversions are unlikely in a reasonable amount of time. However, perhaps photoactive crystal modifications of these diolefins exist.

So far, crystals of only 2-33 and 2-34 have been obtained. The photostability of the triflate salt with a four-carbon methylene bridge, 2-33, is easily explained by its crystal structure, a projection of which is shown in Figure 5-18. Salts with longer methylene bridges may result in the hydrophobic and hydrophilic zone packing proposed by Quina and Whitten, but here in the four-carbon bridge, the pyrylium portion is adjacent to its neighbor's alkyl chain. The same disorder found in the p-methoxy-substituted styrylpyrylium triflate exists in the linked salt as well. Crystal data for this structure is found in Table 5-1. Crystallographic analysis of 2-34 shows incorporation of triflic (trifluoromethane sulfonic) acid, the recrystallization solvent, in the lattice. The photoactivity of these crystals has not been tested. It should be noted that the powdered solids of most of the compounds in Table 2-4 and 2-5 possess some photoactivity. The irradiated powders give signals in the cyclobutane region of their <sup>1</sup>H NMR spectra.

However, these solids, if not completely amorphous, are very finely divided and at least possess a great deal of crystal texture which would lead to random reactive double bond orientations, in the same way crosslinking through [2+2] cycloaddition occurs in amorphous cinnamate-substituted polymers.

### Future Studies

Clearly, work on the diolefins has just begun. The search for a polymerizable crystal continues. When found, its single-crystal-to-single-crystal polymerization could be investigated. Also, the packing in the salts with longer methylene bridges has yet to be studied. The substances in Table 2-4 are Hasegawa-type "four-center" diolefins. Organic salts in this classification have never been investigated. The [2+2] solid state photopolymerization of diolefins linked by a flexible chain has also been realized, but for only three types of olefins-containing species (maleimides, cinnamates and thymine) and never for a salt chromophore.

Further counterion series may be created such as that begun with 2-17,  $\text{SbF}_6^-$ , intended to be part of the octahedral series, including  $\text{PF}_6^-$  and  $\text{AsF}_6^-$  for the same purposes as the existing tetrahedral series. The potential single-crystal-to-crystal back reaction of the tetrahedral series has not been investigated crystallographically, and would be interesting to compare to the triflate salt due to the substantially larger heat evolution involved in the back reaction for these salts.

The most important questions yet to be answered involve a more sensitive investigation into the photodimerization kinetics of the tetrahedral series which may be possible with the holographic techniques discussed in chapter 6. The homogeneous and heterogeneously-formed dimer modifications must still be compared as well.

Finally, as can be seen in Table 2-25, the perrhenate counterion IR band is significantly shifted from the monomer to dimer structure. It would be interesting to correlate the shift with changes in lattice parameters in the homogeneous dimerization.

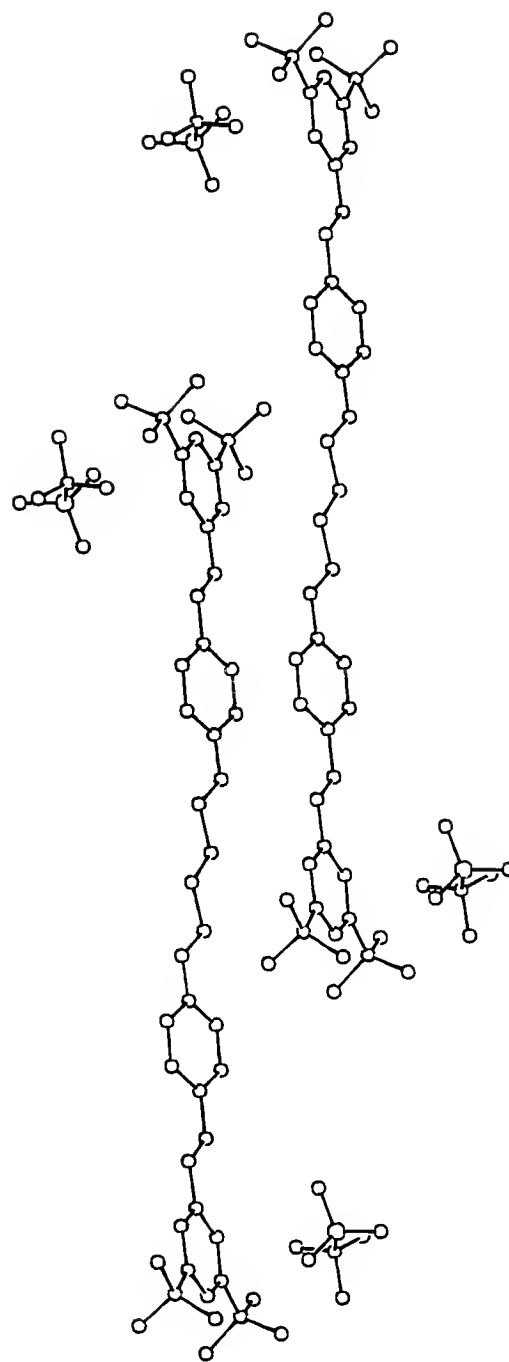


Figure 5-18. Projection of crystal structure for photostable bis(styrylpyrylium triflate), 2-33.

## CHAPTER 6 THERMALLY REVERSIBLE HOLOGRAPHIC GRATINGS

### Introduction

This chapter describes successful attempts to create a spatial distribution of styrylpyrylium monomer and photodimer within a styrylpyrylium triflate crystal. The purpose is to demonstrate the first thermally reversible holographic grating formed in a single crystal of an organic material. The grating is then used to study the kinetics of the photodimerization and thermal cycloreversion of the styrylpyrylium salt. This phenomenon of reversible light-induced spectral modification is photochromism. The introduction to this chapter defines some terms associated with photochromism, as well as related work in the literature and then goes on to outline the experimental set-up required for the experiment. The basis is then laid for relating the information obtained from the diffraction intensity growth and decay curves to kinetic data on the organic solid state photochemistry.

The following section on the results offer evidence that a thick holographic phase grating has been formed and that its behavior is in agreement with the reasoning put forth in the introduction. Then the data and calculations determining the energy of activation for the photodimerization and thermal cycloreversion of the styrylpyrylium system are reported. Finally, further investigations on the kinetics of the styrylpyrylium photodimerization and cycloreversion are suggested.

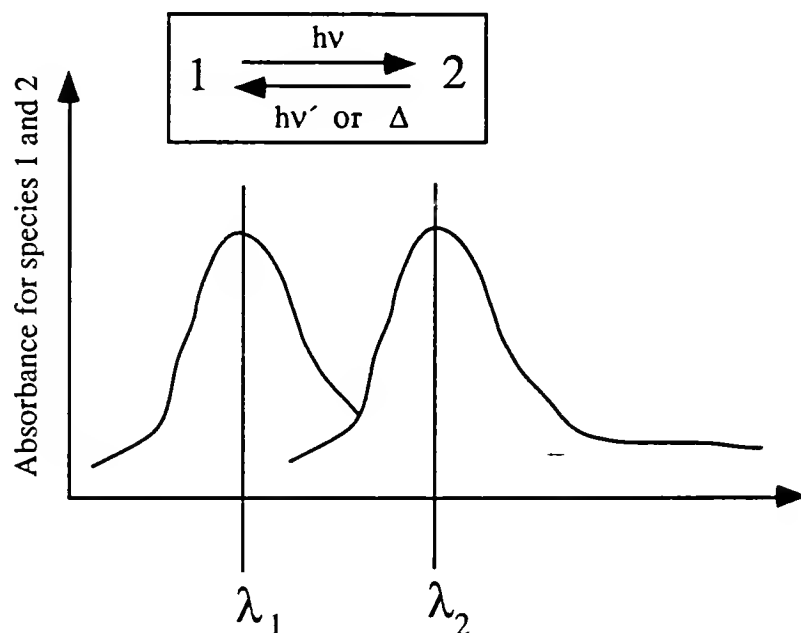
### Background

#### What is photochromism?

Certain chemical species react with light in such a way that their electronic absorption spectra changes. Often this change is reversible on further irradiation or with

heat. Such species that undergo a photo-induced reversible transformation between two states having distinguishable absorption spectra are photochromic. The most thoroughly investigated photochromic systems, such as spiropyrans and the fulgides, are unimolecular. Furthermore they typically react with light so that their absorption shifts to longer wavelengths; in other words, they change from a “bleached” form to a colored form. This is represented below by the transformation of species 1 to 2. Photoreversal, a “P-type” back reaction, occurs when  $\nu' < \nu$ . Thermal reversal is called “T-type”.

A review on photochromism<sup>112</sup> classifies unimolecular [2+2] photocycloadditions according to two types: the valence isomerization type,<sup>113</sup> represented by the intramolecular photoreaction of norbornadiene, and reactions of bis(chromophores), represented by species such as bisacenathylenes, bisphenanthrenes, biscinnamates and bisthymines.<sup>114</sup> The former show only small changes in their absorption spectra; however, the latter are comparable to the intermolecular [2+2] photocycloadditions.



In the intermolecular category, the chromophores listed above for the unimolecular bis-type have been recognized as photochromic, as well as ketosteroids, heteroaromatics and  $\alpha$ ,  $\beta$ -unsaturated carbonyl compounds. “Four-center” photopolymerizations as well as



systems undergoing [2+2] photocrosslinking (styrylpyridinium salts) have also been put forth as examples of photochromic systems.

With the exception of one example in the valence isomerization category, all the species mentioned above fall under the category of *inverse* photochromic systems because they undergo a photo-induced transformation to species absorbing at shorter wavelength. Thus, their initial reaction is from a colored form (2) to a bleached form (1). This is due to the interruption of their  $\pi$ -conjugation on formation of the cyclobutane ring. The back reaction from 1 to 2 then may be thermal or radiation-induced. The [2+2] photodimerization of styrylpyrylium salts discussed in this dissertation, therefore is an inverse photochromic system, T-type.

Photochromic systems are interesting for their potential applications in optical data processing and microdocumentation with a view toward reversible information storage. A general review of organic photochemical imaging systems places photochromism in context with other types of chemical processes in photographic technology.<sup>115</sup>

#### Holographic gratings with photochromic systems

Organic photochromic materials and holographic gratings are two topics which overlap in the literature in two ways: photochromic substances have been investigated as useful media for holographic gratings<sup>116,38-41</sup> and the formation of gratings has been used as a technique to investigate the photochemistry of these substances whether in bulk or imbedded in polymer host matrices.<sup>42,43</sup> Although the use of single crystals of photochromic substances to form holographic gratings has been reported,<sup>1</sup> the only system demonstrated to record a grating through a strictly topochemical, single-crystal-to-single-crystal reaction is that of the polymerization of diacetylene crystals.<sup>40,41</sup> However, this system is not reversible. In the work described in this dissertation, it is demonstrated that a styrylpyrylium triflate is a new system that can record a thermally erasable holographic grating through a topochemical, single-crystal-to-single-crystal [2+2] photodimerization.

In addition, holography is used as a tool to investigate the kinetics of the photodimerization in the crystalline state.

Holographic gratings formed through [4+4] photodimerization reactions involving single crystals are well known in the literature.<sup>116,39</sup> A single crystal of a photodimer may be irradiated at a certain wavelength to create a concentration of “broken dimer”, usually at the surface of the dimer crystal. At longer wavelengths, where now only the newly formed chromophore absorbs, a grating can be written by “remaking” the dimer with light from two interfering laser beams. The classes of substances whose single crystal behavior was investigated in this way were anthracenes, acridizinium and pyridinium salts.

In these cases, the irradiation wavelengths used were well within the absorption bands of the transforming species and thus the photoproduct was built up only at the crystal surface. The microfractures and eventual cracking of the crystal that was observed was probably due to the dimensional mismatch between the reactant and product lattices which causes phase separation. However, in the case of the holograms based on the topochemical polymerization of diacetylenes,<sup>40,41</sup> the transformation is single-crystal-to-single-crystal; that is, a solid solution of the reactant and product was achieved and no phase separation was observed. Up until now such single-crystal-to-single-crystal photoreactions have been rare.

As already described in this work, irradiation of a photoactive crystal far into the tail of its longest-wavelength band is a general method for inducing single-crystal-to-single-crystal photoreactions homogeneously throughout the entire volume of the crystal.<sup>117</sup> This has been demonstrated for the [2+2] photodimerization of a styrylpyrylium salt.<sup>118</sup> Not only can this particular dimerization be made to proceed with retention of the single crystal in the forward direction, the thermal reverse reaction also occurs without destruction of the single crystal. Thus single-crystal-to-single-crystal cycling of this photochromic system is possible. In the following, it will be shown how holography can be used as a highly sensitive tool to investigate the kinetics both of the photoreaction and the thermal back

reaction in the crystalline state. By irradiation of the styrylpyrylium crystal with an optical interference grating at a wavelength within the absorption tail, it is possible to create a periodic spatial distribution of the monomer which and dimer which extends over the entire crystal. By monitoring both the photoinduced growth and the thermal decay of the diffraction efficiency of the resulting refractive index grating, information about the kinetics of the related reactions are obtained. Since irradiation and read-out occurs within the extreme tail of the absorption band, the grating has only negligible absorptive contributions.

### The Setup

Holographic interference gratings with a fringe spacing of approximately 20  $\mu\text{m}$  were written by means of a 30 mW He-Ne laser (633nm) as shown in Figure 6-1. The beam was split then recombined constructively so that an interference pattern was formed. Between the writing periods of typically 10 seconds, one of the writing beams was blocked by a shutter (S) and the intensity of the diffracted reading beam was measured with a photomultiplier tube (PMT) during an integration time of 0.5 seconds. The fringe spacing and the position of the grating were monitored with an optical set-up involving a microscope objective (O), microscope reticle (R) and a video camera. An uncoated glass plate was used as a beam splitter to direct approximately 5% of the intensity to the microscope objective. During the writing periods, the phase of the interference grating, and hence its position on the crystal, was actively stabilized. For this purpose the following control loop was established: The video camera and a video digitizer were connected to a personal computer to monitor the phase of the grating. Software was employed to determine the actual phase of the grating by a nonlinear least square fit of a cosine function to the digitized intensity distribution. Additional software was used to emulate a proportional/integral regulator to determine the deviation of the phase of the observed grating from that of the desired grating and to calculate the voltage necessary to

bring the grating back in line. This voltage was supplied by a digital-to-analog converter which was in turn connected to a speaker (Figure 6-1). The speaker controlled the position of a mounted mirror which could shift the phase of one of the writing beams and thus the position of the grating.

Single crystals with the approximate dimensions 2mm x 2mm x 0.5mm were prepared by cooling 0.015M ethanol solution of the salt at 0.05°C / minute from 60° to 0°C. These crystals were then affixed to glass fibres with epoxy and mounted on a goniometer head. The goniometer head was adjusted so that the [100] face of the crystal was perpendicular to the direction of the laser beam.

The mounted crystal and a Pt 100 resistor, connected to a voltmeter for temperature read-out, were inserted in a cylindrical oven, 20 mm long and 10 mm in diameter which was constructed from heating foil connected to a power supply for temperature control. The crystal was inserted into the oven through an opening in the side of the cylinder, while the laser beam was directed down the long axis of the cylinder.

## Theory

### Formation of the grating

The interference pattern created by the interfering laser beams directed onto the crystal can be expressed as

$$I(x) = I_0 (1 + \cos q x),$$

where  $I$  is the intensity of the unsplit laser beam,  $x$  is the direction perpendicular to the optical axis within the plane of the incident beams, and  $q$  is the absolute value of the grating vector,

$$q = (4\pi / \lambda) \sin \frac{\theta}{2}.$$

Here,  $\lambda$  is the wavelength of the laser and  $\theta$  is the angle between the writing beams.

Where light is absorbed within the crystal, a dimerization reaction occurs, creating a new chemical species with a refractive index different from that of the reactant. The difference in refractive index between the irradiated and unirradiated parts of the crystal,  $\Delta n$ , is called the modulation depth of the sinusoidal refractive index grating and, in the

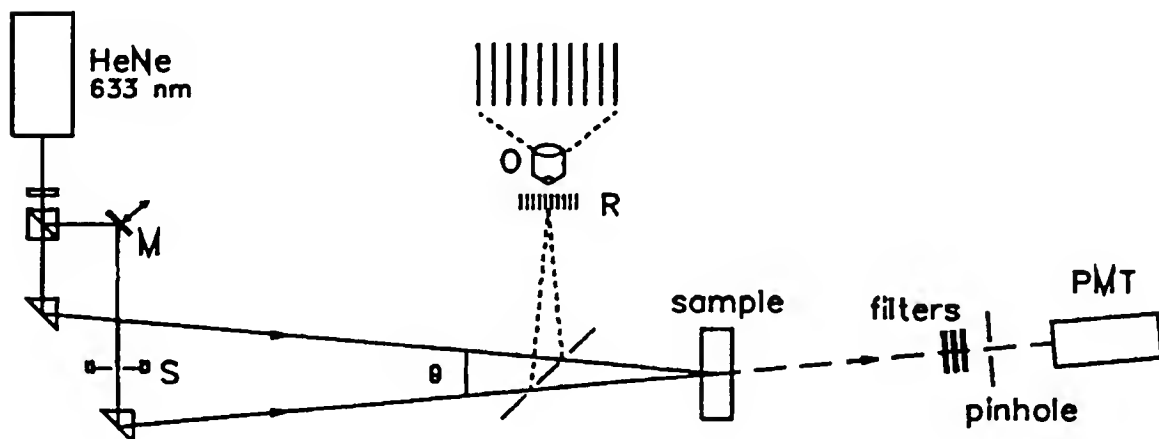


Figure 6-1. The beam from a 30 mW He-Ne laser (633nm) was split and then recombined so that an interference pattern is formed on the sample. The writing beam may be blocked by a shutter (S) and the intensity of the diffracted reading beam measured with a photomultiplier tube (PMT). A beam splitter directed a portion of the intensity to an optical set-up involving a microscope objective (O), microscope reticle (R), and a video camera through which the position of the grating could be monitored.

low conversion limit, is proportional to the difference in the number density of dimer molecules.

This relationship can be derived from the Clausius-Mosotti equation as follows. Here  $n$  is the refractive index at a given point in the crystal;  $N$  is the number density and  $\alpha$  is the polarizability of either,  $m$ , monomer or  $d$ , dimer at that point.  $\epsilon_0$  is vacuum permittivity.

$$\frac{n^2-1}{n^2+1} = \frac{1}{3\epsilon_0} (\alpha_m N_m + \alpha_d N_d) \quad \text{Clausius-Mosotti equation}$$

Taking the differential on both sides,

$$d \left[ \frac{n^2-1}{n^2+1} \right] = \frac{1}{3\epsilon_0} (\alpha_m dN_m + \alpha_d dN_d)$$

Since one dimer molecule is created from every two monomer molecules,  $dN_m = -2dN_d$ ,

$$d \left[ \frac{n^2-1}{n^2+1} \right] = \frac{1}{3\epsilon_0} (\alpha_d - 2\alpha_m) dN_d \quad \text{eq. 1}$$

Furthermore,

$$d \left[ \frac{n^2-1}{n^2+1} \right] = \frac{d \left[ \frac{n^2-1}{n^2+1} \right]}{dn} dn = \frac{6n}{(n^2+1)^2} dn \quad \text{eq. 2}$$

Substituting eq. 2 into eq.1,

$$dn = \frac{(n^2+1)^2}{6n} \frac{1}{3\epsilon_0} (\alpha_d - 2\alpha_m) dN_d$$

Thus for small conversions  $\Delta N_d$

$$\Delta n \sim \Delta N_d$$

Assuming monomer molecules are depleted, and dimer molecules are built up, according to a first order rate law, and the rate of the dimerization is proportional to the intensity,

$$R \sim I_0 (1 + \cos q x),$$

then the growth of the dimer concentration can be described as,

$$N_d \sim 1 - e^{-I_0 t (1 + \cos q x)}$$

or by using the power series expansion for the exponential,

$$N_d \sim I_0 t (1 + \cos qx) - \frac{1}{2} (I_0 t)^2 (1 + \cos qx)^2 + \frac{1}{6} (I_0 t)^3 (1 + \cos qx)^3 + \dots$$

In the low conversion limit, the higher order terms may be neglected and a linear growth of  $N_d$  with time is obtained.

$$N_d \sim I_0 t (1 + \cos qx)$$

Hence both the amplitude of the dimer concentration,  $\Delta N_d$ , and the amplitude of the refractive index grating,  $\Delta n$ , are a linear function of the time,  $t$ :

$$\Delta n \sim \Delta N_d \sim I_0 t$$

The dimer concentration (and thus the modulation depth of the phase grating) along the  $x$ -axis during this initial linear growth period is shown in Figure 6-2a. Only in this initial linear growth period is the grating characterized by an approximation of a simple  $(1 + \cos qx)$  function. Here simple first order diffraction is observed meeting the Bragg condition,  $\lambda = 2n\Lambda \sin(\theta/2)$ , where  $\Lambda$  is the fringe spacing of the grating and  $n$  is an integer, in this case, 1.

At longer times the formation of dimer starts to level off as the system approaches saturation. Now the higher order terms in the expansion become important and conditions for first order Bragg diffraction fail. Figure 6-2b<sup>110</sup> shows how the shape of the function changes as  $t$  increases. Figure 6-3a shows how the grating evolves as the higher order terms become increasingly important in describing the dimer concentration and modulation depth through a cross section of the crystal. Figure 6-3b is a view of Figure 6-3a rotated

180°. As the system deviates from simple  $(1+\cos qx)$  behavior with increasing time, so-called saturation effects may be visually observed in the form of a higher order diffraction pattern.

### Readout of the grating

A thick sinusoidal holographic phase grating, of thickness,  $d$ , will diffract a beam of monochromatic light with the efficiency<sup>119</sup>:

$$\eta = \sin^2 \Delta n \frac{d \pi}{\lambda \cos \frac{\theta}{2}}$$

as long as the refractive index modulation within the crystal is described by a  $(1+\cos qx)$  function. This is the condition in the linear regime, where primarily first order Bragg diffraction is occurring. At the initial stages of the growth of the grating, ie., when  $\Delta n$  is small, the sine function may be expanded and the diffraction efficiency,  $\eta$ , may be approximated as

$$\eta \approx (\Delta n)^2$$

Because the buildup of dimer is initially linear with time ( $\Delta n \sim N_d \sim I_0 t$ ) at the beginning, the diffraction efficiency should show the following time dependence

$$\eta \sim t^2$$

The diffraction efficiency is defined as the ratio of the intensity of the diffracted light to that of the incident beam. In the experiments reported here, it was not possible and not necessary to measure the absolute diffraction efficiency because of losses due to the relatively poor optical quality of the crystals. However, the relative intensity of the diffracted light could be measured very precisely.



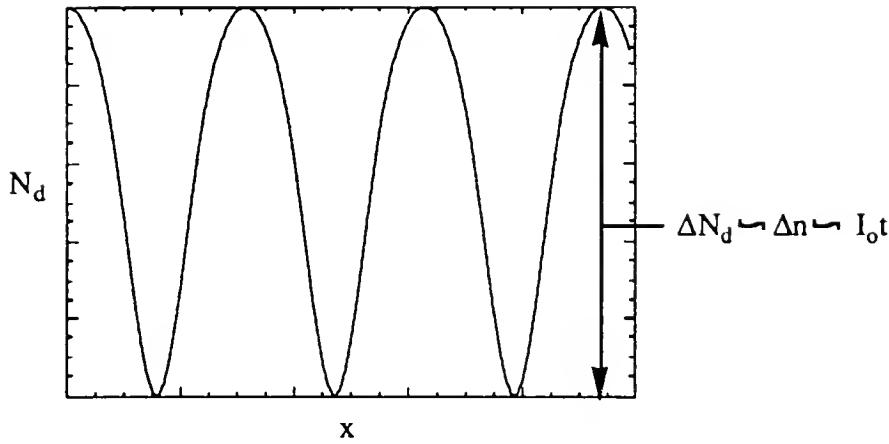


Figure 6-2a. The dimer concentration,  $N_d$ , along a cross section of the crystal,  $x$ , is described by  $N_d \sim 1 - e^{-I_0 t (1 + \cos q x)}$ . At low values for  $t$ , ie., during the initial stages of growth for the grating, this may be approximated,  $N_d \sim I_0 t (1 + \cos q x)$ . This is shown above where the exponential function is plotted for a low value for  $t$ . The difference in dimer concentration between the “light” areas of the crystal, ie., those areas receiving the highest intensity of light from the laser, and “dark” areas,  $\Delta N_d$ , is proportional to  $I_0 t$ . The modulation depth of the grating,  $\Delta n$ , is also proportional  $\Delta N_d$ , and therefore also proportional to  $I_0 t$ .

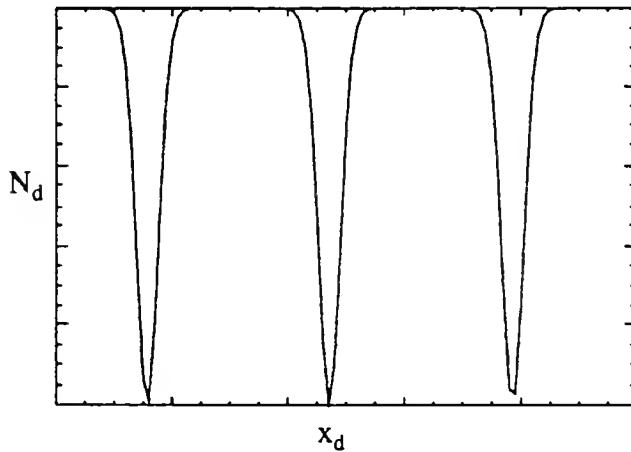
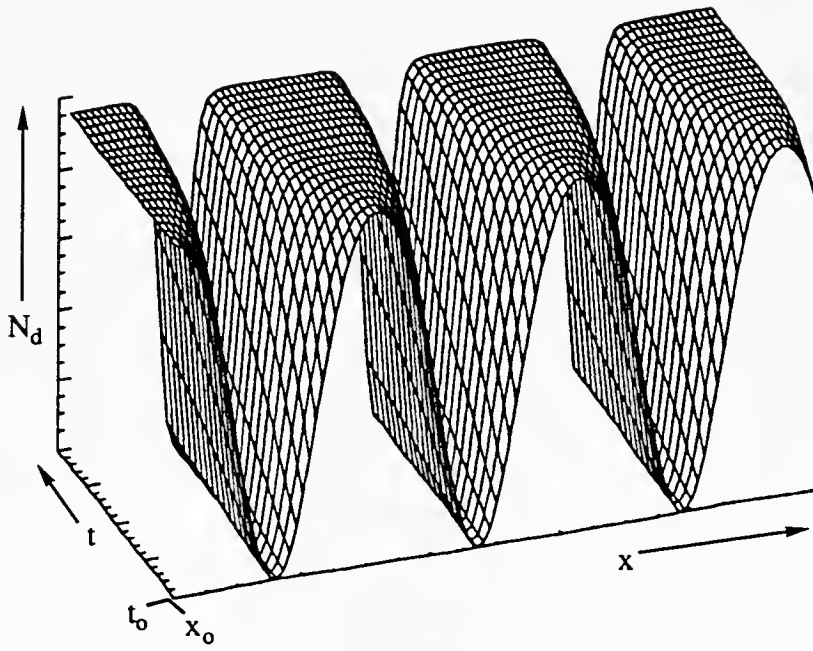


Figure 6-2b. At later stages of growth, ie., high values for  $t$ , the first approximation for  $N_d$  does not hold and the entire  $1 - e^{-I_0 t (1 + \cos q x)}$  function must be used to describe the spatial distribution of the dimer concentration and the modulation depth of the grating. This is shown here where the exponential function is plotted for a high value of  $t$ .



Figures 6-3a. This Figure shows how the plot in Figure 6-2a evolves into that of Figure 6-2b.

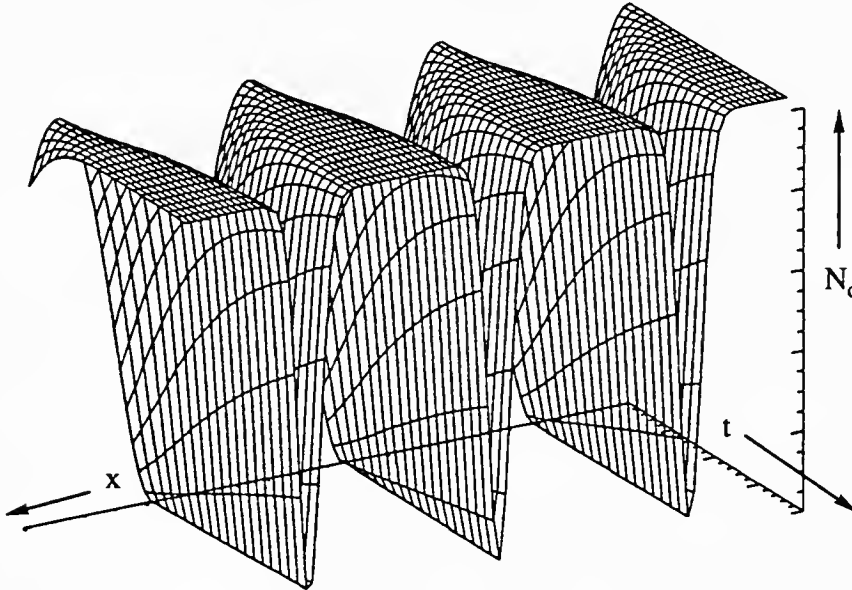


Figure 6-3b. This Figure shows Figure 6-3a from the opposite side, that is, rotated 180°.

Furthermore, in the above discussion, 100% contrast within the interference grating is assumed. In practice this is never achieved because of scattering from the edges and imperfections of the crystal. This, however, does not affect the measurements during the initial linear growth period which are subsequently used for quantitative data analysis. Only the saturation behavior is significantly affected by this “background” or “stray” light.

## Results

### Writing the Grating

Figure 6-4 shows a plot of the intensity of the diffracted light with time for an initial experiment without active stabilization of the grating. From 0 to 1800 seconds, the intensity of the diffracted light oscillates due to the instability of the interference pattern created by the laser. The grating directed onto the crystal was drifting. This led to grating erasure as the unreacted monomer component of the grating received increasingly higher intensities from the interference pattern. When cyclobutane is formed in these unreacted regions,  $\Delta n$  decreases and thus the grating is weakened. The grating shift was visually monitored with the microscope / video camera set-up. From 2200 to 3100 seconds, the stability of the grating *written into the crystal* was tested by deactivating the writing beam and periodically monitoring the intensity of the diffracted reading beam. From 3100 to 3800 seconds, the reading beam was left on continuously with the expected decrease in diffraction intensity due to bleaching was observed.

In the next experiments, interference grating drift was eliminated by active phase stabilization. Once the grating was stabilized, a perfect square-dependence of the initial stages of the grating growth curves with time was seen. Figure 6-5 shows an example of such a curve; the inset shows the data points for the first 1500 seconds of growth with the  $t^2$  fit. In this example, at the later stages of growth, but still on the initial growth curve, a higher order diffraction pattern could be seen, indicating that the phase modulation in the

crystal can no longer be described by a simple sinusoidal function. Thus, the conditions for first order Bragg diffraction broke down before the argument of the  $\sin^2$  function in equation 1 reached  $\pi/2$ . Figure 6-6 shows a micrograph of the grating.

### Energy of Activation for Cyclobutane Cleavage

Because the dimerization is thermally reversible, the grating can be erased by heating the crystal. For measuring the rates of cyclobutane thermal cycloreversion, the grating was written and “read” in a stepwise manner at the given temperature until the desired diffraction intensity had been reached. Filters were then used to reduce the intensity of the reading beam by a factor of approximately 2000 to avoid bleaching. For temperature control, the crystal was inserted together with a Pt 100 resistor in a cylindrical oven of 20 mm in length and 10 mm in diameter. Figure 6-7 shows such a writing / erasing cycle. Both the growth and decay curves are normalized to 1 at  $t = \text{filter insertion}$ . Figure 6-8 shows a series of decay curves at various temperatures. The diffraction efficiency, and therefore the intensity of the diffracted beam, is proportional to the square of the number of cyclobutane molecules in the crystal. Thus, the rate of diffracted intensity decay is directly proportional to twice the rate of disappearance of the cyclobutane. The decay in diffracted intensity with time fit a first order rate law, that is, the plots of  $\ln I_d$  vs. time at various temperatures give straight lines. From these plots, the half-lives and rate constants for the cyclobutane thermal cycloreversion are calculated and shown in Table 6-1.

The temperature dependence of the reaction showed Arrhenius-type behavior, ie., in accordance with the Arrhenius equation,  $\ln k = \ln A - \frac{E_a}{R} \frac{1}{T}$ , a plot of  $\ln k$  vs.  $1/T$  gives a straight line as shown in Figure 6-9:

$$\ln k = 27.81 - 11,897 \frac{1}{T} . \quad \text{eq. 3}$$

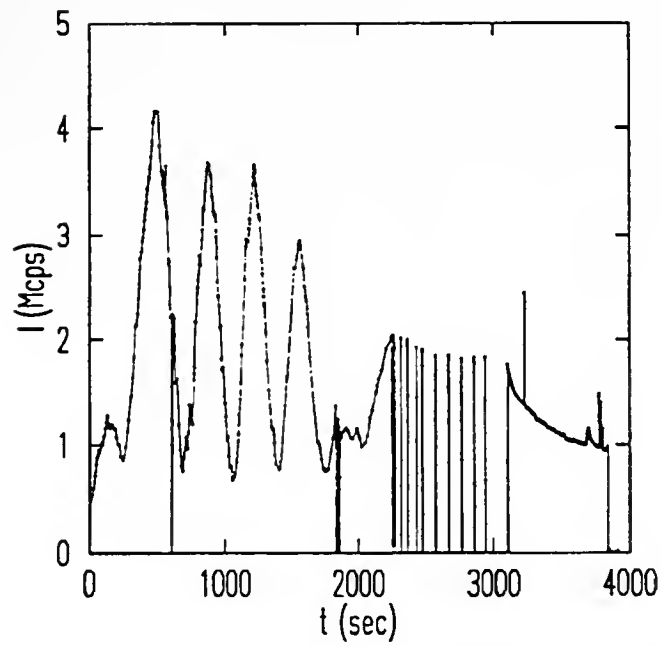


Figure 6-4. Plot of the intensity of the diffracted light with time for an unstabilized interference pattern. From 0 to 1800 seconds, the intensity of the diffracted light is seen to oscillate due to pattern drift. From 2200 to 3100 seconds, the written grating is periodically tested and found to be stable. From 3100 to 3800 seconds, the sample is continuously exposed to the diffracted beam which bleaches out the grating.



Figure 6-6. This is a micrograph of a grating written into a styrylpyrylium crystal with fringe spacing,  $\Lambda \approx 20\mu\text{m}$ .

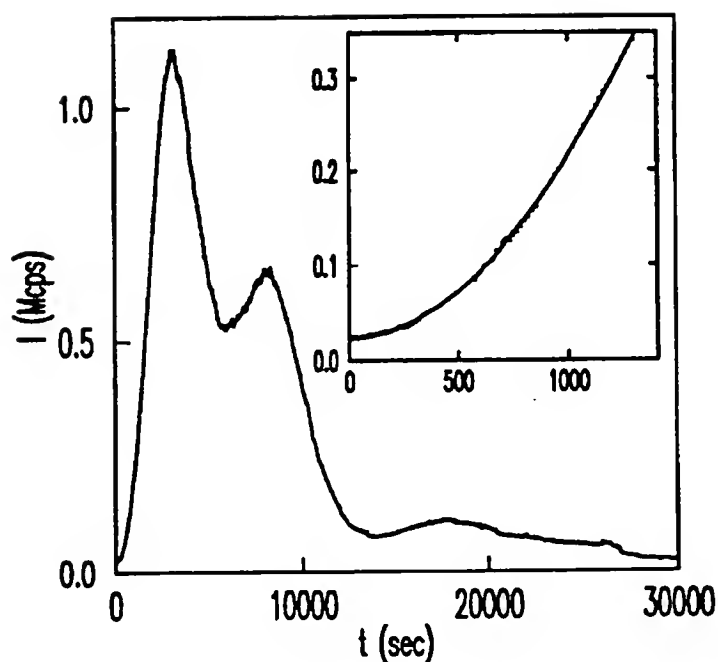


Figure 6-5. The diffraction efficiency for a grating in a crystal irradiated with a stabilized interference pattern. In the first 1500 seconds, a perfect square dependence of the diffraction efficiency with time is seen, as shown in the inset where the data points are fit to a  $t^2$  function. At longer times, but still on the first diffraction efficiency growth curve, a higher order diffraction pattern could be seen, indicating that the system had reached saturation.

Table 6-1. Rate constants from a plot of  $\ln I_d$  vs. time at various temperatures for grating erasure.

$T / ^\circ\text{C}$	$k / \text{s}^{-1}$	$t_{0.5} / \text{s}$
137	0.294	1.64
129.5	0.147	3.26
119.5	0.0893	5.38
118.6	0.0794	6.05
114	0.0450	15.4
111	0.0423	16.4
104	0.0294	23.6
97	0.0137	50.7
97	0.0142	48.6
96	0.0109	63.8
92	0.00942	73.6
85	0.00453	153
79.5	0.00265	262
71.9	0.00105	657

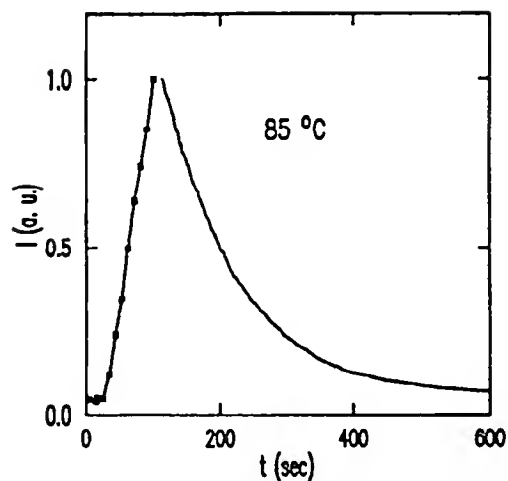


Figure 6-7. Writing / thermal erasing cycle. The grating was written and “read” in a stepwise manner, while being held at a given temperature until the desired diffraction intensity had been reached. Filters were then used to reduce the intensity of the reading beam by a factor of approximately 2000 to avoid bleaching. The crystal was maintained at the given temperature and the diffraction efficiency measured continuously as the grating decayed. Both the growth and decay curves are normalized to 1 at  $t =$  filter insertion.

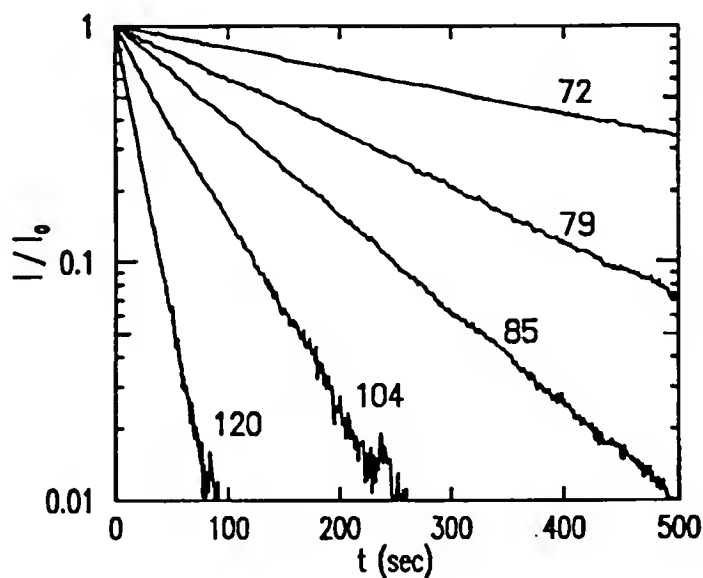


Figure 6-8. A series of decay curves for cyclobutane cleavage at various temperatures:  $\ln$  (diffraction intensity) vs. time for certain temperatures. The straight lines are in accordance with the expected first order decay.

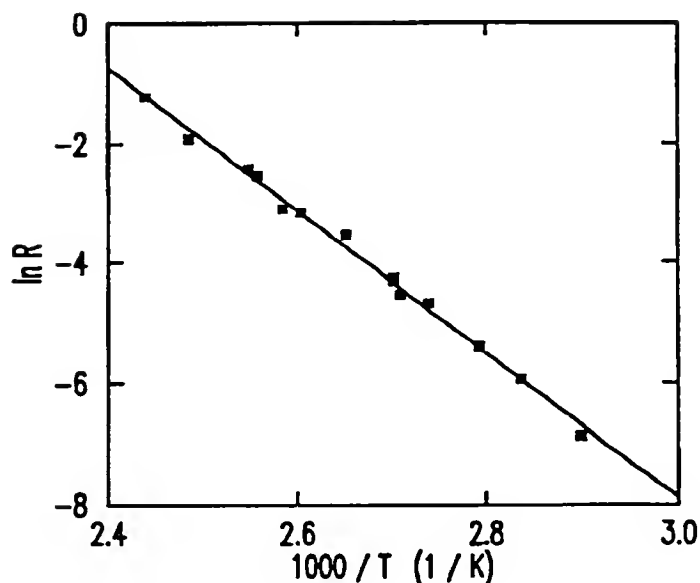


Figure 6-9. An Arrhenius plot of the temperature dependence for the rate of cyclobutane cleavage:  $\ln k = 27.81 - 11,897 \frac{1}{T}$ . For  $R=8.314 \text{ J K}^{-1}\text{mol}^{-1}$ ,  $E_a = 98.9 \text{ kJ mol}^{-1}$  (or for  $R=1.987 \text{ cal K}^{-1}\text{mol}^{-1}$ ,  $E_a=23.6 \text{ kcal mol}^{-1}$ ).

Thus, using  $R=8.314 \text{ J K}^{-1}\text{mol}^{-1}$ ,  $E_a = 98.9 \text{ kJ mol}^{-1}$  or  $R=1.987 \text{ cal K}^{-1}\text{mol}^{-1}$ ,  $E_a=23.6 \text{ kcal mol}^{-1}$ . The pre-exponential factor,  $A$ , is  $1.2 \times 10^{12} \text{ s}^{-1}$  which is on the order of the frequency of a molecular vibration.

Table 6-2 compares data on the energy of activations for the thermal cycloreversion of some cyclobutane-containing compounds. Note that the example of the sterically-strained tricyclo[4.2.0.0]octane is a crystalline state thermolysis. No other examples of kinetic studies on cyclobutane cleavage in the crystalline state could be found. Energies of activation as low as  $22 \text{ kcal mol}^{-1}$  are reported for the strained bicyclo[2.2.0]hexanes. The lowest energy of activation for a nonbridged cyclobutane-containing compound reported in the literature is  $50.9 \text{ kcal mol}^{-1}$  for *cis*-1,3-divinylcyclobutane. The pre-exponential factors range from  $10^{12}$  to  $10^{15} \text{ s}^{-1}$ .



Table 6-2. Comparison of Kinetic Data on Cyclobutane Cleavage.

	A (s <sup>-1</sup> )	E <sub>a</sub> (kcal mol <sup>-1</sup> )
cyclobutane <sup>120</sup>	4x10 <sup>15</sup>	62.5
cis-1,3-divinylcyclobutane <sup>120</sup>		50.9
1,2,5,6-tetracyano-anti-tricyclo[4.2.0.0]octane <sup>121</sup>	4x10 <sup>15</sup>	34.9
styrylpyrylium photodimer (this work)	1.2x10 <sup>12</sup>	23.6

Schaumann and Ketcham<sup>120</sup> have pointed out a qualitative inverse correlation between the strain energy of various types of cyclobutane rings and the energy of activation for their thermal cycloreversion. As previously reported,<sup>122</sup> dramatic bond angle deformation is present in the styrylpyrylium photodimer species trapped in the monomer crystal lattice in low concentrations. This may explain why the energy of activation for the thermal cycloreversion in this study is as low as the energies of activation for cyclobutane-containing molecules with steric strain "built-in". This is supported by two pieces of evidence: The thermal cycloreversion for the styrylpyrylium photodimer is much slower in solution. For example, Hünig, et. al., report that in o-chlorophenol, the thermal cycloreversion is 78% complete after 220 minutes at 155°C.<sup>4</sup> This implies a first order rate constant of  $1.14 \times 10^{-4} \text{ s}^{-1}$ . At T=155°C (428 K),  $k=1.14 \times 10^{-4}$  and  $E_a=23 \text{ kcal mol}^{-1}$ , eq. 3 would require that the pre-exponential factor assumes the unusually low magnitude of  $10^8 \text{ s}^{-1}$ . (Unimolecular reactions have typical pre-exponential factors of  $10^{12} - 10^{15} \text{ s}^{-1}$ , whereas pre-exponential factors for bimolecular reactions are usually in the range of  $10^6 - 10^8 \text{ s}^{-1}$ .) Instead, the energy of activation for the cleavage in solution must be higher than that in the crystal. Thus it is easier to cleave the cyclobutane in the crystal where the strain energy from the bond deformation is present. Furthermore, as reported earlier,<sup>118</sup> the recrystallized cyclobutane dimer crystals fail to cyclorevert to the monomer under the same conditions as the as-dimerized cyclobutane. The cyclobutane dimer molecules in the recrystallized material would be much closer to their equilibrium conformations than the

cyclobutane molecules in the as-dimerized crystals. This underscores the novelty of the dimer lattice that evolves during the irradiation and points to a metastable photodimer conformation being responsible for the high reactivity of the cyclobutane formed in the crystalline state.

The comparatively low energy of activation for this thermal cleavage may also arise from steric strain due to nonbonded interactions. Therefore, the steric crowding around the cyclobutane by the aromatic rings may also lower the energy of activation for the cleavage of this cyclobutane, in comparison with less-substituted cyclobutanes. This effect has been invoked to explain the relative thermal stabilities of certain cyclobutane containing polymers.<sup>123</sup> Furthermore, the aromatic rings are capable of stabilizing the presumed zwitterionic intermediate, an effect which has been demonstrated for a series of bicyclo[2.2.0]hexanes.<sup>120</sup>

#### Energy of Activation for Photodimerization

Figure 6-10 shows diffraction intensity plotted against time for the growth of a grating at increasing temperatures. The growth of the grating was monitored as the crystal was maintained at a given temperature. Recall,  $I_d \sim \eta \sim \Delta n^2$  and  $\Delta n \sim Rt$ , at early times. Thus coefficients proportional to the rates at various temperatures,  $R \sim c$ , were extracted by taking into consideration, background or stray light,  $b$ , and fitting the curves to the function

$$I = b + (c^2) t^2 \quad .$$

The coefficients proportional to the initial growth rates at various temperatures from the fitted curves in Figure 6-10 are shown in Table 6-3.

The temperature dependence of the photodimerization reaction also shows Arrhenius behavior. A plot of  $\ln c$  vs.  $1/T$ , shown in Figure 6-11, indicates a slope,  $E_a / R$  of 1900K. Thus, the energy of activation for the photodimerization is  $15.8 \text{ kJ mol}^{-1}$  or  $3.8 \text{ kcal mol}^{-1}$ . This may be compared with the energy of activation of  $\approx 3 \text{ kcal mol}^{-1}$  for

the photopolymerization of distyrylpyrazine in the crystalline state to form a cyclobutane-containing polymer.<sup>124</sup>

Table 6-3. Coefficients proportional to the initial growth rates for grating formation at increasing temperatures.

T / °C	c / s <sup>-1</sup>
20	2.96
53	6.67
20	3.30
40	4.90
70	8.29
20	3.22
80	9.14

### Future Studies

The highly sensitive technique of holographic imaging can give access to quantitative kinetic data for crystalline state reactions, which is impractical to obtain by any other means. This study has centered around the type of grating that involves creating small amounts of dimer in a monomer lattice, a “dimer in monomer”-type grating. But what can be learned from studying gratings caused by small amounts of monomer in a dimer lattice? For example, the energy of activation for the photodimerization of styrylpyrylium triflate in mixed crystals of the monomer and dimer (formed from tail irradiation) may be measured. Mixed crystals in any percent conversion are available for study. As the percent of dimer in the mixed crystal increases, the monomer must accommodate increasing bond angle deformation. Will this lead to a decrease in the energy of activation for the photodimerization? Furthermore, what can be learned from thermal studies of a “monomer in dimer”-type grating. For example, if the energy of activation for cyclobutane cleavage decreases with increasing bond angle deformation of the dimer in the mixed crystal, then an increase in diffraction efficiency should be observed on heating the grating.

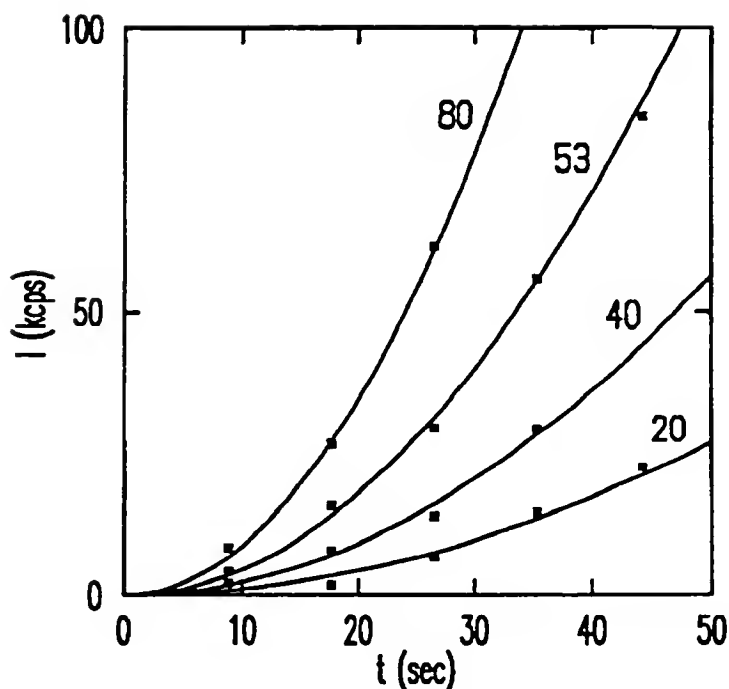


Figure 6-10. A series of growth curves for grating formation as the crystal is held at various temperatures: data points fitted to the function  $I = b + (c^2) t^2$ , where  $b$  is a constant representing background light and  $c$  is proportional to the rate of cyclobutane formation.

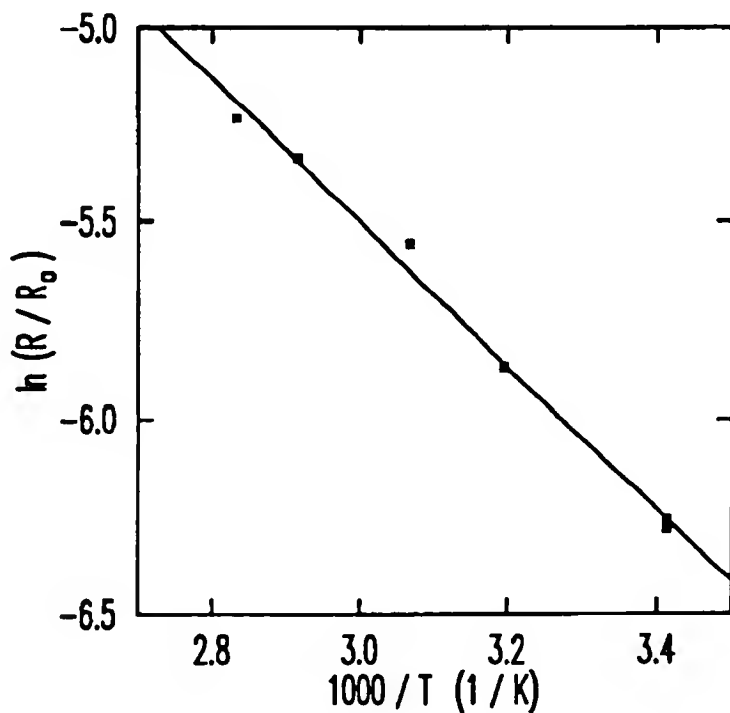


Figure 6-11. An Arrhenius plot of the data contained in Table 6-3 ( $R/R_0=c$ )  $E_a$  for the photodimerization is calculated at  $15.8 \text{ kJ mol}^{-1}$  (or  $3.8 \text{ kcal mol}^{-1}$ ).

APPENDIX  
VISUALIZING PRODUCT PHASE EVOLUTION:  
THE DRAWINGS OF M. C. ESCHER

M.C. Escher's woodcut, *Sky and Water*, shown in Figure A-1, is used by Venkatesan and Ramamurthy<sup>13</sup> to illustrate the single-crystal-to-single-crystal transformation in the [2+2] transformation of BBCP. *Development I*, by Escher, Figure A-2, illustrates how a defect may disrupt a crystal lattice in its immediate vicinity, as pointed out by L. Glasser.<sup>125</sup> Visions of Symmetry: Notebooks, Periodic Drawings, and Related Work of M. C. Escher<sup>126</sup> and M. C. Escher: Art and Science<sup>127</sup> list other references describing issues in topology, symmetry and crystallography demonstrated in Escher's work.

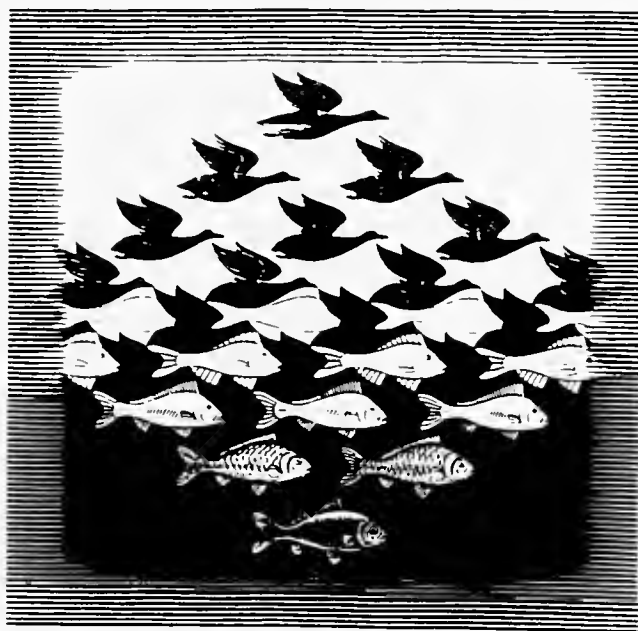


Figure A-1. *Sky and Water* by M. C. Escher illustrates the single-crystal-to-single-crystal photodimerization of BBCP.

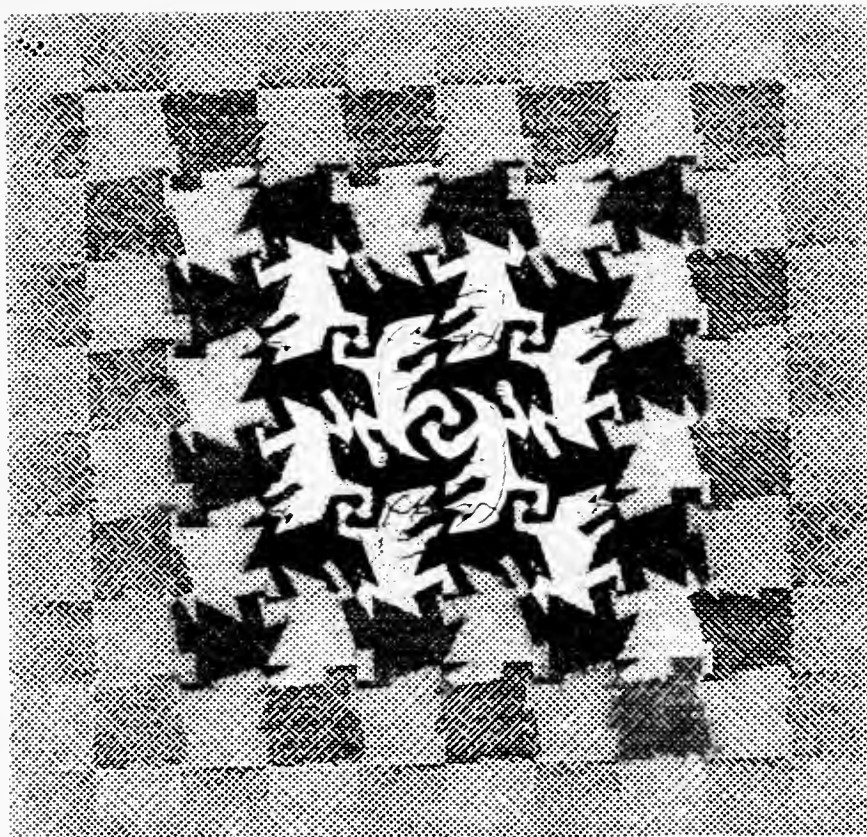


Figure A-2. *Development I* by M. C. Escher illustrates a point defect disrupting the periodicity in a crystal lattice.

## REFERENCES

- (1) Ramamurthy, V.; Venkatesan, K. *Chem. Rev.* 1987, 87, p. 478.
- (2) Rees, R. W. In *Encyclopedia of Polymer Science and Engineering*; J. Kroschwitz, Ed.; John Wiley & Sons: New York, 1988, 4, p. 395.
- (3) Engle, L. P., Doctoral Dissertation, University of Florida, Gainesville, Florida 1991.
- (4) Hesse, K.; Hünig, S. *Liebigs Ann. Chem.* 1985, 715.
- (5) Meyer, W.; Lieser, G.; Wegner, G. *J. Polym. Sci., Polym. Phys. Ed.* 1978, 16, 1365.
- (6) Braun, H.-G.; Wegner, G. *Mol. Cryst. Liq. Cryst.* 1983, 96, 121.
- (7) Braun, H.-G.; Wegner, G. *Makromol. Chem.* 1983, 184, 1103.
- (8) Prasad, P. N. In *Organic Solid State Chemistry*; G. R. Desiraju, Ed.; Elsevier: New York, 1987; p. 117.
- (9) Hasegawa, M. In *Comprehensive Polymer Science*, G. Allen, Ed.; Pergamon Press: Oxford, Great Britain; 1989; 5, p. 217.
- (10) Braun, H.-G.; Enkelmann, V. *Acta Cryst. B* 1984.
- (11) Wegner, G. *Pure & Appl. Chem.* 1977, 49, 443.
- (12) Nakanishi, H.; Jones, W.; Thomas, J. M.; Hursthouse, M. B.; Motevalli, M. *J. Phys. Chem.* 1981, 85, 3636.
- (13) Venkatesan, K.; Ramamurthy, V. In *Photochemistry in Organized and Constrained Media*; V. Ramamurthy, Ed.; VCH: Weinheim, Germany, 1991; p. 133.
- (14) Kaupp, G. *Angewandte Chem.* 1992, 104, 606.
- (15) Kaupp, G. *Angew. Chem. Int. Ed. Engl.* 1992, 3, 592.
- (16) Wegner, G. *Z. Naturforsch.* 1969, 24b, 824.
- (17) Chang, H. C.; Popovitz-Biro, R.; Lahav, M.; Lesierowitz, L. *J. Amer. Chem. Soc.* 1982, 104, 614.
- (18) Ohashi, Y.; Yanagi, K.; Kurihara, T.; Sasada, Y.; Ohgo, Y. *J. Amer. Chem. Soc.* 1982, 104, 6353.

- (19) Tieke, B. J. *J. Polym. Sci. Polym. Chem. Ed. A-1* 1984, 22, 2895.
- (20) Wang, W.-N.; Jones, W. *Tetrahedron* 1987, 43, 1273.
- (21) Williams, J. L. R. *J. Org. Chem.* 1963, 28, 1317.
- (22) Quina, F. H.; Whitten, D. G. *J. Am. Chem. Soc.* 1977, 99, 877.
- (23) Vansant, J.; Toppet, S.; Smets, G.; Declercq, J. P.; Germain, G.; Meersche, M. V. *J. Org. Chem.* 1980, 45, 1565.
- (24) Horner, M.; Hünig, S. *Liebigs Ann. Chem.* 1982, 1183.
- (25) Muira, M.; Kitami, T.; Nagakubo, K. *J. Polym. Sci., B* 1968, 6, 463.
- (26) Schryver, F. C. D.; Feast, W. J.; Smets, G. *J. Polym. Sci., A-1* 1970, 8, 1939.
- (27) Stevens, M. P.; Kardush, N. *J. Polym. Sci., A-1* 1972, 10, 1093.
- (28) Stevens, M. P.; Musa, Y. *J. Polym. Sci., A-1* 1972, 10, 319.
- (29) Leonard, N. J.; McCredie, R. S.; Logue, M. W.; Cundall, R. L. *J. Am. Chem. Soc.* 1973, 95, 2320.
- (30) Schryver, F. C. D.; Boens, N.; Smets, G. *J. Am. Chem. Soc.* 1974, 96, 6463.
- (31) DeSchryver, F. C.; Boens, N.; Smets, G. *J. Polym. Sci., A-1* 1974, 10, 1687.
- (32) Schryver, F. C. D.; Boens, N.; Smets, G. *J. Polym. Sci., Polym. Chem. Ed.* 1975, 13, 201.
- (33) Bernstein, J.; Green, B. S.; Regto, M. *J. Am. Chem. Soc.* 1980, 102, 323.
- (34) Hasegawa, M. In *Adv. Polym. Sci.* Springer-Verlag: Berlin, 1982; p. 1.
- (35) Dilling, W. *Chem. Rev.* 1983, 83, 1.
- (36) Hasegawa, M. *Chem. Rev.* 1983, 83, 507.
- (37) Hasegawa, M. In *Organic Solid State Chemistry*; G. R. Desiraju, Ed.; Elsevier: New York, 1987; p. 153.
- (38) Tomlinson, W. J. *Appl. Optics* 1975, 14, 2456.
- (39) Tomlinson, W. J.; Chandross, E. A. *Adv. Photochem.* 1980, 12, 201.
- (40) Richter, K. H. *Chem. Phys. Letters* 1982, 92, 4.
- (41) Richter, K. H.; Güttler, W.; Schwoerer, M. *Appl. Phys. A* 1983, 1.
- (42) Bjorklund, G. C.; Burland, D. M.; Alvarez, D. C. *J. Chem. Phys.* 1980, 73, 4321.
- (43) Burland, D. M.; Bräuchle, C. *J. Chem. Phys.* 1982, 76, 4502.



- (44) Cross, L. C.; Klyne, W. *Pure Appl. Chem.* 1976, 45, 11.
- (45) Cohen, M. D.; Schmidt, G. M. J. *J. Chem. Soc.* 1964, 1996.
- (46) Thomas, J. M.; Williams, J. O. In *Progress in Solid State Chemistry*; H. Reiss and J. O. McCaldin, Ed.; Pergamon Press: New York, 1971; p. 119.
- (47) Hirshfeld, F. L.; Schmidt, G. M. J. *J. Polym. Sci, A* 1964, 2, 2181.
- (48) Wegner, G. In *Proc. Symp. Uppsala, 1977: Structure and Dynamics in Chemistry*; P. Ahlberg and L.-O. Sundelof, Ed.; Acta Universitatis: Uppsala, Sweden, 1978.
- (49) Cohen, M. D.; Ludmer, Z.; Thomas, J. M.; Williams, J. O. *Proc. Roy. Soc. London, A* 1971, 324, 459.
- (50) Parkinson, G. M.; Goringe, M. J.; Ramdas, S.; Williams, J. O.; Thomas, J. M. *J. Chem. Soc. Chem. Commun.* 1978, 134.
- (51) Bart, J. C. J.; Schmidt, G. M. J. *Israel J. Chem.* 1971, 9, 429.
- (52) Heller, E.; Schmidt, G. M. J. *Israel J. Chem.* 1971, 9, 449.
- (53) Schmidt, G. M. J. *J. Chem. Soc.* 1964, 2014.
- (54) Cohen, M. C.; Schmidt, G. M. J.; Sonntag, F. I. *J. Chem. Soc.* 1964, 2000.
- (55) Schmidt, G. M. J. *Solid State Photochemistry*; D. Ginsburg, Ed.; VCH: New York, 1976.
- (56) Dunitz, J. D. In *Solid State Photochemistry*; D. Ginsburg, Ed.; VCH: New York, 1976; p. 255.
- (57) Wegner, G. *Makromol. Chem., Suppl.* 1984, 6, 347.
- (58) Simpson, W. M., Doctoral Dissertation, University of Oxford, Oxford, Great Britain 1993.
- (59) Heyes, S. *Mol. Cryst., Liq. Cryst.* 1993, *in press*.
- (60) Di, L., Doctoral Dissertation, Brandeis University, Waltham, Massachusetts, 1992.
- (61) Cohen, M. D.; Green, B. S. *Chemistry in Britain* 1973, 9, 490.
- (62) Block, S.; Filippakis, W. E.; Schmidt, G. M. J. *J. Chem. Soc. (B)* 1967, 233.
- (63) Filippakis, S. E.; Schmidt, G. M. J. *J. Chem. Soc. (B)* 1967, 229.
- (64) Schmidt, G. M. J. In *Reactivity of the Photoexcited Organic Molecule*; Interscience: London, 1967; p. 227.
- (65) Lahav, M.; Schmidt, G. M. J. *J. Chem. Soc. (B)* 1967, 239.
- (66) Ramamurthy, V.; Venkatesan, K. *Chem. Rev.* 1987, 87, 433.

- (67) Schmidt, G. M. J.; Rabinovich, D. *J. Chem. Soc., B*, 1967, 286.
- (68) Rabinovich, D.; Schmidt, G. M. J. *J. Chem. Soc., B* 1967, 144.
- (69) Rabinovich, D. *J. Chem. Soc., B* 1967, 140.
- (70) Rabinovich, D. *J. Chem. Soc., B* 1970, 6.
- (71) Green, B. S.; Schmidt, G. M. J. *Tet. Lett.* 1970, 49, 4249.
- (72) Schmidt, G. M. J.; Cohen, M. D., Flavian, S. (in part) *J. Chem. Soc.* 1964, 2041.
- (73) Schmidt, G. M. J. *Pure Appl. Chem.* 1971, 27, 647.
- (74) Cohen, M. D.; Elgavi, A.; Green, B. S.; Ludmer, Z.; Schmidt, G. M. J. *J. Am. Chem. Soc.* 1972, 94, 6776.
- (75) Hung, J. D.; Lahav, M.; Luwisch, M.; Schmidt, G. M. J. *Israel J. Chem.* 1972, 10, 585.
- (76) Penzien, K.; Schmidt, G. M. J. *Angew. Chem. Int. Ed.* 1969, 8, 608.
- (77) Elgavi, A.; Green, B. S.; Schmidt, G. M. J. *J. Am. Chem. Soc.* 1973, 95, 2058.
- (78) Green, B. S.; Lahav, M.; Schmidt, G. M. J. *Mol. Cryst. Liq. Cryst.* 1975, 29, 187.
- (79) Desiraju, G. R. *Crystal Engineering: the Design of Organic Solids*; Elsevier: Amsterdam, 1989.
- (80) Ramamurthy, V., Ed. *Photochemistry in Organized and Constrained Media*; VCH: Weinheim, Germany, 1991.
- (81) Desiraju, G. R., Ed. *Organic Solid State Chemistry*; Elsevier: New York, 1987.
- (82) Enkelmann, V. *Adv. Polym. Sci.* 1984, 63, 92.
- (83) Wegner, G. *Polymerization Reactions and New Polymers, Advances in Chemistry Series* 1973, 129, 255.
- (84) Bloor, D. In *Comprehensive Polymer Chemistry*, G. Allen, Ed.; Pergamon Press: Oxford, Great Britain, 1989; 5, p. 233.
- (85) Baughman, R. H. *J. Chem. Phys.* 1978, 68, 3110.
- (86) Hasegawa, M.; Shiba, S. *J. Phys. Chem.* 1982, 86, 1490.
- (87) Sharp, J. H.; Brindley, G. W.; Achar, B. N. *J. Am. Ceram. Soc.* 1966, 49, 379.
- (88) Hancock, J. D.; Sharp, J. H. *J. Am. Ceram. Soc.* 1971, 55, 74.
- (89) Gnanaguru, K.; Ramasubbu, N.; Venkatesan, K.; Ramamurthy, V. *J. Org. Chem.* 1985, 50, 2337.

- (90) Zimmerman, H. E.; Zuraw, M. J. *J. Am. Chem. Soc.* 1989, *111*, 7974.
- (91) Garcia-Garibay, M.; Scheffer, J. R.; Trotter, J.; Wireko, F. *Tet. Lett.* 1987, *28*, 1741.
- (92) Kearsley, S. K. In *Organic Solid State Chemistry*; G. R. Desiraju, Ed.; Elsevier: New York, 1987; p. 69.
- (93) Cohen, M. D. *Angew. Chem.* 1975, *87*, 439.
- (94) Cohen, M. D. *Angew. Chem. Int. Ed. Engl.* 1975, *14*, 386.
- (95) Ariel, S.; Askari, S.; Scheffer, J. R.; Trotter, J.; Walsh, L. *J. Am. Chem. Soc.* 1984, *106*, 5726.
- (96) Ariel, S.; Askari, S.; Scheffer, J. R.; Trotter, J.; Walsh, L. In *Organic Phototransformations in Nonhomogeneous Media, ACS Symposium Series 278*; American Chemical Society: Washington, D. C., 1985; p. 243.
- (97) Murthy, G. S.; Arjunan, P.; Venkatesan, K.; Ramamurthy, V. *Tetrahedron* 1987, *43*, 1225.
- (98) Gavezzotti, A. *J. Am. Chem. Soc.* 1983, *105*, 5220.
- (99) Kaiser, J.; Wegner, G.; Fischer, E. W. *Israel J. Chem.* 1972, *10*, 157.
- (100) Hasegawa, M.; Suzuki, Z. *Polymer Letters* 1967, *5*, 813.
- (101) Wegner, G.; Fischer, E. W.; Munoz-Escalona, A. *Makromol. Chem. Suppl.* 1975, *1*, 521.
- (102) Cheng, K.; Foxman, B. *J. Amer. Chem. Soc.* 1977, *99*, 8102.
- (103) Balaban, A. T.; Nenitzescu, C. D. *Liebigs Ann. Chem.* 1959, *82*, 625.
- (104) Dimroth, K. *Angew. Chemie* 1960, *72*, 331.
- (105) Stang, P. J.; Anderson, A. G. *J. Org. Chem.* 1976, *41*, 3034.
- (106) Rao, C. N. R. In *New Directions in Solid State Chemistry*; Cambridge University Press: New York, p. 148.
- (107) Berry, R. S.; Rice, S. A.; Ross, J. *Physical Chemistry*; John Wiley & Sons: New York, 1976, p. 864.
- (108) Enkelmann, V.; Wegner, G.; Kroehnke, C. *Mol. Cryst. Liq. Cryst.* 1982, *86*, 103.
- (109) Kitaigorodsky, A. I. *Mixed Crystals*; Springer-Verlag: New York, 1984.
- (110) Plots were done with PV-Wave software, 4.01, on a Unix DecStation 5000/240.
- (111) Eanes, E. D.; Donnay, G. Z. *Krist.* 1959, *111*, 368.

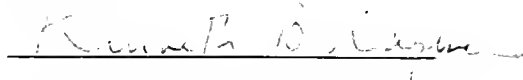
- (112) Dürr, H.; Bouas-Laurent, H., Eds. *Photochromism Molecules and Systems*; Elsevier: Amsterdam, 1990.
- (113) Jones, G. In *Photochromism Molecules and Systems*; H. Dürr and H. Bouas-Laurent, Ed.; Elsevier: Amsterdam, 1990; p. 514.
- (114) Desvergne, J.-P.; Bouas-Laurent, H. In *Photochromism Molecules and Systems*; H. Dürr and H. Bouas-Laurent, Ed.; Elsevier: Amsterdam, 1990; p. 539.
- (115) Delzenne, G. A. *Adv. Photochem.* 1979, *11*, 1.
- (116) Tomlinson, W. J.; Chandross, E. A.; Fork, R. L.; Pryde, C. A.; Lamola, A. A. *Appl. Optics* 1972, *11*, 533.
- (117) Enkelmann, V.; Wegner, G.; Novak, K.; Wagener, K. B. *J. Amer. Chem. Soc.* 1993, *115*, 10390.
- (118) Novak, K.; Enkelmann, V. *Angew. Chem.* 1993, "Crystallographic Studies on a Single-Crystal-to-Single-Crystal Photodimerization and Thermal Back Reaction" *in press*.
- (119) Kogelnik, H. *Bell System Tech. J.* 1969, *48*, 2909.
- (120) Schaumann, E.; Ketcham, R. *Angew. Chem. Intern. Ed. Eng.* 1982, *21*, 225.
- (121) Bellus, D.; Mez, H.-C.; Rihs, G.; Sauter, H. *J. Amer. Chem. Soc.* 1974, *96*, 5007.
- (122) Novak, K.; Enkelmann, V.; Köhler, W.; Wegner, G.; Wagener, K. B. *Mol. Cryst., Liq. Cryst. in press*.
- (123) Takahashi, H.; Sakuragi, M.; Hasegawa, M.; Takahashi, H. *J. Polym. Sci. Polym. Chem. Ed. A-1* 1972, *10*, 1399.
- (124) Nakanishi, H.; Suzuki, Y.; Suzuki, F.; Hasegawa, M. *J. Polym. Sci. Polym. Chem. Ed. A-1* 1969, *7*, 753.
- (125) Glasser, L. *J. Chem. Ed.* 1967, *44*, 502.
- (126) Schattschneider, D. *Visions of Symmetry: Notebooks, Periodic Drawings, and Related Work of M. C. Escher*, W. H. Freeman and Company: New York, 1990.
- (127) Coxeter, H. S. M.; Emmer, M.; Penrose, R.; Teuber, M.I., Eds., *M. C. Escher: Art and Science*, North-Holland: New York, 1986.

## BIOGRAPHICAL SKETCH

Kathleen Novak is the great-granddaughter of immigrants from the central European cities of Minden, Posnan and Ugoszcz and the granddaughter of Mireya Martin, a Cuban immigrant, whose parents were from Spain. The author was born near Chicago, Illinois, and received her early education in the public schools belonging to the small farming community of Marengo, Illinois. After earning her Bachelor of Arts in chemistry from Rockford College, Rockford, Illinois, she moved to the state of Florida to teach high school. In 1987 she resumed her study of chemistry at Purdue University, W. Lafayette, Indiana, transferring to the University of Florida in 1990. There she began doctoral research under the direction of Kenneth B. Wagener. In 1991 she traveled to Mainz, Germany, to continue her doctoral research under the joint direction of Professor Wagener and Professor Gerhard Wegner at the Max Planck Institut für Polymerforschung. This work was completed in 1993. She has coauthored papers to be published in the *Journal of the American Chemical Society*, *Angewandte Chemie*, *Journal of Chemical Physics* and *Molecular Crystals, Liquid Crystals*. She has presented work at the International Conference on the Chemistry of the Organic Solid State, ICCOSS XI, Jerusalem, Israel, July, 1993; at the 206th National American Chemical Society Meeting in Chicago, Illinois, August 1993; and at the 45th Southeast Regional American Chemical Society Meeting in Johnson City, Tennessee, October, 1993. After graduation, the author returned to MPI for postdoctoral work.

:

I certify that I have read this study and that in my opinion it conforms to acceptable standards of scholarly presentation and is fully adequate, in scope and quality, as a dissertation for the degree of Doctor of Philosophy.



Kenneth B. Wagener  
Professor of Chemistry

I certify that I have read this study and that in my opinion it conforms to acceptable standards of scholarly presentation and is fully adequate, in scope and quality, as a dissertation for the degree of Doctor of Philosophy.



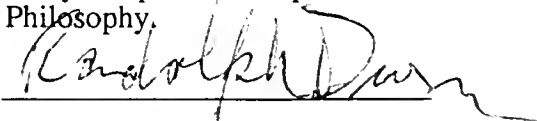
William Dolbier  
Professor of Chemistry

I certify that I have read this study and that in my opinion it conforms to acceptable standards of scholarly presentation and is fully adequate, in scope and quality, as a dissertation for the degree of Doctor of Philosophy.



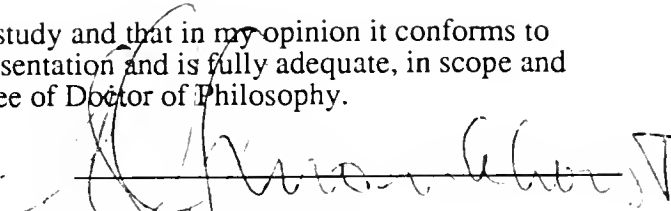
Kirk Schanze  
Associate Professor of  
Chemistry

I certify that I have read this study and that in my opinion it conforms to acceptable standards of scholarly presentation and is fully adequate, in scope and quality, as a dissertation for the degree of Doctor of Philosophy.



Randolph S. Duran  
Assistant Professor of  
Chemistry

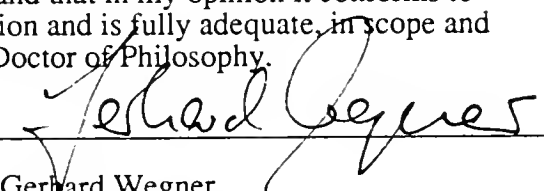
I certify that I have read this study and that in my opinion it conforms to acceptable standards of scholarly presentation and is fully adequate, in scope and quality, as a dissertation for the degree of Doctor of Philosophy.



---

Hendrick Monkhorst  
Professor of Physics

I certify that I have read this study and that in my opinion it conforms to acceptable standards of scholarly presentation and is fully adequate, in scope and quality, as a dissertation for the degree of Doctor of Philosophy.



---

Gerhard Wegner  
Professor of Chemistry  
Max-Planck-Institut-für-Polymerforschung  
Mainz, Germany

This dissertation was submitted to the Graduate Faculty of the Department of Chemistry in the College of Liberal Arts and Sciences and to the Graduate School and was accepted as partial fulfillment of the requirements for the degree of Doctor of Philosophy.

December, 1993

---

Dean, Graduate School

UNIVERSITY OF FLORIDA



3 1262 08556 8482